Università degli Studi di Torino

Tesi di Dottorato di Ricerca in Scienze Biologiche
e Biotecnologie Applicate

PhD Thesis in Biological Sciences
and Applied Biotechnologies

Carotenoid cleavage dioxygenase encoding genes as regulators of development and responses to biotic and abiotic stresses in crop plants

Cristina Votta

Tutor: Luisa Lanfranco
Co-Tutor: Valentina Fiorilli

XXXIV Cycle

TABLE OF CONTENT

Chapter 1: Introduction 4
1.1 Carotenoids and apocarotenoids 4
1.1.1 The Carotenoid Cleavage Dioxygenases enzymatic family 6
1.2 Abscisic acid (ABA) 12
1.2.1 Biological function of ABA 12
1.2.2 ABA biosynthesis and signalling 13
1.3 Strigolactones 15
1.3.1 The biological function of strigolactones 15
1.3.2 Chemistry, biosynthesis and signalling of strigolactones 17
1.4. Novel apocarotenoids 20
1.4.1 β-cyclocitral 20
1.4.2 Anchorene 21
1.4.3 Zaxinone 22
1.5 The role of apocarotenoids in the arbuscular mycorrhizal symbiosis 25
1.5.1 The arbuscular mycorrhizal symbiosis 25
1.5.2 The role of abscisic acid in the AM symbiosis 27
1.5.3 Strigolactones and the AM symbiosis 28
1.5.4 Mycorradicins (C_{14}) and blumenols (C_{13}) 30
1.5.5 The zaxinone involvement in the AM symbiosis 33
1.5.6 Other phytohormones involved in AM colonization 33
1.6 Aim of the work 35
1.7 References 37
Chapter 2: Multi-omics approaches explain the growth-promoting effect of the apocarotenoid growth regulator zaxinone in rice 51
Introduction 53
Results 54
Discussion 57
Summary model 58

Material and methods 59
References 60
2.1 Supplementary material 63
Chapter 3: Zaxinone synthase controls arbuscular mycorrhizal colonization level in rice 64
Introduction 65
Results and discussion 66
Conclusion 72
Summary model 74
Experimental procedures 74
References 76
3.1 Supplementary material 79
Chapter 4: ZAXINONE SYNTHASE 2 regulates growth and arbuscular mycorrhizal symbiosis in rice 79
Introduction 81
Results 82
Discussion 88
Material and methods 92
References 95
4.1 Summary model 98
4.2 Supplementary material 99
Chapter 5: The effect of zaxinone, a natural metabolite derived from carotenoids, on tomato plants 100
5.1 Introduction 100
5.2 Material and methods 104
5.3 Results 112
5.4 Discussion 123
5.5 Summary model 128
5.6 References 129
5.7 Supplementary material 129

Chapter 6: Integration of Apocarotenoid Profile and Expression Pattern of Carotenoid Cleavage Dioxygenases during Mycorrhization in Rice 139
6.1 Introduction 139
6.2 Material and methods..... 144
6.3 Results 148
6.4 Discussion and conclusion 157
6.5 Summary model 162
6.6 References..... 169
6.7 Supplementary material 161
Chapter 7: General conclusions 186
7.1 Reference 189
List of publications 190
Poster and oral presentation conferences 190
Acknowledgments..... 192

Chapter 1: Introduction

1.1 Carotenoids and apocarotenoids

Carotenoids are a class of lipophilic pigments widely diffused in nature, being synthesized by all photosynthetic organisms (bacteria, algae, and plants) and by non-photosynthetic bacteria and fungi (Hirschberg, 2001; Fraser and Bramley, 2004; DellaPenna and Pogson, 2006; Moise *et al.*, 2014; Nisar *et al.*, 2015).

Generally, carotenoids are defined by a common C_{40} polyene backbone carrying 3–11 conjugated double bonds with different stereo configurations. Their diversity derives from the addition of different functional groups, which are commonly attached to the rings or the ends of the molecule, or due to the presence of hydroxylation, oxygenation, and further derivatization (Hirschberg 2001; Moise *et al.* 2014; Wang, Lin, *et al.* 2021). They are classified as carotenes or xanthophylls, with only the latter including oxygen-containing functional groups (Bhosale & Bernstein 2005). The presence of these groups affects the solubility of carotenoids, making xanthophylls more polar than carotenes.

In plants, carotenoids are synthesized in light- and dark-grown tissues, such as leaves, endosperm, and roots. The carotenoid biosynthetic pathway occurs in plastids where they are also stored and accumulated in envelope/thylakoid membranes and plastoglobuli (Jeffrey *et al.* 1974; Austin *et al.* 2006).

Carotenoids derived from two isoprene isomers, isopentenyl diphosphate (IPP) and its allylic isomer dimethylallyl diphosphate (DMAPP), originated from the plastid methylerythritol 4-phosphate (MEP) pathway (Rodríguez-Concepción & Boronat 2002). Thanks to the action of different enzymes present in this metabolic route geranylgeranyl diphosphate (GGPP) is obtained, by the addition of three IPP molecules to DMAPP. GGPP is the direct precursor for carotenoid biosynthesis, as

well as for many other important plastidial isoprenoids, such as gibberellins and chlorophylls (Ruiz-Sola *et al.*, 2016; Zhou *et al.*, 2017; Sun *et al.*, 2020).

In photosynthetic organisms, carotenoids, mainly xanthophylls, are located in specific complexes, serving as accessory pigments to harvest light for photosynthesis and constituting the basic structural units of the photosynthetic apparatus (Britton, 2008). In addition, they also act as photo protectors by quenching the energy excess under high-light stress and preventing the formation of highly reactive singlet oxygen (Heath *et al.*, 2013).
Carotenoids have also ecological functions, providing flowers and fruits with specific colors that play a role in attracting insects and other animals, thus promoting pollination and seed dispersal (Yuan *et al.*, 2015; Giuliano, 2017). Alongside, they can also function as repellents for pathogens and pests(Wang *et al.*, 1999; Ômura *et al.*, 2000; Gruber *et al.*, 2009).

Carotenoids are important antioxidants also in heterotrophic organisms, including humans. Many birds, fishes, and marine invertebrates accumulate these pigments in certain tissues for pigmentation and nutritional purposes too. Normally, animals, except for some aphids that naturally produce torulene (Moran and Jarvik, 2010), are unable to synthesize carotenoids *de novo* and obtain them from their diet. α-carotene, β-carotene, and β-cryptoxanthine are precursors of vitamin A, retinal, and retinoic acid, which play essential roles in nutrition, vision, and cellular differentiation (Krinsky, 1994) (Fraser and Bramley, 2004; DellaPenna and Pogson, 2006; Giuliano, 2014; Nisar *et al.*, 2015; Zheng *et al.*, 2020).

Carotenoids are also the precursor of apocarotenoids, another important class of compounds, which includes the already mentioned retinal and vitamin A, signaling molecules, the fungal pheromone trisporic acid, the plant hormones abscisic acid (ABA) (Nambara and Marion-Poll, 2005) and strigolactones (SLs) (Hou *et al.*, 2016; Wang *et al.*, 2021*b*). Recently, novel plant apocarotenoids have been identified, such

as cyclocitral (Dickinson *et al.*, 2019), zaxinone (Wang *et al.*, 2019), and anchorene (Jia *et al.*, 2019).

Plant apocarotenoids can be generated by non-enzymatic oxidation processes that are triggered by reactive oxygen species (ROS) (Harrison and Bugg, 2014; Ahrazem et al., 2016) or by the action of a ubiquitous family of non-heme iron enzymes, called carotenoid cleavage dioxygenases (CCDs) (Floss *et al.*, 2008; Alder *et al.*, 2008), which incorporate molecular oxygen between adjacent carbon atoms, leading to carbonyl products *via* unstable intermediates. The different specificity concerning substrate structure and stereo-configuration, and the targeted double bond allows distinguishing diverse types of CCDs (Bruno *et al.*, 2014).

1.1.1 The Carotenoid Cleavage Dioxygenases enzymatic family

The CCD family is an ancient family of enzymes present in bacteria, plants, and animals. The CCD members share common features: i) the need for a Fe^{2+} ion for catalytic activity (Schwartz *et al.*, 1997); ii) the presence of four conserved histidines that are thought to coordinate iron binding; and iii) a conserved peptide sequence at their carboxyl terminus (Auldridge *et al.*, 2006).

Plant CCDs constitute the most abundant group identified so far (**Figure 1**). These CCDs have been classified into two large families based on the production or not of abscisic acid (ABA), a hormone involved in drought stress responses and seed dormancy (Schwartz *et al.*, 1997). Those involved in ABA production are the 9-*cis*-epoxy-carotenoid-dioxygenases (NCEDs), which cleave 9-*cis*-violaxanthin and 9-*cis*- neoxanthin to xanthoxin, the precursor of ABA (Nambara and Marion-Poll, 2005; Ahrazem *et al.*, 2016). In the model plant *Arabidopsis thaliana*, the CCD family comprises nine members, including five NCEDs (NCED2, NCED3, NCED5, NCED6, and NCED9) and four CCDs (CCD1, CCD4, CCD7, and CCD8) (Tan *et al.*, 2003; Sui *et al.*, 2013).

The first enzyme found to be specifically involved in the cleavage of carotenoids, viviparous14 (VP14), was identified by the analysis of a viviparous ABA-deficient mutant in maize (Schwartz *et al.*, 1997). NCEDs are plastid-localized and are therefore co-localized with carotenoids (Tan *et al.*, 2003; Floss and Walter, 2009). These enzymes are unique among other CCDs in that they accept only *cis*-isomers of their substrates (Tan *et al.*, 2003). The cleavage reaction, in which they are involved, is the rate-limiting step in ABA biosynthesis (Finkelstein, 2013).

The contribution of CCD1 enzymes to the generation of important apocarotenoid volatile compounds (β-ionone, β-cyclocitral, geranylacetone, and pseudoionone) in fruit and flowers has been demonstrated in a vast number of different plant species (Schwartz *et al.*, 2001; Vogel *et al.*, 2008; Ilg *et al.*, 2009, 2014; Nisar *et al.*, 2015). These enzymes are the only CCDs localized in the cytoplasm (Auldridge *et al.*, 2006), although they may also associate with the outer chloroplast membrane. Due to their subcellular location, CCD1s do not have direct access to the carotenoids located in the plastids (Auldridge *et al.*, 2006). Therefore, plant CCD1 may convert the plastid-released apocarotenoids that have arisen by non-enzymatic oxidative cleavage processes or the activity of other CCDs (CCD4 and/or CCD7). This scenario might explain the multiple cleavage sites and the wide substrate specificity displayed by CCD1 enzymes (Ilg *et al.*, 2010; Beltran and Stange, 2016).
In some species, however, CCD1 gene duplication has occurred leading to functional specialization (Hou *et al.*, 2016). *In vivo*, CCD1 catalyzes the C9-C10; C9'-C10' double bond of β-carotene forming β-ionone; interestingly, *Oryza sativa* and *Zea mays* CCD1s are reported to cleave C5-C6; C5'-C6' and C7-C8; C7'-C8' positions of lycopene (Vogel *et al.*, 2008; Ilg *et al.*, 2009, 2014). Moreover, CCD1 in *Medicago truncatula* may be involved in the generation of mycorradicin, revealing a special role in the production of a non-volatile compound. Mycorradicin is the yellow pigment that accumulates to high levels in the roots of many plants upon colonization

with arbuscular mycorrhizal (AM) fungi (Fester *et al.*, 2002*a*) and is produced from cleavage of root carotenoids (Fester *et al.* 2010).

A CCD subfamily related to the CCD1 family has been identified in *Crocus* species (Frusciante *et al.*, 2014). This subfamily, named CCD2, is involved in the formation of the apocarotenoid crocetin, which accumulates in stigma tissue at high levels (Ahrazem *et al.*, 2015); this enzyme catalyzes the reaction cleaving zeaxanthin at C7-C8 and C7'-C8' position. Similar to CCD1, CCD2 has a cytoplasmic localization, suggesting that it may cleave carotenoids localized in the chromoplast outer envelope (Frusciante *et al.*, 2014). No other CCD2 homologs have been identified in other organisms, probably for the uncommon capability to synthesize crocetin in plants and bacteria (Ahrazem *et al.*, 2016).

CCD4, as well as CCD1 enzymes, are known to produce apocarotenoid-derived pigments, flavours, and aromas *in planta*, but their biochemical functions are quite different (Schwartz *et al.*, 2001; Auldridge *et al.*, 2006; Ilg *et al.*, 2009). Plants produce two different forms of CCD4 enzyme (Huang *et al.*, 2009). The first type mediates the cleavage of bicyclic all-*trans*-cyclic carotenoids, e.g., all-*trans*-β-carotene, at the C9-C10 or C9'-C10' double bond leading to apo-10'-carotenoids (C27), e.g., β-apo-10'-carotenal, and the corresponding C13 cyclohexenone product, e.g., β-ionone (Bruno *et al.*, 2016). Zeaxanthin and β-epoxyxanthophylls may also be substrates for CCD4-mediated 9,10 cleavage in *Arabidopsis* leaves and the apocarotenoids formed may be sequestered as glycosides (Lätari *et al.*, 2015).
Moreover, a second type of CCD4 was identified, in Satsuma mandarin (*Citrus unshiu*); it cleaves bicyclic carotenoid, as β-cryptoxanthin and zeaxanthin, asymmetrically at the C7-C8 or C-7'C-8' positions to yield β-citraurin, a pigment responsible for the color of citrus fruits, and apo-8'-β-carotenal (Ma *et al*., 2013; Rodrigo *et al*., 2013). CCD4 is localized in plastoglobules, the lipoprotein particles inside plastids, which means these enzymes have direct access to carotenoid

substrates, implicating their role in carotenoid degradation and apocarotenoid synthesis within the plastid (Beltran & Stange 2016).
Similar to CCD1, these genes exist as duplicates in many species and often differ in substrate selectivity, tissue localization, and expression pattern (Hou *et al.*, 2016).

CCD7 is a key enzyme for the SL biosynthesis, cleaving at the C9'-C10' and/or C9-C10 double bond of 9-*cis*-β-carotene (C_{40}) to give β-ionone and 9-*cis*-β-apo-10'-carotenal (C_{27}) (Alder *et al.*, 2012; Bruno *et al.*, 2014; Bruno and Al-Babili, 2016; Abuauf *et al.*, 2018). The stereo-and regiospecificity of the CCD7 substrate from *Oryza sativa*, *Pisum sativum*, and *Arabidopsis thaliana* was further studied *in vitro* with different carotenoid isomers, which indicates that CCD7 enzymes preferentially cleave 9-*cis*-configured carotenoids, i.e., 9-*cis*-lutein (C_{40}), 9-*cis*-zeaxanthin (C_{40}), and 9-*cis*-ζ-carotene (C_{40}) resulting in the formation of the corresponding 9-*cis*-apocarotenal (C_{27}) (Alder *et al.*, 2012; Bruno *et al.*, 2014; Bruno and Al-Babili, 2016). Additionally, CCD7 may also catalyze the initial 9,10 cleavage required for mycorradicin synthesis (Floss *et al.* 2008).

CCD8 follows CCD7 in SL biosynthesis by catalyzing the conversion of 9-*cis*-apo-10'-carotenal (C_{27}) into carlactone, the SL precursor (Alder *et al.*, 2012). A study revealed that the combined action of CCD7 and CCD8 in the bryophyte *Physcomitrella* can also produce carlactone, pointing out that SL biosynthesis mediated by these two enzymes has occurred since the primitive land plant (Decker *et al.*, 2017). Moreover, CCD8 can also convert 9-*cis*-3-OH-β-apo-10'-carotenal (C_{27}) produced by CCD7 into the 3-hydroxy-carlactone (3-H-CL, C_{27}), which finds out another branch in the SL biosynthesis pathway.
In addition, *in vitro* CCD8 also catalyzes a typical CCD cleavage reaction, converting the all-*trans*-β-apo-10'-carotenal (C_{27}), at C13-C14 leading to β-apo-13-carotenone (C_{18}), called D'orenone, and an unidentified dialdehyde product (Alder *et al.*, 2012; Bruno *et al.*, 2017). Interestingly, from recent studies on this

apocarotenoid, it is possible to speculate that D'orenone formation may have functions in regulating plant development, signaling precursor in shoot branching, and the interaction with microorganisms, affecting ectomycorrhizal formation by modulating auxin metabolism in both symbiotic partners (Wagner *et al.*, 2016). CCD7 and CCD8 are localized in the chloroplast stroma, although a transient association with the stroma-facing thylakoid membrane has also been observed (Hou *et al.*, 2016).

Recently, other types of CCDs were reported, including the already mentioned CCD2 in *Crocus* species and ZAXINONE SYNTHASE (ZAS), which represents an overlooked CCD subfamily from rice (Wang *et al.*, 2019). *In vitro* ZAS cleaves a molecule of apo-10'-zeaxanthinal (3-OH-β-apo-10'-carotenal, C_{27}) at the C13-C14 double bond, generating zaxinone, a C_{18}-ketone, and an unstable C_9-dialdehyde. In rice, zaxinone acts as a growth-promoting metabolite, a biosynthesis regulator of SLs, and influences mycorrhization (Wang *et al.*, 2019; Votta *et al.*, 2022). Notably, phylogenetic analysis revealed that genomes of plant species that are non-host AM plants, such as *Brassicales* species, do not contain ZAS orthologues.
Newly, Ablazov and colleagues (Ablazov *et al.*, 2022) described the biological function of *OsZAS2*, a rice homolog of *OsZAS*, highlighting that this gene encodes for an additional zaxinone-forming enzyme (for further details see **Chapter 4**).

Research on CCDs has evolved rapidly over the past 20 years, with the breakthrough of genome sequencing projects and transcriptome analyses of many species. The characterization of CCDs and possibly novel apocarotenoids will contribute to a better understanding of their role in plant biology and responses to environmental factors; this knowledge could also be instrumental for the development of agro-biotechnological tools to improve crop performances.

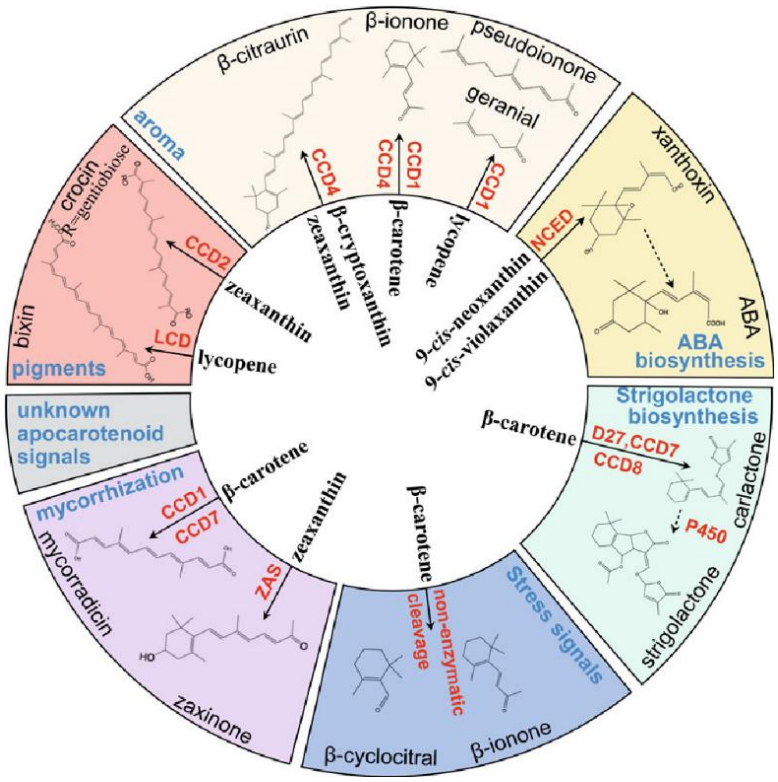

Figure 1. Scheme of the main apocarotenoids produced in plants. *Molecules are divided according to their function (aroma, pigments, signals, mycorrhization, stress signal, and phytohormones-SLs and ABA). For each apocarotenoid is indicated the starting substrate. Non-enzymatic cleavage and enzymatic catabolic processes are annotated in red (Sun* et al. *2020).*

1.2 Abscisic acid (ABA)

1.2.1 Biological function of ABA

The best-studied plant apocarotenoid is the plant hormone ABA, discovered in the early 1960s; it coordinates plant response to stress stimuli and is involved in different developmental processes, like shoot branching and leaves senescence (Finkelstein and Rock, 2002; Finkelstein, 2013) (**Figure 2**). In addition, ABA regulates water uptake (Dodd, 2013; Harris, 2015) and coordinates stomata closure to minimize water loss under drought conditions (Merilo *et al.*, 2015). Furthermore, this hormone controls seed maturation, germination, and dormancy, which prevents germination under unfavorable conditions (Tuan *et al.*, 2018). Substantial evidence has emerged from different AM host plants for a direct role of ABA in mycorrhizal root colonization (Fiorilli *et al.*, 2019). In many of these proposed functions, ABA acts through synergistic and/or antagonistic interactions with other hormones (i.e., gibberellins, ethylene, and auxins) (Hussain *et al.*, 2000; De Vleesschauwer *et al.*, 2010).

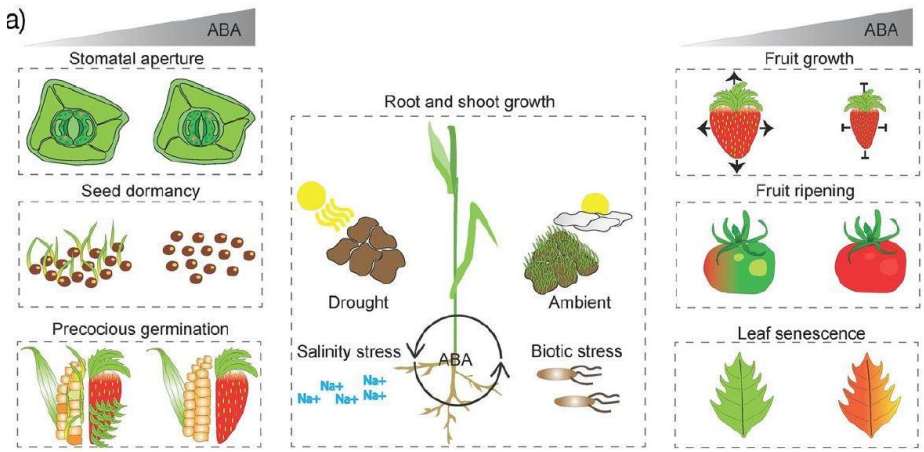

***Figure 2*. ABA functions in plants.** *ABA modulates plant growth and development (shoot branching, leaves senescence, fruit growth, and ripening). This hormone regulates plant responses during abiotic (drought, salinity, ambient) and biotic stress conditions. ABA also controls seed germination and dormancy (Moreno* et al. *2021).*

1.2.2 ABA biosynthesis and signalling

ABA biosynthesis starts with the enzymatic cleavage NCED-mediated of 9-*cis*-violaxanthin or 9'-*cis*-neoxanthin into xanthoxin (C_{15}) and the corresponding C_{25}-apocarotenoid in plastids (Tan *et al.*, 2003). Xanthoxin is then transported to the cytosol, where it is converted by short-chain dehydrogenase reductase (SDR) into an abscisic aldehyde. Oxidation of the latter by abscisic aldehyde oxidase (AAO), leads to forming ABA (Nambara and Marion-Poll, 2005; Finkelstein, 2013).

ABA levels are determined not only by biosynthesis but also by conjugation and hydroxylation processes (Chen *et al.*, 2020). The conjugation of ABA by the uridine diphosphate glucosyltransferases (UGTs) leads to an inactive ABA form, ABA-glucose ester, that can be considered as storage or long-distance, root-to-shoot transport form (Finkelstein, 2013). Under stress conditions, this compound can be rapidly hydrolyzed into ABA by a β-glucosidase and released from vacuoles, providing a fast response to environmental changes (Lee *et al.*, 2006; Xu *et al.*, 2012). In angiosperms, the core of the ABA perception and signaling pathway comprises three major components: PYR (pyrabactin resistance)/PYL (PYR1-LIKE)/RCAR (regulatory component of ABA response) group of ABA receptors, the negative regulator PP2C (protein phosphatase 2C), and the positive regulator SnRK2 (sucrose non fermenting 1–related protein kinase 2) (Todaka *et al.*, 2015; Felemban *et al.*, 2019) (**Figure 3**).

In the absence of ABA, the negative regulator PP2C represses SnRK2 activity by dephosphorylating its kinase activating loop; in the presence of ABA, the receptors PYR/PYL/RCAR5 and PP2C form a complex that prevents the SnRK2 dephosphorylation. This allows the SnRK2 activation and triggers ABA-responsive element (ABRE)–binding protein/ ABRE-binding factor (AREB/ABF) transcription

factors, which bind to promoters of stress-responsive genes (Todaka *et al.*, 2015; Wang *et al.*, 2017; Xie *et al.*, 2019*b*).

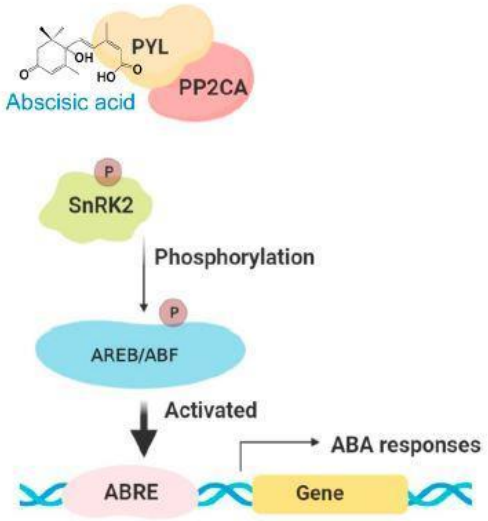

Figure 3. ABA perception and signaling pathway. *The presence of ABA leads to the formation of the complex containing the receptor PYR/PYL/RCAR5 and PP2C, preventing the SNRK2 dephosphorylation. This activation triggers ABA-responsive element (ABRE)–binding protein/ ABRE-binding factor (AREB/ABF) transcription factors that induce the ABA response (modified from Wang et al., 2021).*

1.3 Strigolactones

1.3.1 The biological function of strigolactones

Strigolactones (SLs) are carotenoid-derived plant hormones produced mainly in the root and exuded into the rhizosphere (**Figure 4).** They were described for the first time as an inducer of seed germination of root parasitic plants of the genera *Striga*, *Orobanche*, *Alectra*, and *Phelipanche* (Yoneyama *et al.* 2013). Root parasitic plants have little or no photosynthetic capacity and therefore depend entirely on a host plant to provide them with water, assimilate, and nutrients (Bouwmeester *et al.* 2003). They infect hosts in natural habitats, and, in addition, represent a serious problem also in agriculture, where cause extended yield losses in many major crops (Parker 2009). Besides this negative ecological role, a decade ago, it was demonstrated that SLs mediate the establishment of the beneficial symbiosis between arbuscular mycorrhizal (AM) fungi and roots of land plants by stimulating the branching of the fungal hyphae (Akiyama *et al.* 2005). In addition, SLs are involved in the *Rhizobium*-legume interaction, another root symbiosis of particular relevance in nitrogen-limiting environments (Soto *et al.*, 2010; Foo and Davies, 2011; Peláez-Vico *et al.*, 2016), where SLs were shown to stimulate the surface motility of rhizobia (Peláez-Vico et al., 2016).

Furthermore, SLs are plant hormones involved in many shoot-related developmental processes like the regulation of shoot branching (Gomez-Roldan *et al.*, 2008; Umehara *et al.*, 2008), rice tiller angle by attenuating shoot gravitropism (Sang *et al.*, 2014), promotion of shoot secondary growth, elongation of internodes (Agusti *et al.*, 2011), inhibition of hypocotyl and mesocotyl growth (Hu *et al.*, 2010, 2014; Jia *et al.*, 2014; Wang *et al.*, 2020*b*), induction of leaf senescence (Snowden *et al.*, 2005; Yamada *et al.*, 2014) and decreasing the rice leaf angle in response to nutrient deficiencies (Sang *et al.*, 2014; Shindo *et al.*, 2020) (**Figure 4 a-j, m-n**). However, it is worth to mention that a recent work has clearly demonstrated that in rice

canonical SLs (see next paragraph) are not major determinants of shoot architecture (Ito et al. 2022).

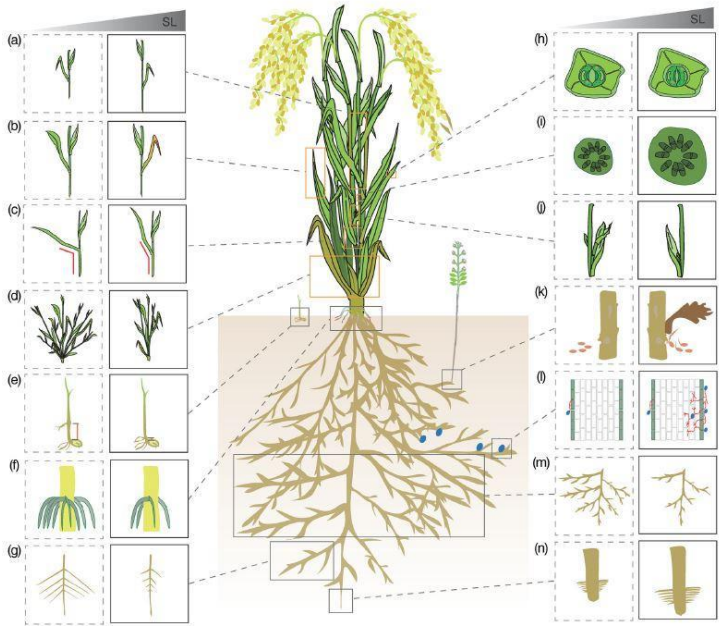

Figure 4. Functions of strigolactones (SLs) in plant development and in rhizosphere communications. *SLs promote or inhibit different plant growth processes, including (a) internode growth, (b) leaf senescence, (c) leaf angle, (d) tillering and tiller angle, (e) mesocotyl elongation, (f) adventitious roots formation, (g) secondary lateral root formation, (h) stomatal closure, (i) stem thickness increase and secondary growth, (j) axillary buds outgrowth, (k) parasitic seeds germination, (l) interactions with arbuscular mycorrhizal fungi, (m) lateral roots of formation and (n) root hair elongation and primary root growth (Moreno et al., 2020).*

1.3.2 Chemistry, biosynthesis, and signalling of strigolactones

There are around 30 characterized natural SLs so far, which are classified based on their chemical structure in canonical and non-canonical SLs (Yoneyama *et al.* 2018). Canonical SLs consist of a butenolide lactone ring (D ring) linked by an enol ether bridge in R-configuration (2′R), to a tricyclic lactone (ABC ring). They are divided into strigol- and orobanchol-like SLs (C-ring in α- orientation/down) and strigol-type SLs (C-ring in β-orientation/up) (Al-Babili and Bouwmeester, 2015; Felemban *et al.*, 2019; Wang *et al.*, 2021*b*). There are also non-canonical SLs, that contain the enol-ether–D-ring moiety but lack the canonical A-, B-, and/or C-rings (Xie, Mori, *et al.* 2019).

Strigolactone biosynthesis (**Figure 5**) is initiated by the reversible conversion of the all-*trans*-β-carotene (C_{40}) into 9-*cis*-β-carotene in the plastids, which is catalyzed by the 9-*cis*/*trans*-all-β-carotene isomerase Dwarf27 (D27), an iron-binding protein with an isomerase activity (Alder *et al.*, 2012; Bruno and Al-Babili, 2016; Abuauf *et al.*, 2018; Ito *et al.*, 2022). Sequential actions of already worded CCD7 and CCD8 on this substrate yield carlactone (CL), the last common precursor for all SLs. At this step, the formation and stereochemical orientation of the D ring is complete, but CL itself does not have appreciable SL activity (Alder *et al.* 2012; Bruno *et al.* 2017). CL is exported into the cytosol where it is further converted by cytochrome P450 enzymes (CYP), of the 711 clades. An investigation on the activity of CYP711 enzymes from different plant species allowed the classification of these enzymes into three types: types A1, A2, and A3. Type A1 enzymes, including the Arabidopsis AtMAX1 and its orthologues, convert CL into carlactonoic acid (CLA) (Yoneyama *et al.* 2018). Type A2 enzymes, represented by the rice Os900, transform CL into the 4-deoxyorobanchol (4DO), which involves the generation of CLA, and additional oxygenation followed by B/C lactone ring closure (Zhang *et al.* 2014). Enzymes of the CYP711 A3 type, represented by the rice Os1400, conduct the hydroxylation of 4DO to produce orobanchol (Sun *et al.* 2014).

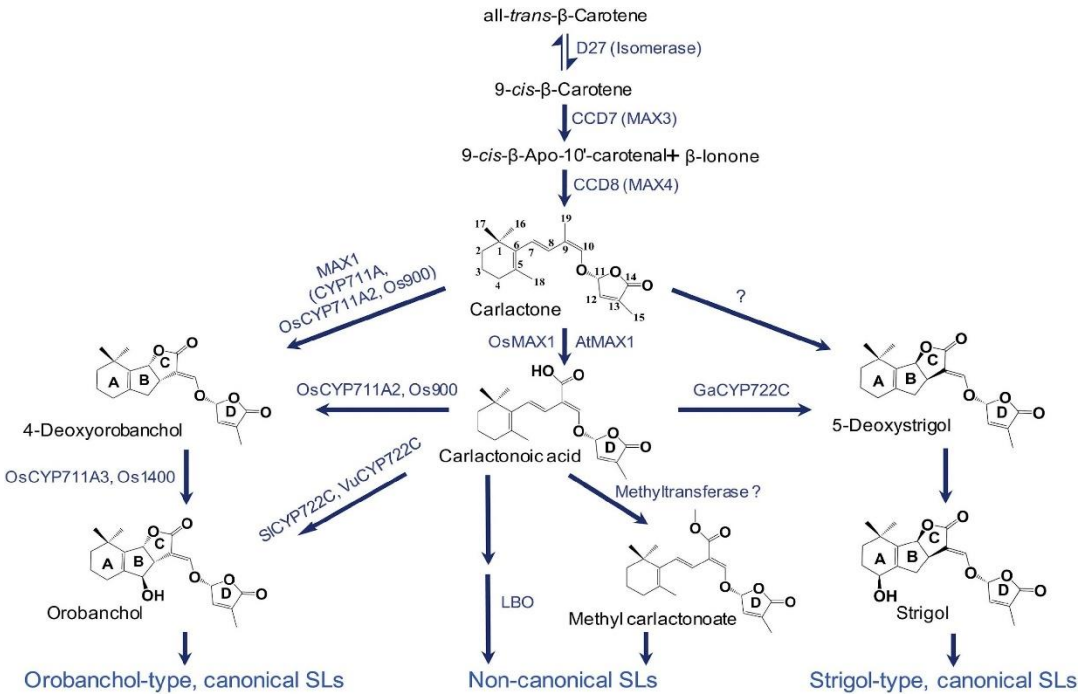

Figure 5. Strigolactones biosynthesis*. The synthesis begins with the action of isomerase D27, then the sequential action of CCD7 and CCD8 yields carlactone (CL), the precursor for all SLs. CL is further modified by cytochrome P450 enzymes to form different types of canonical, e.g., 4-deoxyorobanchol, and non-canonical, SLs (Wang et al., 2021).*

Like many plant growth regulators (auxins, gibberellins, jasmonate), SLs signaling mechanisms are executed by proteasomal degradation (**Figure 6**). SLs signaling machinery comprises at present the α/β-fold hydrolase named Dwarf14 (D14), the F-box leucine-rich protein MAX2, and the D53 a repressor protein that belongs to a small family of proteins [SMAX1-like (SMXL)] (Stanga *et al.* 2013). D14 contains a conserved Ser-His-Asp catalytic triad required for SL hydrolysis and signal transduction (Hamiaux *et al.* 2012; Nakamura *et al.* 2013).

In the absence of SLs, D14 exhibits an open solvent-exposed ligand-binding pocket. During SL hydrolysis, the SL D-ring is cleaved and forms a linked intermediate molecule that is covalently linked to the His residue of the catalytic triad. This connection leads D14 to change conformation and stimulates its interaction with MAX2/DWARF3 (D3 in rice), a component of Skp1/Cullin/F-box (SCF)-type E3

ubiquitin ligase (Yao *et al.* 2016). The formed complex recruits a subset of transcription factors, such as the *Arabidopsis* SUPPRESSOR OF MAX2 1-LIKE (SMXL), and triggers their poly-ubiquitination and proteasomal degradation (Jiang *et al.*, 2013; Al-Babili and Bouwmeester, 2015; Wang *et al.*, 2015).

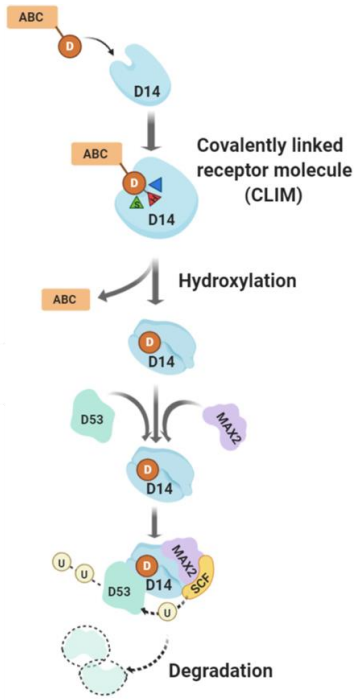

Figure 6. Model of strigolactone signaling. *The receptor D14 binds and hydrolyzes SLs, leading to the ejection of the ABC moiety and retention of the D ring. Hydrolysis also induces a conformational change that helps the D14 interaction with MAX2 and repressor proteins, like the Arabidopsis SMXL or the rice D53. After recruitment into the SCF complex, D53 protein is polyubiquitinated and degraded by the proteasome (modified from Wang et al., 2021).*

1.4. Novel apocarotenoids

In recent years new apocarotenoids have been discovered, some of which are involved in the stress response, such as β-cyclocitral; others seem to play a role in plant growth and beyond, like anchorene and zaxinone (**Figure 7**).

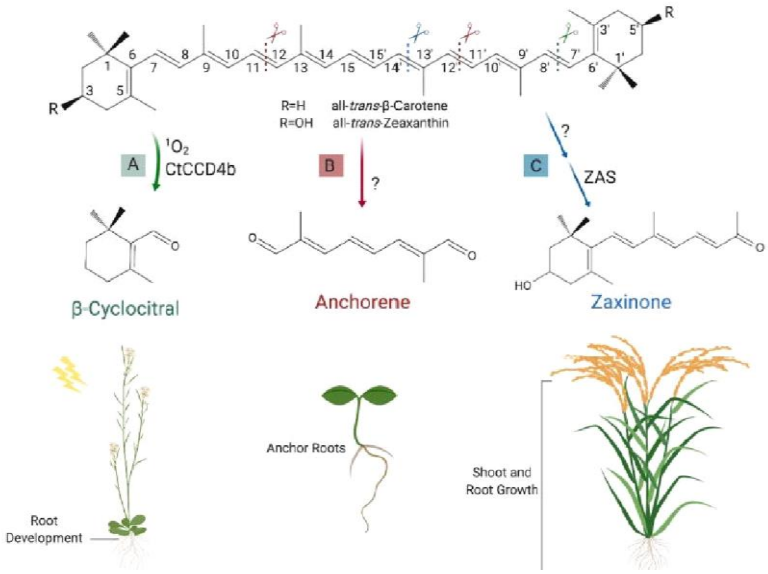

Figure 7. Biosynthesis and function of novel apocarotenoids. ***(A)*** *β-cyclocitral can be formed through the cleavage of all-trans-β-carotene at the (C7'- C8) double bound and, non-enzymatically, through attack by singlet oxygen ($_1O_2$). This volatile molecule acts as a growth regulator of roots and is involved in high-light acclimation.* ***(B)*** *Anchorene, which can be formed by cleaving the (C11- C12) and (C11- C12) double bounds in all carotenoids downstream ζ-carotene in the carotenoid pathway, stimulates anchor roots formation in Arabidopsis seedlings.* ***(C)*** *Zaxinone synthase (ZAS) cleaves a molecule of apo-10'-zeaxanthinal (3-OH-β-apo-10'-carotenal, C_{27}) at the C13-C14 double bond. Zaxinone is required for normal rice growth and development and is a negative regulator of SL biosynthesis (Felemban et al., 2019).*

1.4.1 β-cyclocitral

β-cyclocitral is a volatile β-carotene cleavage product that can be formed by enzymes from a subgroup of the CCD4 clade (Rodrigo *et al.* 2013) and, non-enzymatically, through attack by singlet oxygen ($_1O_2$) (**Figure 7 A**). This second way of formation makes cyclocitral a suitable candidate for sensing high-light/oxidative stress. Indeed, β-cyclocitral acts in *Arabidopsis* as a second messenger that conveys the $_1O_2$ stress

signal to the nucleus, altering the transcription of $_1O_2$-regulated genes *via* a small zinc finger protein called METHYLENE BLUE SENSITIVITY, which enables acclimation to photo-oxidative stress (Wang, Lin, *et al.* 2021). Moreover, the conversion of β-cyclocitral into β-cyclocitric acid, a reaction that spontaneously occurs in water, is an initial step in β-cyclocitral signaling (Havaux 2014; Shumbe *et al.* 2017).

Though the mechanism of action is still unclear, the application of β-cyclocitric acid promoted the expression of several water stress-responsive genes under sufficient water supply and increased *Arabidopsis* tolerance to drought (D'Alessandro *et al.* 2019). Moreover, the positive effect of this apocarotenoid was also observed under salt stress conditions: applied to salt-stressed rice roots rescued the negative effect of salt on root depth and showed in salty soil a positive effect on the vigor of rice plants. Interestingly, β-cyclocitral can act also as a growth regulator, increasing root growth and branching by promoting stem cell divisions (Dickinson *et al.* 2019).

1.4.2 Anchorene

There is a class of less-explored compounds, called diapocarotenoids. Their instability and low abundance impeded the exploration of possible regulatory functions of these molecules, which so far have been mainly studied as precursors of natural pigments, such as crocin in saffron stigma (Frusciante *et al.* 2014).

Recently a screening system was set up to identify known and predicted diapocarotenoids involved in plant development, by looking at alterations in *Arabidopsis* roots. This approach led to the discovery of anchorene, a novel carotenoid-derived bioactive, that promotes the development of anchor roots (ANRs) (**Figure 7 B**). ANRs are a less investigated type of *Arabidopsis* roots, which develop from the collet region situated at the root hypocotyl junction (Lucas *et al.* 2011). Although it is still unclear how anchorene is formed, it is a C_{10} natural metabolite, as confirmed by LC-MS analysis (Mi *et al.* 2019; Jia *et al.* 2019) and its structure indicates that it can be produced by cleaving the (C11-C12) and (C11′-C12′) double

bound from all carotenoids downstream of ζ-carotene in the carotenoid biosynthesis pathway (Felemban *et al.* 2019; Jia *et al.* 2019). Interestingly, the phenotype of the carotenoid-deficient *Arabidopsis psy* mutant, deficient in ANR formation, can be rescued by external anchorene application. Further investigations demonstrated an effect on auxin homeostasis and its involvement in nitrogen deficiency response (Jia *et al.* 2019).

1.4.3 Zaxinone

Zaxinone is a natural apocarotenoid that regulates rice growth and plant architecture and, under certain conditions, suppresses SL biosynthesis (Wang *et al.* 2019) (**Figure 7 C**). As described in the previous section, zaxinone is produced by the action of ZAS, Zaxinone Synthase, which is conserved in most land species but not in *Arabidopsis* or other members of *Brassicaceae*. However, this apocarotenoid was also detected in *Arabidopsis*, suggesting the existence of a ZAS-independent route (Ablazov *et al.* 2020).

Moreover, recently, OsZAS2 was described in rice as a second enzyme involved in zaxinone production. (Ablazov *et al.* 2022, **Chapter 4**).

The analysis of a corresponding rice loss-of-function *zas* mutant, in comparison to the wild type, showed decreased content of zaxinone in roots, accompanied by a reduced crown root length and number, a decrease in root and shoot biomass, and a lower tiller and panicle number, but a higher SL level. The exogenous application of zaxinone rescued the root phenotypes in *zas* mutant and increased root growth in wild-type plants, suggesting that this metabolite is a growth-promoting molecule and is required for normal rice growth and development. Moreover, when this molecule is applied to plants there is a decrease in SL content and release, showing that zaxinone is a negative regulator of SL biosynthesis, by reducing transcript levels of SL genes (Wang *et al.* 2019). Furthermore, the application of zaxinone to a rice variety susceptible to parasitic plant infestations, IAC-165, decreased *Striga*

emergence, pointing out a potential zaxinone application in repressing *Striga* infestation by lowering SL released (Wang *et al.* 2019).
The role of zaxinone was also investigated in *Arabidopsis*: when zaxinone was applied to the plant seedling, the hypocotyl elongation was inhibited and promotion of SL and ABA biosynthesis was observed, in contrast to what was found in rice (Ablazov *et al.* 2020).

Novel research investigated the growth-promoting effect of this new metabolite using an 'omics approach, underlighting that zaxinone acts by increasing the sugar uptake and metabolism in rice roots (Wang, Alseekh, *et al.* 2021). In addition, zaxinone enhances root starch concentration and induces cytokinins (CKs) glycosylation, which significantly reduces their activity and transport. This growth promotion effect is observed also at the cellular level, where zaxinone-treated roots show an increase in apex length, diameter, and the number of cells and cortex cell layers (Wang, Alseekh, *et al.* 2021) (for the entire study see **Chapter 2**).

Finally, Wang and colleagues developed and assessed the activity of phenyl-based compounds mimics of zaxinone (MiZax), which are easy to synthesize and highly efficient. MiZax3 and MiZax5 (**Figure 8**) gave the most promising results and, mimicking the action of zaxinone, they rescued the root growth phenotype of *zas* rice mutant, by promoting growth, and reducing SLs accumulation in wild-type plants (Wang, Jamil, *et al.* 2020).
Another study tested the action of MiZaxs as potential biostimulants, highlighting how their application improved the performance and productivity of horticultural crops (tomato, pepper, squash, and date palm) (Wang *et al.* 2022). MiZax represents suitable tools to investigate zaxinone functions and, at the same time, an agro-

biotechnological approach to enhance crop growth and productivity (Wang, Jamil, *et al.* 2020; Moreno *et al.* 2021).

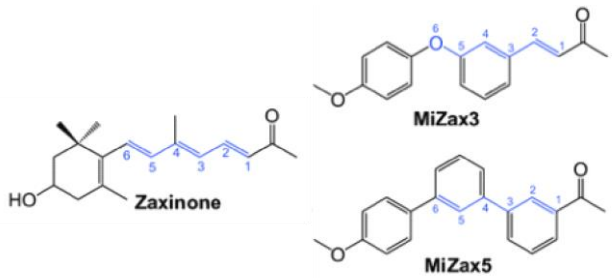

Figure 8. Chemical structure of zaxinone, MiZax3, and MiZax5 *(Wang, Jamil, et al. 2020; Moreno et al. 2021).*

1.5 The role of apocarotenoids in the arbuscular mycorrhizal symbiosis

1.5.1 The arbuscular mycorrhizal symbiosis

The arbuscular mycorrhizal (AM) symbiosis is one of the oldest mutualistic association on Earth, involving soil fungi of the subphylum Glomeromycotina (Spatafora *et al.* 2016) and approximately 70% of land plants, including the most important economic crops (Brundrett & Tedersoo 2018). An estimated 15% of vascular species do not associate with AM fungi. These plants denominated 'non-host' plants, typically occur in disturbed habitats, where competition with other plants is low and soil phosphorus availability is high, or are species without specialized strategies for nutrient acquisition, such as Brassicaceae, the family of *Arabidopsis thaliana*, Polygonaceae, Amaranthaceae, and Caryophyllaceae (Wang & Qiu 2006). These plants presumably lost or suppressed their ability to establish this symbiosis because the costs outweighed the benefits obtained (Lambers & Teste 2013).

Land plant fossils show that AM symbiosis dated back to the time when plants initially colonized the terrestrial environment (Genre *et al.* 2020). Symbiosis with AM fungi is indeed observed also in bryophytes, the basal lineage that diverged from vascular plants more than 400 million years ago (Delaux & Schornack 2021).

In this mutualistic association, AM fungi provide access to phosphorus, which is poorly mobile in the soil, and to a lesser extent, nitrogen, and other mineral nutrients. On the other side, the plant furnishes the fungus with up to 20% of the carbon fixed during photosynthesis, in form of sugars and lipids (Bago *et al.* 2000; Jiang *et al.* 2017; MacLean *et al.* 2017; Brands *et al.* 2018). This symbiosis not only improves mineral nutrition but also raises plant tolerance to biotic and abiotic stresses. Additionally, this colonization impacts the plant developmental processes, like root

architecture, flowering time, fruit and seed formation, and quality (Ruiz-Lozano *et al.* 2012; Zouari *et al.* 2014; Fiorilli *et al.* 2018).

The development of AM symbiosis is an asynchronous event that is divided into different steps (**Figure 9**). In a pre-contact stage, also called the pre-symbiotic stage, the mutual recognition is characterized by a range of responses triggered by SLs, including spore germination, hyphal elongation, and hyphopodia formation (Akiyama *et al.*, 2005; Lanfranco *et al.*, 2018), and the induction of the common symbiotic signalling pathway triggered by fungal diffusible molecules which include (lipo)chito-oligosaccharides (Oldroyd 2013). In response to mechanical and chemical signals emanating from fungal hyphopodia, the contacted plant cell forms an intracellular accommodation structure, the pre-penetration apparatus (PPA) (Genre *et al.* 2005). PPA guides intracellular fungal passage into deeper cell layers. Once in the cortex, fungal hyphae progress longitudinally through the apoplast and form branches to initiate arbuscule formation in cortical cells (Genre *et al.* 2008). The arbuscules are considered the key structure of symbiosis. They are always enveloped by a plant-derived peri-arbuscular membrane (PAM) that forms an extensive interface where nutrients are exchanged (Gutjahr & Parniske 2013). The plant keeps the level of fungal proliferation under control, to prevent excessive carbon loss and to maintain the benefits of symbiosis. To achieve this regulation signals are continuously exchanged between the two symbionts and is required extensive transcriptional reprogramming and cellular remodelling in the plant (MacLean *et al.* 2017; Pimprikar & Gutjahr 2018; Liao *et al.* 2018).

This symbiosis is also regulated by phosphorus (P) availability. In a plant with a high or sufficient P status, initiation of symbiosis is inhibited, while phosphate (Pi) application to an already colonized root rapidly inhibits cortical colonization and the formation of new arbuscules (Koide 1991; Kobae *et al.* 2016). Two recent papers provided convincing evidence that a plant regulatory network, centered on crucial

components of the so-called Pi starvation response, controls the level of root colonization by AM fungi (Shi *et al.* 2021; Das & Gutjahr 2022).

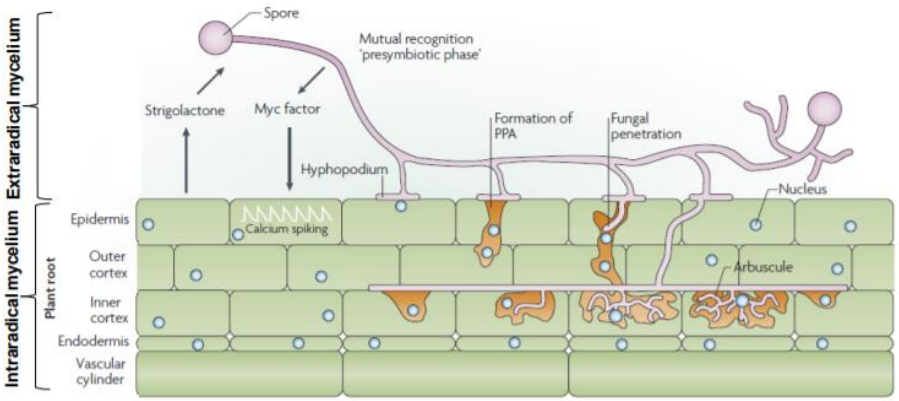

Figure 9. Steps in arbuscular mycorrhiza development*. The plant exudes SLs which are perceived by the AM fungus, which increases its physiological activity and responds by producing "Myc-factors". Consequently, the root prepares for the establishment of the symbiosis. After attachment and hyphopodium formation, the AM fungus enters the root to establish the intraradical mycelium and the formation of arbuscules. (modified from Parniske 2008).*

In addition, many phytohormones may have a role in regulating AM symbiosis (López-Ráez *et al.*, 2015; Pozo *et al.* 2015; Chialva *et al.* 2018; Liao *et al.* 2018; Müller & Harrison 2019). The role of carotenoid metabolism in the AM symbiosis process is not only limited to the well-known plant hormones ABA and SLs, but also involves some novel carotenoid-derived metabolites such as zaxinone (Fiorilli *et al.* 2019). They will be presented in the following sections.

1.5.2 The role of abscisic acid in the AM symbiosis

ABA has been extensively studied due to its primary importance in generating and coordinating the plant's response against abiotic and biotic stress factors (i.e., drought, salt, and pathogens). Recently, a direct role of ABA in mycorrhizal root colonization was described in diverse plant host species.

In *Medicago truncatula*, a dose-dependent effect of ABA modulates the establishment of AM symbiosis by promoting fungal colonization at low

concentrations and its impairment at high concentrations. The ABA positive effect is mediated by the action of the protein phosphatases 2A, PP2A, which is induced during the symbiosis and after ABA treatment (Charpentier *et al.* 2014).

In tomato, the analysis of AM colonization in the tomato mutant *sitiens*, deficient in enzyme activity at the final step of ABA biosynthesis, has demonstrated that this hormone plays a crucial role in the development and functionality of arbuscules (Herrera-Medina *et al.* 2007; Martín-Rodríguez *et al.* 2011). In addition, ABA deficiency enhances ethylene content, thus acting as a negative regulator of mycorrhizal intensity (Herrera-Medina *et al.* 2007; Martín-Rodríguez *et al.* 2011).

Recently, ABA pre-treatment was found to induce in *Solanum tuberosum* (potato) a higher AM colonization and arbuscule level, suggesting that ABA probably acts during the early stage of mycorrhizal formation, developing a suitable metabolic environment for the fungus (Mercy *et al.* 2017; Fiorilli *et al.* 2019).

However, ABA does not act independently during the AM symbiosis, but in negative or positive interaction with other molecules. A correlation between ABA and SLs levels was observed (López-Ráez *et al.* 2010; Visentin *et al.* 2016); their cross-talk may also influence the success of the symbiosis (Fiorilli *et al.* 2019). Alongside, it was demonstrated antagonism between ABA and ethylene (Martín-Rodríguez *et al.* 2011) and gibberellins (GA) (Floss *et al.* 2013; Martín-Rodríguez *et al.* 2016). In detail, ABA could regulate AM development by inhibiting ethylene production (Martín-Rodríguez *et al.* 2011) and contribute to arbuscule formation by mitigating GA-biosynthetic and increasing the catabolic gene expression leading to a reduction in bioactive GAs (Martín-Rodríguez *et al.* 2016).

1.5.3 Strigolactones and the AM symbiosis

When released into the soil, SLs trigger developmental responses of the AM fungi, such as stimulating spore germination and hyphal growth and branching (Akiyama *et al.* 2005; Besserer *et al.* 2006, 2008) thereby enhancing the chance of physical contact with a root. However, it is still unclear how AMF perceives SLs. Moreover,

it has been demonstrated that SLs promote the AMF ATP production and mitochondrial division; and activate the expression of mitochondrial and effector genes (Besserer *et al.* 2006, 2008; Salvioli *et al.* 2016; Tsuzuki *et al.* 2016). In response to this stimulation, the AM fungus exudes some chemical molecules, called "Myc factor", which include chitin oligomers. These fungal molecules can elicit pre-symbiosis responses in root tissues, with the induction of nuclear calcium spiking in the rhizodermis and activation of a common symbiosis signaling pathway (CSSP), which are necessary for initiation of the AM symbiosis (Genre *et al.* 2013).
SL levels are inversely correlated with the plant Pi status (Yoneyama *et al.* 2007) and directly affect the fungal symbiont: in Pi-starved plants, SL production and export to the rhizosphere increase. Interestingly, the expression of SL biosynthetic genes, induced by Pi-starvation, requires two GRAS transcription factors, NSP1 and NSP2 (Liu *et al.* 2011), that also regulate the AM symbiosis signaling pathway. So this provides a point for cross-talk between SL biosynthesis and AM colonization signaling (Kobae *et al.* 2018; Müller & Harrison 2019).

Although it is not yet completely defined how plants release SLs into the rhizosphere, there is evidence that SLs export is associated with an ABC transporter PDR1. In fact, in *Petunia hybrida*, *pdr1* mutants are defective in the SL exudation from their roots, suggesting that PDR1 might function as a cellular SL-exporter (Kretzschmar *et al.* 2012; Sasse *et al.* 2015).

Through the analysis of SL-deficient mutants and applications of SL analogs to the soil, it has been demonstrated the role of SLs as rhizosphere signals in several plant species. Plant mutants with a defect in SL biosynthesis (*ccd7*, *ccd8*, *nsp1/2*) and export (*pdr1*) showed decreased levels of AM colonization and hyphopodium formation, but morphologically normal intraradical fungal structures. The application of the synthetic SL analog GR24 in the pea *ccd8* mutant restored the phenotype of the mutant leading to a similar level of SL compared with the pea wild-

type plants (Akiyama *et al.* 2005; Kretzschmar *et al.* 2012; Kohlen *et al.* 2012; Sasse *et al.* 2015). These findings highlight the important role of SLs involved in the control of early steps of the AM interaction (Kobae *et al.* 2018).

Studying SL-deficient *d17(ccd7) d10(ccd8)* rice double mutants, it has been shown that SLs are also significant for secondary infection (Kobae *et al.* 2018). Despite in these mutants most of the colonization process is normal the hyphopodium formation is severely attenuated, suggesting a continuous requirement for SL (Kobae *et al.* 2018; Müller & Harrison 2019).On the whole, SLs act as positive regulators of the AM symbiosis, they are essential in the pre-symbiotic phase by activating the fungal metabolism, and also their action is necessary to achieve the full extent of mycorrhization during secondary infections (Kobae *et al.* 2018; Fiorilli *et al.* 2019).

From an evolutionary point of view, the identification of an ancestral SL, called bryosymbiol, present in diverse bryophytes such as *Marchantia paleacea*, and vascular plants, and the observation that in *M. paleacea*, bryosymbiol is required for the AM symbiosis but not for development led to the hypothesis that the ancestral function of SLs is as AM symbiosis-inducing rhizosphere signaling molecules and not as plant hormones (Kodama *et al.* 2022).

1.5.4 Mycorradicins (C_{14}) and blumenols (C_{13})

The connection between the AM symbiosis and apocarotenoids is much older than the discovery of SLs. Indeed, already at the beginning of the twentieth century, it was common among scientists to find a yellow coloration of roots colonized by AM fungi (Walter *et al.* 2007; Jones). Afterward, these "pigments" were identified as mycorradicins, yellow C_{14} polyene derivatives (Klingner *et al.* 1995; Walter *et al.* 2010) (**Figure 10 A**) accumulated mainly in connection with AM symbiosis, even if Fester et al. (2002) (Fester *et al.* 2002b) quantified a small amount of these apocarotenoids also in non-mycorrhizal roots in diverse plant species. Moreover,

there are no reports of mycorradicins accumulation in ectomycorrhizas, nodules, or in response to abiotic and biotic stresses (Maier *et al.* 1997; Walter *et al.* 2010). Mycorradicins are stored as globules in root chromoplasts, and their presence leads to changes in root plastid morphology (Scannerini & Bonfante-Fasolo 1977). In addition to these, another type of AM-induced apocarotenoids was described: the colorless C_{13} cyclohexenone derivatives, called blumenols (Walter *et al.* 2010). Blumenols are classified into three major types: blumenol A, blumenol B, and blumenol C. However, only blumenols glycosides containing a blumenol C-based aglycone are positively correlated to mycorrhizal colonization. The aglycone can be additionally hydroxylated at the C11 or carboxylated at the C11 or C12 position (Maier *et al.* 1997, 2000) (**Figure 10 B-C**). Recently, a group of five blumenols (11-hydroxyblumenol C-9-O-Glc, 11-carboxyblumenol C-9-O-Glc, 11-hydroxyblumenol C-9-O-Glc-Glc, blumenol C-9-O-Glc-Glc, and blumenol C-9-O-Glc) was found in shoots and roots of mycorrhizal plants (e.g., tomato, barley, and potato) using a combination of targeted and untargeted metabolomics (Wang, Schäfer, *et al.* 2018). Their abundance is correlated with the AM colonization rate, as reflected in changes in the transcript profile of canonical mycorrhization marker genes. Even if their biological role has not yet been clarified, blumenols can be used as foliar markers that allow rapid detection of AM symbiosis and for the screening of functional AM associations (Walter *et al.* 2010; Wang, Schäfer, *et al.* 2018).

As regards the biosynthesis of these two apocarotenoid types, it seems that they derive from a sequential two-step cleavage of a common C_{40} precursor. The current model suggests the involvement of a CCD enzyme (CCD7 or potentially CCD4) in cleaving the C_{40} carotenoid to form a C_{27} apocarotenoid and C_{13} cyclohexenone, β- or α-ionone (Vogel *et al.* 2010; Walter *et al.* 2010). In the next step, the C_{27} apocarotenoid is cleaved by CCD1, leading to rosafluene-dialdehyde (C_{14}), the mycorradicin precursor, and another cyclohexanone (C_{13}) (Floss *et al.* 2008; Walter *et al.* 2010; Hou *et al.* 2016).

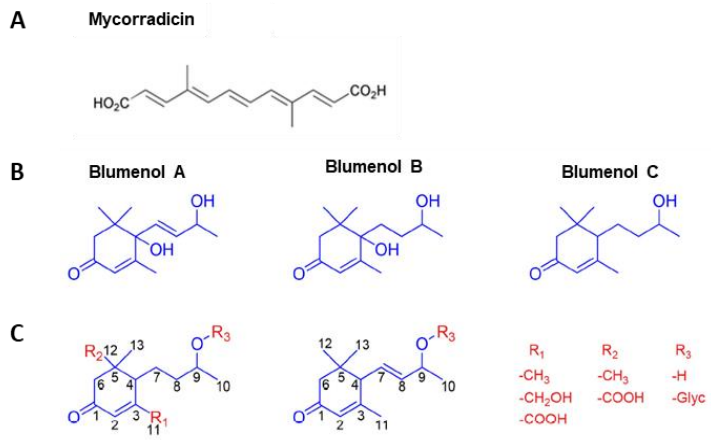

Figure 10. Mycorradicin and blumenol core structures and modifications. *(A) Structure of Mycorradicin (from J. Humphrey et al., 2006. (B) Blumenol A, blumenol B and blumenol, (C) blumenols derivatives structure (modified from Wang et al., 2018).*

Analysis of knockdown mutants affected in carotenoid metabolism demonstrated a positive correlation between C_{13} and C_{14} apocarotenoid content and mycorrhizal functionality (Moreno *et al.* 2021). These apocarotenoids are accumulated locally in arbusculed-contained cells, where their assumed biosynthesis enzymes are present (Fester *et al.* 2002a; Hans *et al.* 2004; Walter *et al.* 2007). In *M. truncatula*, AMF colonization induced the 1-DEOXY-D-XYLULOSE 5-PHOSPHATE SYNTHASE 2 (*MtDXS2*), which catalyses the first step in the plastic isoprenoids biosynthesis. In transgenic roots, obtained repressing *MtDXS2* expression, an equal reduction in the level of both C_{13} and C_{14} levels was described, mirrored by a reduction of mycorrhizal functionality during the later stages of the symbiosis (Floß *et al.* 2008; Fiorilli *et al.* 2019).

In contrast with the *MtDXS2* mutant, *MtCCD1* knockdown lines, displayed a strong reduction in the content of mycorradicin derivatives while the C_{13} cyclohexenone level was only moderately affected, indicating that other enzymes are also involved in blumenols biosynthesis. Moreover, *MtCCD1* down-regulation led to a moderate increase in the relative ratio of degenerated arbuscules, bringing out a more prominent role for blumenols in AM establishment and functioning (Moreno *et al.*

2021). Mycorradicin and blumenols are considered a trademark of AM symbiosis and they are strongly linked with the establishment and maintenance of AM colonization (Walter *et al.* 2007; Hill *et al.* 2018; Wang, Wang, *et al.* 2018; Fiorilli *et al.* 2019).

1.5.5 The zaxinone involvement in the AM symbiosis

Zaxinone was described as a novel regulatory metabolite in rice plants (Wang *et al.* 2019). Moreover, the impact of this molecule on SL biosynthesis and the upregulation of *OsZAS* during the early and later stages of mycorrhization (Fiorilli *et al.* 2019) suggests its possible involvement in AM symbiosis. As shown in Wang et al. (2019) the *oszas* rice mutant, with a reduced root zaxinone content, displays a lower AM colonization level, while the arbuscule morphology is unaltered.
A recent study highlights that the mutant mycorrhizal phenotype is attributable to the lack of SLs accumulation at the early phase of the symbiosis and that OsZAS function as a part of a regulatory network that includes SLs and Dwarf14-Like (D14L) pathways (**Chapter 3**; Votta *et al.* 2022).

1.5.6 Other phytohormones involved in AM colonization

Besides carotenoids and their derivates, other classes of hormones can regulate AM symbiosis. In this paragraph, the involvement of these phytohormones will be concisely reviewed (**Figure 11**).

During the pre-symbiotic stage, salicylates, ethylene, and cytokinins reduced the intensity of mycorrhizal root colonization, with a negative effect on fungal penetration (Pozo *et al.* 2015). Several reports indicate that the gibberellin (GA)-DELLA complex also plays a critical role in symbiotic control (Ho-Plágaro & García-Garrido 2022). In the later stages, GA acts as a repressor of the arbuscules formation (Foo *et al.* 2013; Floss *et al.* 2013; Martín-Rodríguez *et al.* 2015). In agreement with this, DELLA genes, encoding transcription factors that negatively

control the GA signaling, are required for correct mycorrhizal colonization and arbuscule formation (Floss *et al.* 2013).

As regards the auxins have a positive impact on the arbuscule formation and functionality (Martín-Rodríguez *et al.* 2011; Etemadi *et al.* 2014).

For the jasmonate (JA), its role has been investigated in several plant species, *i.e.*, *Medicago*, tomato, tobacco, and rice, however, contradicting results have been reported concerning a neutral, stimulating, or inhibitive effect, depending partially on the plant species and fungal strains (Liao *et al.* 2018).

It is also worth mentioning that often hormones do not act independently, but they interact synergistically or antagonistically and this might occur during the AM symbiosis. For example, as we already mentioned in paragraph 1.5.2, an antagonistic interaction for ABA was described with ethylene (Martín-Rodríguez *et al.* 2011) and GA (Floss *et al.* 2013; Martín-Rodríguez *et al.* 2016). ABA attenuates GA-biosynthesis and increases GA-catabolism, modifying bioactive GA levels; *vice versa* GA activates ABA catabolism, regulating AM formation (Martín-Rodríguez *et al.* 2016).

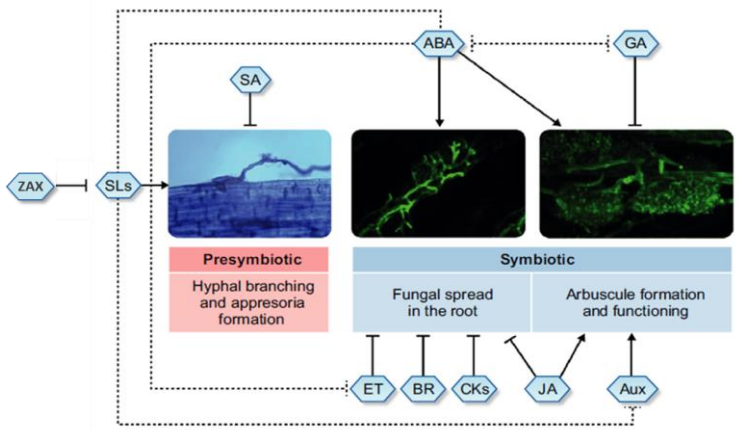

Figure 11. Summary scheme of plant hormones involved in the regulation of the AM symbiosis. *SLs start the dialogue in the pre-symbiotic phase when the fungus is not yet in contact with the root. The other molecules are implicated in the next steps when the fungus starts developing the intraradical mycelium and arbuscules. Positive and negative interactions are represented by arrows and blunt-ended bars, respectively. ABA, abscisic acid; Aux, auxins; BR, brassinosteroids; CKs, cytokinins; ET, ethylene; GA, gibberellins; JA, jasmonates; SA, salicylic acid; SLs, strigolactones; ZAX, zaxinone (modified from Pozo et al., 2015).*

1.6 Aim of the work

The AM symbiosis is a finely regulated process that involves multiple regulatory components. Research in the past years has revealed the critical roles of some phytohormones in modulating the AM interaction, from early recognition events up to the final formation and degradation of arbuscules. Carotenoid-derived metabolites play a role in these different stages, but our knowledge of how these molecules affect symbiosis is still limited.

My PhD thesis aimed at deeper investigating the role of zaxinone, a recently described apocarotenoid, in plant development and in the AM interaction. The work has been carried out in a collaboration with the group of Prof. Salim Al-Babili (KAUST, King Abdullah University of Science and Technology) which in 2019 led to the characterization of zaxinone and the gene responsible for its biosynthesis (Wang *et al.* 2019).

In **Chapter 2**, a combined 'omics approach which includes transcriptomics and metabolomics analyses, was applied to monitor the molecular and metabolic changes after an exogenous zaxinone application in rice plants. We also carried out investigations to highlight alterations in hormone profiles and root organization at the cellular and tissue level (Wang, Alseekh, *et al.* 2021).

Chapter 3 reports investigations on the role of *OsZAS* and zaxinone in the regulation of AM symbiosis. Several experiments and approaches including analyses of mutant lines with altered zaxinone or strigolactones content, exogenous supply of different compounds (zaxinone, the synthetic strigolactones GR24 and a gibberellin inhibitor), hormone analyses, characterization of *OsZAS*-overexpressing transgenic plants and cellular mRNA detection by *in situ* hybridization were performed. We found that this gene guarantees the correct extent of AM root colonization possibly as a component of a regulatory network involving SLs (Votta *et al.* 2022).

In **Chapter 4,** we investigated the biological role of *OsZAS2*, one of the other three *OsZAS* homologs encoded in the rice genome besides *OsZAS*. We studied the enzymatic activity, the expression pattern, and the subcellular localization of OsZAS2, and we generated and characterized the loss-of-function CRISPR/Cas9-*Oszas2* mutants (Ablazov *et al.* 2022).

Considering that zaxinone and the *OsZAS* homologous genes are present in other plant species (Wang *et al.* 2019), the impact of exogenous zaxinone on another crop, *Solanum lycopersicum,* looking at plant development, mycorrhization, and responses to water stress, was analyzed (**Chapter 5**).

Finally, in **Chapter 6**, to identify other apocarotenoids involved in the AM symbiosis, we quantified different non-hydroxylated and hydroxylated apocarotenoids using an ultra-HPLC (UHPLC)-mass spectrometry (MS) method (Mi *et al.* 2018) in rice shoots and roots along a time course mycorrhization experiment. In parallel, the analysis of the expression of *CCD* genes was performed.

1.7 References

Ablazov A, Mi J, Jamil M, Jia K-P, Wang JY, Feng Q, Al-Babili S. 2020. The Apocarotenoid Zaxinone Is a Positive Regulator of Strigolactone and Abscisic Acid Biosynthesis in Arabidopsis Roots. Frontiers in Plant Science 0.

Ablazov A, Votta C, Fiorilli V, et al. 2022. ZAXINONE SYNTHASE 2 regulates growth and arbuscular mycorrhizal symbiosis in rice. Plant Biology.

Abuauf H, Haider I, Jia K-P, Ablazov A, Mi J, Blilou I, Al-Babili S. 2018. The Arabidopsis DWARF27 gene encodes an all-trans-/9-cis-β-carotene isomerase and is induced by auxin, abscisic acid and phosphate deficiency. Plant Science 277, 33–42.

Agusti J, Herold S, Schwarz M, et al. 2011. Strigolactone signaling is required for auxin-dependent stimulation of secondary growth in plants. Proceedings of the National Academy of Sciences 108, 20242–20247.

Ahrazem O, Gómez-Gómez L, Rodrigo MJ, Avalos J, Limón MC. 2016. Carotenoid Cleavage Oxygenases from Microbes and Photosynthetic Organisms: Features and Functions. International Journal of Molecular Sciences 17, 1781.

Ahrazem O, Rubio-Moraga A, Nebauer SG, Molina RV, Gómez-Gómez L. 2015. Saffron: Its Phytochemistry, Developmental Processes, and Biotechnological Prospects. Journal of Agricultural and Food Chemistry 63, 8751–8764.

Akiyama K, Matsuzaki K, Hayashi H. 2005. Plant sesquiterpenes induce hyphal branching in arbuscular mycorrhizal fungi. Nature 435, 824–827.

Al-Babili S, Bouwmeester HJ. 2015. Strigolactones, a Novel Carotenoid-Derived Plant Hormone. Annual Review of Plant Biology 66, 161–186.

Alder A, Holdermann I, Beyer P, Al-Babili S. 2008. Carotenoid oxygenases involved in plant branching catalyse a highly specific conserved apocarotenoid cleavage reaction. Biochemical Journal 416, 289–296.

Alder A, Jamil M, Marzorati M, Bruno M, Vermathen M, Bigler P, Ghisla S, Bouwmeester H, Beyer P, Al-Babili S. 2012. The path from β-carotene to carlactone, a strigolactone-like plant hormone. Science (New York, N.Y.) 335, 1348–1351.

Auldridge ME, McCarty DR, Klee HJ. 2006. Plant carotenoid cleavage oxygenases and their apocarotenoid products. Current Opinion in Plant Biology 9, 315–321.

Austin JR, Frost E, Vidi P-A, Kessler F, Staehelin LA. 2006. Plastoglobules Are Lipoprotein Subcompartments of the Chloroplast That Are Permanently Coupled to Thylakoid Membranes and Contain Biosynthetic Enzymes. The Plant Cell 18, 1693–1703.

Bago B, Pfeffer PE, Shachar-Hill Y. 2000. Carbon metabolism and transport in arbuscular mycorrhizas. Plant Physiology 124, 949–958.

Beltran JCM, Stange C. 2016. Apocarotenoids: A New Carotenoid-Derived Pathway. In: Stange C, ed. Subcellular Biochemistry. Carotenoids in Nature: Biosynthesis, Regulation and Function. Cham: Springer International Publishing, 239–272.

Besserer A, Bécard G, Jauneau A, Roux C, Séjalon-Delmas N. 2008. GR24, a Synthetic Analog of Strigolactones, Stimulates the Mitosis and Growth of the Arbuscular Mycorrhizal Fungus Gigaspora rosea by Boosting Its Energy Metabolism. Plant Physiology 148, 402–413.

Besserer A, Puech-Pagès V, Kiefer P, Gomez-Roldan V, Jauneau A, Roy S, Portais J-C, Roux C, Bécard G, Séjalon-Delmas N. 2006. Strigolactones Stimulate Arbuscular Mycorrhizal Fungi by Activating Mitochondria (J Chory, Ed.). PLoS Biology 4, e226.

Bhosale P, Bernstein PS. 2005. Microbial xanthophylls. Applied Microbiology and Biotechnology 68, 445–455.

Brands M, Wewer V, Keymer A, Gutjahr C, Dörmann P. 2018. The Lotus japonicus acyl-acyl carrier protein thioesterase FatM is required for mycorrhiza formation and lipid accumulation of Rhizophagus irregularis. The Plant Journal 95, 219–232.

Britton G. 2008. Functions of Intact Carotenoids. In: Britton G,, In: Liaaen-Jensen S,, In: Pfander H, eds. Carotenoids. Carotenoids: Volume 4: Natural Functions. Basel: Birkhäuser, 189–212.

Brundrett MC, Tedersoo L. 2018. Evolutionary history of mycorrhizal symbioses and global host plant diversity. New Phytologist 220, 1108–1115.

Bruno M, Al-Babili S. 2016. On the substrate specificity of the rice strigolactone biosynthesis enzyme DWARF27. Planta 243, 1429–1440.

Bruno M, Hofmann M, Vermathen M, Alder A, Beyer P, Al-Babili S. 2014. On the substrate- and stereospecificity of the plant carotenoid cleavage dioxygenase 7. FEBS Letters 588, 1802–1807.

Bruno M, Koschmieder J, Wuest F, Schaub P, Fehling-Kaschek M, Timmer J, Beyer P, Al-Babili S. 2016. Enzymatic study on AtCCD4 and AtCCD7 and their potential to form acyclic regulatory metabolites. Journal of Experimental Botany 67, 5993–6005.

Bruno M, Vermathen M, Alder A, Wüst F, Schaub P, Steen R van der, Beyer P, Ghisla S, Al-Babili S. 2017. Insights into the formation of carlactone from in-depth analysis of the CCD8-catalyzed reactions. FEBS Letters 591, 792–800.

Charpentier M, Sun J, Wen J, Mysore KS, Oldroyd GED. 2014. Abscisic Acid Promotion of Arbuscular Mycorrhizal Colonization Requires a Component of the PROTEIN PHOSPHATASE 2A Complex. Plant Physiology 166, 2077–2090.

Chen K, Li G-J, Bressan RA, Song C-P, Zhu J-K, Zhao Y. 2020. Abscisic acid dynamics, signaling, and functions in plants. Journal of Integrative Plant Biology 62, 25–54.

Chialva M, Fossalunga AS di, Daghino S, Ghignone S, Bagnaresi P, Chiapello M, Novero M, Spadaro D, Perotto S, Bonfante P. 2018. Native soils with their microbiotas elicit a state of alert in tomato plants. New Phytologist 220, 1296–1308.

D'Alessandro S, Mizokami Y, Légeret B, Havaux M. 2019. The Apocarotenoid β-Cyclocitric Acid Elicits Drought Tolerance in Plants. iScience 19, 461–473.

Das D, Gutjahr C. 2022. Old dog, new trick: The PHR-SPX system regulates arbuscular mycorrhizal symbiosis. Molecular Plant 15, 225–227.

De Vleesschauwer D, Yang Y, Vera Cruz C, Höfte M. 2010. Abscisic Acid-Induced Resistance against the Brown Spot Pathogen Cochliobolus miyabeanus in Rice Involves MAP Kinase-Mediated Repression of Ethylene Signaling. Plant Physiology 152, 2036–2052.

Decker EL, Alder A, Hunn S, et al. 2017. Strigolactone biosynthesis is evolutionarily conserved, regulated by phosphate starvation and contributes to resistance against phytopathogenic fungi in a moss, Physcomitrella patens. New Phytologist 216, 455–468.

Delaux P-M, Schornack S. 2021. Plant evolution driven by interactions with symbiotic and pathogenic microbes. Science 371, eaba6605.

DellaPenna D, Pogson BJ. 2006. VITAMIN SYNTHESIS IN PLANTS: Tocopherols and Carotenoids. Annual Review of Plant Biology 57, 711–738.

Dickinson AJ, Lehner K, Mi J, Jia K-P, Mijar M, Dinneny J, Al-Babili S, Benfey PN. 2019. β-Cyclocitral is a conserved root growth regulator. Proceedings of the National Academy of Sciences 116, 10563–10567.

Dodd IC. 2013. Abscisic acid and stomatal closure: a hydraulic conductance conundrum? New Phytologist 197, 6–8.

Etemadi M, Gutjahr C, Couzigou J-M, Zouine M, Lauressergues D, Timmers A, Audran C, Bouzayen M, Bécard G, Combier J-P. 2014. Auxin Perception Is Required for Arbuscule Development in Arbuscular Mycorrhizal Symbiosis. Plant Physiology 166, 281–292.

Felemban A, Braguy J, Zurbriggen MD, Al-Babili S. 2019. Apocarotenoids Involved in Plant Development and Stress Response. Frontiers in Plant Science 0.

Fester T, Hause B, Schmidt D, Halfmann K, Schmidt J, Wray V, Hause G, Strack D. Occurrence and Localization of Apocarotenoids in Arbuscular Mycorrhizal Plant Roots. , 10.

Fester T, Schmidt D, Lohse S, Walter M, Giuliano G, Bramley P, Fraser P, Hause B, Strack D. 2002a. Stimulation of carotenoid metabolism in arbuscular mycorrhizal roots. Planta 216, 148–154.

Fester T, Schmidt D, Lohse S, Walter M, Giuliano G, Bramley P, Fraser P, Hause B, Strack D. 2002b. Stimulation of carotenoid metabolism in arbuscular mycorrhizal roots. Planta 216, 148–154.

Finkelstein R. 2013. Abscisic Acid Synthesis and Response. The Arabidopsis Book / American Society of Plant Biologists 11, e0166.

Finkelstein RR, Rock CD. 2002. Abscisic Acid Biosynthesis and Response. The Arabidopsis Book / American Society of Plant Biologists 1, e0058.

Fiorilli V, Vannini C, Ortolani F, et al. 2018. Omics approaches revealed how arbuscular mycorrhizal symbiosis enhances yield and resistance to leaf pathogen in wheat. Scientific Reports 8, 9625.

Fiorilli V, Wang JY, Bonfante P, Lanfranco L, Al-Babili S. 2019. Apocarotenoids: Old and New Mediators of the Arbuscular Mycorrhizal Symbiosis. Frontiers in Plant Science 0.

Floß DS, Hause B, Lange PR, Küster H, Strack D, Walter MH. 2008. Knock-down of the MEP pathway isogene 1-deoxy-d-xylulose 5-phosphate synthase 2 inhibits formation of arbuscular mycorrhiza-induced apocarotenoids, and abolishes normal expression of mycorrhiza-specific plant marker genes. The Plant Journal 56, 86–100.

Floss DS, Levy JG, Levesque-Tremblay V, Pumplin N, Harrison MJ. 2013. DELLA proteins regulate arbuscule formation in arbuscular mycorrhizal symbiosis. Proceedings of the National Academy of Sciences 110, E5025–E5034.

Floss DS, Schliemann W, Schmidt J, Strack D, Walter MH. 2008. RNA interference-mediated repression of MtCCD1 in mycorrhizal roots of Medicago truncatula causes accumulation of C27 apocarotenoids, shedding light on the functional role of CCD1. Plant Physiology 148, 1267–1282.

Floss DS, Walter MH. 2009. Role of carotenoid cleavage dioxygenase 1 (CCD1) in apocarotenoid biogenesis revisited. Plant Signaling & Behavior 4, 172–175.

Foo E, Davies NW. 2011. Strigolactones promote nodulation in pea. Planta 234, 1073–1081.

Fraser PD, Bramley PM. 2004. The biosynthesis and nutritional uses of carotenoids. Progress in Lipid Research 43, 228–265.

Frusciante S, Diretto G, Bruno M, et al. 2014. Novel carotenoid cleavage dioxygenase catalyzes the first dedicated step in saffron crocin biosynthesis. Proceedings of the National Academy of Sciences of the United States of America 111, 12246–12251.

Genre A, Chabaud M, Balzergue C, et al. 2013. Short-chain chitin oligomers from arbuscular mycorrhizal fungi trigger nuclear Ca2+ spiking in Medicago truncatula roots and their production is enhanced by strigolactone. The New Phytologist 198, 190–202.

Genre A, Chabaud M, Faccio A, Barker DG, Bonfante P. 2008. Prepenetration apparatus assembly precedes and predicts the colonization patterns of arbuscular mycorrhizal fungi within the root cortex of both Medicago truncatula and Daucus carota. The Plant Cell 20, 1407–1420.

Genre A, Chabaud M, Timmers T, Bonfante P, Barker DG. 2005. Arbuscular mycorrhizal fungi elicit a novel intracellular apparatus in Medicago truncatula root epidermal cells before infection. The Plant Cell 17, 3489–3499.

Genre A, Lanfranco L, Perotto S, Bonfante P. 2020. Unique and common traits in mycorrhizal symbioses. Nature Reviews Microbiology 18, 649–660.

Giuliano G. 2014. Plant carotenoids: genomics meets multi-gene engineering. Current Opinion in Plant Biology 19, 111–117.

Giuliano G. 2017. Provitamin A biofortification of crop plants: a gold rush with many miners. Current Opinion in Biotechnology 44, 169–180.

Gomez-Roldan V, Fermas S, Brewer PB, et al. 2008. Strigolactone inhibition of shoot branching. Nature 455, 189–194.

Gruber MY, Xu N, Grenkow L, Li X, Onyilagha J, Soroka JJ, Westcott ND, Hegedus DD. 2009. Responses of the Crucifer Flea Beetle to Brassica Volatiles in an Olfactometer. Environmental Entomology 38, 1467–1479.

Gutjahr C, Parniske M. 2013. Cell and Developmental Biology of Arbuscular Mycorrhiza Symbiosis. Annual Review of Cell and Developmental Biology 29, 593–617.

Hamiaux C, Drummond RSM, Janssen BJ, Ledger SE, Cooney JM, Newcomb RD, Snowden KC. 2012. DAD2 Is an α/β Hydrolase Likely to Be Involved in the Perception of the Plant Branching Hormone, Strigolactone. Current Biology 22, 2032–2036.

Hans J, Hause B, Strack D, Walter MH. 2004. Cloning, characterization, and immunolocalization of a mycorrhiza-inducible 1-deoxy-d-xylulose 5-phosphate reductoisomerase in arbuscule-containing cells of maize. Plant Physiology 134, 614–624.

Harris JM. 2015. Abscisic Acid: Hidden Architect of Root System Structure. Plants 4, 548–572.

Harrison PJ, Bugg TDH. 2014. Enzymology of the carotenoid cleavage dioxygenases: Reaction mechanisms, inhibition and biochemical roles. Archives of Biochemistry and Biophysics 544, 105–111.

Havaux M. 2014. Carotenoid oxidation products as stress signals in plants. The Plant Journal 79, 597–606.

Heath JJ, Cipollini DF, Stireman III JO. 2013. The role of carotenoids and their derivatives in mediating interactions between insects and their environment. Arthropod-Plant Interactions 7, 1–20.

Herrera-Medina MJ, Steinkellner S, Vierheilig H, Ocampo Bote JA, García Garrido JM. 2007. Abscisic acid determines arbuscule development and functionality in the tomato arbuscular mycorrhiza. New Phytologist 175, 554–564.

Hill EM, Robinson LA, Abdul-Sada A, Vanbergen AJ, Hodge A, Hartley SE. 2018. Arbuscular Mycorrhizal Fungi and Plant Chemical Defence: Effects of Colonisation on Aboveground and Belowground Metabolomes. Journal of Chemical Ecology 44, 198–208.

Hirschberg J. 2001. Carotenoid biosynthesis in flowering plants. Current Opinion in Plant Biology 4, 210–218.

Ho-Plágaro T, García-Garrido JM. 2022. Molecular Regulation of Arbuscular Mycorrhizal Symbiosis. International Journal of Molecular Sciences 23, 5960.

Hou X, Rivers J, León P, McQuinn RP, Pogson BJ. 2016. Synthesis and Function of Apocarotenoid Signals in Plants. Trends in Plant Science 21, 792–803.

Hu Z, Yamauchi T, Yang J, et al. 2014. Strigolactone and Cytokinin Act Antagonistically in Regulating Rice Mesocotyl Elongation in Darkness. Plant and Cell Physiology 55, 30–41.

Hu Z, Yan H, Yang J, Yamaguchi S, Maekawa M, Takamure I, Tsutsumi N, Kyozuka J, Nakazono M. 2010. Strigolactones Negatively Regulate Mesocotyl Elongation in Rice during Germination and Growth in Darkness. Plant and Cell Physiology 51, 1136–1142.

Huang F-C, Molnár P, Schwab W. 2009. Cloning and functional characterization of carotenoid cleavage dioxygenase 4 genes. Journal of Experimental Botany 60, 3011–3022.

Hussain A, Black CR, Taylor IB, Roberts JA. 2000. Does an antagonistic relationship between ABA and ethylene mediate shoot growth when tomato (Lycopersicon esculentum Mill.) plants encounter compacted soil? Plant, Cell & Environment 23, 1217–1226.

Ilg A, Beyer P, Al-Babili S. 2009. Characterization of the rice carotenoid cleavage dioxygenase 1 reveals a novel route for geranial biosynthesis: A novel route for geranial formation. FEBS Journal 276, 736–747.

Ilg A, Bruno M, Beyer P, Al-Babili S. 2014. Tomato carotenoid cleavage dioxygenases 1A and 1B: Relaxed double bond specificity leads to a plenitude of dialdehydes, mono-apocarotenoids and isoprenoid volatiles. FEBS Open Bio 4, 584–593.

Ilg A, Yu Q, Schaub P, Beyer P, Al-Babili S. 2010. Overexpression of the rice carotenoid cleavage dioxygenase 1 gene in Golden Rice endosperm suggests apocarotenoids as substrates in planta. Planta 232, 691–699.

Ito S, Braguy J, Wang JY, et al. 2022. Canonical strigolactones are not the major determinant of tillering but important rhizospheric signals in rice. Science Advances 8, eadd1278.

Jeffrey SW, Douce R, Benson AA. 1974. Carotenoid Transformations in the Chloroplast Envelope. Proceedings of the National Academy of Sciences of the United States of America 71, 807–810.

J. Humphrey A, M. Galster A, H. Beale M. 2006. Strigolactones in chemical ecology: waste products or vital allelochemicals ? Natural Product Reports 23, 592–614.

Jia K-P, Dickinson AJ, Mi J, et al. 2019. Anchorene is a carotenoid-derived regulatory metabolite required for anchor root formation in Arabidopsis. Science Advances 5, eaaw6787.

Jia K-P, Luo Q, He S-B, Lu X-D, Yang H-Q. 2014. Strigolactone-Regulated Hypocotyl Elongation Is Dependent on Cryptochrome and Phytochrome Signaling Pathways in Arabidopsis. Molecular Plant 7, 528–540.

Jiang L, Liu X, Xiong G, et al. 2013. DWARF 53 acts as a repressor of strigolactone signalling in rice. Nature 504, 401–405.

Jiang Y, Wang W, Xie Q, et al. 2017. Plants transfer lipids to sustain colonization by mutualistic mycorrhizal and parasitic fungi. Science 356, 1172–1175.

Jones FR. A>MYCORRHIZAL FUNGUS IN THE ROOTS OF LEGUMES AND SOME OTHER PLANTS. , 12.

Klingner A, Bothe H, Wray V, Marner F-J. 1995. Identification of a yellow pigment formed in maize roots upon mycorrhizal colonization. Phytochemistry 38, 53–55.

Kobae Y, Kameoka H, Sugimura Y, Saito K, Ohtomo R, Fujiwara T, Kyozuka J. 2018. Strigolactone Biosynthesis Genes of Rice are Required for the Punctual Entry of Arbuscular Mycorrhizal Fungi into the Roots. Plant and Cell Physiology 59, 544–553.

Kobae Y, Ohmori Y, Saito C, Yano K, Ohtomo R, Fujiwara T. 2016. Phosphate Treatment Strongly Inhibits New Arbuscule Development But Not the Maintenance of Arbuscule in Mycorrhizal Rice Roots1. Plant Physiology 171, 566–579.

Kodama K, Rich MK, Yoda A, et al. 2022. An ancestral function of strigolactones as symbiotic rhizosphere signals. Nature Communications 13, 3974.

Kohlen W, Charnikhova T, Lammers M, et al. 2012. The tomato CAROTENOID CLEAVAGE DIOXYGENASE 8 (S l CCD 8) regulates rhizosphere signaling, plant architecture and affects reproductive development through strigolactone biosynthesis. New Phytologist 196, 535–547.

Koide RT. 1991. Nutrient supply, nutrient demand and plant response to mycorrhizal infection. New Phytologist 117, 365–386.

Kretzschmar T, Kohlen W, Sasse J, Borghi L, Schlegel M, Bachelier JB, Reinhardt D, Bours R, Bouwmeester HJ, Martinoia E. 2012. A petunia ABC protein controls strigolactone-dependent symbiotic signalling and branching. Nature 483, 341–344.

Krinsky NI. 1994. The biological properties of carotenoids. Pure and Applied Chemistry 66, 1003–1010.

Lambers H, Teste FP. 2013. Interactions between arbuscular mycorrhizal and non-mycorrhizal plants: do non-mycorrhizal species at both extremes of nutrient availability play the same game? Plant, Cell & Environment 36, 1911–1915.

Lanfranco L, Fiorilli V, Venice F, Bonfante P. 2018. Strigolactones cross the kingdoms: plants, fungi, and bacteria in the arbuscular mycorrhizal symbiosis. Journal of Experimental Botany 69, 2175–2188.

Lätari K, Wüst F, Hübner M, Schaub P, Beisel KG, Matsubara S, Beyer P, Welsch R. 2015. Tissue-Specific Apocarotenoid Glycosylation Contributes to Carotenoid Homeostasis in Arabidopsis Leaves1. Plant Physiology 168, 1550–1562.

Lee KH, Piao HL, Kim H-Y, Choi SM, Jiang F, Hartung W, Hwang I, Kwak JM, Lee I-J, Hwang I. 2006. Activation of Glucosidase via Stress-Induced Polymerization Rapidly Increases Active Pools of Abscisic Acid. Cell 126, 1109–1120.

Liao D, Wang S, Cui M, Liu J, Chen A, Xu G. 2018. Phytohormones Regulate the Development of Arbuscular Mycorrhizal Symbiosis. International Journal of Molecular Sciences 19, 3146.

Ito S., Braguy J., Wang J. Y., Yoda A., Fiorilli V., Takahashi I., ... & Al-Babili, S. (2022). Canonical strigolactones are not the major determinant of tillering but important rhizospheric signals in rice. Science Advances, 8(44).

Liu W, Kohlen W, Lillo A, et al. 2011. Strigolactone Biosynthesis in Medicago truncatula and Rice Requires the Symbiotic GRAS-Type Transcription Factors NSP1 and NSP2. The Plant Cell 23, 3853–3865.

López-Ráez JA, Kohlen W, Charnikhova T, et al. 2010. Does abscisic acid affect strigolactone biosynthesis? New Phytologist 187, 343–354.

López-Ráez, J. A., Fernández, I., García, J. M., Berrio, E., Bonfante, P., Walter, M. H., & Pozo, M. J. (2015). Differential spatio-temporal expression of carotenoid cleavage dioxygenases regulates apocarotenoid fluxes during AM symbiosis. Plant Science, 230, 59-69.

Lucas M, Swarup R, Paponov IA, et al. 2011. SHORT-ROOT Regulates Primary, Lateral, and Adventitious Root Development in Arabidopsis1[C][W][OA]. Plant Physiology 155, 384–398.

Ma G, Zhang L, Matsuta A, Matsutani K, Yamawaki K, Yahata M, Wahyudi A, Motohashi R, Kato M. 2013. Enzymatic Formation of β-Citraurin from β-Cryptoxanthin and Zeaxanthin by Carotenoid Cleavage Dioxygenase4 in the Flavedo of Citrus Fruit1[W][OPEN]. Plant Physiology 163, 682–695.

MacLean AM, Bravo A, Harrison MJ. 2017. Plant Signaling and Metabolic Pathways Enabling Arbuscular Mycorrhizal Symbiosis. The Plant Cell 29, 2319–2335.

Maier W, Hammer K, Dammann U, Schulz B, Strack D. 1997. Accumulation of sesquiterpenoid cyclohexenone derivatives induced by an arbuscular mycorrhizal fungus in members of the Poaceae. Planta 202, 36–42.

Maier W, Schmidt J, Nimtz M, Wray V, Strack D. 2000. Secondary products in mycorrhizal roots of tobacco and tomato. Phytochemistry 54, 473–479.

Martín-Rodríguez JA, Huertas R, Ho-Plágaro T, Ocampo JA, Turečková V, Tarkowská D, Ludwig-Müller J, García-Garrido JM. 2016a. Gibberellin–Abscisic Acid Balances during Arbuscular Mycorrhiza Formation in Tomato. Frontiers in Plant Science 7, 1273.

Martín-Rodríguez JA, Huertas R, Ho-Plágaro T, Ocampo JA, Turečková V, Tarkowská D, Ludwig-Müller J, García-Garrido JM. 2016b. Gibberellin–Abscisic Acid Balances during Arbuscular Mycorrhiza Formation in Tomato. Frontiers in Plant Science 7.

Martín-Rodríguez JÁ, León-Morcillo R, Vierheilig H, Ocampo JA, Ludwig-Müller J, García-Garrido JM. 2011. Ethylene-dependent/ethylene-independent ABA regulation of tomato plants colonized by arbuscular mycorrhiza fungi. New Phytologist 190, 193–205.

Mercy L, Lucic-Mercy E, Nogales A, Poghosyan A, Schneider C, Arnholdt-Schmitt B. 2017. A Functional Approach towards Understanding the Role of the Mitochondrial Respiratory Chain in an Endomycorrhizal Symbiosis. Frontiers in Plant Science 8.

Merilo E, Jalakas P, Laanemets K, Mohammadi O, Hõrak H, Kollist H, Brosché M. 2015. Abscisic Acid Transport and Homeostasis in the Context of Stomatal Regulation. Molecular Plant 8, 1321–1333.

Mi J, Jia K-P, Balakrishna A, Wang JY, Al-Babili S. 2019. An LC-MS profiling method reveals a route for apocarotene glycosylation and shows its induction by high light stress in Arabidopsis. The Analyst 144, 1197–1204.

Moise AR, Al-Babili S, Wurtzel ET. 2014. Mechanistic Aspects of Carotenoid Biosynthesis. Chemical Reviews 114, 164–193.

Moran NA, Jarvik T. 2010. Lateral transfer of genes from fungi underlies carotenoid production in aphids. Science (New York, N.Y.) 328, 624–627.

Moreno Beltran JC, Stange C. 2016. APOCAROTENOIDS: A NEW CAROTENOID-DERIVED PATHWAY

Moreno JC, Mi J, Alagoz Y, Al-Babili S. 2021. Plant apocarotenoids: from retrograde signaling to interspecific communication. The Plant Journal 105, 351–375.

Müller LM, Harrison MJ. 2019. Phytohormones, miRNAs, and peptide signals integrate plant phosphorus status with arbuscular mycorrhizal symbiosis. Current Opinion in Plant Biology 50, 132–139.

Nakamura H, Xue Y-L, Miyakawa T, et al. 2013. Molecular mechanism of strigolactone perception by DWARF14. Nature Communications 4, 2613.

Nambara E, Marion-Poll A. 2005. Abscisic Acid Biosynthesis and Catabolism. Annual Review of Plant Biology 56, 165–185.

Nisar N, Li L, Lu S, Khin NC, Pogson BJ. 2015. Carotenoid Metabolism in Plants. Molecular Plant 8, 68–82.

Oldroyd GED. 2013. Speak, friend, and enter: signalling systems that promote beneficial symbiotic associations in plants. Nature Reviews Microbiology 11, 252–263.

Ômura H, Honda K, Hayashi N. 2000. Floral Scent of Osmanthus fragrans Discourages Foraging Behavior of Cabbage Butterfly, Pieris rapae. Journal of Chemical Ecology 26, 655–666.

Parniske M. 2008. Arbuscular mycorrhiza: the mother of plant root endosymbioses. Nature Reviews. Microbiology 6, 763–775.

Peláez-Vico MA, Bernabéu-Roda L, Kohlen W, Soto MJ, López-Ráez JA. 2016. Strigolactones in the Rhizobium-legume symbiosis: Stimulatory effect on bacterial surface motility and down-regulation of their levels in nodulated plants. Plant Science 245, 119–127.

Pimprikar P, Gutjahr C. 2018. Transcriptional Regulation of Arbuscular Mycorrhiza Development. Plant and Cell Physiology 59, 678–695.

Pozo MJ, López-Ráez JA, Azcón-Aguilar C, García-Garrido JM. 2015. Phytohormones as integrators of environmental signals in the regulation of mycorrhizal symbioses. New Phytologist 205, 1431–1436.

Rodrigo MJ, Alquézar B, Alós E, Medina V, Carmona L, Bruno M, Al-Babili S, Zacarías L. 2013. A novel carotenoid cleavage activity involved in the biosynthesis of Citrus fruit-specific apocarotenoid pigments. Journal of Experimental Botany 64, 4461–4478.

Rodríguez-Concepción M, Boronat A. 2002. Elucidation of the methylerythritol phosphate pathway for isoprenoid biosynthesis in bacteria and plastids. A metabolic milestone achieved through genomics. Plant Physiology 130, 1079–1089.

Ruiz-Lozano JM, Porcel R, Azcón C, Aroca R. 2012. Regulation by arbuscular mycorrhizae of the integrated physiological response to salinity in plants: new challenges in physiological and molecular studies. Journal of Experimental Botany 63, 4033–4044.

Ruiz-Sola MÁ, Barja MV, Manzano D, Llorente B, Schipper B, Beekwilder J, Rodriguez-Concepcion M. 2016. A Single Arabidopsis Gene Encodes Two Differentially Targeted Geranylgeranyl Diphosphate Synthase Isoforms. Plant Physiology 172, 1393–1402.

Salvioli A, Ghignone S, Novero M, Navazio L, Venice F, Bagnaresi P, Bonfante P. 2016. Symbiosis with an endobacterium increases the fitness of a mycorrhizal fungus, raising its bioenergetic potential. The ISME Journal 10, 130–144.

Sang D, Chen D, Liu G, et al. 2014. Strigolactones regulate rice tiller angle by attenuating shoot gravitropism through inhibiting auxin biosynthesis. Proceedings of the National Academy of Sciences 111, 11199–11204.

Sasse J, Simon S, Gübeli C, Liu G-W, Cheng X, Friml J, Bouwmeester H, Martinoia E, Borghi L. 2015. Asymmetric localizations of the ABC transporter PaPDR1 trace paths of directional strigolactone transport. Current biology: CB 25, 647–655.

Scannerini S, Bonfante-Fasolo P. 1977. Unusual plasties in an endomycorrhizal root. Canadian Journal of Botany 55, 2471–2474.

Schwartz SH, Qin X, Zeevaart JD. 2001. Characterization of a Novel Carotenoid Cleavage Dioxygenase from Plants *. Journal of Biological Chemistry 276, 25208–25211.

Schwartz SH, Tan BC, Gage DA, Zeevaart JAD, McCarty DR. 1997. Specific Oxidative Cleavage of Carotenoids by VP14 of Maize. Science 276, 1872–1874.

Shi J, Zhao B, Zheng S, et al. 2021. A phosphate starvation response-centered network regulates mycorrhizal symbiosis. Cell 184, 5527-5540.e18.

Shindo M, Yamamoto S, Shimomura K, Umehara M. 2020. Strigolactones Decrease Leaf Angle in Response to Nutrient Deficiencies in Rice. Frontiers in Plant Science 0.

Shumbe L, D'Alessandro S, Shao N, Chevalier A, Ksas B, Bock R, Havaux M. 2017. METHYLENE BLUE SENSITIVITY 1 (MBS1) is required for acclimation of Arabidopsis to singlet oxygen and acts downstream of β-cyclocitral. Plant, Cell & Environment 40, 216–226.

Snowden KC, Simkin AJ, Janssen BJ, Templeton KR, Loucas HM, Simons JL, Karunairetnam S, Gleave AP, Clark DG, Klee HJ. 2005. The Decreased apical dominance1/Petunia hybrida CAROTENOID CLEAVAGE DIOXYGENASE8 Gene Affects Branch Production and Plays a Role in Leaf Senescence, Root Growth, and Flower Development. The Plant Cell 17, 746–759.

Soto MJ, Fernández-Aparicio M, Castellanos-Morales V, García-Garrido JM, Ocampo JA, Delgado MJ, Vierheilig H. 2010. First indications for the involvement of strigolactones on nodule formation in alfalfa (Medicago sativa). Soil Biology and Biochemistry 42, 383–385.

Spatafora JW, Chang Y, Benny GL, et al. 2016. A phylum-level phylogenetic classification of zygomycete fungi based on genome-scale data. Mycologia 108, 1028–1046.

Stanga JP, Smith SM, Briggs WR, Nelson DC. 2013. SUPPRESSOR OF MORE AXILLARY GROWTH2 1 Controls Seed Germination and Seedling Development in Arabidopsis1[W][OPEN]. Plant Physiology 163, 318–330.

Sui X, Kiser PD, Lintig J von, Palczewski K. 2013. Structural basis of carotenoid cleavage: From bacteria to mammals. Archives of Biochemistry and Biophysics 539, 203–213.

Sun T, Tadmor Y, Li L. 2020. Pathways for Carotenoid Biosynthesis, Degradation, and Storage. In: Rodríguez-Concepción M,, In: Welsch R, eds. Methods in Molecular Biology. Plant and Food Carotenoids: Methods and Protocols. New York, NY: Springer US, 3–23.

Sun H, Tao J, Liu S, Huang S, Chen S, Xie X, Yoneyama K, Zhang Y, Xu G. 2014. Strigolactones are involved in phosphate- and nitrate-deficiency-induced root development and auxin transport in rice. Journal of Experimental Botany 65, 6735.

Tan B-C, Joseph LM, Deng W-T, Liu L, Li Q-B, Cline K, McCarty DR. 2003. Molecular characterization of the Arabidopsis 9-cis epoxycarotenoid dioxygenase gene family. The Plant Journal: For Cell and Molecular Biology 35, 44–56.

Todaka D, Shinozaki K, Yamaguchi-Shinozaki K. 2015. Recent advances in the dissection of drought-stress regulatory networks and strategies for development of drought-tolerant transgenic rice plants. Frontiers in Plant Science 6, 84.

Tsuzuki S, Handa Y, Takeda N, Kawaguchi M. 2016. Strigolactone-Induced Putative Secreted Protein 1 Is Required for the Establishment of Symbiosis by the Arbuscular Mycorrhizal Fungus Rhizophagus irregularis. Molecular Plant-Microbe Interactions® 29, 277–286.

Tuan PA, Kumar R, Rehal PK, Toora PK, Ayele BT. 2018. Molecular Mechanisms Underlying Abscisic Acid/Gibberellin Balance in the Control of Seed Dormancy and Germination in Cereals. Frontiers in Plant Science 0.

Umehara M, Hanada A, Yoshida S, et al. 2008. Inhibition of shoot branching by new terpenoid plant hormones. Nature 455, 195–200.

Visentin I, Vitali M, Ferrero M, Zhang Y, Ruyter-Spira C, Novák O, Strnad M, Lovisolo C, Schubert A, Cardinale F. 2016. Low levels of strigolactones in roots as a component of the systemic signal of drought stress in tomato. New Phytologist 212, 954–963.

Vogel JT, Tan B-C, McCarty DR, Klee HJ. 2008. The Carotenoid Cleavage Dioxygenase 1 Enzyme Has Broad Substrate Specificity, Cleaving Multiple Carotenoids at Two Different Bond Positions. Journal of Biological Chemistry 283, 11364–11373.

Vogel JT, Walter MH, Giavalisco P, et al. 2010. SlCCD7 controls strigolactone biosynthesis, shoot branching and mycorrhiza-induced apocarotenoid formation in tomato. The Plant Journal 61, 300–311.

Votta C, Fiorilli V, Haider I, et al. 2022. Zaxinone Synthase controls arbuscular mycorrhizal colonization level in rice. The Plant Journal, tpj.15917.

Wagner K, Krause K, David A, Kai M, Jung E-M, Sammer D, Kniemeyer O, Boland W, Kothe E. 2016. Influence of zygomycete-derived D'orenone on IAA signalling in T richoloma -spruce ectomycorrhiza: D'orenone effect on ectomycorrhiza. Environmental Microbiology 18, 2470–2480.

Walter MH, Floß DS, Hans J, Fester T, Strack D. 2007. Apocarotenoid biosynthesis in arbuscular mycorrhizal roots: Contributions from methylerythritol phosphate pathway isogenes and tools for its manipulation. Phytochemistry 68, 130–138.

Walter MH, Floss DS, Strack D. 2010. Apocarotenoids: hormones, mycorrhizal metabolites and aroma volatiles. Planta 232, 1–17.

Wang JY, Alseekh S, Xiao T, et al. 2021a. Multi-omics approaches explain the growth-promoting effect of the apocarotenoid growth regulator zaxinone in rice. Communications Biology 4, 1–11.

Wang S, Ghisalberti EL, Ridsdill-Smith J. 1999. Volatiles from Trifolium as feeding deterrents of redlegged earth mites. Phytochemistry 52, 601–605.

Wang JY, Haider I, Jamil M, et al. 2019. The apocarotenoid metabolite zaxinone regulates growth and strigolactone biosynthesis in rice. Nature Communications 10, 810.

Wang JY, Jamil M, Hossain MdG, et al. 2022. Evaluation of the Biostimulant Activity of Zaxinone Mimics (MiZax) in Crop Plants. Frontiers in Plant Science 13.

Wang JY, Jamil M, Lin P-Y, et al. 2020a. Efficient Mimics for Elucidating Zaxinone Biology and Promoting Agricultural Applications. Molecular Plant 13, 1654–1661.

Wang T, Li C, Wu Z, Jia Y, Wang H, Sun S, Mao C, Wang X. 2017. Abscisic Acid Regulates Auxin Homeostasis in Rice Root Tips to Promote Root Hair Elongation. Frontiers in Plant Science 0.

Wang JY, Lin P-Y, Al-Babili S. 2021b. On the biosynthesis and evolution of apocarotenoid plant growth regulators. Seminars in Cell & Developmental Biology 109, 3–11.

Wang B, Qiu Y-L. 2006. Phylogenetic distribution and evolution of mycorrhizas in land plants. Mycorrhiza 16, 299–363.

Wang M, Schäfer M, Li D, et al. 2018a. Blumenols as shoot markers of root symbiosis with arbuscular mycorrhizal fungi (D Weigel and M Parniske, Eds.). eLife 7, e37093.

Wang L, Wang B, Jiang L, Liu X, Li X, Lu Z, Meng X, Wang Y, Smith SM, Li J. 2015. Strigolactone Signaling in Arabidopsis Regulates Shoot Development by Targeting D53-Like SMXL Repressor Proteins for Ubiquitination and Degradation. The Plant Cell 27, 3128–3142.

Wang Y, Wang M, Li Y, Wu A, Huang J. 2018b. Effects of arbuscular mycorrhizal fungi on growth and nitrogen uptake of Chrysanthemum morifolium under salt stress (L-SP Tran, Ed.). PLOS ONE 13, e0196408.

Wang L, Xu Q, Yu H, et al. 2020b. Strigolactone and Karrikin Signaling Pathways Elicit Ubiquitination and Proteolysis of SMXL2 to Regulate Hypocotyl Elongation in Arabidopsis[OPEN]. The Plant Cell 32, 2251–2270.

Xie X, Mori N, Yoneyama K, Nomura T, Uchida K, Yoneyama K, Akiyama K. 2019a. Lotuslactone, a non-canonical strigolactone from Lotus japonicus. Phytochemistry 157, 200–205.

Xie Z, Nolan TM, Jiang H, Yin Y. 2019b. AP2/ERF Transcription Factor Regulatory Networks in Hormone and Abiotic Stress Responses in Arabidopsis. Frontiers in Plant Science 10, 228.

Xu Z-Y, Lee KH, Dong T, et al. 2012. A Vacuolar β-Glucosidase Homolog That Possesses Glucose-Conjugated Abscisic Acid Hydrolyzing Activity Plays an Important Role in Osmotic Stress Responses in Arabidopsis[W]. The Plant Cell 24, 2184–2199.

Yamada Y, Furusawa S, Nagasaka S, Shimomura K, Yamaguchi S, Umehara M. 2014. Strigolactone signaling regulates rice leaf senescence in response to a phosphate deficiency. Planta 240, 399–408.

Yao R, Ming Z, Yan L, et al. 2016. DWARF14 is a non-canonical hormone receptor for strigolactone. Nature 536, 469–473.

Yoneyama K, Xie X, Kusumoto D, Sekimoto H, Sugimoto Y, Takeuchi Y, Yoneyama K. 2007. Nitrogen deficiency as well as phosphorus deficiency in sorghum promotes the production and exudation of 5-deoxystrigol, the host recognition signal for arbuscular mycorrhizal fungi and root parasites. Planta 227, 125–132.

Yoneyama K, Xie X, Yoneyama K, Kisugi T, Nomura T, Nakatani Y, Akiyama K, McErlean CSP. 2018a. Which are the major players, canonical or non-canonical strigolactones? Journal of Experimental Botany 69, 2231–2239.

Yoneyama K, Xie X, Yoneyama K, Kisugi T, Nomura T, Nakatani Y, Akiyama K, McErlean CSP. 2018b. Which are the major players, canonical or non-canonical strigolactones? Journal of Experimental Botany 69, 2231–2239.

Yuan H, Zhang J, Nageswaran D, Li L. 2015. Carotenoid metabolism and regulation in horticultural crops. Horticulture Research 2, 15036.

Zhang Y, van Dijk ADJ, Scaffidi A, et al. 2014. Rice cytochrome P450 MAX1 homologs catalyze distinct steps in strigolactone biosynthesis. Nature Chemical Biology 10, 1028–1033.

Zheng X, Giuliano G, Al-Babili S. 2020. Carotenoid biofortification in crop plants: citius, altius, fortius. Biochimica et Biophysica Acta (BBA) - Molecular and Cell Biology of Lipids 1865, 158664.

Zhou F, Wang C-Y, Gutensohn M, Jiang L, Zhang P, Zhang D, Dudareva N, Lu S. 2017. A recruiting protein of geranylgeranyl diphosphate synthase controls metabolic flux toward chlorophyll biosynthesis in rice. Proceedings of the National Academy of Sciences 114, 6866–6871.

Zouari I, Salvioli A, Chialva M, Novero M, Miozzi L, Tenore GC, Bagnaresi P, Bonfante P. 2014. From root to fruit: RNA-Seq analysis shows that arbuscular mycorrhizal symbiosis may affect tomato fruit metabolism. BMC Genomics 15, 221.

Chapter 2: Multi-omics approaches explain the growth-promoting effect of the apocarotenoid growth regulator zaxinone in rice

The study reported in this chapter aimed to investigate the mechanisms underlying the growth-promoting effect of zaxinone on rice plants. As reported by Wang et al. (2019) this novel apocarotenoid positively affects rice growth and suppresses SLs biosynthesis.

Using a combined ‘omics approach, which includes transcriptomics and metabolomics analyses, we investigated the molecular and metabolic changes after an exogenous zaxinone application. Zaxinone triggered sugar accumulation, stimulated glycolysis, and other sugar-related metabolic processes in rice roots. In addition, the treatment with the molecule led to an increased root starch content and induced glycosylation of cytokinins (CK). Zaxinone not only modulates SL biosynthesis and release but also the CK signaling pathway, modulating, through glycosylation, CK activity, and transport. Finally, we discovered that the hormonal and metabolic changes were accompanied by alterations at the histological level, with an increase in root apex length, diameter, and the number of cells and cortex cell layers.

In conclusion, we clarified the mode of action of zaxinone and emphasized its potential as a growth-promoting compound.

My specific contribution to this paper was to analyse the histological features of roots upon zaxinone application and to evaluate the root starch content.

communications biology

ARTICLE

https://doi.org/10.1038/s42003-021-02740-8 OPEN

Multi-omics approaches explain the growth-promoting effect of the apocarotenoid growth regulator zaxinone in rice

Jian You Wang[1,7], Saleh Alseekh[2,3,7], Tingting Xiao[4], Abdugaffor Ablazov[1], Leonardo Perez de Souza[2], Valentina Fiorilli[5], Marita Anggarani[6], Pei-Yu Lin[1], Cristina Votta[5], Mara Novero[5], Muhammad Jamil[1], Luisa Lanfranco[5], Yue-Ie C. Hsing[6], Ikram Blilou[4], Alisdair R. Fernie[2] & Salim Al-Babili[1✉]

The apocarotenoid zaxinone promotes growth and suppresses strigolactone biosynthesis in rice. To shed light on the mechanisms underlying its growth-promoting effect, we employed a combined omics approach integrating transcriptomics and metabolomics analysis of rice seedlings treated with zaxinone, and determined the resulting changes at the cellular and hormonal levels. Metabolites as well as transcripts analysis demonstrate that zaxinone application increased sugar content and triggered glycolysis, the tricarboxylic acid cycle and other sugar-related metabolic processes in rice roots. In addition, zaxinone treatment led to an increased root starch content and induced glycosylation of cytokinins. The transcriptomic, metabolic and hormonal changes were accompanied by striking alterations of roots at cellular level, which showed an increase in apex length, diameter, and the number of cells and cortex cell layers. Remarkably, zaxinone did not affect the metabolism of roots in a strigolactone deficient mutant, suggesting an essential role of strigolactone in the zaxinone growth-promoting activity. Taken together, our results unravel zaxinone as a global regulator of the transcriptome and metabolome, as well as of hormonal and cellular composition of rice roots. Moreover, they suggest that zaxinone promotes rice growth most likely by increasing sugar uptake and metabolism, and reinforce the potential of this compound in increasing rice performance.

[1] The BioActives Lab, Center for Desert Agriculture (CDA), Biological and Environment Science and Engineering (BESE), King Abdullah University of Science and Technology, Thuwal 23955-6900, Saudi Arabia. [2] Max-Planck-Institute of Molecular Plant Physiology, Am Mühlenberg 1, 14476 Potsdam-Golm, Germany. [3] Center of Plant Systems Biology and Biotechnology, 4000 Plovdiv, Bulgaria. [4] The Laboratory of Plant Cell and Developmental Biology (LPCDB), Biological and Environment Science and Engineering (BESE), King Abdullah University of Science and Technology, Thuwal 23955-6900, Saudi Arabia. [5] Department of Life Sciences and Systems Biology, University of Turin, Turin, Italy. [6] Institute of Plant and Microbial Biology, Academia Sinica, No. 128, Section 2, Yien-Chu-Yuan Road, Taipei 11529, Taiwan. [7] These authors contributed equally: Jian You Wang, Saleh Alseekh. ✉email: salim.babili@kaust.edu.sa

Carotenoids are widespread pigments fulfilling vital functions in plants, by protecting the photosynthetic apparatus from photo-oxidation and harnessing light energy[1]. In addition, they are the precursor of a structurally diverse set of metabolites, generally called apocarotenoids, which include volatiles, colorants, signaling/regulatory molecules, and hormones. Apocarotenoids arise through oxidative break down of carotenoids, which is initiated by reactive oxygen species (ROS) attack or catalyzed by Carotenoid Cleavage Dioxygenases (CCDs), an evolutionarily conserved family of non-heme Fe^{2+}-dependent enzymes[2–4]. The primary cleavage products are frequently modified by different enzymes, before acquiring their biological function. For instance, the apocarotenoid plant hormone strigolactone (SL) is formed by the sequential action of CCD7, CCD8, more axillary growth1 (MAX1, a cytochrome P450 monooxygenase), and other enzymes[4–8]. SLs and abscisic acid (ABA), a further carotenoid-derived plant hormone, are key metabolites in establishing plant's response to abiotic and biotic stress, and major determinants of plant development[4,9]. Besides, SLs modulate plant's architecture in response to nutrients availability, particularly phosphorus, and mediate, when released in the rhizosphere, the communication with arbuscular mycorrhizal fungi that supply plants with water and minerals[10,11]. However, SLs are also perceived by seeds of parasitic plants, such as *Striga*, which use them as germination stimulus ensuring the availability of a host required for the survival of these obligate parasitic weeds[5]. To fulfill their role in plant growth and development, SLs are embedded in a complex hormonal network in which they affect and are influenced by the activity of other plant hormones. Indeed, auxin and gibberellins were reported to interact with SL biosynthesis or signaling in rice and *Arabidopsis*[12]. Vice versa, it was shown that SLs enhance cytokinins (CKs) catabolism by modulating *CYTOKININ OXIDASE/DEHYDROGENASE 9* (*CKX9*) expression to inhibit rice tillering[13]. Similarly, CKs and SLs exert opposite effects on rice mesocotyl elongation[14,15].

Metabolism is a central process required for the uptake and utilization of energy and nutrients to ensure the survival, reproduction, growth, and development of living organisms[16]. Thus, primary metabolites such as sugars, amino acids, nucleotides, organic acids, and fatty acids are essential for maintaining cellular homeostasis and for organismal life[17]. In fact, metabolites are direct physiological signatures that are highly correlated with end-phenomes in plants[17,18]. In addition, some primary metabolites act as signaling molecules regulating plant growth and development. For instance sugars, such as sucrose, interact with different plant hormones and regulate bud development and shoot branching by modulating the signaling of auxin and SLs[12,19,20].

Besides the established plant hormones ABA and SLs, the apocarotenoid family includes growth regulators, such as anchorene that specifically promotes the growth of anchor roots in *Arabidopsis*[21], and signaling molecules, such as cyclocitral that mediates the response of plants to high-light and drought stress, and regulates roots growth[4,22]. Recently, we have identified zaxinone, an apocarotenoid hormone candidate, as a metabolite required for proper rice growth and development, and characterized a rice CCD, called ZAXINONE SYNTHASE (ZAS), involved in its biosynthesis[23]. A rice loss-of-function *zas* mutant showed shoot and root growth impairment, a lower root zaxinone level, and higher SL content in roots and root exudates. Exogenous application of zaxinone rescued several *zas* phenotypes and resulted in a decrease in SL content and release, and in promoted root growth[23,24]. Treatment of WT seedlings with zaxinone led also to an obvious increase in root growth and a suppression of SL formation[23,24]. Transcript analysis showed that zaxinone is a negative regulator of SL biosynthesis at the transcript level. However, zaxinone application did not enhance root growth in SL biosynthesis and perception rice mutants, which indicates an interaction between zaxinone and SLs and suggests the requirement of a functional SL pathway for zaxinone's growth-promoting activity[23].

In the current study, we set out to understand how zaxinone promotes rice growth. For this purpose, we characterized its effect on rice primary metabolism and transcriptome in WT and the SL-deficient *d17* mutant rice plants, and determined zaxinone's impact on hormone content and root anatomy. Our results unraveled enhanced root sugar metabolism as a major reason for zaxinone growth-promoting activity and point to modulation of cytokinin content as a likely reason for increased root cell division activity and enhanced number of cortex cell layers, which we observed in roots.

Results

Zaxinone treatment increases sugar content and metabolism. To determine the effects of zaxinone on rice at a metabolomic and transcriptomic level and to get an insight into the dynamics of triggered changes, we grew rice seedlings hydroponically, applied the compound at a 5 µM concentration into the growth medium, and collected root and shoot samples 2, 6 and 24 h after application. A scheme of the experimental design is shown in Supplementary Fig. 1. Gas chromatography–mass spectrometry (GC–MS) analysis of primary metabolites in treated roots revealed an up to a 1.5-fold increase in the level of many sugars, glycolysis- and tricarboxylic acid (TCA)-cycle intermediates, such as glucose, citric acid, and 2-oxoglutarate (Fig. 1a). The position of these metabolites in cellular sugar catabolism pathways is shown in Fig. 1b. At the same time point, i.e., 6 h after zaxinone application, we also observed an increase in the content of most of the free amino acids and many of other analyzed primary metabolites. However, the content of some amino acids, e.g., leucine, dropped at the 24 h time point to below control level (Fig. 1a). Principal component analysis (PCA) revealed that the zaxinone effect on root metabolome was more pronounced at 6 and 24 h, compared with the early 2 h time point, with a peak of primary metabolites accumulation at 6 h (Fig. 1a and Supplementary Figs. 2a, Supplementary Fig. 3). In more detail, we observed a significant increase in the levels of the major sugars sucrose, glucose, and fructose at 2 and 6 h after application of zaxinone, which was followed by a sharp decrease at 24 h. In contrast, trehalose showed the highest increase after 24 h, similar to maltose, glucose-1-phosphate, and glucose-6-phosphate, which indicates a biphasic response to zaxinone application. In shoot tissues, we also detected a quick enhancement in the level of sucrose and trehalose 2 h after zaxinone application. However, many other primary metabolites, including several sugars, TCA intermediates, and free amino acids, showed an increase only at the late, 24 h, time point (Fig. 1d and Supplementary Figs. 2b, 4). These results suggest that zaxinone application to roots in hydroponically grown seedlings causes a rapid global change in the primary metabolism of roots and, with a slight delay, in shoots. In particular, it affects sugar content and catabolism, which are essential for adenosine triphosphate (ATP) generation and supply of C skeletons for cellular building blocks.

Assuming that excess sugars may be stored as starch, we measured the starch level in roots of hydroponically grown seedlings after two weeks of treatment with zaxinone (5 µM). Indeed, we detected around two-fold higher starch content in treated roots (Fig. 1c), compared to the mock condition. Taking into consideration that plants produce sugars through photosynthesis, we investigated the effect of zaxinone on this process. For this purpose, we performed a time-course measurement of chlorophyll content and stomatal conductance, two parameters of photosynthetic activity, in a 3-weeks-old hydroponic grown rice

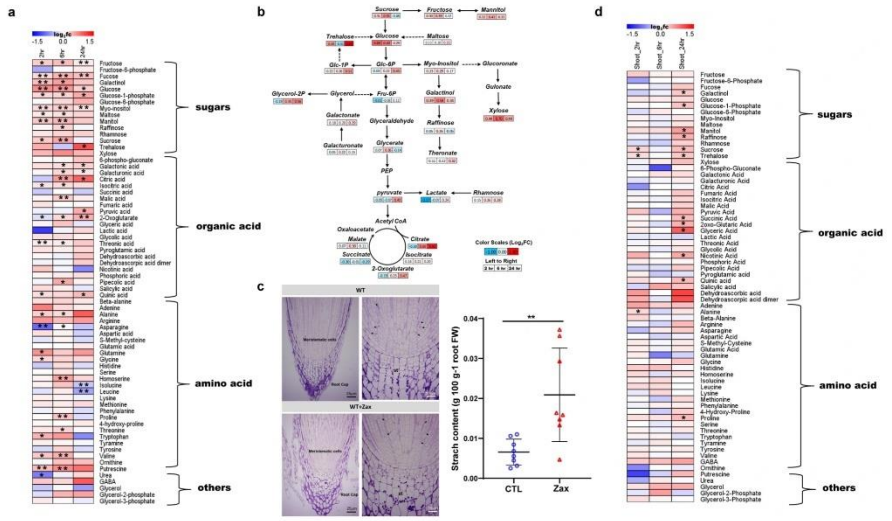

Fig. 1 The dynamic primary metabolite profiles upon zaxinone treatment. Primary metabolites extracted from roots for GC–MS, which were annotated and listed in Supplementary Data 6. Three independent harvests were concurrently subjected to GC–MS analysis. $n \geq 4$ biological replicates. **a** Heatmap of root tissue showing relative accumulation of each metabolite as compared to those in control plants. For each metabolite, the value of the corresponding wild type was set to 1. Asterisks indicate statistically significant differences as compared to control by *t*-test (*$p < 0.05$, **$p < 0.01$). **b** The scheme of major metabolic changes in the sugar-related metabolites after zaxinone treatment, which adapted from **a**. Blue and red color depict a decrease and increase in metabolic levels compared to the non-treated root samples, respectively. The data are presented as log2 (fold changes) from left to right as follows: 2, 6, and 24 h. **c** Longitudinal-sections of WT and WT treated with 5 µM zaxinone roots tips after resin-embedding and staining by the Periodic Acid-Schiff (PAS) reaction for the visualization of amyloplasts. At higher magnification (15 µm) the statoliths (st) in the root cap, as well as some tiny amyloplasts (arrows), are present in the cytoplasm of meristematic cells. The starch level was quantified in the root tissues. Bar presented as mean ± SD, $n = 8$ biological replicates. **d** Heatmap of shoot tissue of relative accumulated metabolites in comparison with control. For each metabolite, the value of the corresponding wild type was set to 1. Asterisks indicate statistically significant differences as compared to wild type by *t*-test (*$p < 0.05$, **$p < 0.01$). CTL control, Zax zaxinone.

plant treated with 5 µM zaxinone under greenhouse condition. As shown in Supplementary Fig. 5a, b, we observed an enhancement of both parameters in leaves of treated rice plants, which indicated an increased photosynthetic activity and may explain the elevated sugar levels.

Zaxinone application increases transcript level of genes involved in root sugar metabolism. We also analyzed the impact of zaxinone treatment on rice transcriptome, using RNA sequencing (RNA-Seq). A heatmap visualization of mean-centered, normalized log-expression values for correlated highly variable genes (HVGs) of the RNA-Seq data confirmed the high quality of each replicate, which was supported by the PCA plots of HVGs (Supplementary Fig. 6). A Volcano plot of differentially expressed genes (DEGs), following Deseq2 analysis, revealed the gene expression pattern at different cutting points with $\log_2$FoldChange, adjusted *Q*-value (False discovery rate, FDR), or a combination of both (Supplementary Fig. 7). In order to have a better picture of the transcriptome, we decided to use the FDR < 0.05 as a criterion for further analysis (Supplementary Data 1). Zaxinone application led to significant changes in the transcriptome over time, by increasing the transcript level of 324, 551, and 350 genes after 2, 6, and 24 h, respectively, including 38 genes that showed an induction at the three time points. The application also decreased the transcript level of 136 (2 h), 501 (6 h), and 71 (24 h) genes, ten of which were downregulated at the three time points (Fig. 2a, b). To validate the RNA-Seq data, we determined the transcript level of 15 selected genes that showed low to high response to zaxinone treatment, by qRT-PCR. The resulting correlation analysis ($R^2 = 0.87$–0.93) indicated that the RNA-Seq dataset was highly reliable and thus appropriate for pathway enrichment analysis (Supplementary Fig. 8). Gene Ontology (GO term) analysis of molecular function and biological process showed that most of the genes regulated by zaxinone were related to metabolic processes [upregulation: 45 (2 h), 108 (6 h), and 50 (24 h) genes; downregulation: 16 (2 h), 70 (6 h), and 8 (24 h) genes] and catalytic activity [upregulation: 72 (2 h), 148 (6 h), and 90 (24 h) genes; downregulation: 36 (2 h), 124 (6 h), and 22 (24 h) genes] (Supplementary Data 2). Further enrichments with Kyoto Encyclopedia of Genes and Genomes (KEGG) and PlantCyc pathway unraveled the induction of genes mediating several annotated sugar metabolism pathways, including pyruvate metabolism, citric acid cycle, sucrose degradation, glycolysis, and gluconeogenesis, particularly 6 h after zaxinone application (Fig. 2c), which is in line with the change in the profile of primary metabolites (Fig. 1a). We also confirmed the annotated pathways (the plant glycolytic pathway and the TCA cycle) by MapMan software (Supplementary Fig. 9). To validate these changes, we chose ten genes from the OyzaCyc 6.0 database, which are involved in root glycolysis (Supplementary Data 3), and validated their expression pattern by performing qRT-PCR analysis of the

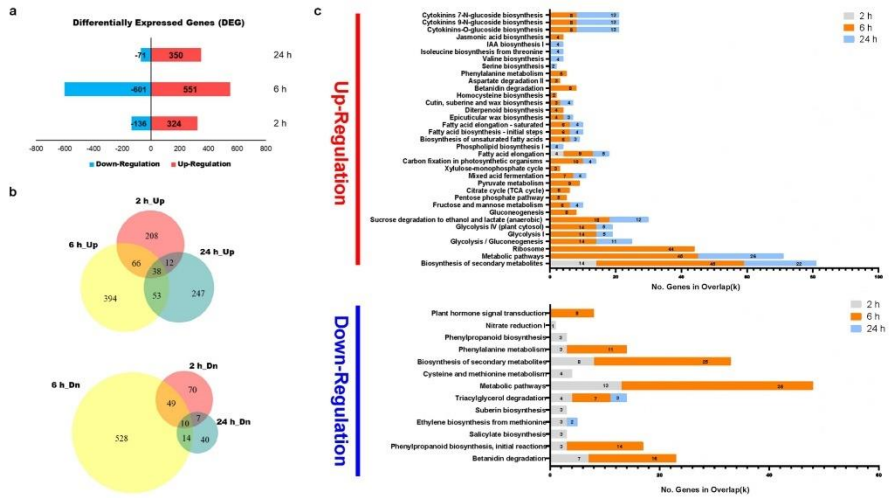

Fig. 2 Analysis of differentially expressed genes (DEGs) in response to zaxinone at different time points. a Numbers of the significantly expressed genes upon zaxinone treatment (FDR < 0.05). The numbers on the vertical axis represent the three time points while the horizontal axis reflects the numbers of up- and down-regulated genes. Up- and down-regulated genes are shown in red and blue bars, respectively. **b** Venn diagrams showing the numbers of down (Dn) and upregulated (Up) genes that overlap between different time points. **c** Kyoto Encyclopedia of Genes and Genomes (KEGG) and PlantCyc pathway enrichment analysis for up- and down-regulated genes, which were analyzed by The Plant GeneSet Enrichment Analysis Toolkit (PlantGSEA) (http://structuralbiology.cau.edu.cn/PlantGSEA/index.php).

same samples used for the RNA-seq experiment (Supplementary Fig. 10). Results obtained correlated with and explained the increase in sugar metabolites in root tissues. In contrast to roots, we detected a less significant impact on the shoot transcriptome presented in the PCA plots and DEGs analysis (Supplementary Fig. 11 and Supplementary Data 4), which may be anticipated given that the effect of zaxinone was mainly visible in root tissues, when using the hydroponic system. To further confirm the results, we performed a parallel transcript analysis with roots of WT and the *zas* mutant that contains less zaxinone and displays retarded growth (Supplementary Fig. 12a). We observed an upregulated transcript pattern of five glycolytic genes following the zaxinone treatment (Supplementary Fig. 12b), which could explain the capability of zaxinone in rescuing *zas* phenotype. Taken together, the transcriptome analysis supported the hypothesis that the growth-promoting effect is strongly linked with an increase of sugar metabolism in rice roots.

Zaxinone application does not induce sugar metabolism in the absence of strigolactones. In our previous study, we showed that zaxinone application did not promote root growth in rice SL biosynthesis and perception mutants, indicating that zaxinone's growth-promoting effect depends on functional SL biosynthesis and perception[23]. This opened the question of whether the changes in sugar metabolism caused by zaxinone are also linked to SLs. To answer this question, we applied zaxinone to *d17* and *zas* mutants and the corresponding WT varieties for 6 h, following the experimental design shown in Supplementary Fig 1, and analyzed the metabolome of collected root tissues. Results of metabolome analysis confirmed the accumulation of sugars and TCA cycle metabolites upon zaxinone treatment in both WT and *zas* mutants, while this response was largely absent in the *d17* mutant (Fig. 3), demonstrating that the sensitivity of sugar metabolism towards zaxinone application depends on the presence of a functional SL biosynthetic pathway.

Lipids are further important metabolites required for plant's growth. To assess the effect of zaxinone on lipid metabolism, we analyzed the lipid profile of treated root samples 6 h after zaxinone application. However, we did not detect a positive effect of zaxinone on lipid metabolism (Supplementary Fig. 13).

Zaxinone application promotes cell division in the root apical meristem and increases the number of cortex layers. It can be assumed that the growth-promoting effect of zaxinone in rice roots is caused by an increase in cell number and/or size. To determine changes at a cellular level, we applied zaxinone (at 5 µM concentration) to hydroponically grown rice seedlings for 2 weeks and investigated the roots using cotton blue staining. As shown in Supplementary Fig. 14, the treatment with zaxinone enhanced the length of the root apex, suggesting an increase of cell division or cell elongation activity. To test this hypothesis, we used 5-Ethynyl-2′-deoxyuridine (EdU) staining that visualizes proliferating cells and can be monitored by a fluorescent dye. This experiment revealed that the meristem length and diameter, as well as the number of cell layers (counted from epidermis to vascular tissue), increased upon zaxinone application in both primary and the longest crown roots (Fig. 4a, b). To confirm the increase in the number of cell layers, we performed cross sections of primary and the longest crown roots of treated WT and *zas* mutant seedlings, by staining the cell wall with SCRI Renaissance 2200. In the main root cortex as well as in the longest crown roots, zaxinone application led to a remarkable increase in the number of cortex layers from around three to around five, and of the number of cells in the circumference by ten, which caused an around 50 µm enlargement of root diameters (Fig. 4c, d).

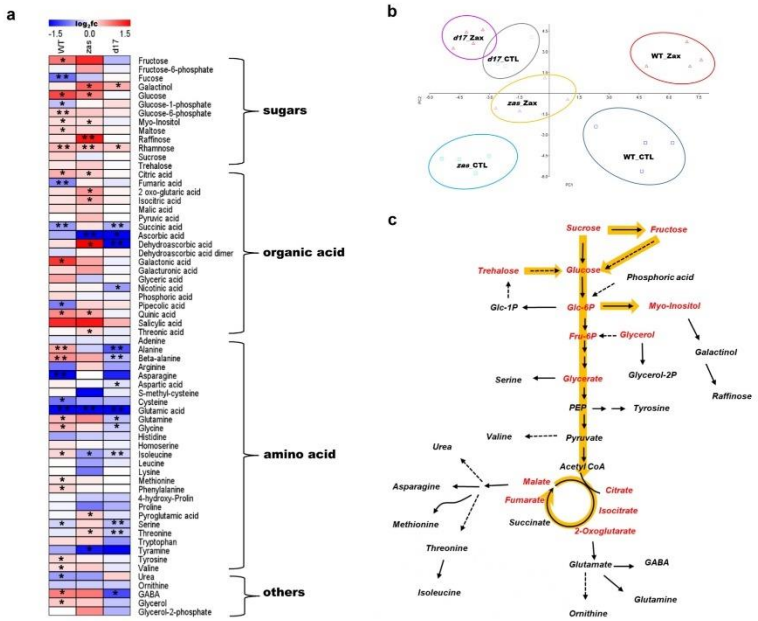

Fig. 3 The profile of primary metabolites in roots of WT, *zas*, and *d17* mutant. Primary metabolites extracted from roots for GC-MS, which were annotated and listed in Supplementary Data 7. $n = 4$ biological replicates. **a** Heatmap of root tissue showing relative accumulation of each metabolite as compared to those in control plants. For each metabolite, the value of the corresponding control was set to 1. Asterisks indicate statistically significant differences as compared to control by *t*-test (*$p < 0.05$, **$p < 0.01$). **b** Principal component analysis (PCA) of root metabolites was performed using Past3 software. **c** The scheme of major metabolic changes in central metabolism after zaxinone treatment, which adapted from a. Orange arrows indicate sugar-related metabolites that mainly accumulated upon zaxinone treatment in WT and/or the *zas* mutant, but not in *d17*. CTL control, Zax zaxinone.

Moreover, the enhancement in the number of cortex layers, root diameters, and cell numbers upon zaxinone application was much more conspicuous in the crown roots of *zas* mutant (Supplementary Fig. 15).

Zaxinone enhances cytokinin glycosylation in rice roots. The changes in root morphology at the cellular level indicate that zaxinone may affect the hormonal composition in roots, in addition to its role in determining SL biosynthesis and sugar metabolism. Analysis of the RNA-Seq data indicated that zaxinone might affect several genes related to hormone metabolism, including genes involved in jasmonic acid and auxin biosynthesis and in the glycosylation of CKs (Fig. 2c). Therefore, we determined the changes in the hormone profile and content of abscisic acid (ABA), gibberellin (GA), auxin (IAA), salicylic acid (SA), jasmonic acid (JA), and cytokinins (CKs: *trans*-zeatin, isopentyladenine, isopentyladenosine, and benzyladenine) in rice roots 2, 6, and 24 h after zaxinone application. We did not detect significant changes in the levels of GA, IAA, or SA, compared to the control, but observed an increase in ABA and JA levels at 2 and 6 h, respectively (Supplementary Fig. 16). Notably, the application of zaxinone led to a significant decrease in the content of isopentenyladenosine in all treated samples, a reduction of isopentenyladenine and benyzladenine in the 6, and 6 and 24 h samples, respectively, and an increase in levels of glycosylated, inactive *trans*-zeatin forms. We also observed an increase in *trans*-zeatin content 2 h after application (Supplementary Fig. 17). These data indicate that zaxinone may regulate the abundance and pattern of CKs. To gain insights into the long-term effect of zaxinone on CKs level, we applied the compound for two weeks and quantified the hormone. In this experiment, we also included the *zas* mutant that showed at the cellular level a stronger response than WT (Supplementary Fig. 15). As shown in Fig. 4e, prolonged treatment with zaxinone led to significant accumulation in the glycosylated, deactivated *trans*-zeatin. Finally, we chose four genes annotated by Kyoto Encyclopedia of Genes and Genomes analysis as cytokinin glycosyltransferases (Supplementary Data 5), and validated their expression levels in the samples used for the RNA-seq experiment, using qRT-PCR. As anticipated, these genes were highly induced following 24 h of zaxinone treatment (Fig. 2c and Supplementary Fig. 18). We obtained similar results in *zas* mutant seedlings exposed to zaxinone treatment (Supplementary Fig. 19). The induction of these genes may explain the accumulation of the glycosylated forms of CKs. To further validate that reduction of cytokinin signaling via CK glycosylation is a part of the downstream effect of zaxinone, we applied 2.5 µM zaxinone to CK biosynthetic (*Os03g49050*, *Os05g51390*, and *Os10g33900*) and regulatory (*Os06g08440*) rice T-DNA insertion mutants (Supplementary Fig. 20a). Interestingly, none of these mutants showed an increased root growth in

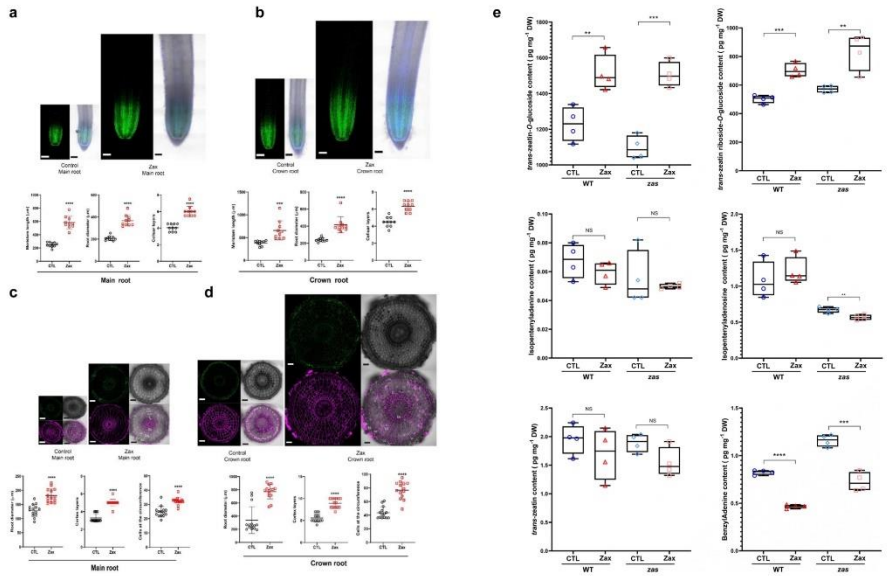

Fig. 4 Characterization of root development at cellular level upon zaxinone treatment. a, **b** Ethynyl deoxyuridine (EdU) staining for cell proliferation analysis. Confocal images of rice root showing dividing cells as captured by EdU staining in Zeiss LSM 710 inverted confocal microscope. Root meristem length, root diameter, and cell layers (counted from epidermis to vascular tissue) in both primary roots and crown roots after 5 µM zaxinone treatment (twice per week) in Nipponbare WT rice seedlings. Dividing EdU-stained nuclei are shown in green; nuclei counterstained with Hoechst 33258 are shown in magenta. Images were acquired using the tile scan function in the Zen software with automatized stitching. Regions of interest were divided into multiple tiles and imaged individually. The tiles were then combined via automatic stitching to create a large overview image. Images are representative of the total number ($n = 10$) of seedlings that were studied. Scale bar: 50 µm. **c**, **d** Cross section of the mock and zaxinone-treated roots stained with SCRI Renaissance 2200. Magenta indicates the cell wall staining; green shows the auto-fluorescence marking lignin and suberin deposition ($n = 14$ biological replicates). Examples of cell layer and circumference cell number count are indicated in the cross section d, scale bar: 50 µm. **e** Quantification of cytokinins in root tissues of WT and *zas* mutant after 2-week zaxinone treatment. Box plot presented as min to max, $n = 4$ biological replicates. Asterisks indicate statistically significant differences as compared to control by *t*-test (*$p < 0.05$, **$p < 0.01$; ***$p < 0.001$; ****$p < 0.0001$). CTL control, Zax zaxinone. Ep epidermis, Ex exodermis, Sc sclerenchyma, Co cortex, En endodermis.

response to zaxinone treatment, in contrast to the corresponding WT controls (Supplementary Fig. 20b). This result supported the hypothesis that the root growth-promoting effect of zaxinone is dependent on CKs.

Discussion

As the main product of photosynthetic carbon assimilation, sucrose plays an energy source and an essential role in plant growth and development. In addition, this sugar acts as a signaling molecule interacting with hormonal networks and regulating metabolic pathways[25–27]. In this paper, we show that zaxinone application promotes sugar metabolism in growing plants, leading to the accumulation of soluble sugars in different tissues, and might enhance the photosynthetic activity in rice seedlings (Fig. 5). We observed this effect also in *zas* mutant plants (Supplementary Fig. 5c), which contain less zaxinone in their roots[23]. Compared to WT, these plants also showed a lower chlorophyll content under control conditions, suggesting that endogenous zaxinone level might affect the photosynthetic capacity (Supplementary Fig. 5c). The alterations in shoot metabolism were of considerably lower magnitude and slower in response, compared to those of root metabolism. The alterations in root sugar metabolism appear to be biphasic with an initial accumulation of the major sugars sucrose, glucose, and fructose whose levels subsequently decreased, whilst those of downstream metabolites including trehalose, glucose-1-phosphate, glucose-6-phosphate alongside TCA cycle intermediates increased 24 h following zaxinone treatment. We observed similar metabolic changes to the initial effect also in *zas* mutant plants (Fig. 3a). Yet, we cannot rule out that zaxinone might not directly act as signaling molecules as it may need further modification or trigger its response via unknown component(s), which might explain the low response at the 2 h time point and the delay of metabolic changes the root and shoot tissues. Supporting the metabolomics data, the transcriptomic results indicated that zaxinone induces several sugar-related metabolic pathways, such as glycolysis that catabolizes hexose units to produce energy and building blocks for different cellular components (Fig. 5). We also showed that prolonged treatment with zaxinone led to an increased starch accumulation in roots, which is synthesized from mobilized sucrose that is produced by photosynthesis in leaves[26]. In rice, disruption in sucrose synthesis or transport mutations of rice causes growth retardation[28–30]. It might be a possibility that

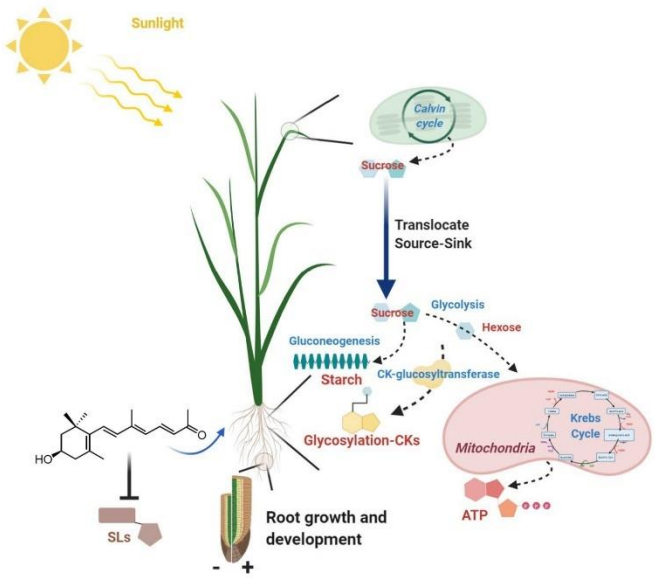

Fig. 5 Model of the mechanisms underlying the growth-promoting effect of zaxinone in rice. Application of zaxinone might enhance photosynthesis activity (Calvin cycle) that produces sucrose that is translocated from the shoot (source) to developing root tissues (sink). Sucrose then can either be hydrolyzed (glycolysis) into hexose that enters glycolysis and citric acid cycle (to produce ATP and C-building blocks), or stores as starch formed by gluconeogenesis. The glucose can also be used for cytokinin glycosylation that regulates the bioactivity of CKs in rice root tissues. A combination of these effects results in root phenotypical changes and cellular events, such as a larger meristem size. In addition, zaxinone suppresses SL biosynthesis and release, while it cannot rescue the SL biosynthesis and perception mutants[22] and does not affect the central metabolism in the SL biosynthetic *d17* mutant. Created with "Biorender".

sucrose provides the energy and C-atoms for the plant to grow and develop, depending on zaxinone, as we saw that zaxinone rescued *Oszas* mutant phenotype[23]. This trend correlates with the observed increase in transcript levels of sucrose metabolic genes. Moreover, we observed some of the sugar metabolites were highly accumulated in *zas* mutant compared to WT at control condition, which may argue that the endogenous zaxinone level is involved in the sugar metabolism. However, *zas* also shows high SL content[22] that indicates the endogenous relative amount of zaxinone and SLs might contribute to the observed sugar metabolites as well as phenotypic changes.

Roots and young leaves are the major sinks during early developmental stages, whereas fruit and seeds are the ones accumulating starch during the reproductive stages[31]. Consequently, zaxinone treatment, which led to an increased starch accumulation in roots, improved the sink capacity of this organ. However, we cannot currently demonstrate whether the increase in chlorophyll abundance and stomatal conductance is due to an enhanced sink-strength of the zaxinone-treated roots, or a direct effect of zaxinone/derivative thereof. Regardless, our results demonstrate zaxinone remarkably increases sugar metabolism and might modulate photosynthesis in rice plants.

The root system is essential for plants to absorb nutrients and water, which determine plant growth and performance. Application of zaxinone remarkably increased crown root numbers[23], root apex length as well as cortex layers and cell numbers in both rice WT and *zas* mutant, which indicates a possible interplay with Auxin or CKs. Indeed, CKs orchestrate root growth and development; and previous studies documented that this hormone inhibits root elongation by decreasing root meristem size[32–34]. For example, disruption of *CROWN ROOTLESS5* (*CRL5*) encoding an ERF transcription factor led to a loss of rice crown root initiation through repression of two negative regulators of CK signaling (*OsRR1* and *OsRR2*)[35]. Indeed, we detected significant upregulation of the transcript level of *OsRR6*, (*Os04g57720*) and *OsRR10*, (*Os02g35180*), two homologs of *OsRR1* and *OsRR2*, at 2 h after zaxinone application (Supplementary Data 1). Similarly, overexpressing *CK OXIDASE/DEHYDROGENASE 4* (*OsCKX4*, *Os01g71310*) led to lower amounts of CKs, which was accompanied by longer roots and a larger root apical meristem with more cellular layers[34,36]. In this study, we observed an upregulation of *OsCKX4* expression (2 and 24 h; Supplementary Data 1) upon zaxinone treatment, which may contribute to the increased activity of root meristems and alterations in root architecture. Besides, the plant hormones profile and transcript analysis showed that zaxinone reduced the free-form CKs and enhanced glycosylated-CKs biosynthesis, which can be considered as fine-tuning of their synthesis, metabolism, and function. Indeed, glycosylation was shown to significantly reduce the activity of CKs and to affect their transport, signal transduction, and impact on growth and development[37]. The changes in root architecture caused by CK glycosylation

resemble those observed upon zaxinone treatment to CK biosynthesis and signaling mutants. Therefore, CKs-glycosylation is of great significance for understanding the effects of zaxinone and its impact on rice root development (Fig. 5). Previously, we showed that zaxinone did not enhance the root growth in SL-deficient rice mutants, indicating the requirement for intact SL biosynthesis[23]. Here, we further found that zaxinone did not increase the sugar metabolism in the SL-deficient rice *d17* mutant, which indicates that the effect of zaxinone on sugar metabolism is mediated by SLs. Taken together, zaxinone not only modulates the SL biosynthesis and release[23], but also acts on the CK signaling pathway by modulating CK activity through glycosylation. The latter may be the result of increasing sugar content in the root tissues.

In summary, we provide experimental evidence at the metabolite, transcript, and cellular level, which demonstrates the role of zaxinone in regulating central metabolism, determining hormone profile, and promoting cell division in rice roots (Fig. 5). The results presented explain zaxinone's growth-promoting effect in rice plants and may help to develop new strategies to increase the performance of this and other crops towards sustainable agriculture.

Methods

Plant material and growth conditions. Nipponbare background *zas*[23], *d17*[38], and WT rice plants were grown under controlled conditions (a 12 h photoperiod, 200-µmol photons m^{-2} s^{-1} and day/night temperature of 27/25 °C). Rice seeds were surface-sterilized in a 50% sodium hypochlorite solution with 0.01 % Tween-20 for 15 min. The seeds were rinsed with sterile water and germinated in the dark overnight. The pre-germinated seeds were transferred to Petri dishes containing half-strength liquid Murashige and Skoog (MS) medium and incubated in a growth chamber for 7 days. Thereafter, the seedlings were transferred into black falcon tubes filled with half-strength modified Hoagland nutrient solution with adjusted pH to 5.8. The nutrient solution consisted of 5.6 mM NH_4NO_3, 0.8 mM $MgSO_4{\cdot}7H_2O$, 0.8 mM K_2SO_4, 0.18 mM $FeSO_4{\cdot}7H_2O$, 0.18 mM $Na_2EDTA{\cdot}2H_2O$, 1.6 mM $CaCl_2{\cdot}2H_2O$, 0.8 mM KNO_3, 0.023 mM H_3BO_3, 0.0045 mM $MnCl_2{\cdot}4H_2O$, 0.0003 mM $CuSO_4{\cdot}5H_2O$, 0.0015 mM $ZnCl_2$, 0.0001 mM $Na_2MoO_4{\cdot}2H_2O$ and 0.4 mM $K_2HPO_4{\cdot}2H_2O$.

For metabolomic and transcriptomic analysis, 3-weeks-old seedlings were grown hydroponically in half-strength modified Hoagland nutrient solution. Seedlings were further treated with 5 µM zaxinone for 2, 6, or 24 h, and tissues were collected.

For phenomic experiments, one-week-old seedlings were grown hydroponically in half-strength modified Hoagland nutrient solution with or without 5 µM zaxinone for two weeks. Thereafter, plant tissues were collected for analysis.

For zaxinone application to CK mutants, 1-week-old seedling (IN67 background) were grown hydroponically in ½ strength Hoagland nutrient solution containing 2.5 µM zaxinone for 2 weeks. The solution was changed two times per week.

Synthetic zaxinone was purchased (custom synthesis) from Buchem B.V. (Apeldoorn, The Netherlands).

Analysis of primary metabolites using GC-MS. Frozen ground material, spiked with 60 µg phenyl-β-glucopyranosides, was homogenized in 750 µL of methanol at 70 °C for 15 min and then 375 µL of chloroform followed by adding 750 µL of water. The polar fraction was dried under vacuum, and the residue was derivatized for 40 min at 37 °C (in 50 µL of 20 mg mL^{-1} methoxyamine hydrochloride in pyridine) followed by a 30 min treatment at 37 °C with 70 µL of MSTFA. The GC-MS system used was a gas chromatograph coupled to a time-of-flight mass spectrometer (Leco Pegasus HT TOF-MS). A Gerstel Multi Purpose autosampler system injected the samples. Helium was used as carrier gas at a constant flow rate of 2 mL s^{-1} and gas chromatography was performed on a 30 m DB-35 column. The injection temperature was 230 °C and the transfer line and ion source were set to 250 °C. The initial temperature of the oven (85 °C) increased at a rate of 15 °C min^{-1} up to a final temperature of 360 °C. After a solvent delay of 180 s mass spectra were recorded at 20 scans s^{-1} with *m/z* 70–600 scanning range. Chromatograms and mass spectra were evaluated by using Chroma TOF 4.5 (Leco) and TagFinder 4.2 software[39,40].

Lipid profile by LC–MS. Lipids were extracted based on the protocol published in[41]. In brief, 5 mg of freeze-dry materiel was homogenized and extracted with 1 mL of pre-cooled (−20 °C) extraction buffer (homogenous methanol/methyl-*tert*-butyl-ether [1:3] mixture). After 10 min incubation at 4 °C and sonication for 10 min in a sonic bath, 500 µL of water/methanol mixture was added. Samples were then centrifuged (5 min, 14,000×g), which led to the formation of two phases: a lipophilic phase and a polar phase. Five hundred microliters of the lipophilic phase were collected and dried under vacuum and resuspended in 200 µL of ASN/isopropanol and used for lipid analysis. Samples were processed using UPLC-FT-MS on a C_8 reverse-phase column (100 × 2.1 mm × 1.7 µm particle size, Waters) at 60 °C. The mobile phases consisted of 1% 1 M NH_4OAc and 0.1 % acetic acid in water (buffer A) and acetonitrile/isopropanol (7:3, UPLC grade BioSolve) supplemented with 1 M NH_4Ac and 0.1% acetic acid (buffer B). The dried lipid extracts were resuspended in 500 µL of buffer B. The following gradient profile was applied: 1 min 45% A, 3 min linear gradient from 45% A to 35 % A, 8 min linear gradient from 25 to 11% A, 3 min linear gradient from 11 to 1% A. Finally, after washing the column for 3 min with 1% A, the buffer was set back to 45% A, and the column was re-equilibrated for 4 min, leading to a total run time of 22 min. The flow rate of the mobile phase was 400 µL min^{-1}. The mass spectra were acquired using an Exactive mass spectrometer (ThermoFisher, http://www.thermofisher.com) equipped with an ESI interface. All the spectra were recorded using altering full-scan and all-ion fragmentation scan mode, covering a mass range from 100–1500 *m/z* at a capillary voltage of 3.0 kV, with a sheath gas flow value of 60 and an auxiliary gas flow of 35. The resolution was set to 10,000 with 10 scans per second, restricting the Orbitrap loading time to a maximum of 100 ms with a target value of 1E6 ions. The capillary temperature was set to 150 °C, while the drying gas in the heated electrospray source was set to 350 °C. The skimmer voltage was held at 25 V, while the tube lens was set to a value of 130 V. The spectra were recorded from minute 1 to 20 of the UPLC gradients. Processing of chromatograms, peak detection, and integration was performed using REFINER MS 10.0 (GeneData, http://www.genedata.com) or Xcalibur (Version 3.1, ThermoFisher, Bremen, Germany). In the first approach, the molecular masses, retention time, and associated peak intensities for the three replicates of each sample were extracted from the raw files, which contained the full-scan MS and the all-ion fragmentation MS Data Processing of MS data included the removal of the fragmentation information, isotopic peaks, and chemical noise. Further peak filtering on the manually extracted spectra or the aligned data matrices was performed. Obtained features (*m/z* at a certain retention time) were queried against an in-house lipid database for further annotation

RNA library preparation and transcriptomic analysis. Total rice root RNA was extracted with TRIzol (Invitrogen, https://www.thermofisher.com/de/de/home.html.) using a Direct-zol RNA Miniprep Plus Kit following the manufacturer's instructions (ZYMO RESEARCH; USA). RNA quality was checked with a Agilent 2100 Bioanalyzer, and RNA concentration was measured using a Qubit 3.0 Fluorometer. The cDNA libraries were constructed following standard Illumina protocols and paired-end sequenced on an Illumina HiSeq 4000 machine by the Bioscience core lab of KAUST. RNA-Seq reads were aligned to the *O. sativa* genome v7.0 downloaded from Phytozome v12.1 (http://phytozome.jgi.doe.gov/). Data processing and analysis were performed using the LSTrAP workflow[42], which included all steps described below. Adapter sequences were removed from fastq files by Trimmomatic[43], and aligned to the genome using HISAT2[44]. Read counts aligned to each annotated gene were computed with HTSeq[45]. The results were passed through LSTrAP quality control and TPM normalized. The mean data were used to cluster and resistance level was visualized as a heatmap using a hierarchical clustering R script. Principal component analysis (PCA), a multivariate statistical technique, was further conducted to examine links between samples. All analyses were performed using the R statistical package. For differential gene expression, read counts from HTSeq were analyzed using the R package DESeq2[46]. Genes were considered differentially expressed based on a *P*-value adjusted by the Benjamini–Hochberg procedure[47] below 0.05. Gene Ontology (GO) enrichment analysis of all the differentially were selected at FDR < 0.05 and analyzed by Panther-Gene list analysis[48] (http://pantherdb.org/). Kyoto Encyclopedia of Genes and Genomes and PlantCyc pathway enrichment analysis for up- and down-regulated genes, were then analyzed by The Plant GeneSet Enrichment Analysis Toolkit (PlantGSEA)[49] (http://structuralbiology.cau.edu.cn/PlantGSEA/index.php). Visualization of DEGs in MapMan followed the instructions as described[50].

Gene expression analysis. Roots of rice seedlings were ground and homogenized in liquid nitrogen, and total RNA was isolated using a Direct-zol RNA Miniprep Plus Kit following the manufacturer's instructions (ZYMO RESEARCH; USA). cDNA was synthesized from 1 µg of total RNA using iScript cDNA Synthesis Kit (BIO-RAD Laboratories, Inc, 2000 Alfred Nobel Drive, Hercules, CA; USA), according to the instructions in the user manual. Transcript levels were detected by real-time quantitative RT-PCR (qRT-PCR) which was performed using SYBR Green Master Mix (Applied Biosystems; www.lifetechnologies.com) in a CFX384 Touch™ Real-Time PCR Detection System (BIO-RAD Laboratories, Inc, 2000 Alfred Nobel Drive, Hercules, CA; USA). Primers used for qRT-PCR analysis are listed in Supplementary Data 8. The gene expression level was calculated by normalization to the rice housekeeping gene Ubiquitin (OsUBQ) (Supplementary Data 8). The relative gene expression level was calculated according to $2^{-\Delta\Delta CT}$ method[51].

Cotton blue staining for root apex. Apex length and width were assessed in WT rice roots with or without 5 μM zaxinone (applied twice a week). Plants were grown hydroponically in Hoagland solution (400 μM Pi), and data were collected 3 weeks post-germination. The primary crown root apex was stained with Cotton Blue 0.1 %. The apex length was calculated considering the segment between the root tip and the first root hair.

Ethynyl deoxyuridine (EdU) staining for cell proliferation analysis. Cell proliferation in rice seedlings was evaluated using the Click-iT EdU Alexa Fluor 488 imaging kit (C10637, Invitrogen) followed the procedure[52]. Plants were incubated in Murashige and Skoog medium with EdU for 12 h. For each plant, the primary root and the longest crown root (prior to the formation of lateral roots) were harvested and fixed in 3.7% formaldehyde for 1 h under vacuum. Then samples were permeabilized with PBS containing 0.5 % Triton X-100 for 1 h and incubated for 1 h in the dark with a click-it-reaction cocktail that was prepared according to the manual, followed by DNA counterstaining using Hoechst 33342 in PBS under vacuum in the dark for 1 h. Samples were mounted in clearing solution and incubated in the dark for 2 weeks at 4 °C as described in the protocol published in ref. [53]. Images were captured by a Zeiss LSM 880 inverted confocal microscope and automatically stitched to generate the overview image of the root tip in ZEN 2.0 while imaging. Dividing EdU-stained nuclei are shown in green; nuclei counterstained with Hoechst 33258 are shown in blue. Images are representative of the total number ($n = 10$) of seedlings that were studied.

Root cross section, staining, and microscopy. Fresh root segments starting from the root hair emergence zone to the direction of the shoot (an upward direction, about 0.5 cm from in differentiation zone) were embedded in 10% low melting agarose and sectioned using a Leica VT1000S vibratome. The SCRI Renaissance 2200 (SR2200) stain was used to visualize cell walls while the berberine hemisulfate stain was used to visualize suberin[54]. Images were captured using a Zeiss LSM 880 inverted confocal microscope with excitation of 405 nm for SCRI or 488 nm for berberine.

Quantification of starch. For starch extraction, excised root systems were rapidly blot-dried on filter paper and weighed. Samples were then frozen in liquid nitrogen, transferred to 2-mL Eppendorf tubes (Eppendorf, Hamburg, Germany), and thoroughly homogenized using a pestle in liquid nitrogen. The samples were further homogenized in 0.5 mL of absolute ethanol. After the addition of 0.5 mL of 80% ethanol, the tubes were incubated at 70 °C for 90 min and then centrifuged for 10 min at 11,337 × *g* and the pellet was resuspended in 1 mL of 80% ethanol. Two more washings were performed with 1 mL of 80% ethanol (and 10 min of centrifugation). The pellets were finally resuspended in 400 μL of 0.2 m KOH and incubated at 95 °C for 60 min. After neutralization with 70 μL of acetic acid, the samples were centrifuged for 10 min and the supernatant was used for starch quantification (Starch Test-Combination enzymatic analysis kit, cat. no. 207748; Boehringer, Mannheim, Germany), according to the manufacturer's instructions. At least three independent experiments, including at least three plants each, were performed to obtain all results of enzymatic starch quantification.

Quantification of plant hormones. For the quantification of endogenous hormone levels, 20 mg of freeze-dried ground tissues were spiked with internal standards D_6-ABA (3.2 ng), D_2-GA1 (0.08 ng), D_2-IAA (5.4 ng), D_4-SA (0.05 ng), D_2-JA (0.1 ng), D_5-*trans*-zeatin (1.5 ng), D_5-*trans*-zeatin-O-glucoside (2 ng), D_5-*trans*-zeatin riboside-O-glucoside (2 ng), D_6-N^6-Isopentenyladenine (2 ng), N_{15}-N^6-isopentenyladenosine (2 ng), and D_7-N^6-Benzyladenine (2 ng) along with 1.5 mL of methanol as described procedure[51]. The mixture was sonicated for 15 min in an ultrasonic bath (Branson 3510 ultrasonic bath), followed by centrifugation for 10 min at 14,000 × *g* at 4 °C. The supernatant was collected, and the pellet was re-extracted with 1.5 mL of the same solvent. Then, the two supernatants were combined and dried under a vacuum. The sample was re-dissolved in 150 μL of acetonitrile:water (25:75, v-v) and filtered through a 0.22 μm filter for LC–MS analysis. Plant hormones were analyzed using HPLC-Q-Trap-MS/MS with Multiple Reaction Monitoring (MRM) mode. Chromatographic separation was achieved on a ZORBAX Eclipse plus C_{18} column (150 × 2.1 mm; 3.5 μm; Agilent). Mobile phases consisted of water:acetonitrile (95:5, v-v) and acetonitrile, both containing 0.1% formic acid. A linear gradient was optimized as follows (flow rate, 0.4 mL min^{-1}): 0 − 17 min, 10–100% B, followed by washing with 100% B and equilibration with 10% B. The injection volume was 5 μL and the column temperature was maintained at 40 °C for each run. Mass spectrometry was conducted in electrospray and MRM mode, in positive ion mode for cytokinins, and in negative ion mode for the other hormones. Relevant instrumental parameters were set as follows: ion source of turbo spray, ion spray voltage of (±) 4500 V, curtain gas of 25 psi, collision gas of medium, gas 1 of 45 psi, gas 2 of 30 psi, turbo gas temperature of 500 °C, entrance potential of −10 V. The characteristic MRM transitions (precursor ion → product ion) were 263.2 → 153.1 for ABA; 347.1 → 261.1 for GA1; 174.0 → 129.6 for IAA; 136.6 → 92.8 for SA; 209.0 → 59.0 for JA; 269.2 → 159.1 for D_6-ABA; 349.1 → 261.1 for D_2-GA1; 176.0 → 131.6 for D_2-IAA; 141.0 → 97.0 for D_4-SA ; 211.0 → 61.0 for D_2-JA. 225.2 → 136.7 for D_5-*trans*-zeatin; 387.2 → 225.4 for D_5-*trans*-zeatin- *O* -glucoside; 519.2 → 225.2 for D_5-*trans*-zeatin riboside-*O*-glucoside; 210.2 → 137.0 for D_6-N^6-Isopentenyladenine; 337.0 → 205.0 for N_{15}-N^6-isopentenyladenosine; 233.1 → 98.0 for D_7-N^6-Benzyladenine; 220.2 → 136.0 for *trans*-zeatin; 382.2 → 220.2 for *trans*-zeatin-*O*-glucoside; 514.2 → 220.2 for *trans*-zeatin riboside-*O*-glucoside; 204.2 → 136.1 N^6-Isopentenyladenine; 336.0 → 204.0 for N^6-isopentenyladenosine; 226.1 → 91.0 for N^6-Benzyladenine.

Measurement of photosynthetic parameters. Three-week-old seedlings were grown hydroponically in a half-strength-modified Hoagland nutrient solution. Seedlings were further treated with 5 μM zaxinone for 2, 6, or 24 h. Leaf chlorophyll content was measured by CCM-200 plus chlorophyll content meter (Opti-Sciences, Hudson, USA), and leaf stomatal conductance was measured by AP4 Porometer (Delta-T, Cambridge, UK).

Chlorophyll quantification. Chlorophyll was extracted from the leaf segment by following the procedure according to ref. [55] with a slight modification. Briefly, an equal amount of frozen leaf tissue was measured in a 2 mL Eppendorf tube and ground into a fine powder with 2 mm metal beads. One mL of 80% acetone was added to each tube and the mixture was vortex for 30 s. The extracted mixture was incubated at room temperature for 10 min. Each sample was subjected to centrifugation at 4282 × *g*, 4, at room temperature for 90 s. Then 200 μL of supernatant was collected from the top of each tube and added to 96 well plates. The plate was run in the microplate reader (Tecan Infinite M1000 Pro). The absorbance of Chlorophyll-*a* (Chla) and Chlorophyll-*b* (Chlb) was determined by UV-spectrophotometry at 645 and 663 nm wavelength. Chlorophyll-*a*, Chlorophyll-*b*, and total chlorophyll content were calculated from each extract by using the following equations:

$$\mathrm{Chl}a\,(\mathrm{mg\ g^{-1}}) = 12.7(\mathrm{A663}) - 2.69(\mathrm{A645}) \times V/1000 \times W \quad (1)$$

$$\mathrm{Chl}b\,(\mathrm{mg\ g^{-1}}) = 22.9(\mathrm{A645}) - 4.68(\mathrm{A663}) \times V/1000 \times W \quad (2)$$

$$\mathrm{Total\ Chl}\,(\mathrm{mg\ g^{-1}}) = 20.2(\mathrm{A645}) + 8.02(\mathrm{A663}) \times V/1000 \times W \quad (3)$$

where
A = absorbance at specific wavelengths
V = final volume of chlorophyll extract
W = fresh weight of tissue extracted

Statistics and reproducibility. A minimum of three independent biological replicates to ensure reproducibility in all the experiments. Exact biological samples (n) and mean with error bars are indicated in individual figure captions and methods. Statistical tests were carried out through one-way analysis of variance (one-way ANOVA) and Tukey's post hoc test or two-tailed Student's *t*-tests, using a probability level of $P < 0.05$, which was considered to be statistically significant.

Reporting summary. Further information on research design is available in the Nature Research Reporting Summary linked to this article.

Data availability

All data generated or analyzed during this study are included in this published article, Supplementary Information, and Supplementary Data 10 and 11. RNA-Seq data can be accessed at NCBI's Gene Expression Omnibus (GEO) via accession number (GSE184529).

Received: 18 February 2021; Accepted: 24 September 2021;
Published online: 25 October 2021

References

1. Zheng, X., Giovanni, G. & Al-Babili, S. Carotenoid biofortification in crop plants: citius, altius, forties. *Biochim. Biophys. Acta Mol. Cell. Biol. Lipids* **1865**, 158664 (2020).
2. Havaux, M. Carotenoid oxidation products as stress signals in plants. *Plant J.* **79**, 597–606 (2014).
3. Hou, X., Rivers, J., Leo, N. P., McQuinn, R. P. & Pogson, B. J. Synthesis and function of apocarotenoid signals in plants. *Trends Plant Sci.* **21**, 792–803 (2016).
4. Wang, J. Y., Lin, P.-Y., & Al-Babili, S. On the biosynthesis and evolution of apocarotenoid plant growth regulators. *Semin. Cell. Dev. Biol.* **109**, 3–11 (2020)
5. Al-Babili, S. & Bouwmeester, H. J. Strigolactones, a novel carotenoid-derived plant hormone. *Annu. Rev. Plant Biol.* **66**, 161–186 (2015).
6. Alder, A. et al. The path from beta-carotene to carlactone, a strigolactone-like plant hormone. *Science* **335**, 1348–1351 (2012).

7. Bruno, M. et al. Insights into the formation of carlactone from in-depth analysis of the CCD8-catalyzed reactions. *FEBS lett.* **591**, 792–800 (2017).
8. Brewer, P. B. et al. LATERAL BRANCHING OXIDOREDUCTASE acts in the final stages of strigolactone biosynthesis in *Arabidopsis*. *Proc. Natl Acad. Sci. USA* **113**, 6301–6306 (2016).
9. Nisar, N., Li, L., Lu, S., Khin, N. C. & Pogson, B. J. Carotenoid metabolism in plants. *Mol. Plant.* **8**, 68–82 (2015).
10. Lanfranco, L., Fiorilli, V., Venice, F. & Bonfante, P. Strigolactones cross the kingdoms: plants, fungi, and bacteria in the arbuscular mycorrhizal symbiosis. *J. Exp. Bot.* **69**, 2175–2188 (2018).
11. Fiorilli, V., Wang, J. W., Bonfante, P., Lanfranco, L. & Al-Babili, S. Apocarotenoids: old and new mediators of the arbuscular mycorrhizal symbiosis. *Front. Plant Sci.* **10**, 1186 (2019).
12. Barbier, F. F., Dun, E. A., Kerr, S. C., Chabikwa, T. G. & Beveridge, C. A. An update on the signals controlling shoot branching. *Trends Plant Sci.* **24**, 220–236 (2019).
13. Duan, J. et al. Strigolactone promotes cytokinin degradation through transcriptional activation of CYTOKININ OXIDASE/DEHYDROGENASE 9 in rice. *Proc. Natl Acad. Sci. USA* **116**, 14319–14324 (2019).
14. Dun, E. A. et al. Antagonistic action of strigolactone and cytokinin in bud outgrowth control. *Plant Physiol.* **158**, 487–498 (2012).
15. Hu, Z. et al. Strigolactone and cytokinin act antagonistically in regulating rice mesocotyl elongation in darkness. *Plant Cell Physiol.* **55**, 30–41 (2014).
16. Baghalian, K., Hajirezaei, M. R. & Schreiber, F. Plant metabolic modeling: achieving new insight into metabolism and metabolic engineering. *Plant Cell* **26**, 3847–3866 (2014).
17. Sulpice, R. & McKeown, P. C. Moving toward a comprehensive map of central plant metabolism. *Annu. Rev. Plant Biol.* **66**, 187–210 (2015).
18. Patti, G. J., Yanes, O. & Siuzdak, G. Innovation: Metabolomics: the apogee of the omics trilogy. *Nat. Rev. Mol. Cell. Biol.* **13**, 263–269 (2012).
19. Li, G. D. et al. Strigolactones are involved in sugar signaling to modulate early seedling development in *Arabidopsis*. *Plant Biotechnol.* **33**, 87–97 (2016).
20. Bertheloot, J. et al. Sugar availability suppresses the auxin-induced strigolactone pathway to promote bud outgrowth. *N. Phytol.* **225**, 866–879 (2020).
21. Jia, K. et al. Anchorene is a carotenoid-derived regulatory metabolite required for anchor root formation in *Arabidopsis*. *Sci. Adv.* **5**, eaaw6787 (2019).
22. Dickinson, A. J. et al. β-cyclocitral is a conserved root growth regulator. *Proc. Natl. Acad. Sci. USA* **116**, 10563–10567 (2019).
23. Wang, J. Y. et al. The apocarotenoid metabolite zaxinone regulates growth and strigolactone biosynthesis in rice. *Nat. Commun.* **10**, 810 (2019).
24. Wang, J. Y. et al. Efficient mimics for elucidating zaxinone biology and promoting agricultural applications. *Mol. Plant.* **13**, 1654–1661 (2020).
25. Lastdrager, J., Hanson, J. & Smeekens, S. Sugar signals and the control of plant growth and development. *J. Exp. Bot.* **65**, 799–807 (2014).
26. Ljung, K., Nemhauser, J. L. & Perata, P. New mechanistic links between sugar and hormone signalling networks. *Curr. Opin. Plant Biol.* **25**, 130–137 (2015).
27. Ruan, Y. L. Sucrose metabolism: gateway to diverse carbon use and sugar signaling. *Annu. Rev. Plant Biol.* **65**, 33–67 (2014).
28. Eom, J. S. et al. Impaired function of the tonoplast-localized sucrose transporter in rice, OsSUT2, limits the transport of vacuolar reserve sucrose and affects plant growth. *Plant Physiol.* **157**, 109–119 (2011).
29. Hirose, T. et al. Analysis of gene-disruption mutants of a sucrose phosphate synthase gene in rice, OsSPS1, shows the importance of sucrose synthesis in pollen germination. *Plant Sci.* **225**, 102–106 (2014).
30. Lee, S. K. et al. Loss of cytosolic fructose-1,6-bisphosphatase limits photosynthetic sucrose synthesis and causes severe growth retardations in rice (*Oryza sativa*). *Plant Cell Environ.* **31**, 1851–1863 (2008).
31. Wardlaw, I. F. Tansley Review No. 27. The control of carbon partitioning in plants. *N. Phytol.* **116**, 341–381 (1990).
32. Beemster, G. & Baskin, T. S'UNTED PLAN'I' 1 mediates effects of cytokinin, but not of auxin, on cell division and expansion in the root of *Arabidopsis thaliana*. *Plant Physiol.* **124**, 1718–1727 (2000).
33. Dello Ioio, R. et al. Cytokinins determine *Arabidopsis* root-meristem size by controlling cell differentiation. *Curr. Biol.* **17**, 678–682 (2007).
34. Werner, T. et al. Cytokinin-deficient transgenic *Arabidopsis* plants show multiple developmental alterations indicating opposite functions of cytokinins in the regulation of shoot and root meristem activity. *Plant Cell* **15**, 2532–2550 (2003).
35. Kitomi, Y. et al. The auxin responsive AP2/ERF transcription factor CROWN ROOTLESS5 is involved in crown root initiation in rice through the induction of OsRR1, a type-A response regulator of cytokinin signaling. *Plant J.* **67**, 472–484 (2011).
36. Gao, S. et al. CYTOKININ OXIDASE/DEHYDROGENASE4 integrates cytokinin and auxin signaling to control rice crown root formation. *Plant Physiol.* **165**, 1035–1046 (2014).
37. Mok, D. W. & Mok, M. C. Cytokinin metabolism and action. *Annu. Rev. Plant Physiol. Plant Mol. Biol.* **52**, 89–118 (2001).
38. Butt, H., Jamil, M., Wang, J. Y., Al-Babili, S. & Mahfouz, M. Engineering plant architecture via CRISPR/Cas9-mediated alteration of strigolactone biosynthesis. *BMC Plant Biol.* **18**, 174 (2018).
39. Roessner, U. et al. Metabolic profiling allows comprehensive phenotyping of genetically or environmentally modified plant systems. *Plant Cell* **13**, 11–29 (2001).
40. Schauer, N. et al. GC-MS libraries for the rapid identification of metabolites in complex biological samples. *FEBS Lett.* **579**, 1332–1337 (2005).
41. Hummel, J. et al. Ultra performance liquid chromatography and high resolution mass spectrometry for the analysis of plant lipids. *Front. Plant Sci.* **2**, 54 (2011).
42. Proost, S., Krawczyk, A. & Mutwil, M. LSTrAP: efficiently combining RNA sequencing data into co-expression networks. *BMC Bioinformatics* **18**, 444 (2017).
43. Bolger, A. M., Lohse, M. and Usadel, B. Trimmomatic: a flexible trimmer for Illumina sequence data. *Bioinformatics* **30**, 2114–2120 (2014).
44. Kim, D., Paggi, J. M., Park, C., Bennett, C. & Salzberg, S. L. Graph-based genome alignment and genotyping with HISAT2 and HISAT-genotype. *Nat. Biotechnol.* **37**, 907–915 (2019).
45. Anders, S., Pyl, P. T. & Huber, W. HTSeq—a Python framework to work with high-throughput sequencing data. *Bioinformatics* **31**, 166–169 (2015).
46. Love, M. I., Huber, W. & Anders, S. Moderated estimation of fold change and dispersion for RNA-seq data with DESeq2. *Genome Biol.* **15**, 550 (2014).
47. Benjamini, Y. & Hochberg, Y. Controlling the false discovery rate: a practical and powerful approach to multiple testing. *J. R. Stat. Soc. B* **57**, 289–300 (1995).
48. Mi, H. et al. Protocol update for large-scale genome and gene function analysis with the PANTHER classification system (v.14.0). *Nat. Protoc.* **14**, 703–721 (2019).
49. Yi, X., Du, Z. & Su, Z. PlantGSEA: a gene set enrichment analysis toolkit for plant community. *Nucleic Acids Res.* **41**, 98–103 (2013).
50. Thimm, O. et al. MAPMAN: a user-driven tool to display genomics data sets onto diagrams of metabolic pathways and other biological processes. *Plant J.* **37**, 914–939 (2004).
51. Livak, K. J. & Schmittgen, T. D. Analysis of relative gene expression data using real-time quantitative PCR and the $2^{\Delta\Delta}$CT method. *Methods* **25**, 402–408 (2001).
52. Xiao, T. T. et al. Emergent protective organogenesis in date palms: a morpho-devo-dynamic adaptive strategy during early development. *Plant Cell* **31**, 1751–1766 (2019).
53. Kirschner, G. K., Stahl, Y., Von Korff, M. & Simon, R. Unique and conserved features of the barley root meristem. *Front. Plant Sci.* **8**, 1240 (2017).
54. Musielak, T. J., Schenkel, L., Kolb, M., Henschen, A. & Bayer, M. A simple and versatile cell wall staining protocol to study plant reproduction. *Plant Reprod.* **28**, 161–169 (2015).
55. Sudhakar, P., Latha, P. & Reddy, P. *Phenotyping Crop Plants for Physiological and Biochemical Traits* 121–127 (Academic Press, 2016).

Acknowledgements

We thank Dr. Kennedy Odokonyero for technical support in photosynthesis experiments and Dr. Hendrik N. J. Kuijer for reading and correcting the manuscript. We are grateful to the KAUST bioscience core lab for RNA-seq, the members of the Bioactives lab in KAUST, members of AG Fernie in MPIMP, and Prof. Anna Fusconi and Prof. Paola Bonfante in the University of Torino for their helpful discussions and assistance. This work was supported by baseline funding and Competitive Research Grants (CRG2017 and CRG2020) given to S.A.-B. from King Abdullah University of Science and Technology (KAUST), and by grants from the European Union's Horizon 2020 research and innovation programme, project PlantaSYST (SGA-CSA No. 739582 under FPA No. 664620) to A.R.F. and S.A.

Author contributions

S.A.-B. and A.R.F. proposed the concept and designed the experiments. J.Y.W. and S.A. performed metabolomics, lipid profiles, and phytohormone experiments. A.A. and J.Y.W. prepared RNA library for RNA sequence. P.d.L. and J.Y.W. performed RNA-Seq data analysis. A.A. and P.-Y.L. performed expression analyses. T.T.X. and I.B. prepared and perform cellular level analysis. V.F., C.V., and M.N. performed root apex analysis, starch quantification, and localization. M.A. and Y.-I.C.H. investigated the effect of zaxinone on cytokinin mutants. J.Y.W. and M.J. conducted photosynthetic activities analysis. J.Y.W., S.A., I.B., V.F., L.L., A.R.F. and S.A.-B. analyzed the data. J.Y.W., S.A., A.R.F., and S.A.-B. wrote the manuscript. All authors read and approved the manuscript.

Competing interests

King Abdullah University of Science and Technology (KAUST) has filed a patent (WO2017001927-A1 EP3322294-A1) on zaxinone and its applications.

Additional information

Supplementary information The online version contains supplementary material available at https://doi.org/10.1038/s42003-021-02740-8.

Correspondence and requests for materials should be addressed to Salim Al-Babili.

Peer review information *Communications Biology* thanks the anonymous reviewers for their contribution to the peer review of this work. Primary Handling Editors: Yuan Qin and George Inglis.

Reprints and permission information is available at http://www.nature.com/reprints

Publisher's note Springer Nature remains neutral with regard to jurisdictional claims in published maps and institutional affiliations.

Open Access This article is licensed under a Creative Commons Attribution 4.0 International License, which permits use, sharing, adaptation, distribution and reproduction in any medium or format, as long as you give appropriate credit to the original author(s) and the source, provide a link to the Creative Commons license, and indicate if changes were made. The images or other third party material in this article are included in the article's Creative Commons license, unless indicated otherwise in a credit line to the material. If material is not included in the article's Creative Commons license and your intended use is not permitted by statutory regulation or exceeds the permitted use, you will need to obtain permission directly from the copyright holder. To view a copy of this license, visit http://creativecommons.org/licenses/by/4.0/.

© The Author(s) 2021

2.1 Supplementary material

The supplementary data referred to the Chapter 2 are available at the following link:

https://static-content.springer.com/esm/art%3A10.1038%2Fs42003-021-02740-8/MediaObjects/42003_2021_2740_MOESM1_ESM.pdf

Chapter 3: Zaxinone synthase controls arbuscular mycorrhizal colonization level in rice

The following study, representing the focus of my PhD research across these years, aimed to investigate the role of *OsZAS* and its enzymatic product, zaxinone, in arbuscular mycorrhizal (AM) symbiosis regulation in rice.

As described previously by Wang and colleagues (Wang *et al.* 2019) the loss-of-function *oszas* mutant line showed a reduced AM colonization level. We observed that the zaxinone exogenous application rescued the root growth, but not the mycorrhizal decreased level of the mutant line, and even reduced mycorrhization in wild-type plants. We described that the lower AM colonization level in *oszas* lines is attributable to its lack of strigolactones (SLs) at the early stages of the symbiosis and suggests that, during this phase, OsZAS activity is required for the SLs production, possibly mediated by the Dwarf14-Like (D14L) signaling pathway.
Moreover, we reported that *OsZAS* is expressed in arbuscule-containing cells, and the overexpression of this gene in arbusculed cells (*OsPT11*prom::*OsZAS* transgenic lines) leads to an increased AM colonization level.

Overall, our findings highlighted the importance of *OsZAS* to guarantee the correct extent of AM colonization, acting as a novel part of a regulatory network that involved SLs, which could not be mimicked by an exogenous application of its product zaxinone.

the plant journal

The Plant Journal (2022) **111**, 1688–1700 doi: 10.1111/tpj.15917

Zaxinone synthase controls arbuscular mycorrhizal colonization level in rice

Cristina Votta[1,†], Valentina Fiorilli[1,†], Imran Haider[2], Jian You Wang[2], Raffaella Balestrini[3], Ivan Petřík[4], Danuse Tarkowská[4], Ondřej Novák[4], Akmaral Serikbayeva[2], Paola Bonfante[1], Salim Al-Babili[2,*] and Luisa Lanfranco[1,*]

[1]*Department of Life Sciences and Systems Biology, University of Turin, Turin 10125, Italy,*
[2]*The BioActives Lab, Center for Desert Agriculture (CDA), Biological and Environment Science and Engineering (BESE), King Abdullah University of Science and Technology, Thuwal 23955, Saudi Arabia,*
[3]*National Research Council, Institute for Sustainable Plant Protection, Turin 10135, Italy, and*
[4]*Laboratory of Growth Regulators, Faculty of Science, Palacký University and Institute of Experimental Botany, The Czech Academy of Sciences, Olomouc 78371, Czech Republic*

Received 2 January 2022; revised 5 July 2022; accepted 21 July 2022; published online 25 July 2022.
*For correspondence (e-mail luisa.lanfranco@unito.it or salim.babili@kaust.edu.sa).
†These authors contributed equally to this work.

SUMMARY

The *Oryza sativa* (rice) carotenoid cleavage dioxygenase *OsZAS* was described to produce zaxinone, a plant growth-promoting apocarotenoid. A *zas* mutant line showed reduced arbuscular mycorrhizal (AM) colonization, but the mechanisms underlying this behavior are unknown. Here, we investigated how *OsZAS* and exogenous zaxinone treatment regulate mycorrhization. Micromolar exogenous supply of zaxinone rescued root growth but not the mycorrhizal defects of the *zas* mutant, and even reduced mycorrhization in wild-type and *zas* genotypes. The *zas* line did not display the increase in the level of strigolactones (SLs) that was observed in wild-type plants at 7 days post-inoculation with AM fungus. Moreover, exogenous treatment with the synthetic SL analog GR24 rescued the *zas* mutant mycorrhizal phenotype, indicating that the lower AM colonization rate of *zas* is caused by a deficiency in SLs at the early stages of the interaction, and indicating that during this phase OsZAS activity is required to induce SL production, possibly mediated by the Dwarf14-Like (D14L) signaling pathway. *OsZAS* is expressed in arbuscule-containing cells, and *OsPT11*-prom::*OsZAS* transgenic lines, where *OsZAS* expression is driven by the *OsPT11* promoter active in arbusculated cells, exhibit increased mycorrhization compared with the wild type. Overall, our results show that the genetic manipulation of OsZAS activity *in planta* leads to a different effect on AM symbiosis from that of exogenous zaxinone treatment, and demonstrate that OsZAS influences the extent of AM colonization, acting as a component of a regulatory network that involves SLs.

Keywords: apocarotenoids, arbuscular mycorrhizal symbiosis, GR24, *in situ* hybridization, *OsPT11*, *Oryza sativa*, strigolactones, zaxinone, zaxinone synthase.

INTRODUCTION

Most terrestrial plants, including major crops, establish a root mutualistic association called arbuscular mycorrhizal (AM) symbiosis (Genre *et al.*, 2020) with soil fungi belonging to Glomeromycotina (Spatafora *et al.*, 2016). This evolutionarily ancient interaction implies a reciprocal delivery of nutrients: host plants receive mineral nutrients, mainly phosphorus (P), whereas AM fungi rely on plant-derived fixed carbon (Rich *et al.*, 2017). Additional benefits at organism and ecosystem levels make AM symbiosis a promising component of sustainable agricultural production (Chen *et al.*, 2018; Rillig *et al.*, 2019).

The establishment of AM symbiosis follows a finely tuned colonization pattern. The pre-symbiotic phase is characterized by a molecular dialog involving the release of diffusible signals (Lanfranco, Fiorilli, & Gutjahr, 2018; Lanfranco, Fiorilli, Venice, & Bonfante, 2018) that leads to the activation of the so-called common symbiosis signaling pathway (MacLean *et al.*, 2017). Upon reaching the roots epidermis, the fungus develops adhesion structures

© 2022 The Authors.
The Plant Journal published by Society for Experimental Biology and John Wiley & Sons Ltd.
This is an open access article under the terms of the Creative Commons Attribution License, which permits use, distribution and reproduction in any medium, provided the original work is properly cited.

called hyphopodia that enable the fungus to penetrate host tissues and proliferate *via* intercellular and/or intracellular routes. The symbiotic phase culminates when the fungal hyphae penetrate single cells of the inner cortical layer and form highly branched, tree-shaped structures, called arbuscules. Arbuscules are always enveloped by a plant-derived periarbuscular membrane (PAM) that forms an extensive interface for nutrient exchange (Gutjahr & Parniske, 2013). The PAM is indeed populated by a unique set of proteins, such as Pht1 phosphate (Pi) transporters that are responsible for the uptake of Pi delivered by the fungus (Harrison *et al.*, 2002; Yang *et al.*, 2012).

Phytohormones and other signaling molecules have been shown to play a role mainly in the control of the extent of fungal colonization of the root system (Müller & Harrison, 2019). Strigolactones (SLs), a group of carotenoid-derived hormones, are the best-known molecules active in early plant–AM fungal interaction (Lanfranco, Fiorilli, & Gutjahr, 2018; Lanfranco, Fiorilli, Venice, & Bonfante, 2018). SLs are produced by roots of Pi-starved plants and exported to the rhizosphere, where they stimulate AM fungal metabolism, gene expression and hyphal branching, enhancing the chances of the fungus intercepting host plants (Akiyama *et al.*, 2005; Besserer *et al.*, 2006, 2008). However, the dynamics of SL production and their role during the later steps of AM colonization remain elusive.

The involvement of carotenoid metabolism in AM symbiosis is not restricted to SLs and to the early steps of colonization. Indeed, several lines of evidence suggest the initiation and the development of AM symbiosis are influenced by other apocarotenoids (Fiorilli *et al.*, 2019 and reference therein). Among them, the well-characterized plant hormone abscisic acid (ABA; C_{15}) plays key roles in plant response to abiotic stress (Felemban *et al.*, 2019; Peleg & Blumwald, 2011), regulates plant growth and development, and promotes pathogen defense responses (Ma *et al.*, 2018; Ton *et al.*, 2009) and mycorrhizal colonization (Charpentier *et al.*, 2014; Herrera-Medina *et al.*, 2007; Martín-Rodríguez *et al.*, 2011). The role of ABA in AM symbiosis remains enigmatic: *Solanum lycopersicum* (tomato) ABA mutants showed reduced levels of AM colonization compared with the wild type; however, in *Medicago truncatula*, ABA treatment promotes AM colonization at low concentrations (Charpentier *et al.*, 2014; Herrera-Medina *et al.*, 2007; Martín-Rodríguez *et al.*, 2011). Other works have highlighted an antagonistic interaction between ABA and other hormones involved in AM symbiosis, such as ethylene (Martín-Rodríguez *et al.*, 2011) and gibberellins (GAs) (Floss *et al.*, 2013; Martín-Rodríguez *et al.*, 2016).

In addition, other specific classes of apocarotenoids, such as mycorradicins (C_{14}) and blumenols (C_{13}), are nowadays considered a signature for the establishment of AM symbiosis, as they are specifically accumulated in mycorrhizal plants (Hill *et al.*, 2018; Moreno *et al.*, 2021; Walter *et al.*, 2007; Wang *et al.*, 2018).

The formation of most of the plant apocarotenoid hormones and signaling molecules involves carotenoid cleavage dioxygenases (CCDs), an evolutionarily conserved family of non-heme Fe^{2+}-dependent enzymes (Giuliano *et al.*, 2003; Hou *et al.*, 2016; Moise *et al.*, 2005; Wang *et al.*, 2021). The recent characterization of a member of the overlooked sixth CCD subfamily led to the identification of zaxinone (3-OH-all-*trans*-apo-13-carotenone), an important growth-regulating apocarotenoid metabolite in plants (Ablazov *et al.*, 2020; Wang *et al.*, 2019). The enzyme responsible for its biosynthesis in *Oryza sativa* (rice), zaxinone synthase (ZAS), has a wide distribution in the plant kingdom although a homolog gene is absent in the genomes of non-AM host species, such as *Arabidopsis thaliana* (Wang *et al.*, 2019). A rice mutant (*zas*), defective in *OsZAS*, showed lower zaxinone content and higher levels of SLs in roots, as well as severely retarded root and shoot growth. Exogenous application of zaxinone not only rescued the *zas* root phenotype but also promoted root growth in wild-type plants and reduced SL biosynthesis and exudation under Pi-limited and non-mycorrhizal conditions (Wang *et al.*, 2019). Despite the increased SL content the rice *zas* mutant displayed a reduced, by half, level of AM colonization, compared with wild-type plants. However, the mechanisms leading to the impaired mycorrhization of the mutant line are not known.

The aim of this study was to understand the role of *OsZAS* and its product zaxinone in the regulation of AM symbiosis. It has been shown that zaxinone has no effect on *Gigaspora margarita* spore germination (Wang *et al.*, 2020), suggesting that perturbation of the fungal asymbiotic phase is unlikely. We therefore hypothesized that zaxinone controls the rate of colonization success through interactions with SLs and other hormones. To address these issues we investigated the phytohormone contents of wild-type and *zas* genotypes; we performed different exogenous treatments with the aim to restore the expected colonization level in the *zas* mutant. In addition, we analyzed *OsZAS* gene expression at cellular resolution and we characterized transgenic lines in which the expression of *OsZAS* is driven by a promoter active in arbusculated cells (*OsPT11*prom::*OsZAS* lines). Our findings highlight that the SL profiles of wild-type and *zas* genotypes depend on the plant developmental stage as well as the AM colonization process. In this context we demonstrate that *OsZAS* plays a regulatory role in SL production, possibly through D14-Like signaling, during the early colonization process and, when expressed under the *OsPT11* promoter, promotes fungal intraradical development.

RESULTS AND DISCUSSION

The low colonization level of the *zas* mutant is rescued by SLs, but not by exogenous treatments with zaxinone

As the *zas* mutant displayed decreased mycorrhizal colonization (Wang *et al.*, 2019), we tested whether this

© 2022 The Authors.

phenotype could be restored by an exogenous treatment with zaxinone. Therefore, we applied zaxinone at different concentrations (5, 0.5 and 0.05 μM) on 10-day-old wild-type and *zas* mycorrhizal plants. Although the application of zaxinone successfully rescued most plant phenotypic defects in the mutant, i.e. crown root number, shoot length and biomass (Figure S1), it did not restore the expected AM colonization level, as shown by the quantitative reverse transcription polymerase chain reaction (qRT-PCR) on plant AM marker genes *OsPT11* (Figure 1a) and *OsLysM*, and the fungal *18S* rRNA, and also by a morphological assessment (Figures S2, S3 and S4). In wild-type plants the lowest zaxinone concentration (0.05 μM) had no impact on mycorrhization but the 0.5 or 5 μM concentrations strongly reduced the AM colonization (Figures 1a, S2, S3 and S4). We hypothesize that the reduced mycorrhization of wild-type plants might be caused by the negative impact of exogenous zaxinone on SL biosynthesis (Wang *et al.*, 2019) or to alterations to other plant hormones involved in AM symbiosis. As the terpenoid-derived phytohormones ABA and GAs were shown to play a role in regulating the extent of the AM colonization (Liao *et al.*, 2018; Pozo *et al.*, 2015), we determined their profile in wild-type and *zas* genotypes in non-mycorrhizal and mycorrhizal

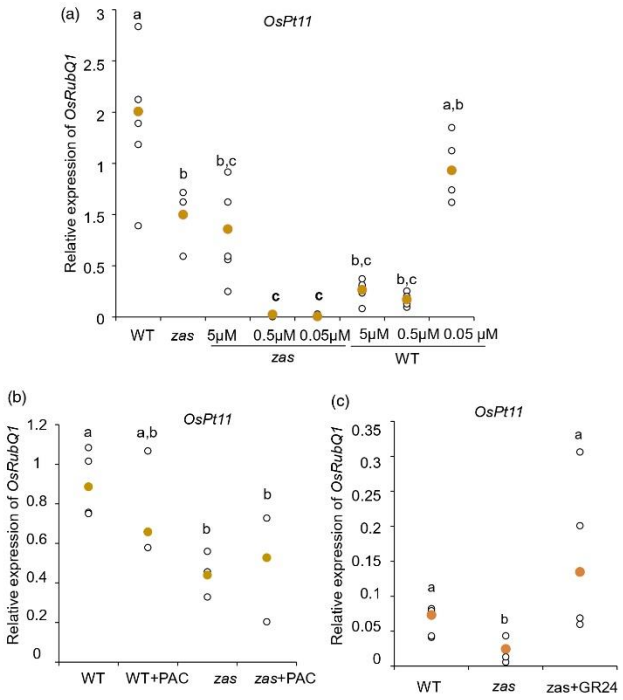

Figure 1. Mycorrhization level in wild-type and *zas* mutant *Oryza sativa* (rice) plants grown under different treatments, evaluated on the abundance of *phosphate transporter 11* gene (*OsPT11*) transcripts. (a) The relative expression levels of *OsPT11* in mycorrhizal Nipponbare wild-type (WT) and *zas* mutant (*zas*) roots, treated or not with different zaxinone concentrations (5, 0.5 and 0.05 μM). Mock treatment has the respective % of acetone used for 5-μM treatments. (b) The relative expression levels of *OsPT11* in mycorrhizal Nipponbare wild-type (WT) and *zas* mutant (*zas*) roots, treated or not with paclobutrazol (PAC). (c) The relative expression level of *OsPT11* in mycorrhizal roots of wild-type (WT), *zas* and *zas* + GR24 plants. All plants were harvested at 35 days post inoculation (35 dpi) with *Funneliformis mosseae*. Zaxinone and PAC treatments were performed once a week directly in the nutrient solution, starting 10 days after mycorrhizal inoculation. GR24 (10 nM) treatment was applied once a week directly in the nutrient solution for the entire growing period. *Ubiquitin* was used as a reference gene. Individual data for each condition are shown as white dots and the median values are shown as yellow dots. For each experiment we considered at least $n = 4$ plants. Different letters represent statistically significant differences ($P < 0.05$, one-way ANOVA; nsd, not statistically different). All experiments were repeated twice with equivalent results.

© 2022 The Authors.

conditions. In non-mycorrhizal conditions, the *zas* mutant displayed a decrease in ABA level at 10 days post germination (10 dpg) and at 45 dpg, whereas we observed an increase in gibberellin (GA_3, GA_{20}, GA_{13} and GA_{29}) content in at least one of the considered time points (Tables S1 and S2). In mycorrhizal plants, *zas* showed an increase in ABA and GA (particularly GA_1 and GA_{20}) content compared with the wild type (Tables S1 and S2). As it has been shown that biologically active GAs suppress arbuscule development and negatively affect the frequency of mycorrhization (Floss *et al.*, 2013), we tested whether an increased level of GA could be responsible for the low level of mycorrhizal colonization in the *zas* mutant. We treated wild-type and *zas* mycorrhizal plants with paclobutrazol (PAC), which reduces GA levels by inhibiting the ent-kaurene oxidase/CYP701 (Rademacher, 2000). The effect of the PAC treatment was verified by the plant growth inhibition in both genotypes (Figure S5). In the *zas* mutants, PAC supply rescued neither the growth phenotype nor the mycorrhizal phenotype (Figures 1b, S5 and S6), indicating that the low level of mycorrhization of the mutant line was not cause by a perturbation in GA levels.

So far, the only well-characterized hormones that promote the establishment of AM symbiosis are SLs, which are active at the early stage of AM interaction (Lanfranco, Fiorilli, Venice, & Bonfante, 2018).

We therefore treated the *zas* mutant with a racemic solution of GR24, an SL synthetic analog, and evaluated the AM colonization at 35 dpi. Notably, the GR24 treatment completely rescued the *zas* mutant mycorrhizal defect (Figures 1c and Figure S7), including the number of hyphopodia and arbuscules that were severely reduced in the untreated *zas* mutant compared with the wild type (Figures 1c and S7). These data suggest that the lower AM colonization rate of *zas* was linked to a deficiency in SLs at the early stage of the AM interaction. In addition, and notably, GR24 treatments did not rescue the *zas* root defects in non-mycorrhizal (Figure S8) and mycorrhizal (Figure S9) conditions, which were by contrast rescued by the exogenous supply of zaxinone (Wang *et al.*, 2019). These results indicate that the mycorrhizal and root defects of the *zas* mutant could be restored by distinct molecules: SLs and zaxinone, respectively, confirming the prominent role of zaxinone in controlling root development (Wang *et al.*, 2019).

We therefore hypothesized a lower SL content in the *zas* mutant during the early stages of AM symbiosis. To investigate this hypothesis we quantified the 4DO content in both genotypes, along a time-course experiment and during the colonization process. A different trend in 4DO content was observed in non-mycorrhizal roots, with the 4DO content increasing along with the developmental stages (7, 21 and 35 dpi; Figure 2a). In mycorrhizal roots the highest 4DO content was observed at 7 dpi (Figure 2a), in agreement with the hypothesis that 4DO content facilitates host plant–AM fungus contact during the early stages (López-Ráez *et al.*, 2015), whereas at later stages (21 and 35 dpi) the 4DO content decreased, as previously observed in different plant species (Figure 2a; Lanfranco, Fiorilli, Venice, & Bonfante, 2018). Concerning the *zas* mutant, in non-mycorrhizal roots the 4DO content increased over time and a higher 4DO content compared with the wild type was observed at 21 dpi, as described by Wang *et al.* (2019). Notably, this difference was not statistically significant at earlier (7 dpi) and later (35 dpi) developmental stages (Figure 2a). These data indicate that, under our growth conditions, the increase in SL content in the *zas* mutant varies depending on the developmental stage, which is a rather common phenomenon for plant hormones (Rizza & Jones, 2019). In mycorrhizal conditions the 4DO profile of the *zas* mutant was similar to that of wild-type plants at 21 and 35 dpi, whereas at 7 dpi no 4DO increment was detected (Figure 2a), suggesting that OsZAS activity is involved in the increase in SLs required at this specific stage of the interaction. The different 4DO contents in wild-type and *zas* mycorrhizal roots at 7 dpi was also supported by the upregulation of *OsCCD8* (*D10*), a key SL biosynthetic gene, which was exclusively observed in wild-type roots upon AM fungal inoculation (Figure S10). These results suggest the occurrence of a regulatory link between OsZAS function and SL production during the early colonization process. The increase of *OsZAS* mRNA abundance and zaxinone content observed at the early stage of AM colonization in wild-type mycorrhizal plants (Wang *et al.*, 2019) is also in line with this model.

The increase of SLs induced by the presence of AM fungus seems, therefore, to be dependent on a fully functional *OsZAS*. To follow this hypothesis we investigated the impact of short-chain chito-oligosaccharides (COs), the early signaling molecules released by AM fungi that are known to trigger symbiotic responses in the host (Genre *et al.*, 2013; Volpe *et al.*, 2020), on SL biosynthetic gene expression in the wild type and the *zas* mutant. We monitored the expression of *OsCCD8* (Figure 2b,c) and *OsMAX1-1400* at 6 h (Figure S10b) and 12 h after treatment with COs (hpt) (Figure S10). As previously reported in other host plants (Giovannetti *et al.*, 2015), no differences were observed in wild-type plants treated with COs, whereas, interestingly, both SL biosynthetic genes were downregulated in the *zas* mutant after the treatment with COs. This accords with a reduced accumulation of SLs in the *zas* mutant at 7 dpi compared with the wild type in mycorrhizal conditions (Figure 2a). Altogether, these data indicate that at the early stage of the AM interaction, *OsZAS* regulates SLs biosynthesis during the plant–fungus molecular dialog.

The cooperation between SLs and zaxinone biosynthesis during the mycorrhizal colonization of rice is also revealed by recent findings on the signaling pathway mediated by

© 2022 The Authors.
The Plant Journal published by Society for Experimental Biology and John Wiley & Sons Ltd.,

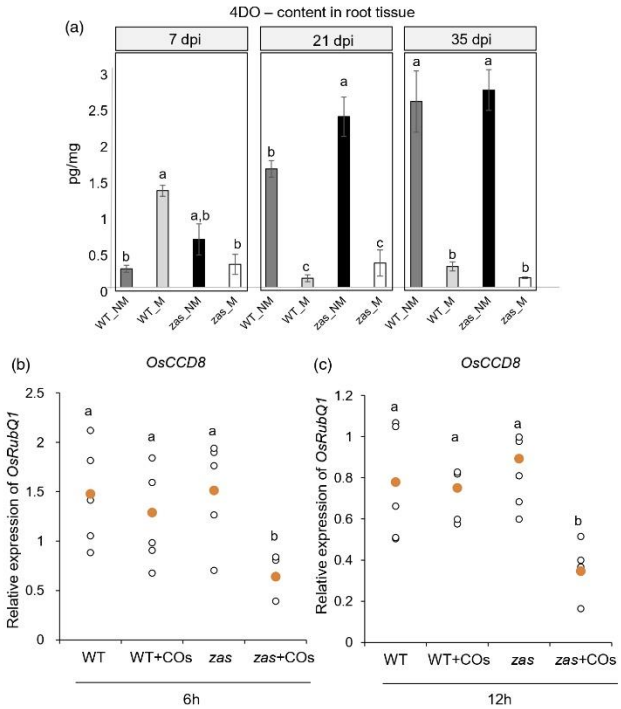

Figure 2. Strigolactone (SL) content and effect of treatment with short-chain chito-oligosaccharides (COs) on *OsCCD8* in wild-type and *zas Oryza sativa* (rice) plants. (a) SL, 4-deoxyorobanchol (4DO), quantification in wild-type and *zas* mutant roots in mycorrhizal and non-mycorrhizal conditions. Roots from mycorrhizal (MYC) and non-mycorrhizal (NM) plants were collected at 7, 21 and 35 days post fungal inoculation (dpi). Three independent biological replicates (each replicate is a pool of 40 plants) have been considered for the analysis. Different letters represent statistically significant differences within time points ($P < 0.05$, one-way ANOVA). (b, c) The relative expression level of *OsCCD8* in non-mycorrhizal roots of wild-type (WT) and *zas* plants treated (+COs) or not with COs. All plants were harvested at 7 days of growth: (b) after 6 hours post-COs treatment (hpt); (c) and after 12 hpt. *Ubiquitin* was used as a reference gene ($n = 5$ plants). Different letters represent statistically significant differences ($P < 0.05$, one-way ANOVA).

the α/β-fold hydrolase Dwarf14-Like (D14L) (Choi *et al.*, 2020), which has been demonstrated to be indispensable for the establishment of AM symbiosis in rice (Gutjahr *et al.*, 2015). It has been shown that D14L signaling positively regulates SL biosynthesis, and therefore AM symbiosis, by eliminating the negative regulator SMAX1 (Choi *et al.*, 2020). Notably, the removal of SMAX1 leads to the upregulation not only of genes involved in SL biosynthesis (i.e. *D10* and *D17*), but also several genes evolutionarily conserved in AM hosts, including *OsZAS*. Therefore, *OsZAS* transcription appears to depend on the activation of the D14L signaling pathway, which is also required to induce SL biosynthetic genes. To support the connection between OsZAS and D14L and SMAX1, we investigated the gene expression level of *OsD14L* and *OsSMAX1* in wild-type and *zas* genotypes and observed a downregulation of both genes in the mutant compared with wild-type plants (Figure 3). Intriguingly, these data suggest that the low colonization level of *zas* could also be related to a downregulation of the D14L signaling pathway, which also negatively impacts SL biosynthesis.

Taken as a whole, our data indicate that OsZAS takes part in the mechanisms underpinning the early symbiotic programs that are instrumental in achieving normal mycorrhization levels, influencing both SLs and D14-L signaling pathways.

© 2022 The Authors.

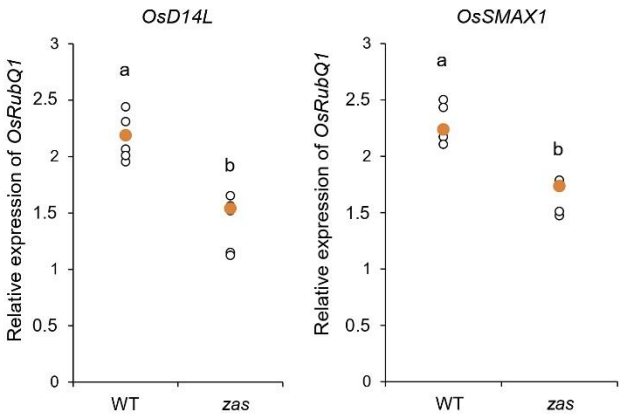

Figure 3. Expression levels of the *Dwarf14-Like* (D14L) signaling pathway in wild-type and *zas* mutant *Oryza sativa* (rice) plants. The relative expression levels of (a) *D14L* and (b) *OsSMAX1* in non-mycorrhizal Nipponbare wild-type (WT) and *zas* mutant (*zas*) roots at 7 days post growth (dpg). *Ubiquitin* was used as a reference gene ($n = 5$ plants). Different letters represent statistically significant differences ($P < 0.05$, one-way ANOVA).

OsZAS mRNA is localized in the arbusculated cells

We showed that *OsZAS* gene expression is induced in rice roots upon mycorrhizal colonization at 7 and 35 dpi (Wang *et al.*, 2019). With the aim to gain data on *OsZAS* spatial expression, *in situ* hybridization assays were performed on roots of 35-dpi plants, which correspond to mature mycorrhizas. *OsZAS* mRNA accumulated in cells with fully developed arbuscules where a strong chromogenic signal was observed (Figure 4a,b). By contrast, no signal was detected in non-colonized cells from mycorrhizal roots (Figure 4a,b) or in sections from mycorrhizal roots hybridized with the *OsZAS* sense probe (Figure 4c,d). Although it was expected to detect *OsZAS* mRNA in non-mycorrhizal roots, no hybridization signal was observed (Figure 4e,f). We hypothesize that in non-mycorrhizal cortical cells the level of *OsZAS* mRNA is relatively low, making it undetectable by *in situ* hybridization; an alternative explanation is that *OsZAS* expression is associated with other parts of the root. *OsZAS* spatial expression in mycorrhizal roots is consistent with transcript accumulation observed in the late stages of mycorrhization (Wang *et al.*, 2019) and suggests an involvement of OsZAS in the functioning of arbusculated cells.

*OsPT11*prom::*OsZAS* lines show higher root colonization and normal arbuscule morphology

As *in situ* hybridization experiments revealed that *OsZAS* mRNA accumulates in arbusculated cells, we then investigated whether the *OsZAS* expression level has an impact on the intraradical phase and, in particular, on arbuscule formation and development. We thus generated rice transgenic lines, called *OsPT11*prom::*OsZAS* (Figure S11), where *OsZAS* expression is driven by the *OsPT11* promoter that is active in arbuscule-containing cells (Paszkowski *et al.*, 2002). Two independent, hygromycin-selected lines, *PT11*prom:*OsZAS_6* (*PT11p::zas6*) and *PT11*prom:*OsZAS_18* (*PT11p::zas18*), were identified by PCR (Figure S11). Both lines were then phenotyped in non-mycorrhizal (Figure S12) and mycorrhizal conditions (Figure S13). The two lines under non-mycorrhizal conditions showed an increased crown root length compared with the wild type (Figure S12). This phenotype was similar to that observed in wild-type plants treated with exogenous zaxinone (Wang *et al.*, 2019). As it has been shown that in the legumes *Medicago truncatula* and *Lotus japonicus* the *OsPT11* homologs are also expressed in root tips when plants are grown under Pi-limiting conditions (Volpe *et al.*, 2016), we verified whether *OsPT11* was also expressed in rice root apexes. Indeed, *OsPT11* transcripts were detected in root tips of both the wild type and *PT11p::zas6* (Figure S14); notably, we also found that also *OsZAS* is expressed in root apexes and, as expected, transcripts were more abundant in the transgenic line compared with the wild type (Figure S14).

These findings clearly show that in non-mycorrhizal roots the *OsPT11* promoter is active in root apices, and that the *OsZAS* gene is also expressed in this root tissue. This spatial expression, together with the fact that *OsZAS* expression is induced by Pi starvation (Wang *et al.*, 2019),

© 2022 The Authors.
The Plant Journal published by Society for Experimental Biology and John Wiley & Sons Ltd.

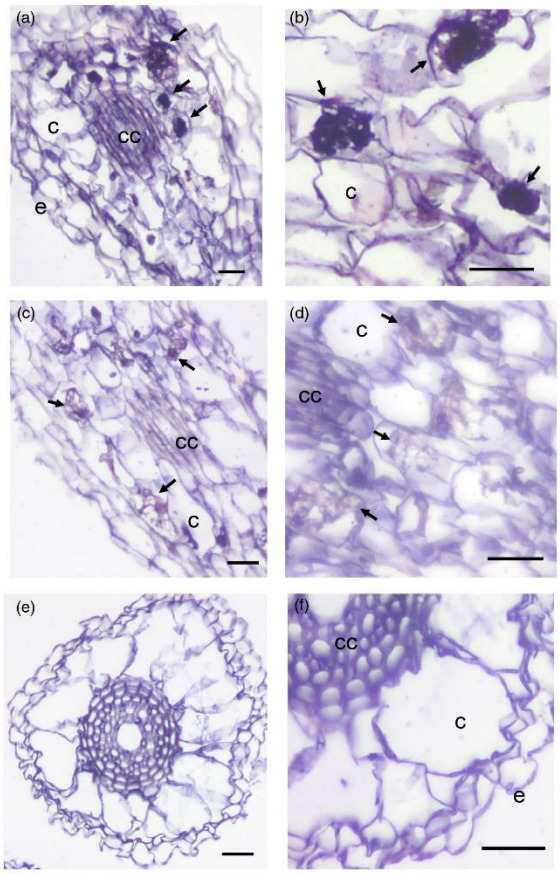

Figure 4. Spatial expression of *OsZAS*. Localization of *OsZAS* mRNA in sections from differentiated regions of inoculated (a–d) and non-inoculated (e, f) roots of *Oryza sativa* (rice) by cold *in situ* hybridization. (a, b) Section of mycorrhizal roots treated with *OsZAS* antisense probe. A strong chromogenic signal, which mirrors the presence of the *OsZAS* transcripts, is visible in arbuscule-containing cells (arrows). (c, d) Section of mycorrhizal roots treated with *OsZAS* sense probe, where a hybridization signal is not evident. Arrows indicate the arbuscule-containing cells that are not labeled. (e, f). Only a very low background is present in uninoculated root segments. c, non-colonized cortical cells; cc, central cylinder; e, epidermal cells. Scale bars: 50 μm.

suggests that OsZAS may be involved in Pi sensing, as has been proposed for the *OsPT11* homologs in legumes (Volpe *et al.*, 2016). The recent discovery that promoters of both *OsZAS* and *OsPT11* genes carry the conserved Pi starvation-responsive motif P1BS, and are transactivated by the central regulator of Pi signaling, PHR2, has strengthened the idea that these genes have been co-opted for the Pi sensing pathway and the establishment of AM symbiosis (Das *et al.*, 2021; Shi *et al.*, 2021).

Moreover, the enhanced growth observed in *OsPT11*-prom::*OsZAS* non-mycorrhizal roots could be the result of localized *OsZAS* upregulation. Indeed, a higher zaxinone content was detected in roots of the non-mycorrhizal *PT11p::zas6* line, whereas the *PT11p::zas18* line showed a

© 2022 The Authors.

higher but not statistically different level compared with the wild type (Figure 5a). At the same growth stage non-mycorrhizal wild-type and *OsPT11*prom::*OsZAS* plants showed similar levels of SLs in the roots (Figure 5b). Remarkably, a higher trend of 4DO level was detected in root exudates of both transgenic lines compared with the wild type (Figure 5c).

It has been shown that hyphopodium formation is severely attenuated in SL-deficient *d17* (*CCD7*) *d10* (*CCD8*) rice double mutants, suggesting that a continuous requirement of SLs is essential for hyphopodia formation and the promotion of secondary infection (Kobae *et al.*, 2018). In accordance with these data, *OsPT11*prom::*OsZAS* lines showed an increased AM colonization level in terms of mycorrhization frequency, number of arbuscules and number of hyphopodia, compared with the wild type (Figure 6a–c), whereas the arbuscule morphology was unaltered (Figure 6e). The morphological results were also confirmed by gene expression analyses in the plant *OsPT11* (Figure 6d).

The data obtained from *OsPT11*prom::*OsZAS* lines confirmed the role of *OsZAS* in promoting the AM colonization level, probably by inducing SL biosynthesis, which triggers hyphopodia formation that in turn promotes arbuscule formation; they also provide evidence that localized *OsZAS* overexpression in arbusculated cells does not have an impact on intracellular fungal morphology (Figure 6e).

CONCLUSION

Overall, the data we present here demonstrate the importance of *OsZAS* to guarantee the correct extent of AM root colonization. In the early stages of the AM interaction, OsZAS modulates AM colonization and exerts its function as a component of a regulatory network that involves SLs and D14L pathways. The overexpression of *OsZAS* in arbusculated cells (*OsPT11*prom::*OsZAS* lines) leads to increased mycorrhization, including an increased abundance of hyphopodia and arbuscules (Figure 7), that could

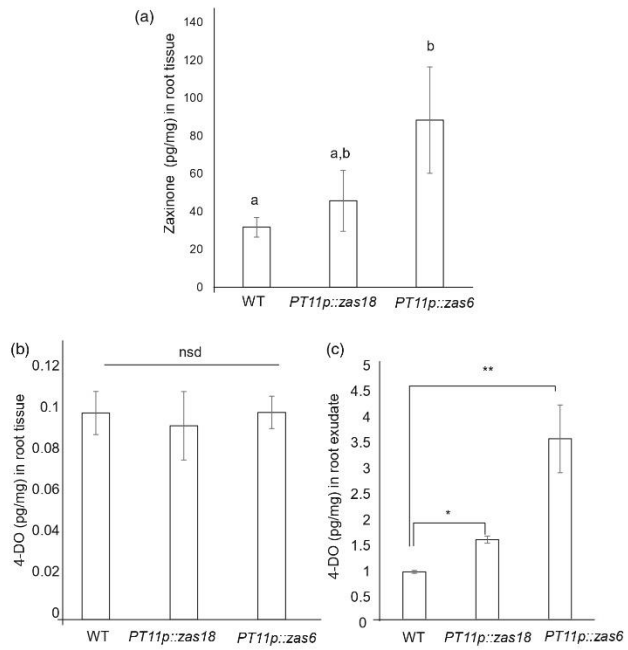

Figure 5. Zaxinone and 4-deoxyorobanchol (4DO) quantification in *OsPT11*prom::*OsZAS* (*PT11p::ZAS*) lines of *Oryza sativa* (rice). Zaxinone (a) and 4DO content in root tissue (b) and in root exudate (c) were quantified in wild-type (WT) and *OsPT11*prom::*OsZAS* (*PT11p::ZAS*) lines in non-mycorrhizal conditions at 21 days post-germination. Means and standard errors of four biological replicates are shown. Different letters indicate significant differences (*$P < 0.05$, **$P < 0.01$).

© 2022 The Authors.
The Plant Journal published by Society for Experimental Biology and John Wiley & Sons Ltd.,
The Plant Journal, (2022), **111**, 1688–1700

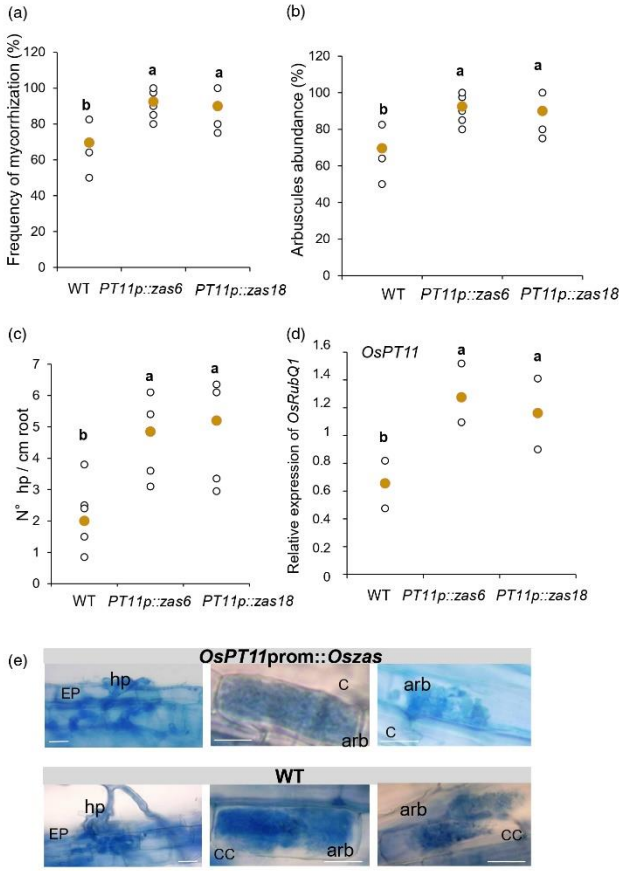

Figure 6. Molecular and phenotypic evaluation of mycorrhizal colonization in *OsPT11*prom::*OsZAS* lines of *Oryza sativa* (rice). After blue cotton staining: (a) the frequency of mycorrhizal (F%) colonization; (b) arbuscule abundance (A%); and (c) number of hyphopodia per cm of roots were evaluated in the wild-type (WT) and *OsPT11*prom::*OsZAS* lines (*PT11p::zas6*; *PT11p::zas18*) ($n = 5$ plants). (d) The relative expression levels of *OsPT11* in mycorrhizal wild-type (WT) and *OsPT11*prom::*OsZAS* lines (*PT11p::zas6*; *PT11p::zas18*). *Ubiquitin* was used as a reference gene ($n = 4$ plants). (e) Root epidermal cells (EP) and cortical cells (CC) from wild-type (WT) and *OsPT11*prom::*OsZAS* lines where hyphopodia (hp) and arbuscules (arb) are shown, respectively; the blue color indicates the cotton blue staining. Scale bars: 80 μm. All plants were harvested 21 days post inoculation with *Funneliformis mosseae*. Individual data for each condition are shown as white dots and median values are shown as yellow dots. Different letters represent statistically significant differences ($P < 0.05$, one-way ANOVA).

be related to the higher content of SLs in the *OsPT11*-prom::*OsZAS* root exudates.

Our results show that the genetic manipulation of OsZAS activity *in planta* leads to a different effect on the AM symbiosis from that of an exogenous zaxinone treatment. Although we found a clear positive correlation between the expression level of *OsZAS* and the extent of colonization, exogenous zaxinone repressed the AM symbiosis, probably through the strong negative impact of a continuous application of this compound on SL biosynthesis (Wang *et al.*, 2019; Figure 7). This highlights that appropriate levels of this apocarotenoid are needed to assist

© 2022 The Authors.

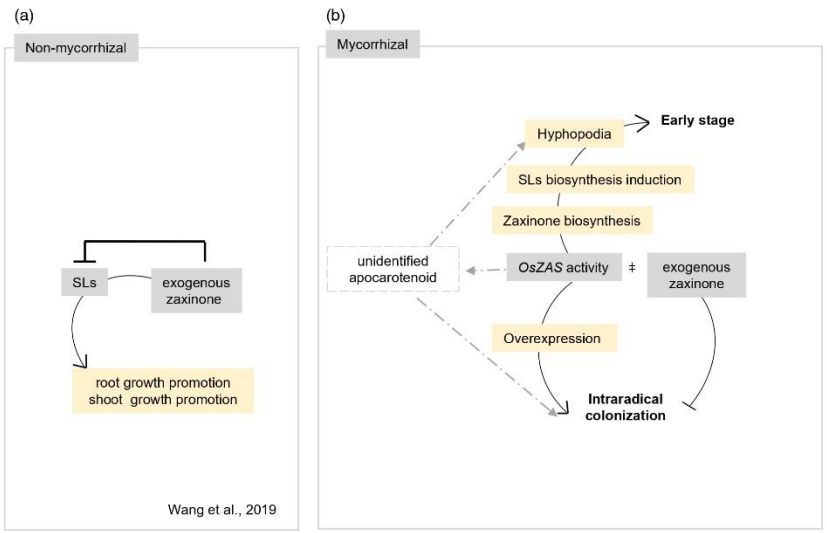

Figure 7. Schematic model for OsZAS and exogenous zaxinone regulation in wild-type *Oryza sativa* (rice) plants grown in non-mycorrhizal (a) and mycorrhizal (b) conditions. (a) In low-Pi conditions, exogenous zaxinone treatment negatively regulates rice SL biosynthesis and release. The zaxinone root and shoot growth promotion requires functional strigolactone (SL) biosynthesis (Wang et al., 2019). (b) OsZAS activity increases zaxinone content and promotes the biosynthesis of SLs and hyphopodia formation in the early stage of mycorrhizal colonization. Overexpression of *OsZAS* under the *OsPT11* promoter increases the intraradical colonization. By contrast, exogenous application of zaxinone negatively impact AM colonization. The discrepancy between the impacts on AM symbiosis of exogenous and endogenous (by OsZAS localized overexpression) accumulation of zaxinone suggests that, besides zaxinone, OsZAS can form *in planta* a yet unidentified apocarotenoid required for optimal mycorrhization (dashed arrow and lines). Positive and negative effects are illustrated by arrows and blunt-ended bars, respectively.

root colonization by AM fungi and that OsZAS activity is involved in a complex network that could not be mimicked by an exogenous supply of its product. One could also speculate that, besides zaxinone, OsZAS can form *in planta* a yet unidentified apocarotenoid required for optimal mycorrhization.

EXPERIMENTAL PROCEDURES

Plant and fungal material

For all the experiments, seeds of the Nipponbare wild-type cultivar, the mutants *zas* (Wang *et al.*, 2019) and *d17* (Butt *et al.*, 2018), and two independent *OsPT11*prom::*Oszas* lines (see Supplemental methods) cv. Nipponbare were germinated as described by Fiorilli *et al.* (2015). Mycorrhizal plants were colonized with *Funneliformis mosseae* (BEG 12; MycAgroLab, http://www.mycagrolab.com) using a fungal inoculum mixed (25%) with sterile quartz sand. Plants were grown and watered as described by Vallino *et al.* (2014). Mycorrhizal roots were stained with cotton blue and the level of mycorrhizal colonization was assessed according to the method described by Trouvelot *et al.* (1986). Hyphopodia were counted manually in each root section.

In situ hybridization and detection

To generate the probe for *in situ* hybridization, a primer pair (Table S3) was used to amplify an *Oszas* sequence of 470 bp. The amplicon was cloned in the sense and antisense orientation into the pCR2.1-TOPO (TA Cloning®; ThermoFisher Scientific, https://www.thermofisher.com) with respect to the T7 promoter. Digoxigenin-labeled RNA probes were synthesized from PCR fragments with T7 or SP6 RNA polymerase, as described by Balestrini *et al.* (1997). Root segments of 1 cm in length were fixed in 4% paraformaldehyde in PBS overnight at 4°C. Samples were then dehydrated in an ethanol series, embedded in Paraplast Plus and sectioned to 8-μm thickness using a rotary microtome. *In situ* hybridization and color development were performed as described by Balestrini *et al.* (1997) (see Supplemental methods). Sections were observed under a light microscope (Primo Star Zeiss; Carl Zeiss, https://www.zeiss.com) with a Leica DFC425 digital camera (Leica Microsystems, https://www.leica-microsystems.com). The experiment was repeated twice with equivalent results.

Phytohormone quantification

For the quantification of targeted plant hormones and related compounds, 20-mg (fresh weight) portions of separately

© 2022 The Authors.

harvested roots were frozen in liquid nitrogen. Concentration levels of endogenous phytohormones (ABA and GAs) were determined in four biological replicates according to the modified method described by Šimura *et al.* (2018) (see Supplemental methods).

To measure SLs and zaxinone contents, the protocol described by Wang *et al.* (2019) was followed for different stages of mycorrhizal symbiosis in a time-course experiment: plants inoculated or not with *F. mosseae* were sampled at 7, 20 and 35 dpi. To measure SL content in root exudate of *OsPT11*prom::*Oszas* lines, the protocol described by Wang *et al.* (2019) was followed.

Plant treatments

For zaxinone treatment, a set of wild-type and *zas* mycorrhizal plants were watered twice a week, once by applying 5, 0.5 or 0.05 μM of the compound in the nutrient solution, starting at 10 dpi to avoid a decrease of SL content during the early phase of AM symbiosis. For SL treatment, 10 nM of the SL analog GR24 (racemic solution) was applied once a week on non-mycorrhizal and mycorrhizal wild-type and *zas* plants. Both zaxinone and GR24 were dissolved in acetone. For treatment with paclobutrazol (PAC), an inhibitor of GA biosynthesis, 10 μM PAC was applied 10 days after AM fungal inoculation once a week for a total period of 4 weeks.

For the chitooligosaccharides (COs; CO4–CO5) treatment, rice seeds of wild-type and *zas* mutant plants were germinated in pots containing sand and incubated for 10 days in a growth chamber under a 14-h light (23°C)/10-h dark (21°C) photoperiod. Seedlings were transferred to 5-ml Eppendorf tubes (https://www.eppendorf.com) and were grown hydroponically in a modified Long Ashton (LA) solution containing 3.2 μM $Na_2HPO_4{\cdot}12H_2O$. A set of wild-type (WT + CO) and *zas* (*zas* + CO) plants were treated with a concentration of 10^{-5} M (Carotenuto *et al.*, 2017) of COs mix, previously withthe protocol from Crosino *et al.* (2021), for 6 and 12 h, and then roots were collected for gene expression analysis.

Nucleic acid extraction and cDNA synthesis

Total RNA was extracted from rice roots using the Plant RNeasy Kit (Qiagen, https://www.qiagen.com). Samples were treated with TURBO™ DNase (Ambion, now ThermoFisher Scientific, https://www.thermofisher.com). The RNA samples were routinely checked for DNA contamination using PCR analysis, using primers for *OsRubQ1* (Güimil *et al.*, 2005). For single-strand cDNA synthesis, about 1000 ng of total RNA was reverse-transcribed using Super-Script II (Invitrogen, now ThermoFisher Scientific, https://www.thermofisher.com).

Real-time quantitative RT-PCR

Quantitative RT-PCR (qRT-PCR) was performed using a Rotor-Gene Q 5plex HRM Platform (Qiagen). Each PCR reaction was carried out as described by Fiorilli *et al.* (2015). All reactions were performed on at least four biological and two technical replicates. The transcript levels of rice *OsPT11* (Güimil *et al.*, 2005), *OsLysM* (Fiorilli *et al.*, 2015), *OsCCD8* and *OsMAX1* (Wang *et al.*, 2019), and *OsD14L* (Gutjahr *et al.*, 2015) and *OsSMAX1* (Choi *et al.*, 2020) and fungal housekeeping *Fm18S* (Balestrini *et al.*, 2007) were normalized using the *OsRubQ1* housekeeping gene (Table S3).

Statistics

Statistical tests were carried out through one-way analysis of variance (one-way ANOVA) and Tukey's *post hoc* test, using a probability level of $P < 0.05$. All statistical elaborations were performed using PAST 2.16 (Hammer *et al.*, 2001).

ACKNOWLEDGEMENTS

This work was supported by baseline funding of the University of Turin (LL and VF) and the Competitive Research Grant (CRG2017) given to SA-B and LL from King Abdullah University of Science and Technology, by the Ministry of Education, Youth and Sports of the Czech Republic (European Regional Development Fund-Project 'Centre for Experimental Plant Biology' no. CZ.02.1.01/0.0/0.0/16_019/0000738), and by the Internal Grant Agency of Palacký University (IGA_PrF_2021_011) to ON. The authors thank Dr Mara Novero and Dr Mara Politi for their technical assistance and Prof. Andrea Genre for providing chito-olisaccharides. Open Access Funding provided by Universita degli Studi di Torino within the CRUI-CARE Agreement.

AUTHOR CONTRIBUTIONS

VF, SA-B, PB and LL designed the investigation. CV and VF performed the cellular and molecular experiments concerning mycorrhization. RB contributed with the *in situ* hybridization. JYW carried out the quantification of zaxinone and SLs. IH and AS generated the transgenic lines. IP, DT and ON conducted the quantification of hormones. All authors contributed to the results and discussion, and VF, SA-B, PB and LL wrote the article.

CONFLICT OF INTEREST

The authors declare that they have no conflicts of interest associated with this work.

DATA AVAILABILITY STATEMENT

The data that support the findings of this study are available from the corresponding authors, upon reasonable request.

SUPPORTING INFORMATION

Additional Supporting Information may be found in the online version of this article.

Figure S1. Phenotypic evaluation of sand-grown *Oryza sativa* (rice) wild-type (WT) and *zas* mycorrhizal plants treated with 5 μM zaxinone.

Figure S2. Analysis of arbuscular mycorrhizal level in wild-type (WT) and *zas* mutant plants under 5 μM zaxinone treatment.

Figure S3. Analysis of arbuscular mycorrhizal level in wild-type (WT) and *zas* mutant plants under 0.5 μM zaxinone treatment.

Figure S4. Analysis of arbuscular mycorrhizal level in wild-type (WT) and *zas* mutant plants under 0.05 μM zaxinone treatment.

Figure S5. Phenotypic evaluation of sand-grown *Oryza sativa* (rice) wild-type (WT) and *zas* plants treated or not with 10 μM paclobutrazol (PAC).

Figure S6. Analysis of arbuscular mycorrhizal level in wild-type (WT) and *zas* mutant plants under 10 μM paclobutrazol (PAC) treatment.

Figure S7. Analysis of arbuscular mycorrhizal level in wild-type (WT) and *zas* mutant plants under 10 nM GR24 treatment.

Figure S8. Effect of GR24 treatment on the shoot and root phenotypes of wild-type (WT) and *zas* mutant plants grown in non-mycorrhizal conditions.

Figure S9. Effect of GR24 treatment on the shoot and root phenotypes of wild-type (WT) and *zas* mutant plants in mycorrhizal conditions.

© 2022 The Authors.

Figure S10. Relative expression level of SL biosynthesis genes (*OsCCD8* and *OsMAX1*) in wild-type (WT) and *zas* mutant plants in the early stage of the AM interaction; the number of hyphopodia per cm of root evaluated in WT, *zas* and *zas* + GR24 plants at 35 dpi; and relative expression level of *OsMAX1-1400* in non-mycorrhizal roots of wild type (WT) and *zas* mutant plants treated (+COs) or not with COs.

Figure S11. Molecular analysis of the *OsPT11prom:OsZAS* transgenic *Oryza sativa* (rice) lines.

Figure S12. Phenotypic evaluation of *Oryza sativa* (rice) wild-type (WT) and *OsPT11*prom::*OsZAS* lines grown in sand in non-mycorrhizal conditions.

Figure S13. Phenotypic evaluation of *Oryza sativa* (rice) wild-type (WT) and *OsPT11*prom::*OsZAS* lines in mycorrhizal conditions grown in sand at 21 days post-inoculation.

Figure S14. Gel electrophoresis of RT-PCR products obtained from RNA of root apexes of non-mycorrhizal wild-type (WT) and *OsPT11*prom::*OsZAS*(*Pt11_6*) line samples using specific primers.

Table S1. ABA quantification (pmol/gFW) in wild-type (WT) and *zas* non-mycorrhizal and mycorrhizal roots in a time-course experiment.

Table S2. Gibberellin quantification (pmol/gFW) in wild-type (WT) and *zas* non-mycorrhizal and mycorrhizal roots.

Table S3. Primer sequences used in this study.

Supplemental methods

REFERENCES

Ablazov, A., Mi, J., Jamil, M., Jia, K.P., Wang, J.Y., Feng, Q. *et al.* (2020) The apocarotenoid zaxinone is a positive regulator of strigolactone and abscisic acid biosynthesis in arabidopsis roots. *Frontiers in Plant Science*, **11**, 578. https://doi.org/10.3389/fpls.2020.00578

Akiyama, K., Matsuzaki, K. & Hayashi, H. (2005) Plant sesquiterpenes induce hyphal branching in arbuscular mycorrhizal fungi. *Nature*, **435**, 824–827.

Balestrini, R., Estanyol, M.J., Puigdoménech, P. & Bonfante, P. (1997) Hydroxyproline-rich glycoprotein mRNA accumulation in maize root cells colonized by an arbuscular mycorrhizal fungus as revealed by in situ hybridization. *Protoplasma*, **198**, 36–42.

Balestrini, R., Gómez-Ariza, J., Lanfranco, L. & Bonfante, P. (2007) Laser microdissection reveals that transcripts for five plant and one fungal phosphate transporter genes are contemporaneously present in arbusculated cells. *Molecular Plant-Microbe Interactions*, **20**, 1055–1062.

Besserer, A., Bécard, G., Jauneau, A., Roux, C. & Séjalon-Delmas, N. (2008) GR24, a synthetic analogue of strigolactones, stimulates the mitosis and growth of the arbuscular mycorrhizal fungus *Gigaspora rosea* by boosting its energy metabolism. *Plant Physiology*, **148**, 402–413.

Besserer, A., Puech-Pagès, V., Kiefer, P., Gomez-Roldan, V., Jauneau, A., Roy, S. *et al.* (2006) Strigolactones stimulate arbuscular mycorrhizal fungi by activating mitochondria. *PLoS Biology*, **4**, e226.

Butt, H., Jamil, M., Wang, J.Y., Al-Babili, S. & Mahfouz, M. (2018) Engineering plant architecture via CRISPR/Cas9-mediated alteration of strigolactone biosynthesis. *BMC Plant Biology*, **18**, 174.

Carotenuto, G., Chabaud, M., Miyata, K., Capozzi, M., Takeda, N., Kaku, H., et al. (2017) The rice LysM receptor-like kinasesOsCERK1 is required for the perception of short-chain chitin oligomers in arbuscularmycorrhizal signaling. *New Phytologist*, **214**, 1440–1446.

Charpentier, M., Sun, J., Wen, J., Mysore, K.S. & Oldroyd, G.E.D. (2014) Abscisic acid promotion of arbuscular mycorrhizal colonization requires a component of the PROTEIN PHOSPHATASE 2A complex. *Plant Physiology*, **166**, 2077–2090.

Chen, M., Arato, M., Borghi, L., Nouri, E. & Reinhardt, D. (2018) Beneficial services of arbuscular mycorrhizal fungi – from ecology to application. *Frontiers in Plant Science*, **9**, 1270.

Choi, J., Lee, T., Cho, J., Servante, E.K., Pucker, B., Summers, W. *et al.* (2020) The negative regulator SMAX1 controls mycorrhizal symbiosis and strigolactone biosynthesis in rice. *Nature Communications*, **11**, 2114.

Crosino, A., Moscato, E., Blangetti, M., Carotenuto, G., Spina, F., Bordignon, S. *et al.* (2021) Extraction of short chain chitooligosaccharides from fungal biomass and their use as promoters of arbuscular mycorrhizal symbiosis. *Scientific Reports*, **11**, 3798.

Das, D., Paries, M., Hobecker, K., Gigl, H., Dawid, C., Lam, H.M. *et al.* (2021) Phosphate starvation response enables arbuscular mycorrhiza symbiosis. bioRxiv preprint https://doi.org/10.1101/2021.11.05.467437

Felemban, A., Braguy, J., Zurbriggen, M.D. & Al-Babili, S. (2019) Apocarotenoids Involved in Plant Development and Stress Response. *Frontiers in Plant Science*, **10**, 1168. https://doi.org/10.3389/fpls.2019.01168

Fiorilli, V., Vallino, M., Biselli, C., Faccio, A., Bagnaresi, P. & Bonfante, P. (2015) Host and non-host roots in rice: cellular and molecular approaches reveal differential responses to arbuscular mycorrhizal fungi. *Frontiers in Plant Science*, **6**, 636.

Fiorilli, V., Wang, J.Y., Bonfante, P., Lanfranco, L. & Al-Babili, S. (2019) Apocarotenoids: old and new mediators of the arbuscular mycorrhizal symbiosis. *Frontiers in Plant Science*, **10**, 1186.

Floss, D.S., Levy, J.G., Levesque-Tremblay, V., Pumplin, N. & Harrison, M.J. (2013) DELLA proteins regulate arbuscule formation in arbuscular mycorrhizal symbiosis. *Proceeding of the National Academy of Science U S A*, **110**, E5025–E5034.

Genre, A., Chabaud, M., Balzergue, C., Puech-Pagès, V., Novero, M., Rey, T. *et al.* (2013) Short-chain chitin oligomers from arbuscular mycorrhizal fungi trigger nuclear Ca2+ spiking in Medicago truncatula roots and their production is enhanced by strigolactone. *New Phytologist*, **198**, 190–202.

Genre, A., Lanfranco, L., Perotto, S. & Bonfante, P. (2020) Unique and common traits in mycorrhizal symbioses. *Nature Review Microbiology*, **18**, 649–660.

Giovannetti, M., Mari, A., Novero, M. & Bonfante, P. (2015) Early Lotus japonicus root transcriptomic responses to symbiotic and pathogenic fungal exudates. *Frontiers in Plant Science*, **6**, 480.

Giuliano, G., Al-Babili, S. & von Lintig, J. (2003) Carotenoid oxygenases: cleave it or leave it. *Trends in Plant Science*, **8**, 145–149.

Güimil, S., Chang, H.S., Zhu, T., Sesma, A., Osbourn, A., Roux, C. *et al.* (2005) Comparative transcriptomics of rice reveals an ancient pattern of response to microbial colonization. *Proceeding of the National Academy of Science U S A*, **102**, 8066–8070.

Gutjahr, C., Gobbato, E., Choi, J., Riemann, M., Johnston, M.G., Summers, W. *et al.* (2015) Rice perception of symbiotic arbuscular mycorrhizal fungi requires the karrikin receptor complex. *Science*, **350**, 1521–1524.

Gutjahr, C. & Parniske, M. (2013) Cell and developmental biology of arbuscular mycorrhiza symbiosis. *Annual Review of Cell and Developmental Biology*, **29**, 593–617.

Hammer, Ø., Harper, D.A.T. & Ryan, P.D. (2001) PAST: paleontological statistics software package for education and data analysis. *Palaeontologia Electronica*, **4**, 9.

Harrison, M.J., Dewbre, G.R. & Liu, J. (2002) A phosphate transporter from *Medicago truncatula* involved in the acquisition of phosphate released by arbuscular mycorrhizal fungi. *The Plant Cell*, **14**, 2413–2429.

Herrera-Medina, M.J., Steinkellner, S., Vierheilig, H., Ocampo Bote, J.A. & García Garrido, J.M. (2007) Abscisic acid determines arbuscule development and functionality in the tomato arbuscular mycorrhiza. *New Phytologist*, **175**, 554–564.

Hill, E.M., Robinson, L.A., Abdul-Sada, A., Vanbergen, A.J., Hodge, A. & Hartley, S.E. (2018) Arbuscular mycorrhizal fungi and plant chemical defence: effects of colonisation on aboveground and belowground metabolomes. *Journal of Chemical Ecology.*, **44**, 198–208.

Hou, X., Rivers, J., León, P., McQuinn, R.P. & Pogson, B.J. (2016) Synthesis and function of apocarotenoid signals in plants. *Trends in Plant Science*, **21**, 792–803.

Kobae, Y., Kameoka, H., Sugimura, Y., Saito, K., Ohtomo, R., Fujiwara, T. *et al.* (2018) Strigolactone biosynthesis genes of rice are required for the punctual entry of arbuscular mycorrhizal fungi into the roots. *Plant Cell Physiology*, **59**, 544–553.

Lanfranco, L., Fiorilli, V. & Gutjahr, C. (2018) Partner communication and role of nutrients in the arbuscular mycorrhizal symbiosis. *New Phytologist*, **220**, 1031–1046.

Lanfranco, L., Fiorilli, V., Venice, F. & Bonfante, P. (2018) Strigolactones cross the kingdoms: plants, fungi, and bacteria in the arbuscular mycorrhizal symbiosis. *Jornal of Experimental Botany*, **69**, 2175–2188.

© 2022 The Authors.
The Plant Journal published by Society for Experimental Biology and John Wiley & Sons Ltd.,

Liao, D., Wang, S., Cui, M., Liu, J., Chen, A. & Xu, G. (2018) Phytohormones regulate the development of arbuscular mycorrhizal symbiosis. *International Journal of Molecular Sciences*, **19**, 3146.

López-Ráez, J.A., Fernández, I., García, J.M., Berrio, E., Bonfante, P., Walter, M.H. *et al.* (2015) Differential spatio-temporal expression of carotenoid cleavage dioxygenases regulates apocarotenoid fluxes during AM symbiosis. *Plant Science*, **230**, 59–69.

Ma, Y., Cao, J., He, J., Chen, Q., Li, X. & Yang, Y. (2018) Molecular mechanism for the regulation of ABA homeostasis during plant development and stress responses. *International Journal of Molecular Sciences*, **19**, 3643.

MacLean, A.M., Bravo, A. & Harrison, M.J. (2017) Plant signaling and metabolic pathways enabling arbuscular mycorrhizal symbiosis. *The Plant Cell*, **29**, 2319–2335.

Martin-Rodríguez, J.A., Huertas, R., Ho-Plágaro, T., Ocampo, J.A., Turečková, V., Tarkowská, D. *et al.* (2016) Gibberellin–abscisic acid balances during arbuscular mycorrhiza formation in tomato. *Frontiers of Plant Science*, **7**, 1273.

Martin-Rodríguez, J.A., León-Morcillo, R., Vierheilig, H., Ocampo, J.A., Ludwig-Müller, J. & García-Garrido, J.M. (2011) Ethylene-dependent/ethylene-independent ABA regulation of tomato plants colonized by arbuscular mycorrhiza fungi. *New Phytologist*, **190**, 193–205.

Moise, A., Vonlintig, J. & Palczewski, K. (2005) Related enzymes solve evolutionarily recurrent problems in the metabolism of carotenoids. *Trends in Plant Science*, **10**, 178–186.

Moreno, J.C., Mi, J., Alagoz, Y. & Al-Babili, S. (2021) Plant apocarotenoids: from retrograde signaling to interspecific communication. *The Plant Journal*, **105**, 351–375.

Müller, L.M. & Harrison, M.J. (2019) Phytohormones, miRNAs, and peptide signals integrate plant phosphorus status with arbuscular mycorrhizal symbiosis. *Current Opinion in Plant Biology*, **50**, 132–139.

Paszkowski, U., Kroken, S., Roux, C. & Briggs, S.P. (2002) Rice phosphate transporters include an evolutionarily divergent gene specifically activated in arbuscular mycorrhizal symbiosis. *Proceeding of the National Academy of Science U S A*, **99**, 13324–13329.

Peleg, Z. & Blumwald, E. (2011) Hormone balance and abiotic stress tolerance in crop plants. *Current Opinion in Plant Biology*, **14**, 290–295.

Pozo, M.J., López-Ráez, J.A., Azcón-Aguilar, C. & García-Garrido, J.M. (2015) Phytohormones as integrators of environmental signals in the regulation of mycorrhizal symbioses. *New Phytologist*, **205**, 1431–1436.

Rademacher, W. (2000) Growth retardants: effects on gibberellin biosynthesis and other metabolic pathways. *Annual Review of Plant Physiology and Plant Molecular Biology*, **51**, 501–531.

Rich, M.K., Nouri, E., Courty, P.E. & Reinhardt, D. (2017) Diet of arbuscular mycorrhizal fungi: bread and butter? *Trends in Plant Science*, **22**, 652–660.

Rillig, M., Aguilar-Trigueros, C.A., Camenzind, T., Cavagnaro, T.R., Degrune, F., Hohmann, P. *et al.* (2019) Why farmers should manage the arbuscular mycorrhizal symbiosis. *New Phytologist*, **222**, 1171–1175.

Rizza, A. & Jones, A.M. (2019) The makings of a gradient: spatiotemporal distribution of gibberellins in plant development. *Current Opinion in Plant Biology*, **47**, 9–15.

Shi, J., Zhao, B., Zheng, S., Zhang, X., Wang, X., Dong, W. *et al.* (2021) A phosphate starvation response-centered network regulates mycorrhizal symbiosis. *Cell 28*, **184**(22), 5527-5540.e18.

Šimura, J., Antoniadi, I., Široká, J., Tarkowská, D., Strnad, M., Ljung, K. *et al.* (2018) Plant hormonomics: multiple phytohormone profiling by targeted metabolomics. *Plant Physiology*, **177**, 476–489.

Spatafora, J.W., Chang, Y., Benny, G.L., Lazarus, K., Smith, M.E., Berbee, M.L. *et al.* (2016) A phylum-level phylogenetic classification of zygomycete fungi based on genome-scale data. *Mycologia*, **108**, 1028–1046.

Ton, J., Flors, V. & Mauch-Mani, B. (2009) The multifaceted role of ABA in disease resistance. *Trends in Plant Science*, **14**, 310–317.

Trouvelot, A., Kough, J. & Gianinazzi-Pearson, V. (1986) Evaluation of VA infection levels in root systems. Research for estimation methods having a functional significance. In: Gianinazzi-Pearson, V. & Gianinazzi, S. (Eds.) *Physiological and Genetical Aspects of Mycorrhizae*. France: INRA-Press, pp. 217–221.

Vallino, M., Fiorilli, V. & Bonfante, P. (2014) Rice flooding negatively impacts root branching and arbuscular mycorrhizal colonization, but not fungal viability. *Plant Cell Environment*, **37**, 557–572.

Volpe, V., Giovannetti, M., Sun, X.G., Fiorilli, V. & Bonfante, P. (2016) The phosphate transporters LjPT4 and MtPT4 mediate early root responses to phosphate status in non mycorrhizal roots: Characterization of AM-induced Pi transporters. *Plant Cell Environment*, **39**, 660–671.

Volpe, V., Carotenuto, G., Berzero, C., Cagnina, L., Puech-Pagès, V. & Genre, A. (2020) Short chainchito-oligosaccharides promote arbuscular mycorrhizal colonization in Medicagotruncatula. *Carbohydrate Polymers*, **229**. 115505

Walter, M.H., Floß, D.S., Hans, J., Fester, T. & Strack, D. (2007) Apocarotenoid biosynthesis in arbuscular mycorrhizal roots: contributions from methylerythritol phosphate pathway isogenes and tools for its manipulation. *Phytochemistry*, **68**, 130–138.

Wang, J.Y., Haider, I., Jamil, M., Fiorilli, V., Saito, Y., Mi, J. *et al.* (2019) The apocarotenoid metabolite zaxinone regulates growth and strigolactone biosynthesis in rice. *Nature Communications*, **10**, 810.

Wang, J.Y., Jamil, M., Lin, P.Y., Ota, T., Fiorilli, V., Novero, M. *et al.* (2020) Efficient mimics for elucidating zaxinone biology and promoting agricultural applications. *Molecular Plant*, **13**, 1654–1661.

Wang, J.Y., Lin, P.Y. & Al-Babili, S. (2021) On the biosynthesis and evolution of apocarotenoid plant growth regulators. *Seminars in Cell and Devlopmental Biology*, **109**, 3–11.

Wang, M., Schäfer, M., Li, D., Halitschke, R., Dong, C., McGale, E. *et al.* (2018) Blumenols as shoot markers of root symbiosis with arbuscular mycorrhizal fungi. *eLife*, **7**, e37093.

Yang, S.Y., Grønlund, M., Jakobsen, I., Grotemeyer, M.S., Rentsch, D., Miyao, A. *et al.* (2012) Non redundant regulation of rice arbuscular mycorrhizal symbiosis by two members of the *PHOSPHATE TRANSPORTER1* gene family. *The Plant Cell*, **24**, 4236–4251.

© 2022 The Authors.

3.1 Supplementary material

The supporting information referred to the Chapter 3 are available at the following link:

https://onlinelibrary.wiley.com/action/downloadSupplement?doi=10.1111%2Ftpj.15917&file=tpj15917-sup-0001-FigureS1-S14-TableS1-S4.pdf

Chapter 4: ZAXINONE SYNTHASE 2 regulates growth and arbuscular mycorrhizal symbiosis in rice

In the following chapter, we investigated the biological function of *OsZAS2*, one of the other three *OsZAS* homologs encoded by the rice genome (Ablazov *et al.* 2022).

From the phylogenetic analysis, OsZAS2 is placed in a clade different from that including ZAS (from now on called ZAS1) and the other two homologs ZAS1b and ZAS1c, indicating a potentially different biological role and possibly enzymatic activity. In this first study, we focused our attention on the expression pattern, subcellular localization, and enzymatic activity of OsZAS2, and we characterized the loss-of-function CRISPR/Cas9-*Oszas2* mutant.
We discovered that OsZAS2 is a plastid-localized enzyme expressed in the root cortex under phosphate deficiency, able to synthetise zaxinone *in vitro.* The *oszas2* mutant lines showed severe growth defects compared and a lower AM colonization level to WT plants, indicating that *OsZAS2* is required for proper rice development and mycorrhization. In conclusion, besides *OSZAS*, *OsZAS2* encodes a zaxinone-forming enzyme that controls rice growth and architecture, strigolactones (SLs) content, and mycorrhization.

In this work, my contribution was to study the involvement of *OsZAS2* in mycorrhization. Using different approaches, I investigated the spatial expression of *OsZAS2* during the AM symbiosis (*in situ* hybridization assay and mycorrhized *pZAS2::GUS* reporter lines), and I characterized with molecular and morphological analysis the *oszas2* mutant mycorrhizal phenotype.

https://doi.org/10.1093/plphys/kiac472 PLANT PHYSIOLOGY 2022: 00: 1–18

Plant Physiology®

Research Article

ZAXINONE SYNTHASE 2 regulates growth and arbuscular mycorrhizal symbiosis in rice

Abdugaffor Ablazov [1,2], Cristina Votta [3], Valentina Fiorilli [3], Jian You Wang [1], Fatimah Aljedaani [2,4], Muhammad Jamil [1], Aparna Balakrishna [1], Raffaella Balestrini [5], Kit Xi Liew [1], Chakravarthy Rajan [1], Lamis Berqdar [1], Ikram Blilou [2,4], Luisa Lanfranco [3] and Salim Al-Babili [1,2,*]

1 Biological and Environmental Sciences and Engineering Division, Center for Desert Agriculture (CDA), King Abdullah University of Science and Technology (KAUST), The BioActives Lab, Thuwal, 23955-15 6900, Saudi Arabia
2 The Plant Science Program, Biological and Environmental Science and Engineering Division, King Abdullah University of Science and Technology (KAUST), Thuwal, Saudi Arabia
3 Department of Life Sciences and Systems Biology, University of Torino, Torino 10125, Italy
4 Plant Cell and Developmental Biology, Biological and Environmental Sciences and Engineering (BESE), King Abdullah University of Science and Technology (KAUST), Thuwal 23955-6900, Saudi Arabia
5 National Research Council, Institute for Sustainable Plant Protection, Turin 10135, Italy

*Author for correspondence: salim.babili@kaust.edu.sa
These authors contributed equally (A.A and C.V.).
S.A.B. and A.A. conceived and designed the research. S.A.B. supervised the experiments. A.A. generated transgenic lines with the help of CR. C.V., V.F., R.B., and L.L. planned and performed the mycorrhization experiments. M.J. and A.A. conducted the Striga seed germination assays. A.B. performed the in vitro assays. A.A. characterized the transgenic lines with help of M.J. and L.B. J.Y.W., K.X.L., and A.A. performed the metabolite analysis. F.A. performed the subcellular localization experiment. I.B. supervised the subcellular localization and microscopy experiments. A.A. analyzed the data and generated the figures and wrote the manuscript with the help of J.Y.W., V.F., C.V., L.L., and F.A. S.A.B. edited and approved the article.
The author responsible for distribution of materials integral to the findings presented in this article in accordance with the policy described in the Instructions for Authors (https://academic.oup.com/plphys/pages/general-instructions) is Salim Al-Babili (salim.babili@kaust.edu.sa).

Abstract

Carotenoid cleavage, catalyzed by CAROTENOID CLEAVAGE DIOXYGENASEs (CCDs), provides signaling molecules and precursors of plant hormones. Recently, we showed that zaxinone, a apocarotenoid metabolite formed by the CCD ZAXINONE SYNTHASE (ZAS), is a growth regulator required for normal rice (*Oryza sativa*) growth and development. The rice genome encodes three *OsZAS* homologs, called here *OsZAS1b*, *OsZAS1c*, and *OsZAS2*, with unknown functions. Here, we investigated the enzymatic activity, expression pattern, and subcellular localization of OsZAS2 and generated and characterized loss-of-function CRISPR/Cas9 (clustered regularly interspaced short palindromic repeats and associated protein 9)-*Oszas2* mutants. We show that OsZAS2 formed zaxinone in vitro. OsZAS2 was predominantly localized in plastids and mainly expressed under phosphate starvation. Moreover, *OsZAS2* expression increased during mycorrhization, specifically in arbuscule-containing cells. *Oszas2* mutants contained lower zaxinone content in roots and exhibited reduced root and shoot biomass, fewer tillers, and higher strigolactone (SL) levels. Exogenous zaxinone application repressed SL biosynthesis and partially rescued the growth retardation of the *Oszas2* mutant. Consistent with the *OsZAS2* expression pattern, *Oszas2* mutants displayed a lower frequency of arbuscular mycorrhizal colonization. In conclusion, *OsZAS2* is a zaxinone-forming enzyme that, similar to the previously reported OsZAS, determines rice growth, architecture, and SL content, and is required for optimal mycorrhization.

Received July 21, 2022. Accepted September 09, 2022. Advance access publication October 12, 2022
© The Author(s) 2022. Published by Oxford University Press on behalf of American Society of Plant Biologists.
This is an Open Access article distributed under the terms of the Creative Commons Attribution License (https://creativecommons.org/licenses/by/4.0/), which permits unrestricted reuse, distribution, and reproduction in any medium, provided the original work is properly cited.

Open Access

Introduction

Carotenoids are tetraterpene (C_{40}) pigments consisting of long hydrocarbon chains with a conjugated double-bond system. In plants, carotenoids serve as a crucial component of photosynthesis, colorants, and antioxidants (Bouvier et al., 2003; Fraser and Bramley, 2004; Ballottari et al., 2014; Nisar et al., 2015; Hashimoto et al., 2016; Rodriguez et al., 2018; Zheng et al., 2020). In addition, the breakdown of carotenoids gives rise to a diverse group of metabolites called apocarotenoids, which includes pigments, scents, signaling molecules, growth regulators, and the precursors of the phytohormones strigolactone (SL) and abscisic acid (ABA) (Felemban et al., 2019; Moreno et al., 2021; Wang et al, 2021a; Liang et al., 2021; Zheng et al., 2021). ABA is the most-studied plant apocarotenoid hormone and a key player in plant response to abiotic and biotic stress (Peleg and Blumwald, 2011), regulation of seed maturation, dormancy, and shoot and root growth (Nambara and Marion-Poll, 2005; Moreno et al., 2021). SLs regulate a series of developmental processes. They are best known for inhibiting shoot branching/tillering, regulating root architecture, secondary growth, and senescence, and for their contribution to biotic and abiotic stress responses (Gomez-Roldan et al., 2008; Umehara et al., 2008; Ha et al., 2014; Al-Babili and Bouwmeester, 2015; Decker et al., 2017; Waters et al., 2017; Jia et al., 2019). However, SLs were originally discovered as host root-released germination stimulants for seeds of root parasitic weeds (Xie et al., 2010). Later on, they were identified as the plant-released hyphal branching factor for arbuscular mycorrhizal (AM) fungi, which paved the way for establishing plant–AM symbiosis (Akiyama et al., 2005). AM fungi symbiotic association provides the host plant with minerals, mainly phosphorus (P) and nitrogen (N), and the AM fungi with carbohydrates and lipids (Wang et al., 2017). AM symbiosis is widely distributed and formed by most of the land plants, mirroring its importance for their growth and survival (Gutjahr and Parniske, 2013; Wang et al., 2017; Fiorilli et al., 2019).

Recent studies unraveled the presence of several apocarotenoid signaling molecules, such as anchorene, iso-anchorene, β-cyclocitral, and zaxinone. Anchorene is a carotenoid-derived dialdehyde responsible for anchor root formation in Arabidopsis (*Arabidopsis thaliana*) (Jia et al., 2019), while its structural isomer iso-anchorene inhibits Arabidopsis root growth (Jia et al., 2021). β-Cyclocitral regulates root growth and is a retrograde signaling molecule that mediates singlet oxygen response and improves the high light tolerance by modulating the expression of oxidative stress-responsive genes (Ramel et al., 2012; Dickinson et al., 2019). Zaxinone is a regulatory metabolite, which is required for normal rice (*Oryza sativa*) growth and development and negatively regulates SL biosynthesis (Wang et al., 2019, 2020). Multi-omics study revealed that zaxinone also modulates cytokinin homeostasis and that its growth-promoting effect is likely caused by increased sugar metabolism in rice roots (Wang et al., 2021a, 2021b). However, exogenous application of zaxinone to Arabidopsis simultaneously increased both SL and ABA content (Ablazov et al., 2020), suggesting that it might act as a stress signal in Arabidopsis (Ablazov et al., 2020).

Apocarotenoid production in plants is mediated by carotenoid cleavage dioxygenases (CCDs), which cleave double bonds in carotenoid backbones and exhibit different substrate and cleavage site specificities (Moise et al., 2014; Dhar et al., 2020). The diversity of CCDs gives rise to a wide spectrum of apocarotenoids with unique features and functions (Giuliano et al., 2003; Auldridge et al., 2006; Ahrazem et al., 2016). Based on phylogenetic analysis and enzymatic activity, plant CCDs build six subfamilies; NINE-CIS-EPOXY CAROTENOID DIOXYGENASEs (NCEDs), CCD1, CCD4, CCD7, CCD8, and ZAXINONE SYNTHASE (ZAS) (Wang et al., 2019). NCEDs are involved in ABA biosynthesis and catalyze the cleavage of the C11, C12 (or C11′, C12′) double bond in 9-cis-epoxy carotenoids to yield the ABA precursor xanthoxin (Schwartz et al., 1997; Chernys and Zeevart, 2000). In contrast to other CCD types investigated so far, CCD1 enzymes are localized in the cytosol. Moreover, they are characterized by wide substrate and regio-specificity, cleaving many carotenoid and apocarotenoid substrates and producing dialdehyde products and volatiles that contribute to the flavor and aroma in many plants (Vogel et al., 2008; Ilg et al., 2009, 2014). CCD4 enzymes cleave the C9–C10 or C9′–C10′ double bond in bicyclic carotenoids, giving rise to C_{13} volatiles and C_{27}-apocarotenoids (Bruno et al., 2015, 2016). CCD7 and CCD8 act sequentially on 9-cis-β-carotene to produce carlactone, the central intermediate of SL biosynthesis, via the intermediate 9-cis-β-apo-10′-carotenal formed by CCD7 along with the volatile β-ionone (Alder et al., 2012; Bruno et al., 2014). Carlactone is further modified by cytochrome P450s (711 clades), such as the Arabidopsis MORE AXILLARY GROWTH1 or the rice carlactone oxidase, leading to the formation of canonical and noncanonical SLs (Abe et al., 2014; Zhang et al., 2014; Jia et al., 2018; Ito et al., 2022).

ZAS is a recently discovered member of the CCD family, which cleaves the apocarotenoid apo-10-zeaxanthinal (C_{27}) at the C13, C14 double bond, forming the C_{18}-apocarotenoid zaxinone (Wang et al., 2019). Zaxinone is a growth-promoting metabolite required for normal rice growth and a negative regulator of SL biosynthesis and release (Wang et al., 2019, 2020). A rice loss-of-function *zas* mutant showed reduced root zaxinone level, retarded growth, that is, lower root and shoot biomass, tiller number, and higher SL content (Wang et al., 2019). Confirming its biological function, the exogenous application of zaxinone restored several phenotypes of the *zas* mutant (Wang et al., 2019). Though all other CCD subfamilies are conserved, nonmycorrhizal species, such as *A. thaliana* and other members of the *Brassicales*, lack ZAS orthologs, indicating a role of ZAS in AM symbiosis (Fiorilli et al., 2019; Wang et al., 2019). Indeed, the *zas* mutant displayed a lower level of AM colonization compared to the wild-type (WT; Wang et al., 2019).

The rice genome contains three *OsZAS* homologs, previously called *OsZAS-L1* (renamed here to *OsZAS1b*), *OsZAS-L2* (renamed here to *OsZAS1c*), and *OsZAS-L3* (renamed here to *OsZAS2*) with unknown function (Wang et al., 2019). In this study, we investigated the biological function of OsZAS2 by studying its enzymatic activity and by generating and characterizing the corresponding mutant and GUS reporter lines. Obtained data suggest that OsZAS2 is a non-redundant, root- and arbusculated cell-localized zaxinone-forming enzyme required for proper growth and normal SL homeostasis and mycorrhization level.

Results

OsZAS2 represents a separate clade in the ZAS CCD subfamily

To clarify the phylogenetic relationship of *OsZASs* (*OsZAS*, *OsZAS-L1*, *OsZAS-L2*, and *OsZAS-L3*) with other plant ZAS genes, we first constructed a phylogenetic tree, using ZAS sequences from selected monocot and dicot species (Supplemental Table S2; Supplemental File S1). This analysis divided the ZAS proteins into five clades (I–V) (Figure 1A). Three OsZAS enzymes, including OsZAS (Os09g0321200), OsZAS-L1 (Os08g0369800), and OsZAS-L2 (Os08g0371608) grouped in clade I, while OsZAS-L3 (Os06g0162550) clustered in clade II. Based on this analysis we renamed OsZAS-L1, OsZAS-L2, and OsZAS-L3 to OsZAS1b, OsZAS1c, and OsZAS2, respectively (Figure 1A). The clades III, IV, and V contain only enzymes from dicot species, which we called ZAS3, ZAS4, and ZAS5 (Supplemental Table S3).

OsZAS2 is a zaxinone-forming enzyme

Next, we investigated the enzymatic activity of OsZAS2: we expressed OsZAS2 fused to maltose-binding protein (MBP) in *Escherichia coli* cells and incubated the soluble fraction of these cells with different apocarotenoids, that is, β-apo-10′-(C_{27}), 9-cis-β-apo-10′-(C_{27}), β-apo-12′-(C_{25}), and apo-8′-zeaxanthinal (3-OH-β-apo-8′-carotenal, C_{30}) (Supplemental Figure S1). In addition, we incubated the MBP–OsZAS2 fusion with carotenoids, that is, β-carotene, zeaxanthin, and lutein (Supplemental Figure S1). Finally, we performed in vivo activity test by expressing a thioredoxin–OsZAS2 fusion in β-carotene, zeaxanthin, and lycopene-accumulating *E. coli* cells. In all these assays, we only detected a conversion of apo-10′-zeaxanthinal (C_{27}) that was cleaved by OsZAS2 at the C13, C14 double bond, yielding zaxinone (3-OH-β-apo-13-carotenone, C_{18}) and a predicted C_9-dialdehyde (Figure 1B). We confirmed the identity of zaxinone by UHPLC (Ultra High Performance Liquid Chromatography) and LC–MS (Liquid chromatography–mass spectrometry) analysis, using a synthetic standard (Figure 1, C and D).

OsZAS2 is predominantly localized in the plastid

The ChloroP Server program (Emanuelsson et al., 1999) predicts the presence of a plastid transit peptide in the OsZAS2, indicating a plastid localization of this enzyme. To confirm this prediction, we transiently expressed *OsZAS2* cDNA fused with the sequence encoding mNeonGreen fluorescence protein under the control of the 35S promoter (*35S:OsZAS2:mNeonGreen*) in *Nicotiana benthamiana* leaves epidermal cells, alone or together with the gene encoding the plasma membrane specific Turquoise2 marker protein (*35S::Lit6BmTurquoise2*) (Cutler et al., 2000). As shown in Figure 2A, the green fluorescent signal of the OsZAS2 fusion clearly overlapped with the red autofluorescence of chlorophyll A. However, it also showed co-localization with the 35S::Lit6B Turquoise marker of the plasma membrane. Overall, we observed a stronger green fluorescent signal of the OsZAS2 fusion in plastids than in plasma membranes, supporting a plastid localization of this enzyme.

OsZAS2 is expressed in roots and induced under low Pi

To determine the expression pattern of *OsZAS2*, we generated the *GUS* reporter lines *pOsZAS2::GUS11* and *pZAS2::GUS18* by fusing a 1.2-kb upstream *OsZAS2* fragment to *GUS* and transforming the resulting *pZAS2-MDC162* plasmid into rice. The staining of the two reporter lines showed that *OsZAS2* expression significantly increased under low Pi conditions, while the GUS signal was not detectable at all under normal conditions (Figure 2B). Moreover, the GUS signal increased substantially toward the tip of the primary and crown roots. The RT-qPCR (Reverse transcription-quantitative polymerase chain reaction) analysis also showed that the *OsZAS2* transcript level increased about 20-fold under low Pi compared to normal (+ Pi) conditions in roots (Figure 2D). We further investigated OsZAS2 localization at the cellular level using cross-sectioning. Using a confocal microscope, we detected a strong GUS signal in the exodermis of primary roots, while the cortex, epidermis, and other root tissues showed only mild signals (Figure 2C).

CRISPR/Cas9-generated *Oszas2* mutant lines show severe growth defects

Next, we generated *Oszas2* mutant knockout lines in the Dongjin (DJ) variety by employing CRISPR/Cas9. For this purpose, we used two guide RNAs, gRNA1 and gRNA2, which target coding sequence in exons 1 and 2, respectively (Figure 3A). We identified three independent *Oszas2* mutants, *zas2-d*, *zas2-g*, and *zas2-a*, with mutations in the first and second exon (Figure 3A), which resulted in premature stop codons (Supplemental Figure S5). To validate the function of OsZAS2 as a zaxinone synthesizing enzyme in planta, we quantified zaxinone in roots of the three mutant lines grown hydroponically under normal and low Pi supply. Compared to WT, zaxinone content was reduced up to 45% in *Oszas2* mutant lines under normal conditions (Figure 3C), but was unchanged under low Pi conditions (Supplemental Figure S4A). Next, we grew the mutant lines in soil and characterized them at the seedling and mature stage. At seedling stage, *Oszas2* mutants displayed shorter roots and shoots and a striking reduction in root and shoot biomass (Figure 3, B and E–H). Moreover, they produced one tiller on average, while the WT developed three (Figure 3D). The low-tillering and reduced shoot biomass phenotypes remained pronounced after growing the mutants for 3 months in GH and

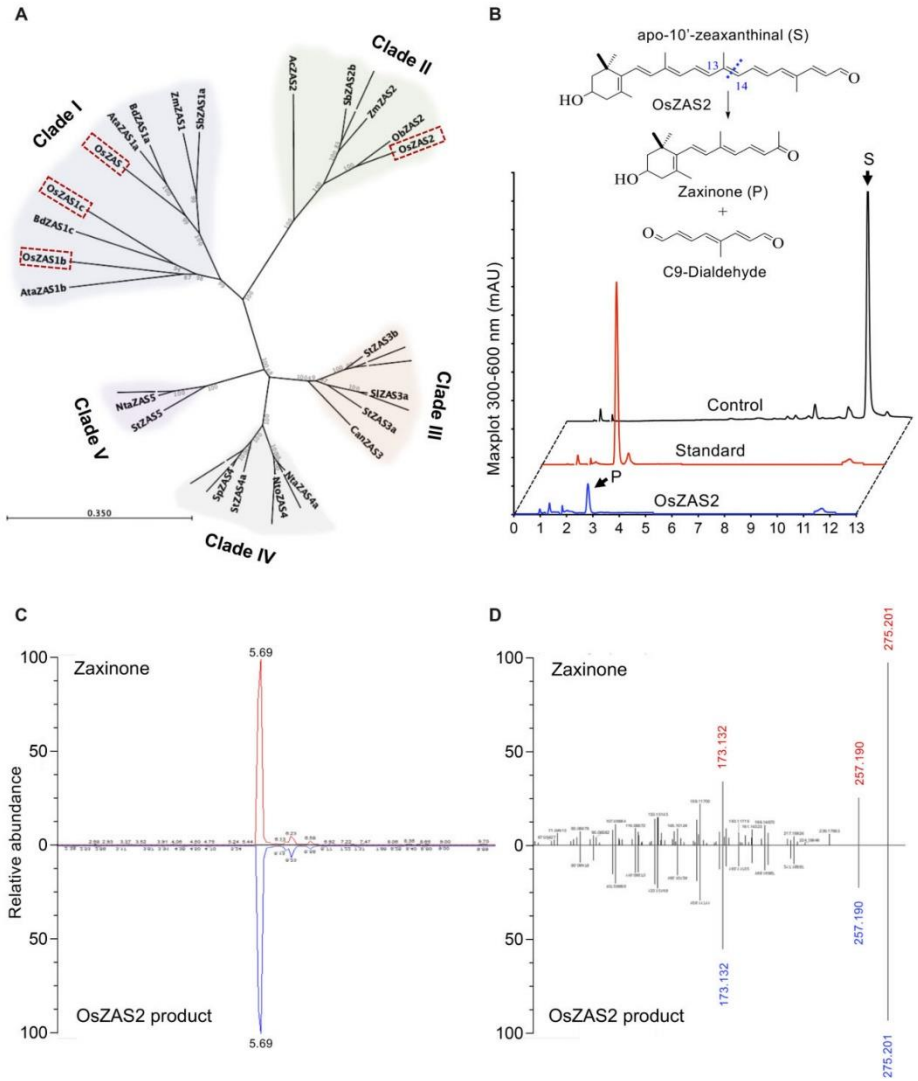

Figure 1 Phylogenetic analysis of ZAS enzymes and analysis of OsZAS2 enzymatic activity. A, Phylogenetic tree analysis of ZAS orthologs from selected monocot and dicot plants, showing bootstrap values on nodes of each cluster. Dashed rectangles represent rice ZAS members. The scale bar represents the number of amino acid change per site. B, HPLC chromatogram of in vitro incubation of OsZAS2 with apo-10′-zeaxanthinal (I) yielded zaxinone (II) and a presumed C_9-dialdehyde. The maximum absorbance (mAU) peak for substrate and product is shown at 347 and 450 nm (mAU), respectively. The representation of zaxinone production in the Figure B adapted from Wang et al. (2019), which is permitted to adaptation under a Creative Commons Attribution 4.0 International License. C, Verification of OsZAS2 in vitro product, based on retention time, (D) accurate mass and MS/MS pattern and in comparison to zaxinone standard.

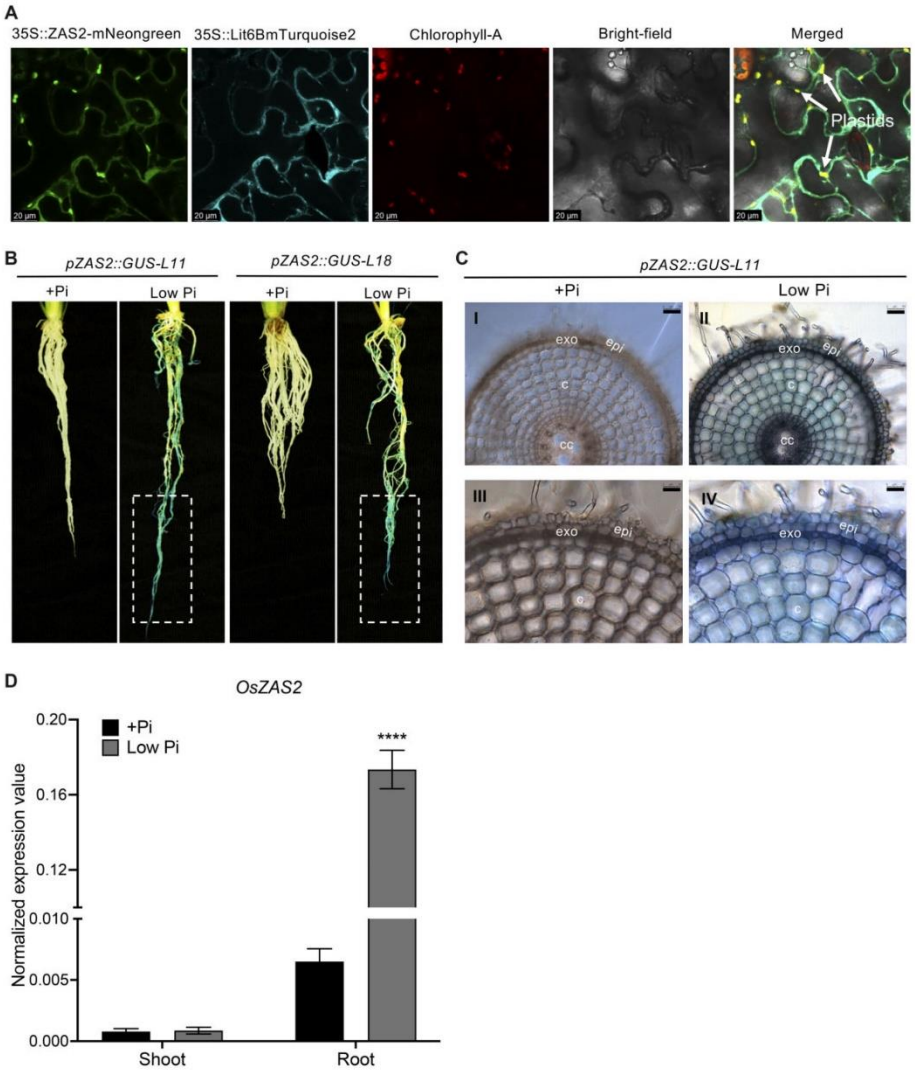

Figure 2 *OsZAS2* subcellular localization and expression pattern. A, Subcellular localization of OsZAS2 transiently expressed in *N. benthamiana* epidermis leave tissue. B, GUS staining of roots of two independent *pZAS2:GUS* reporter lines (*pZAS2::GUS-L11*, *pZAS2::GUS-L18*) under normal (+Pi) and low Pi conditions. Dash rectangle emphasizes the root tip. C, Cross-section of *pZAS2:GUS11* line primary root was examined with two different resolutions under microscope: in the first resolution (parts I and II, bars correspond to 50 μm) all types of tissues were observed while the second resolution of the same samples (parts III and IV, bars correspond to 25 μm) showed a close view of epidermal and cortex cells. Exo, exoderms; epi, epidermis; c, cortex; cc, central cylinder. D, Normalized expression value of OsZAS2 under normal (+Pi) and low Pi conditions in root and shoot tissue of 21-day-old rice plants. Values in (D) are means ± SD ($n = 4$). Student's t test used for the statistical analysis (****$P \leq 0.0001$).

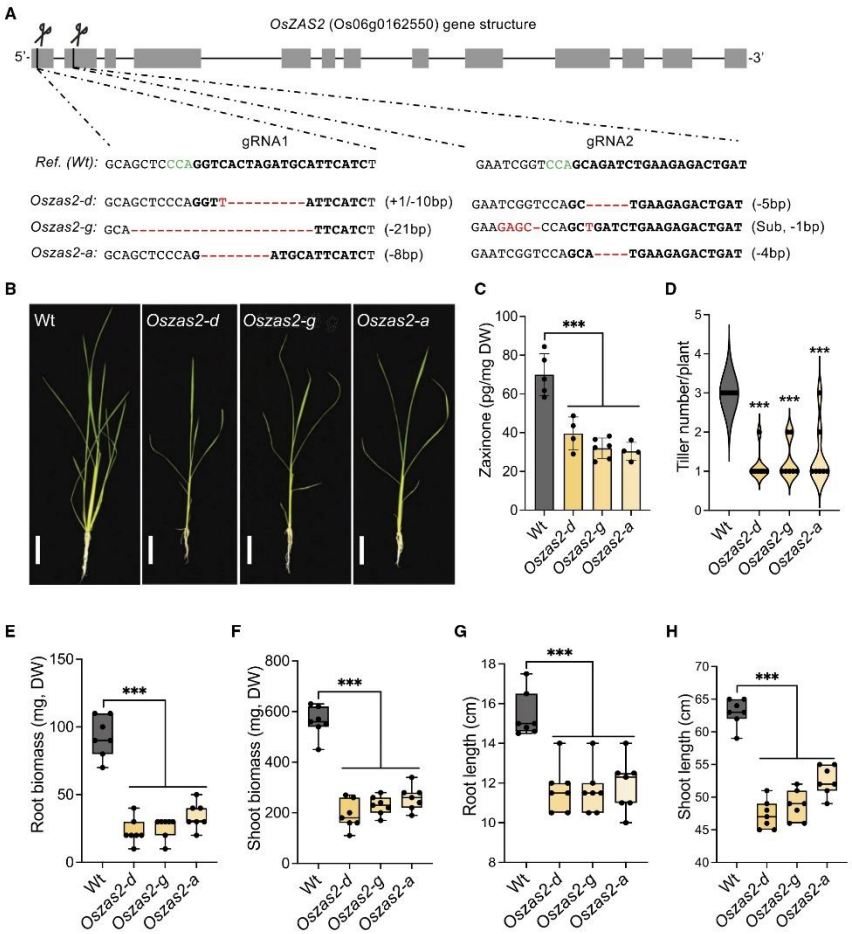

Figure 3 Characterization of CRISPR/Cas9-mediated *Oszas2* mutant lines at the seedling stages. A, Schematic representation of three individual mutations of *OsZAS2* gene generated by CRISPR–Cas9. B, The seedling phenotype of WT (DJ) and three independent *Oszas2* mutants. The scale bar in the pictures represents 7.5 cm. C, Quantification of zaxinone content in WT and *Oszas2* mutants roots. D–H, Root biomass (D), shoot biomass (E), root length (F), shoot length (G), and tiller number (H) of the WT and *Oszas2* mutants are shown in (B). Boxes in boxplots represent the median, first and third quartile. The minimum and maximum values are shown with the length of the whiskers. Dots represent the biological replicates. Values in (C–H) are means ± SD ($n \geq 4$). Student's *t* test used for the statistical analysis (***$P \leq 0.001$).

caused a significant reduction in grain weight per plant, compared to the corresponding WT (Figure 4, A–E).

OsZAS2 is involved in AM colonization

The expression analysis of *OsZAS2* in whole roots at early and late stages of AM colonization revealed an upregulation at 21 days postinoculation (dpi) (Supplemental Figure S2A), when arbuscules are present, as witnessed by the abundance of the AM-inducible plant marker *OsPT11* transcript (Paszkowski et al., 2002; Supplemental Figure S2B). To obtain deeper insights into the spatial expression of *OsZAS2* during mycorrhization, we inoculated *pZAS2::GUS* reporter lines

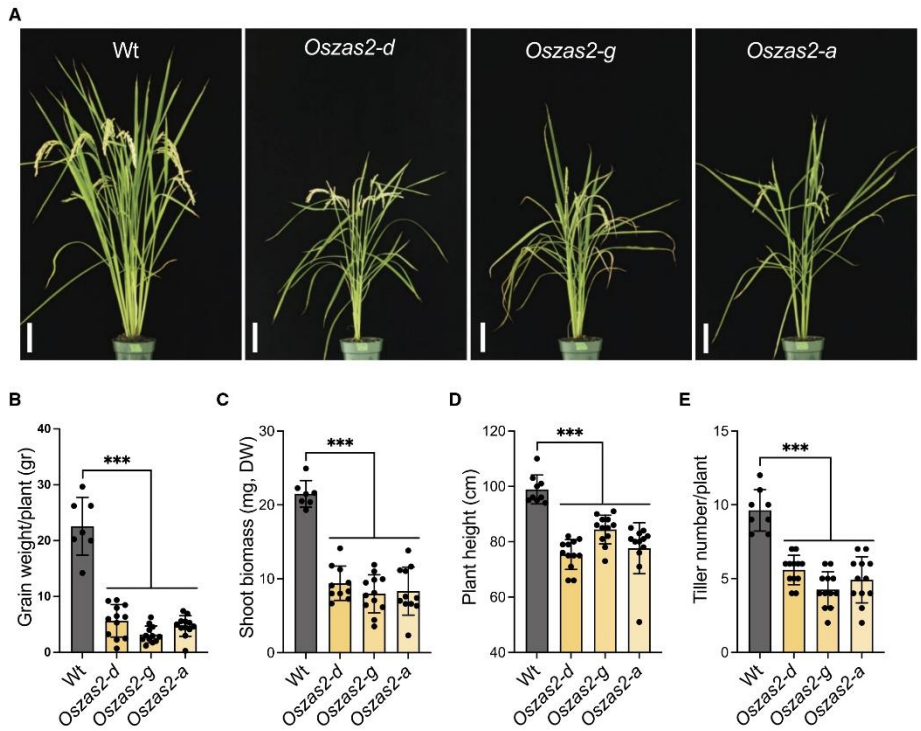

Figure 4 Characterization of Oszas2 mutant lines at the maturing stage. A, The picture of the 3-month-old WT and *Oszas2* mutants grown in the greenhouse. The scale bar in the pictures represents 7.5 cm. B–E, Grain weight per plant (B), shoot biomass (C), plant height (D), and tiller number (E) of the WT and *Oszas2* mutants represented in (A). Values in (B–E) are means ± SD ($n \geq 7$). Student's *t* test was applied for the statistical analysis (***$P \leq 0.001$).

with AM fungi and monitored the GUS signal. Interestingly, we detected GUS activity only in arbusculated cells (Figure 5A; Supplemental Figure S2C), and did not observe any signal in any other root cells, including cortical cells and cells crossed by fungal hyphae. We further validated this observation by using in situ hybridization assays on mycorrhizal roots of WT plants. *Os*ZAS2 mRNA exclusively accumulated in cells with fully developed arbuscules, in which we detected a strong chromogenic signal (Figure 5B). We did not observe any signal in noncolonized cells or upon using the *Os*ZAS2 sense probe (Figure 5B).

To determine the impact of *Os*ZAS2 on AM symbiosis, we inoculated the *Oszas2* mutant lines with AM fungi and assessed the colonization level by morphological analysis and by monitoring the transcript abundance of *OsPT11* at two time points (14 and 50 dpi) and of the fungal genes *RiEF* and *RiPeip1* (Fiorilli et al., 2016) at 50 dpi. Both mutant lines showed a lower frequency of mycorrhizal colonization (F%), intensity of colonization (M%), and total number of arbuscules (A%), compared to WT plants (Figure 5E). Molecular analysis confirmed these results: the expression level of fungal and plant genes was significantly lower in the mutant lines (Figure 5, C and D).

SL biosynthesis increased in *Oszas2* mutants

The low-tillering phenotype of *Oszas2* mutants (Figures 3, D and 4, E) indicated that they may have higher SL content. To test this hypothesis, we profiled their SLs in both roots and root exudates under low Pi conditions. We also analyzed the expression level of SL biosynthetic genes in roots. In roots, the contents of a noncanonical SL, a tentative 4-oxo-methylcarlactonate (4-oxo-MeCLA) (Yoneyama et al., 2018; Ito et al., 2022), and of the canonical SL 4-deoxyorobanchol (4DO) were significantly increased in *Oszas2* lines

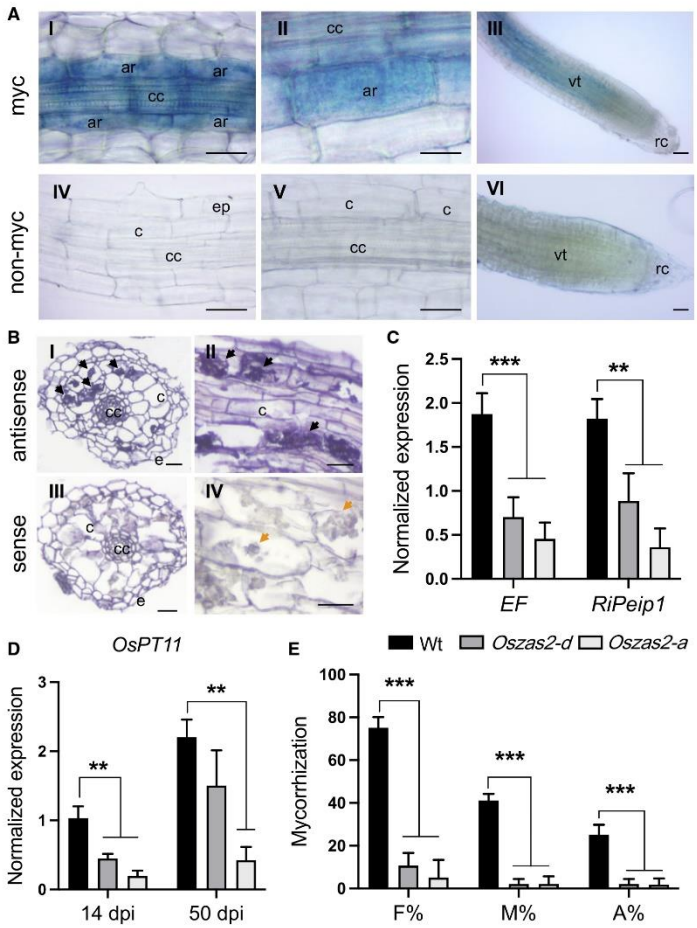

Figure 5 *OsZAS2* is required for AM establishment. A, GUS staining of roots of pZAS2:GUS-L18 reporter line inoculated (I, II, and III) for 35 days with *F. mosseae* and noninoculated (IV, V, and VI). B, Localization of *OsZAS2* mRNA in sections from differentiated regions of inoculated roots by cold in situ hybridization. Sections of mycorrhizal roots treated with *OsZAS2* antisense probe are shown in parts I and II; arrows highlight the strong chromogenic signal, which mirrors the presence of the *OsZAS2* transcript in arbuscule-containing cells. Sections of mycorrhizal roots treated with the *OsZAS2* sense probe are shown in parts III and IV; arrows in part IV indicate arbusculated cells that are not labeled. C, Relative expression of fungal genes; *RiEF* and *RiPeip1* in WT and *Oszas2* mutants at 50 dpi. D, Relative expression of *OsPT11* at 14 and 40 dpi in WT and *Oszas2* mutants. E, Frequency of mycorrhizal colonization (F%), the intensity of colonization (M%), and a total number of arbuscules (A%) in WT and *Oszas2* mutants at 50 dpi. cc, central cylinder; c, noncolonized cortical cells; e, epidermal cells; vt, vascular tissue; ar, arbuscule containing cells; rc, root cap. Bars (A and B) correspond to 50 μm. Values in (C–E) are means ± SD ($n \geq 3$). Student's *t* test was applied for the statistical analysis (**$P \leq 0.01$; ***$P \leq 0.001$).

compared to WT (Figure 6A). As shown in Figure 6B, we also observed an increase in the transcript level of SL biosynthetic genes, that is, *D27*, *CCD7*, *CCD8*, and *OsCO*. To confirm the increase in SLs, we conducted *a Striga* seed germination assay with root extracts. Extracts of *Oszas2* roots showed a significantly higher germination rate (around

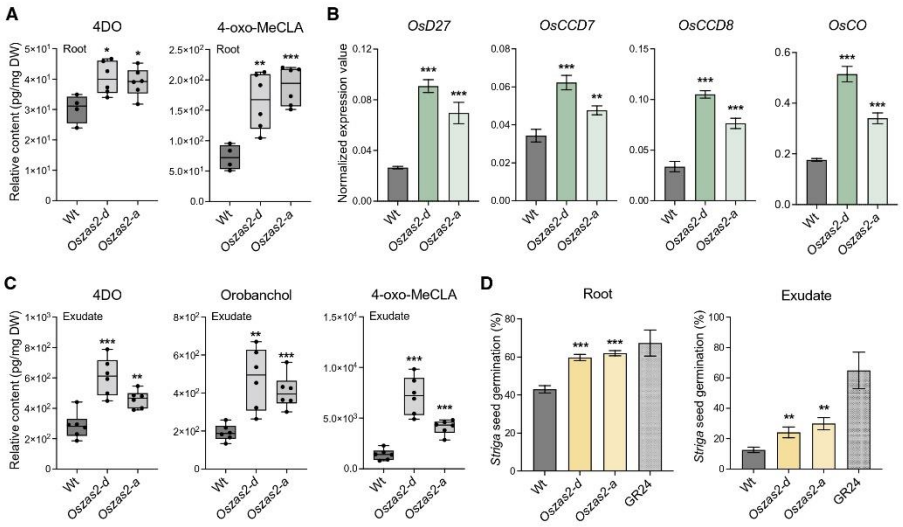

Figure 6 SL biosynthesis increased in *Oszas2* mutants. A, Relative quantification of 4DO and 4-oxo-MeCLA in root tissue of *Oszas2* mutants. B, Normalized expression value of SL biosynthetic genes in *Oszas2* mutants. C, Relative quantification of canonical (4DO, Orobanchol) and noncanonical (4-oxo-MeCLA) SL in root exudate of *Oszas2* mutants. D, *Striga* seed germination assay conducted with root exudate and tissue of *Oszas2* mutants. For both root exudate and tissue bioassay, 1 μM of GR24 was used as control, which showed about 65% and 67% of *Striga* seed germination, respectively. Boxes in boxplots in (A) and (C) represent the median, first and third quartile. The minimum and maximum values are showed with the length of the whiskers. Dots represent the biological replicates. Values in (A–D) are means ± SD ($n \geqslant 4$) and student's *t* test was applied for the statistical analysis (*$P \leqslant 0.05$; **$P \leqslant 0.01$; ***$P \leqslant 0.001$).

60%), compared to those of WT (around 42%, Figure 6D). In root exudates, both canonical (4DO, orobanchol) and noncanonical (4-oxo-MeCLA) SLs were significantly increased in *Oszas2* mutants, compared to WT (Figure 6C). Here again, we performed a *Striga* seed germination assay, in which *Oszas2* mutant lines displayed about15% higher activity compared to WT (Figure 6D), which confirms the LC–MS quantification.

Exogenous zaxinone application repressed SL biosynthesis in *Oszas2* mutant

Next, we treated 3 weeks old, hydroponically grown *Oszas2* seedlings (grown 1 week in Hoagland agar and 2 weeks in low Pi) with 5 μM zaxinone for 6 h. As shown in Figure 7A, zaxinone treatment repressed transcript levels of the SL biosynthetic genes *D27*, *CCD7*, *CCD8*, and *OsCO* in *Oszas2-d* back to the WT level. Furthermore and as shown before (Wang et al., 2019, 2020), exogenous zaxinone application decreased the transcript level of SL biosynthetic genes in WT as well (Figure 7A). Zaxinone application also decreased the content of the noncanonical SL 4-oxo-MeCLA in roots and root exudates of *Oszas2-d* and WT (Figure 7B). In addition, it caused a reduction in the level of the canonical SL orobanchol in root exudates of both *Oszas2-d* and WT (Figure 7C). Surprisingly, 4DO content was slightly increased upon zaxinone treatment in root tissues of both *Oszas2-d* and WT while it was not affected in root exudates (Supplemental Figure S3). Moreover, root exudates of both *Oszas2* and WT plants showed, upon zaxinone treatment, decreased Striga seed germination (Figure 7D).

Zaxinone treatment partially rescued the growth defects of *Oszas2* mutant

Next, we supplied *Oszas2* seedlings, grown in soil, with exogenous zaxinone at a concentration of 10 μM. After 2 weeks, we observed an increase in the tiller number of *Oszas2-d* mutant, but not of that of the WT (Figure 8, A and B). Moreover, zaxinone treatment significantly increased root and shoot biomass and shoot length of *Oszas2-d* (Figure 8, C–F). We also observed an increase in root length and root and shoot biomass of treated WT plants upon zaxinone treatment, while their shoot length remained unaffected (Figure 8, C, D, and F).

Discussion

The identification of a zaxinone synthase, the rice ZAS, revealed the presence of a widely distributed plant CCD

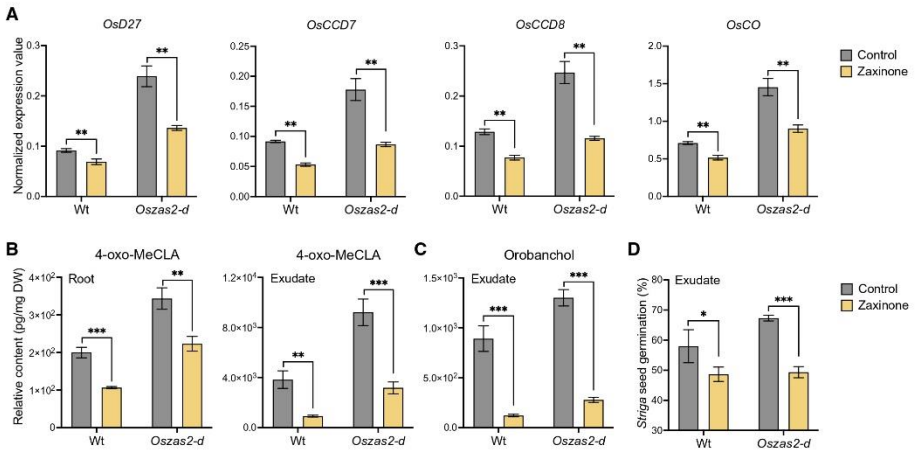

Figure 7 Zaxinone treatment reduced SL biosynthesis in *Oszas2* mutant. A, SL biosynthetic genes; *OsD27*, *OsCCD7*, *OsCCD8*, and *OsCO* expression in WT and *Oszas2* mutant upon zaxinone (5 μM) treatment. B, Relative content of 4-oxo-MeCLA after zaxinone (5 μM) treatment in root tissue and exudate of WT and *Oszas2* mutant. C, Relative content of Orobanchol after zaxinone (5 μM) treatment in root exudate of WT and *Oszas2* mutant. D, *Striga* seed germination assay with exudate of WT and *Oszas2* mutant upon zaxinone (5 μM) treatment. About 1 μM of GR24 was used as control, which showed about 63% of *Striga* seed germination. Values in (A–D) are means ± SD ($n \geqslant 4$). Student's *t* test was applied for the statistical analysis (*$P \leqslant 0.05$; **$P \leqslant 0.01$; ***$P \leqslant 0.001$).

subfamily (Wang et al., 2019). Functional studies and characterization of a corresponding T-DNA insertion mutant demonstrated the importance of ZAS for plant growth, interaction with AM fungi, and SL homeostasis. Furthermore, exogenous treatment with zaxinone revealed the growth-promoting effect of this apocarotenoid and its impact on hormone homeostasis and sugar metabolism, indicating that it may be a candidate for a novel plant hormone (Wang et al., 2019, 2021a, 2021b). Rice contains three *OsZAS* homologs (Wang et al., 2019), called here *ZAS1b*, *ZAS1c*, and *ZAS2*, with unknown functions. The severe phenotypes of *zas* mutant indicate the importance of this gene and suggest that its activity cannot be compensated by that of its homolog(s), and that the latter may exert different function(s). Therefore, we were interested in investigating the biological function of these enzymes.

Phylogenetic analysis placed OsZAS2 in a clade different from that of ZAS, ZAS1b, and 1c, indicating a different biological role and maybe enzymatic activity (Figure 1A). Therefore, we focused in this study on OsZAS2. However, the enzymatic studies performed here demonstrate that OsZAS2 catalyzes the same reaction as ZAS, that is, it converts apo-10′-zeaxanthinal into zaxinone (Figure 1B). Indeed, the enzyme did not convert other substrates tested, for example, β-carotene, zeaxanthin, or different apocarotenoids, or produced other products, pointing to zaxinone formation as its enzymatic function. The same activity was reported for OsZAS. However, OsZAS cleaved, in addition to apo-10′-zeaxanthinal, apo-12′- and apo-8′-zeaxanthinal, but with lower activity (Wang et al., 2019). This difference might be caused by a wider substrate specificity. However, it is also possible that the heterologously expressed OsZAS is generally more active than ZAS2.

To explore the biological function of OsZAS2 in planta, we generated *Oszas2* knockout lines using the CRISPR/Cas9 technology. Disrupting *OsZAS2* led to around 40% decrease in roots zaxinone content. This decrease supports the in vitro enzymatic activity of OsZAS2 and suggests that OsZAS2 is an enzyme, besides OsZAS, responsible for zaxinone biosynthesis in rice. *Oszas2* mutants still contained a substantial amount of zaxinone in roots. This could be due to the activity of OsZAS, which might compensate for the zaxinone production in rice roots. Nevertheless, zaxinone is common at higher levels in green tissues than in roots and is also present in plant species, such as Arabidopsis, which lacks ZAS genes, indicating that it can be synthesized via alternative route(s) independent of ZAS enzymes (Mi et al., 2019; Wang et al., 2019; Ablazov et al., 2020). However, the phenotypes observed with *Oszas* and *Oszas2* mutants suggest the importance of these enzymes and indicate the zaxinone content in roots is crucial for normal growth and development. We are currently generating *Oszas*/*Oszas2* double mutants, which could give us a hint about the involvement of other route(s) in zaxinone biosynthesis.

Zaxinone is a negative regulator of SL biosynthesis in rice (Wang et al., 2019). Indeed, the *Oszas* mutant contained and

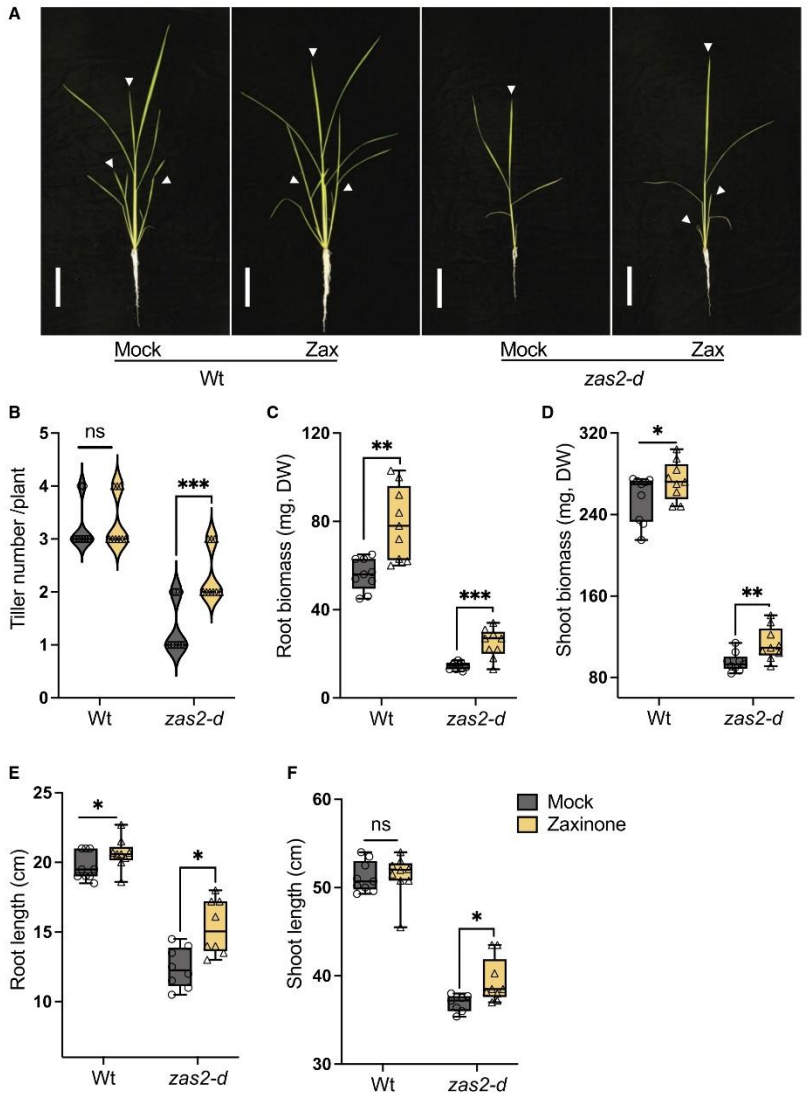

Figure 8 Exogenous zaxinone application rescued the growth defects of *Oszas2* mutant. A, The images of the WT (DJ) and *Oszas2-d* mutant grown for 2 weeks in soil supplemented with 10 μM of zaxinone and tap water (0.01% [v/v] acetone) as mock. The white bar represents 10 cm of scale. The white arrows represent main tillers. B–F, Tiller number (B), root biomass (C), shoot biomass (D), root length (E), and shoot length (F) of the WT and Oszas2 mutants are shown in (A). Boxes in boxplots represent the median, first and third quartile. The minimum and maximum values are showed with the length of the whiskers. Dots represent the biological replicates. Values in (B–F) are means ± SD ($n \geqslant 7$). Student's *t* test used for the statistical analysis (*$P \leqslant 0.05$; **$P \leqslant 0.01$; ***$P \leqslant 0.001$; ns, not significant).

released higher amounts of SLs (Wang et al., 2019) under Pi starvation, and this increase could be suppressed by exogenous zaxinone application. Based on its zaxinone-forming activity and the low-tillering phenotype of the *Oszas2* mutants, we assumed that the loss of OsZAS2 may also cause an increase in SL content. Therefore, we quantified the SL and zaxinone content in *Oszas2* mutants under low Pi conditions. Indeed, transcript levels of the SL biosynthetic genes *OsD27*, *OsCCD7*, *OsCCD8*, and *OsCO* transcript levels were upregulated in *Oszas2* compared to WT (Figure 6A). In parallel, both canonical and noncanonical SLs were significantly increased in roots and root exudates of *Oszas2* mutants (Figure 6, A and C), as confirmed by LC–MS analysis and by using the *Striga* seed germination bioassay. Interestingly, zaxinone content was not changed in *Oszas2* mutants under low Pi conditions (Supplemental Figure S4A), compared to the WT, albeit an increase in SL biosynthesis that is assumed to be caused by a decrease in zaxinone content. Since OsZAS is still functional in the *Oszas2* mutant, we hypothesized that it might compensate for the loss of *Oszas2* activity. In fact, *OsZAS* expression was upregulated, but not that of its homologs *OsZAS1b* and *OsZAS1c*, in *Oszas2* mutant under low Pi conditions (Supplemental Figure S4B). It might be speculated that changes in zaxinone content in certain root cells are crucial for regulating SL biosynthesis and that the increase in OsZAS activity may lead to a generally higher zaxinone content but cannot replace OsZAS2 in cells expressing this enzyme. Clarifying this point requires precise localization of both enzymes under low Pi conditions.

Oszas2 mutants showed severe reduction in root and shoot biomass (Figure 3, E and F) and developed fewer tillers compared to WT (Figure 3D). The retarded growth of *Oszas2* mutants demonstrates that *OsZAS2* is necessary for normal rice growth and development. In general, the phenotypes of the *Oszas2* mutants, reduced zaxinone content, retarded growth, and reduced tiller number, are similar to that of the *Oszas* mutant under normal conditions (Wang et al., 2019). Hence, it can be concluded that rice requires both *ZAS* and *ZAS2* genes to keep the root zaxinone concentration at a certain level, as well as for normal rice growth and development under normal conditions.

We checked the expression pattern of *OsZAS2* at tissue and cellular level using RT-qPCR and promoter–GUS–reporter lines. Similar to *OsZAS* (Wang et al., 2019), *OsZAS2* is expressed in roots and induced upon Pi starvation. A robust upregulation of both *OZAS* and *OsZAS2* in rice roots in response to Pi starvation indicates their involvement in the plant's response to Pi deficiency. Interestingly, analysis of the GUS reporter lines (*pOsZAS2::GUS11* and *pZAS2::GUS18*) demonstrated that the *OsZAS2* expression level was higher in root tips (Figure 2A). The cross-sectioning of the primary roots of the *pOsZAS2::GUS11* further showed that *OsZAS2* is highly expressed in exoderms. Here again, it would be very interesting to monitor *OsZAS* expression patterns at the cellular level to get insights into the function of *OsZAS* and *OsZAS2* and understand why both of them are important for proper rice growth.

In a previous work, we demonstrated that *zas* mutant showed a lower AM colonization level, compared to WT plants (Wang et al., 2019). Moreover, we revealed that the *ZAS* gene family is absent in genomes of nonmycorrhizal species, such as Arabidopsis (Fiorilli et al., 2019; Wang et al., 2019), suggesting a strong link between *ZAS* and AM symbiosis. To investigate the role of OsZAS2 in the different steps of AM colonization, we monitored its expression level during a time course experiment in mycorrhizal and nonmycorrhizal roots. Contrarily to *OsZAS* which was upregulated during both early and later stages, *OsZAS2* was only upregulated at the maximum of arbuscules formation (21 dpi), suggesting an involvement in arbuscules development/formation. This assumption is supported by in situ hybridization and using the *pZAS2::GUS* reporter lines: indeed both assays revealed that *OsZAS2* expression is localized in arbusculated cells. To further clarify the *OsZAS2* involvement during the AM symbiosis, we assessed the *Oszas2* mutant lines (*Oszas2-d* and *Oszas2-a*) colonization level at the morphological level and using molecular analyses. Although *Oszas2* mutants displayed in nonmycorrhizal condition a higher level of SLs in roots and root exudates, they showed a severe reduction of AM colonization level; however, no defects in arbuscules morphology were detected. A similar phenotype was also observed in the *Oszas* mutant (Wang et al., 2019). We recently demonstrated that the lower AM colonization rate of the *Oszas* mutant is due to SL deficiency at the early stage of the AM interaction (Votta et al., 2022): during this phase OsZAS activity is required to induce SL production possibly through the Dwarf14-Like (D14L) signaling pathway which was shown to regulate AM colonization in rice (Gutjahr et al., 2015). We can hypothesize that also OsZAS2 acts as a component of a regulatory network that involves SL and D14L pathways. Although further experiments are needed to prove this hypothesis, all the above data demonstrate that OsZAS2, in analogy to OsZAS, is required to reach a correct level of AM colonization.

We assume that the growth retardation of the *Oszas2* mutants is more likely due to decreased root zaxinone levels under normal conditions. Therefore, we applied zaxinone exogenously in to the *Oszas2-d* seedlings grown in soil. The exogenous application of zaxinone partially rescued the low-tillering, reduced root and shoot biomass, and shorter root and shoot length phenotypes of *Oszas2-d* mutant (Figure 8, C–F). This result indicates that a certain level of zaxinone is required to keep normal SL homeostasis and, hence, maintain normal tillering degree. Moreover, the effects of zaxinone treatment highlight again the importance of appropriate zaxinone concentrations of this apocarotenoid for regular growth and development of rice and support the idea of its function as a growth-promoting metabolite.

In conclusion, we revealed the function of *OsZAS2*, a member of the *CCD* gene family, which is crucial for normal rice growth and development. Besides OsZAS, OsZAS2 contributes to zaxinone production in rice roots and is a further determinant of SL content. Moreover, it is involved in regulating the levels of mycorrhizal colonization. Thus, manipulation

of OsZAS2 expression level could be a tool to modulate rice architecture and improve AM symbiosis.

Materials and methods

Plant material and phenotyping

Rice seedlings (*O. sativa* L. cv DJ) were grown in a Biochamber under the following conditions: a 12-h photoperiod, 500 µmol photons m^{-2} s^{-1} and day/night temperature of 27/25°C. Briefly, rice seeds were surface sterilized in a 50% (v/v) household bleach for 15 min and rinsed 5 times with distilled water. Then, sterilized seeds were germinated in the dark for 2 days in the magenta boxes containing 50 mL of 0.4% (w/v) agarose half-strength Hoagland medium with pH 5.8 at 30°C. The pregerminated seeds were transferred to the biochamber and kept for 5 days.

For metabolite quantification, gene expression analysis, and *Striga* seed germination assay, 1-week-old rice seedlings were transferred into 50-mL black falcon tubes filled with half-strength modified Hoagland nutrient solution with adjusted pH to 5.8. The nutrient solution consisted of 5.6-mM NH_4NO_3, 0.8-mM $MgSO_4.7H_2O$, 0.8-mM K_2SO_4, 0.18-mM $FeSO_4.7H_2O$, 0.18-mM $Na_2EDTA.2H_2O$, 1.6-mM $CaCl_2.2H_2O$, 0.8-mM KNO_3, 0.023-mM H_3BO_3, 0.0045-mM $MnCl_2.4H_2O$, 0.0003-mM $CuSO_4.5H_2O$, 0.0015-mM $ZnCl_2$, 0.0001-mM $Na_2MoO_4.2H_2O$, and 0.4-mM $K_2HPO_4.2H_2O$. For normal conditions (+Pi), the 1-week-old seedlings were grown in the Hoagland nutrient solutions (+Pi) for another 2 weeks. For phosphate starvation, the seedlings were grown for 2 weeks in lower phosphate (4 µM, $K_2HPO4{\cdot}2H_2O$) nutrient solution. The nutrient solution was replaced every 3 days. For zaxinone treatment, 3-week-old seedlings were treated with 5 µM of zaxinone for 6 h: tissues were collected and immediately frozen into liquid N_2.

For phenotyping, 1-week-old *Oszas2* seedlings were transferred into pots filled with soil and grown in growth chamber under the above-mentioned conditions. Tap water was supplied when needed. After 18 days, roots were cleaned off from the soil. Then, the seedlings were photographed with a digital camera, and root and shoot lengths were measured. To analyze the dry weight (DW) of roots and shoots biomass, samples were kept for 3 days in a 65°C oven. For phenotyping of *Oszas2* mutants at the mature stage, 1-week-old seedlings were transferred into greenhouse and grown until the mature stage with a day/night temperature of 28°C/25°C. One-time tap water and a one-time half-strength nutrient solution were supplied when necessary. After 3 months, yield-related traits were recorded. This experiment was repeated twice.

For rescue experiments, 7-days-old seedlings were transferred into 1-L pots filled with soil and grown in Biochamber. Initially, for zaxinone treatment 200 mL of 10-µM zaxione solution (pH 5.8) was added per pot. The same volume of tap water containing 0.01% (v/v) acetone was used as control. Every 3 days, 50 mL of 10 µM of zaxione solution and an equivalent amount of water were added to the treatment and control groups, respectively. After 2 weeks of treatment, seedlings were phenotyped as above.

Generation of transgenic lines

The CRISPR/Cas9 genome-editing technique was used to knock out *OsZAS2* (*Os06g0162550*) in *O. sativa ssp. japonica* variety DJ. The gRNA sequences were designed using the CRISPR-PLANT webserver (www.genome.arizona.edu/crispr/). Two different gRNA sites targeted *OsZAS2* in exon regions; at exon 1 which encodes (5′-GGTCACTAGATGCATTCATC-3′) and exon 2 which encodes (5′-GCAGATCTGAAGAGA CTGAT-3′). The gRNA spacers were fused to a tRNA sequence as described by Xie et al. (2015) (Supplemental Figure S6) and synthesized from GENEWIZ (South Plainfield, NJ, USA). Then, the corresponding fragment was cloned into pRGEB32 (Kanamycin) using 5′-BsaI and 3′-BsaI sites. The *pRGEB32-OsZAS2* construct was further introduced into *Agrobacterium tumefaciens* strain *EHA105* competent cells via electroporation. To construct the *pOsZAS2::GUS* reporter plasmid, the 1.2-kb promoter region of *OsZAS2* was amplified with the Phusion enzyme from the genomic DNA of rice using promoter-specific primers (Supplemental Table S1). The PCR product was ligated into pJet1.2 intermediate plasmid following the instruction of CloneJET PCR Cloning Kit (K1232; Thermo Scientific). The *pOsZAS2* sequence was amplified from the pJet1.2 plasmid with specific primers (Supplemental Table S1) and cloned into the pENTR/D-TOPO plasmid. Then, OsZAS2:pENTR/D-TOPO were inserted into pMDC162 (Curtis and Grossniklaus, 2003) by Gateway cloning.

Rice transformation was conducted according to Hiei and Komari (2008). The mutations of transformed lines were analyzed by PCR using a Thermo Scientific Phire Plant Direct PCR Master Mix Kit. Gene-specific primers (Supplemental Table S1) were used for PCR amplification to detect the mutation sites. Then, PCR products were cleaned up using ExoSAP-IT PCR Product Cleanup Reagent and submitted to the Sanger sequencing core lab team, at KAUST. The Sanger sequencing data (abi file) were analyzed following the instruction of DSDecode (Degenerate Sequence Decode; http://skl.scau.edu.cn/dsdecode/). Three independent homozygote mutant lines were identified and grown until T3 generation.

Metabolite quantification

For quantification, plant material was lyophilized with freeze-dryer and ground with Geno Grinder 2010. D_3-zaxinone (customized synthesis; Buchem B.V., Apeldoorn, the Netherlands) was used as an internal standard. Zaxinone was extracted according to Wang et al. (2019). SLs were extracted from the root tissues as described by Mi et al. (2018). SL extraction from the root exudates was performed according to Wang et al. (2022). In the final step, the dried extract was dissolved in 110 µL of acetonitrile: water (90:10,

v:v) and filtered through a 0.22-μm filter for LC–MS/MS analysis. The samples were run on UHPLC- Triple-Stage Quadrupole Mass Spectrometer (TSQ-Altis) with parameters as described in Wang et al. (2022).

Striga seed germination bioassays

Striga seeds were preconditioned as described by Jamil et al. (2019). After 10 days, the preconditioned *Striga* seeds were treated with rice root extracts and exudates, using 50 μL per disc (n = 3–6). Root extracts were prepared following the above described SL extraction method. For treatment, 5 μL of root extracts were diluted in 400 μL of MilliQ water before application. Root exudates were collected following the above described protocol. For treatment, 200 μL of SL enriched solution was diluted in 1,800 μL of MilliQ water before application. The discs were also treated with water and GR24 (1 μM) as negative and positive control, respectively. The plates were sealed with parafilm and incubated at 30°C for 24 h. The discs were scanned in a microscope and germinated and nongerminated seeds were counted from these scanned images by using the software SeedQuant (Braguy et al., 2021) to calculate the percentage of germination.

RT-qPCR analysis

Rice tissues were ground and homogenized in liquid nitrogen, and total RNA was isolated using a Direct-zol RNA Miniprep Plus Kit following the manufacturer's instructions (ZYMO RESEARCH, Irvine, CA, USA). Briefly, a 1-μg RNA sample was reverse transcribed using an iScript cDNA Synthesis Kit (BIO-RAD Laboratories Inc., 2000 Alfred Nobel Drive, Hercules, CA, USA). The RT-qPCR was performed using SYBR Green Master Mix (Applied Biosystems, Waltham, MA, USA; http://www.lifetechnologies.com) in a CFX384 Touch Real-Time PCR Detection System (BIO-RAD Laboratories, Inc., 2000 Alfred Nobel Drive, Hercules, CA, USA). Primer-BLAST webserver (Ye et al., 2012) was used to design the gene-specific RT-qPCR primers (Supplemental Table S1) and Ubiquitin was used as an internal control. The relative gene expression level was calculated according to 2^{Δ}CT method.

In vitro assays

The OsZAS2 cDNA was amplified using primers listed in Supplemental Table S1 and cloned into the pET-His6 MBP N10 TEV LIC cloning vector (2C-T vector; http://www.addgene.org/29706/) with MBP tags at the N-terminus. OsZAS2-MBP construct transformed into the BL21 Rosetta *E. coli* cells. A single colony of the transformed *E. coli* was cultured overnight and 0.5 mL of this culture was inoculated into 50-mL liquid media and grown at 37°C to OD (optical density) 0.6 at 600 nm. Then, bacteria were induced by IPTG (150 μM final concentration) and kept shaking at 28°C for 4 h. Cells were harvested by centrifugation and resuspended in lysis buffer (sodium phosphate buffer pH 8 containing 1% (v/v) Triton X-100 and 10 mM of dithiothreitol, lysozyme (1 mg mL^{-1})) and incubated on ice for 30 min. Next, the crude lysate was sonicated and centrifuged at 12,000 rpm and 4°C for 10 min, and the supernatant containing the protein was collected for in vitro incubation with the substrate. Synthetic substrates were purchased from Buchem B. V. (Apeldoorn, the Netherlands). Substrates were prepared according to Wang et al. (2019). Dried substrates were resuspended in 0.4% (v/v) Triton X-100 dissolved in ethanol. The mixture was then dried using a vacuum centrifuge to produce an apocarotenoid-containing gel. The gel was resuspended in incubation buffer (2-mM tris 2-carboxyethylphosphine, 0.4-mM $FeSO_4$, and 2-mg/mL catalase in 200-mM Hepes/NaOH, pH 8). OsZAS2 crude cell lysate, that is, 50 μL of the soluble fraction of overexpressing cells, was added to the assay. The assay was incubated for 4 h under shaking at 140 rpm at 28°C in dark. The reaction was stopped by adding two volumes of acetone and the lipophilic compounds were separated by partition extraction with petroleum ether: diethyl ether 1: 4 (v/v), dried, and resuspended in methanol for HPLC (High Performance Liquid Chromatography) analysis. For this purpose, we used an Ultimate 3000 UHPLC system and a YMC Carotenoid C30 column (150 × 3.0 mm, 5 μm) following the parameters described in Wang et al. (2019). This experiment was repeated at least 3 times.

Subcellular localization

The 35S::*OsZAS2*:*mNeongreen* was constructed by amplifying the coding sequence of *OsZAS2* using specific primers (Supplemental Table S1). The PCR product was sub-cloned into the pDONR221 entry vector by BP recombination reaction. Then, the *OsZAS2*::*pDONR221* fragment was fused into pB7FWG2,0 by Gateway cloning. The construct was introduced into *A. tumefaciens* strain GV3101 by electroporation. *Nicotiana benthamiana* infiltration was performed as described by Aljedaani et al. (2021). 35S::*OsZAS2*-*mNeongreen*, membrane protein marker (35S::*Lit6BmTurquoise2*) and p19 helper plasmid were co-infiltrated into the abaxial leave side of *N. benthamiana*. The fluorescence expression was checked 3-day postinfiltration by the confocal microscope. Leaf tissues of the infiltrated *N. benthamiana* was mounted with water on microscope slides and visualized by using a high-resolution laser confocal microscope (STELLARIS 8 FALCON, Leica). Images were acquired using an HC PL APO CS2 63x/1.20 WATER immersion objective, with 512 × 512 pixel resolution with a line average of 8. The mNeongreeen was excited with a 488 laser, and emission was collected at 500–558 nm. The laser was with 40% intensity, the gain was 180 gain and the pinhole was 1 air unit (AU) pinhole. The mTurquoise2 was excited with a 440 laser and the emission was collected at 445–479. The laser power was 12% intensity. The gain was 74 and the pinhole was 1 AU. This experiment repeated at least 3 times.

Mycorrhization

Rice seeds of WT cv. DJ, *Oszas2* (*Oszas2-d* and *Oszas2-a*) were germinated in pots containing a sand and incubated for 10 days in a growth chamber under a 14-h light (23°C)/10-h dark (21°C). All genotypes were colonized with approximately 1,000 sterile spores of *Rhizophagus irregularis* DAOM

197198 (Agronutrition, Labège, France). Mycorrhizal plants were grown in sand and watered with a modified Long-Ashton solution containing 3.2-μM $Na_2HPO_4 \cdot 12H_2O$ and kept in a growth chamber as described before. WT and *Oszas2* mutant plants were sampled at 14 and 50 dpi. To analyze *OsZAS2* gene expression profiles WT plants were inoculated with a fungal inoculum of *Funneliformis mosseae* (BEG 12, MycAgroLab, France) mixed (25% [w/v]) with sterile quartz. Nonmycorrhizal and mycorrhizal plants were sampled at 7 and 21 dpi. For all experiments, mycorrhizal roots were stained with cotton blue, and the level of mycorrhizal colonization was assessed according to Trouvelot et al. (1986) using MYCOCALC (http://www2.dijon.inra.fr/mychintec/Mycocalc-prg/download.html). For molecular analyses, roots were immediately frozen in liquid nitrogen and stored at −80°C. This experiment repeated at least 2 times.

In situ hybridization and GUS staining

For sample preparation and embedding, rice roots were fixed in 4% (v/v) paraformaldehyde in phosphate-buffered saline (PBS; 130-mM NaCl; 7-mM Na_2HPO_4; 3-mM NaH_2PO_4, pH 7.4) overnight at 4°C. To facilitate the fixation, samples were placed under vacuum for the first 15–30 min. Then the tissues were dehydrated in successive steps, each of 30–60 min duration, in 30%, 50%, 70%, 80%, 95%, and 100% (v/v) ethanol and 100% (v/v) Neo-Clear (Xylene substitute; Sigma-Aldrich, St Louis, MO, USA). Finally, samples were embedded in paraffin wax (Paraplast plus; Sigma) at 60°C. Sections of 7–8 μm were then transferred to slides treated with 100 mg mL^{-1} poly-L-Lys (Sigma) and dried on a warm plate at 40°C overnight. In parallel, DIG-labeled RNA probes were synthesized starting with 1 μg of PCR-obtained template (Langdale, 1993). DIG-labeled riboprobes (antisense and sense probes) were produced with DIG-UTP by in vitro transcription using the *Sp6* and *T7* promoters, according to the manufacturer's protocol (RNA-labeling kit; Roche, Basel, Switzerland). The sections were treated as follows: they were de-paraffinized in Neo-Clear, rehydrated through an ethanol series, treated with 0.2-M HCl for 20 min, washed in sterile water for 5 min, incubated in 2× SSC for 10 min, washed in sterile water for 5 min, incubated with proteinase K (1 mg mL^{-1} in 100-mM Tris–HCl, pH 8.0, 50-mM EDTA; Roche) at 37°C for 30 min, washed briefly in PBS, and then treated with 0.2% (w/v) Glycine in PBS for 5 min. After two rinses in PBS, slides were incubated in 4% paraformaldehyde in PBS for 20 min, washed in PBS (2, 3, and 5 min), and then dehydrated in an ethanol series from 30% to 100% (v/v). Hybridizations were carried out overnight at 55°C with denatured DIG-labeled RNA probes in 50% (v/v) formamide, 20× SSC, 20% (w/v) SDS (Sodium dodecyl sulfate), 50-mg mL^{-1} tRNA, 40-μg mL^{-1} Salmon Sperm DNA. Slides were then washed twice in 1× SSC, 0.1% (w/v) SDS at room temperature, and rinsed with 0.2× SSC, 0.1% (w/v) SDS at 55°C (2, 3, and 10 min). After rinsing with 2× SSC for 5 min at room temperature, the nonspecifically bound DIG-labeled probe was removed by incubating in 10-mg mL^{-1} RNase A in 2× SSC at 37°C for 30 min. Slides were then rinsed twice in 2% (v/v) SSC before proceeding to the next stage. The hybridized probe was detected using an alkaline phosphatase antibody conjugate (Roche). After rinsing in TBS (100-mM Tris–HCl, pH 7.5, 400-mM NaCl) for 5 min, slides were treated with 0.5% (w/v) blocking reagent in TBS (Tris Buffered Saline) for 1 h, incubated for 2 h with the anti-DIG alkaline phosphatase conjugate diluted 1:500 in 0.5% (v/v) Bovine Serum Albumin Fraction V in TBS, and then washed in TBS (3 × 5 min). Color development was carried out according to Torres et al. (1995). The color reaction was stopped by washing in distilled water, and the sections were then dehydrated through an ethanol series, deparaffinized in Neo-Clear, and mounted in Neomount (Merck, Kenilworth, NJ, USA) (Balestrini et al., 1997).

The GUS assay was performed on roots of *pOsZAS2:GUS-L11* and *L18* colonized by *F. mosseae* and sampled at 35 dpi. Rice mycorrhizal root segments were cut and placed in single wells of a Multiwell plate and covered with freshly prepared GUS buffer (0.1-M sodium phosphate buffer pH 7.0, 5-mM $K_4Fe(CN)_6$, 5-mM $K_3Fe(CN)_6$, 0.3% (v/v) Triton X, 0.3% (w/v) x-Glc). To improve buffer penetration into the root segments, they were placed under vacuum for 10 min. Finally, samples were incubated at 37°C for 16 h in the dark, de-stained with 70% (v/v) ethanol, and observed under an optical microscope (Nikon Eclipse E300).

Accession numbers

The cDNA and promoter sequence of rice ZAS2 is available in NCBI under the accession number LOC107275952. Accessions of SL biosynthetic genes; LOC_Os11g37650 (OsD27), LOC_Os04g46470 (OsCCD7), LOC_Os01g54270 (OsCCD8), and LOC_Os01g50520 (OsCO).

Supplemental data

The following materials are available in the online version of this article.

Supplemental Figure S1. Structures of carotenoids and apocarotenoids used as substrates in ZAS2 in vitro and vivo assays.

Supplemental Figure S2. *OsZAS2* expression during AM establishment.

Supplemental Figure S3. Relative content of 4DO after zaxinone (5 μM) treatment in root tissue and exudate of Wt and *Oszas2* mutant.

Supplemental Figure S4. Zaxinone quantification and *OsZAS* genes expression analysis in *Oszas2* mutants under low Pi conditions.

Supplemental Figure S5. Truncated amino acid sequences of *Oszas2* mutant lines after CRISPR-Cas9 genome editing.

Supplemental Figure S6. gRNA targets of OsZAS2 were fused to tRNA sequences (Xie et al., 2015).

Supplemental File S1. Clustal alignment of ZAS members.

Supplemental Table S1. Primer sequences used in this study.

Supplemental Table S2. Distribution of ZAS members across monocot and dicot plants.

Supplemental Table S3. Protein accessions of ZAS members in different organisms.

Acknowledgments

We are thankful to Dr. Imran Haider for helping with rice transformation, and Mr. Saad Hammad and Ms. Vijayalakshmi Ponnakanti for their help with greenhouse work.

Funding

This work was supported by baseline funding and Competitive Research Grants (CRG 2017 and CRG 2020) given to Salim Al-Babili from King Abdullah University of Science and Technology.

Conflict of interest statement. The authors declare that the research was conducted in the absence of any commercial or financial relationships that could be construed as a potential conflict of interest.

References

Abe S, Sado A, Tanaka K, Kisugi T, Asami K, Ota S, Kim HI, Yoneyama K, Xie X, Ohnishi T (2014) Carlactone is converted to carlactonoic acid by MAX1 in Arabidopsis and its methyl ester can directly interact with AtD14 in vitro. Proc Natl Acad Sci USA **111**: 18084–18089

Ablazov A, Mi J, Jamil M, Jia KP, Wang JY, Feng Q, Al-Babili S (2020) The apocarotenoid zaxinone is a positive regulator of strigolactone and abscisic acid biosynthesis in Arabidopsis roots. Front Plant Sci **11**: 578

Ahrazem O, Gómez-Gómez L, Rodrigo MJ, Avalos J, Limón MC (2016) Carotenoid cleavage oxygenases from microbes and photosynthetic organisms: features and functions. Int J Mol Sci **17**: 1781

Akiyama K, Matsuzaki KI, Hayashi H (2005) Plant sesquiterpenes induce hyphal branching in arbuscular mycorrhizal fungi. Nature **435**: 824–827

Al-Babili S, Bouwmeester HJ (2015) Strigolactones, a novel carotenoid-derived plant hormone. Ann Rev Plant Biol **66**: 161–186

Alder A, Jamil M, Marzorati M, Bruno M, Vermathen M, Bigler P, Ghisla S, Bouwmeester H, Beyer P, Al-Babili S (2012) The path from β-carotene to carlactone, a strigolactone-like plant hormone. Science **335**: 1348–1351

Aljedaani F, Rayapuram N, Blilou I (2021) A semi-in vivo transcriptional assay to dissect plant defense regulatory modules. *In* S Mukhtar, ed, Modeling Transcriptional Regulation. Salmon Tower Building, NY, Springer US, pp. 203–214.

Auldridge ME, Block A, Vogel JT, Dabney-Smith C, Mila I, Bouzayen M, Magallanes-Lundback M, DellaPenna D, McCarty DR, Klee HJ (2006a) Characterization of three members of the Arabidopsis carotenoid cleavage dioxygenase family demonstrates the divergent roles of this multifunctional enzyme family. Plant J **45**: 982–993

Auldridge ME, McCarty DR, Klee HJ (2006b) Plant carotenoid cleavage oxygenases and their apocarotenoid products. Curr Opin Plant Biol **9**: 315–321

Balestrini R, Jose-Estanyol M, Puigdomenech P, Bonfante P (1997) Hydroxyproline-rich glycoprotein mRNA accumulation in maize root cells colonized by an arbuscular mycorrhizal fungus as revealed by in situ hybridization. Protoplasma **198**: 36–42

Ballottari M, Alcocer MJ, D'Andrea C, Viola D, Ahn TK, Petrozza A, Polli D, Fleming GR, Cerullo, G, Bassi R (2014) Regulation of photosystem I light harvesting by zeaxanthin. Proc Natl Acad Sci USA **111**: E2431–E2438

Bouvier F, Dogbo O, Camara B (2003) Biosynthesis of the food and cosmetic plant pigment bixin (annatto). Science **300**: 2089–2091

Braguy J, Ramazanova M, Giancola S, Jamil M, Kountche BA, Zarban R, Felemban A, Wang JY, Lin PY, Haider I, et al (2021) SeedQuant: a deep learning-based tool for assessing stimulant and inhibitor activity on root parasitic seeds. Plant Physiol **186**: 1632–1644

Bruno M, Beyer P, Al-Babili S (2015) The potato carotenoid cleavage dioxygenase 4 catalyzes a single cleavage of β-ionone ring-containing carotenes and non-epoxidated xanthophylls. Arch Biochem Biophys **572**: 126–133

Bruno M, Hofmann M, Vermathen M, Alder A, Beyer P, Al-Babili S (2014) On the substrate-and stereospecificity of the plant carotenoid cleavage dioxygenase 7. FEBS Lett **588**: 1802–1807

Bruno M, Koschmieder J, Wuest F, Schaub P, Fehling-Kaschek M, Timmer J, Beyer P, Al-Babili S (2016) Enzymatic study on AtCCD4 and AtCCD7 and their potential to form acyclic regulatory metabolites. J Exp Bot **67**: 5993–6005

Chernys JT, Zeevaart JA (2000) Characterization of the 9-cis-epoxycarotenoid dioxygenase gene family and the regulation of abscisic acid biosynthesis in avocado. Plant Physiol **124**: 343–354

Curtis MD, Grossniklaus U (2003) A gateway cloning vector set for high-throughput functional analysis of genes in planta. Plant Physiol **133**: 462–469

Cutler SR, Ehrhardt DW, Griffitts JS, Somerville, CR (2000) Random GFP::cDNA fusions enable visualization of subcellular structures in cells of *Arabidopsis* at a high frequency. Proc Natl Acad Sci USA **97**: 3718–3723

Decker EL, Alder A, Hunn S, Ferguson J, Lehtonen MT, Scheler B, Kerres KL, Wiedemann G, Safavi-Rizi V, Nordzieke S (2017) Strigolactone biosynthesis is evolutionarily conserved, regulated by phosphate starvation and contributes to resistance against phytopathogenic fungi in a moss, Physcomitrella patens. New Phytologist **216**: 455–468

Dhar MK, Mishra S, Bhat A, Chib S, Kaul S (2020) Plant carotenoid cleavage oxygenases: structure–function relationships and role in development and metabolism. Brief Funct Genom **19**: 1–9

Dickinson AJ, Lehner K, Mi J, Jia KP, Mijar M, Dinneny J, Al-Babili S, Benfey PN (2019) β-Cyclocitral is a conserved root growth regulator. Proc Natl Acad Sci USA **116**: 10563–10567

Emanuelsson O, Nielsen H, Von Heijne G (1999) ChloroP, a neural network-based method for predicting chloroplast transit peptides and their cleavage sites. Protein Sci **8**: 978–984

Felemban A, Braguy J, Zurbriggen MD, Al-Babili S (2019) Apocarotenoids involved in plant development and stress response. Front Plant Sci **10**: 1168

Fiorilli V, Belmondo S, Khouja HR, Abbà S, Faccio A, Daghino S, Lanfranco L (2016) RiPEIP1, a gene from the arbuscular mycorrhizal fungus Rhizophagus irregularis, is preferentially expressed in planta and may be involved in root colonization. Mycorrhiza **26**: 609–621

Fiorilli V, Wang JY, Bonfante P, Lanfranco L, Al-Babili S (2019) Apocarotenoids: old and new mediators of the arbuscular mycorrhizal symbiosis. Front Plant Sci **10**: 1186

Fraser PD, Bramley PM (2004) The biosynthesis and nutritional uses of carotenoids. Prog Lipid Res **43**: 228–265

Giuliano G, Al-Babili S, Von Lintig J (2003) Carotenoid oxygenases: cleave it or leave it. Trends Plant Sci **8**: 145–149

Gomez-Roldan V, Fermas S, Brewer PB, Puech-Pagès V, Dun EA, Pillot JP, Letisse F, Matusova R, Danoun S, Portais JC (2008) Strigolactone inhibition of shoot branching. Nature **455**: 189–194

Gutjahr C, Gobbato E, Choi J, Riemann M, Johnston MG, Summers W, Carbonnel S, Mansfield C, Yang SY, Nadal M, et al (2015) Rice perception of symbiotic arbuscular mycorrhizal fungi requires the karrikin receptor complex. Science **350**: 1521–1524

Gutjahr C, Parniske M (2013) Cell and developmental biology of arbuscular mycorrhiza symbiosis. Ann Rev Cell Dev Biol **29**: 593–617

Ha CV, Leyva-González MA, Osakabe Y, Tran UT, Nishiyama R, Watanabe Y, Tanaka M, Seki M, Yamaguchi S, Dong NV (2014) Positive regulatory role of strigolactone in plant responses to drought and salt stress. Proc Natl Acad Sci USA **111**: 851–856

Hashimoto H, Uragami C, Cogdell RJ (2016) Carotenoids and photosynthesis. Carotenoids in Nature. Springer, Berlin, Germany, pp. 111–139

Hiei Y, Komari T (2008) Agrobacterium-mediated transformation of rice using immature embryos or calli induced from mature seed. Nat Protocol **3**: 824–834

Ilg A, Beyer P, Al-Babili S (2009) Characterization of the rice carotenoid cleavage dioxygenase 1 reveals a novel route for geranial biosynthesis. FEBS J **276**: 736–747

Ilg A, Bruno M, Beyer P, Al-Babili S (2014) Tomato carotenoid cleavage dioxygenases 1A and 1B: relaxed double bond specificity leads to a plenitude of dialdehydes, mono-apocarotenoids and isoprenoid volatiles. FEBS Open Biol **4**: 584–593

Ito S, Braguy J, Wang JY, Yoda A, Fiorilli V, Takahashi I, Jamil M, Felemban A, Miyazaki S, Mazzarella T (2022) Canonical strigolactones are not the tillering-inhibitory hormone but rhizospheric signals in rice. BioRxiv https://doi.org/10.1101/2022.04.05.487102

Jamil M, Kountche BA, Haider I, Wang JY, Aldossary F, Zarban RA, Jia KP, Yonli D, Shahul Hameed UF, Takahashi I (2019) Methylation at the C-3′ in D-ring of strigolactone analogs reduces biological activity in root parasitic plants and rice. Front Plant Sci **10**: 353

Jia KP, Baz L, Al-Babili S (2018) From carotenoids to strigolactones. J Exp Bot **69**: 2189–2204

Jia KP, Dickinson AJ, Mi J, Cui G, Xiao TT, Kharbatia NM, Guo X, Sugiono E, Aranda M, Blilou I (2019) Anchorene is a carotenoid-derived regulatory metabolite required for anchor root formation in Arabidopsis. Sci Adv **5**: eaaw6787

Jia KP, Mi J, Ablazov A, Ali S, Yang Y, Balakrishna A, Berqdar L, Feng Q, Blilou I, Al-Babili S (2021) Iso-anchorene is an endogenous metabolite that inhibits primary root growth in Arabidopsis. Plant J **107**: 54–66

Langdale JA (1993) In situ hybridization. *In* M Freeling, V Walbot, eds, The Maize Handbook. Springer-Verlag, New York, pp 165–180

Liang MH, He YJ, Liu DM, Jiang JG (2021) Regulation of carotenoid degradation and production of apocarotenoids in natural and engineered organisms. Critic Rev Biotechnol **41**: 513–534

Mi J, Jia KP, Wang JY, Al-Babili S (2018) A rapid LC-MS method for qualitative and quantitative profiling of plant apocarotenoids. Anal Chim Acta **1035**: 87–95

Mi J, Jia KP, Balakrishna A, Wang JY, Al-Babili S (2019) An LC-MS profiling method reveals a route for apocarotene glycosylation and shows its induction by high light stress in Arabidopsis. Analyst **144**: 1197–1204

Moise AR, Al-Babili S, Wurtzel ET (2014) Mechanistic aspects of carotenoid biosynthesis. Chem Rev **114**: 164–193

Moreno JC, Mi J, Alagoz Y, Al-Babili S (2021) Plant apocarotenoids: from retrograde signaling to interspecific communication. Plant J **105**: 351–375

Nambara E, Marion-Poll A (2005) Abscisic acid biosynthesis and catabolism. Annu Rev Plant Biol **56**: 165–185

Nisar N, Li L, Lu S, Khin NC, Pogson BJ (2015) Carotenoid metabolism in plants. Mol Plant **8**: 68–82

Paszkowski U, Kroken S, Roux C, Briggs SP (2002) Rice phosphate transporters include an evolutionarily divergent gene specifically activated in arbuscular mycorrhizal symbiosis. Proc Natl Acad Sci USA **99**: 13324–13329

Peleg Z, Blumwald E (2011) Hormone balance and abiotic stress tolerance in crop plants. Curr Opin Plant Biol **14**: 290–295

Ramel F, Birtic S, Ginies C, Soubigou-Taconnat L, Triantaphylidès C, Havaux M (2012) Carotenoid oxidation products are stress signals that mediate gene responses to singlet oxygen in plants. Proc Natl Acad Sci USA **109**: 5535–5540

Rodriguez-Concepcion M, Avalos J, Bonet ML, Boronat A, Gomez-Gomez L, Hornero-Mendez D, Limon MC, Meléndez-Martínez AJ, Olmedilla-Alonso B (2018) A global perspective on carotenoids: metabolism, biotechnology, and benefits for nutrition and health. Prog Lipid Res **70**: 62–93

Schwartz SH, Tan BC, Gage DA, Zeevaart JA, McCarty DR (1997) Specific oxidative cleavage of carotenoids by VP14 of maize. Science **276**: 1872–1874

Torres MA, Rigau J, Puigdomenech P, Stiefel V (1995) Specific distribution of mRNAs in maize growing pollen tubes observed by whole-mount in situ hybridization with non-radioactive probes. Plant J **8**: 317–321

Trouvelot A, Kough JL, Gianinazzi-Pearson V (1986) Estimation of vesicular arbuscular mycorrhizal infection levels. Research for methods having a functional significance. Physiological and Genetical Aspects of Mycorrhizae = Aspects Physiologiques et Genetiques des Mycorhizes: Proceedings of the 1st European Symposium on Mycorrhizae, Dijon, 1–5 July 1985. Institut National de le Recherche Agronomique, Paris

Umehara M, Hanada A, Yoshida S, Akiyama K, Arite T, Takeda-Kamiya N, Magome H, Kamiya Y, Shirasu K (2008) Inhibition of shoot branching by new terpenoid plant hormones. Nature **455**: 195–200

Vogel JT, Tan BC, McCarty DR, Klee HJ (2008) The carotenoid cleavage dioxygenase 1 enzyme has broad substrate specificity, cleaving multiple carotenoids at two different bond positions. J Biol Chem **283**: 11364–11373

Votta C, Fiorilli V, Haider I, Wang JY, Balestrini R, Petřík I, Tarkowská D, Novák O, Serikbayeva A, Bonfante P, et al. (2022). Zaxinone synthase controls arbuscular mycorrhizal colonization level in rice. Plant J **111**: 1688–1700

Wang JY, Alseekh S, Xiao T, Ablazov A, Perez de Souza L, Fiorilli V, Anggarani M, Lin PY (2021a) Multi-omics approaches explain the growth-promoting effect of the apocarotenoid growth regulator zaxinone in rice. Commun Biol **4**: 1–1

Wang JY, Chen GT, Jamil M, Braguy J, Sioud S, Liew KX, Balakrishna A, Al-Babili S (2022) Protocol for characterizing strigolactones released by plant roots. STAR Protocol **3**: 101352

Wang JY, Haider I, Jamil M, Fiorilli V, Saito Y, Mi J, Baz L, Kountche BA, Jia KP, Guo X (2019) The apocarotenoid metabolite zaxinone regulates growth and strigolactone biosynthesis in rice. Nat Commun **10**: 1–9

Wang JY, Jamil M, Lin PY, Ota T, Fiorilli V, Novero M, Zarban RA, Kountche BA (2020) Efficient mimics for elucidating zaxinone biology and promoting agricultural applications. Mol Plant **13**: 1654–1661

Wang JY, Lin PY, Al-Babili S (2021b) On the biosynthesis and evolution of apocarotenoid plant growth regulators. Semin Cell Dev Biol **109**: 3–11

Wang W, Shi J, Xie Q, Jiang Y, Yu N, Wang E (2017) Nutrient exchange and regulation in arbuscular mycorrhizal symbiosis. Mol Plant **10**: 1147–1158

Waters MT, Gutjahr C, Bennett T, Nelson DC (2017) Strigolactone signaling and evolution. Ann Rev Plant Biol **68**: 291–322

Xie K, Minkenberg B, Yang Y (2015) Boosting CRISPR/Cas9 multiplex editing capability with the endogenous tRNA-processing system. Proc Natl Acad Sci USA **112**: 3570–3575

Xie X, Yoneyama K, Yoneyama K (2010) The strigolactone story. Ann Rev Phytopathol **48**: 93–117

Ye J, Coulouris G, Zaretskaya I, Cutcutache I, Rozen S, Madden TL (2012) Primer-BLAST: a tool to design target-specific primers for polymerase chain reaction. BMC Bioinform **13**: 1

Yoneyama K, Xie X, Yoneyama K, Kisugi T, Nomura T, Nakatani Y, Akiyama K, McErlean CS (2018) Which are the major players, canonical or non-canonical strigolactones? J Exp Bot **69**: 2231–2239

Zhang Y, Van Dijk AD, Scaffidi A, Flematti GR, Hofmann M, Charnikhova T, Verstappen F, Hepworth J, Van Der Krol S (2014) Rice cytochrome P450 MAX1 homologs catalyze distinct steps in strigolactone biosynthesis. Nat Chem Biol **10**: 1028–1033

Zheng X, Giuliano G, Al-Babili S (2020) Carotenoid biofortification in crop plants: citius, altius, fortius. Biochim Biophys Acta Mol Cell Biol Lipids **1865**: 158664

Zheng X, Yang Y, Al-Babili S (2021) Exploring the diversity and regulation of apocarotenoid metabolic pathways in plants. Front Plant Sci **12**: 787049

4.1 Summary model

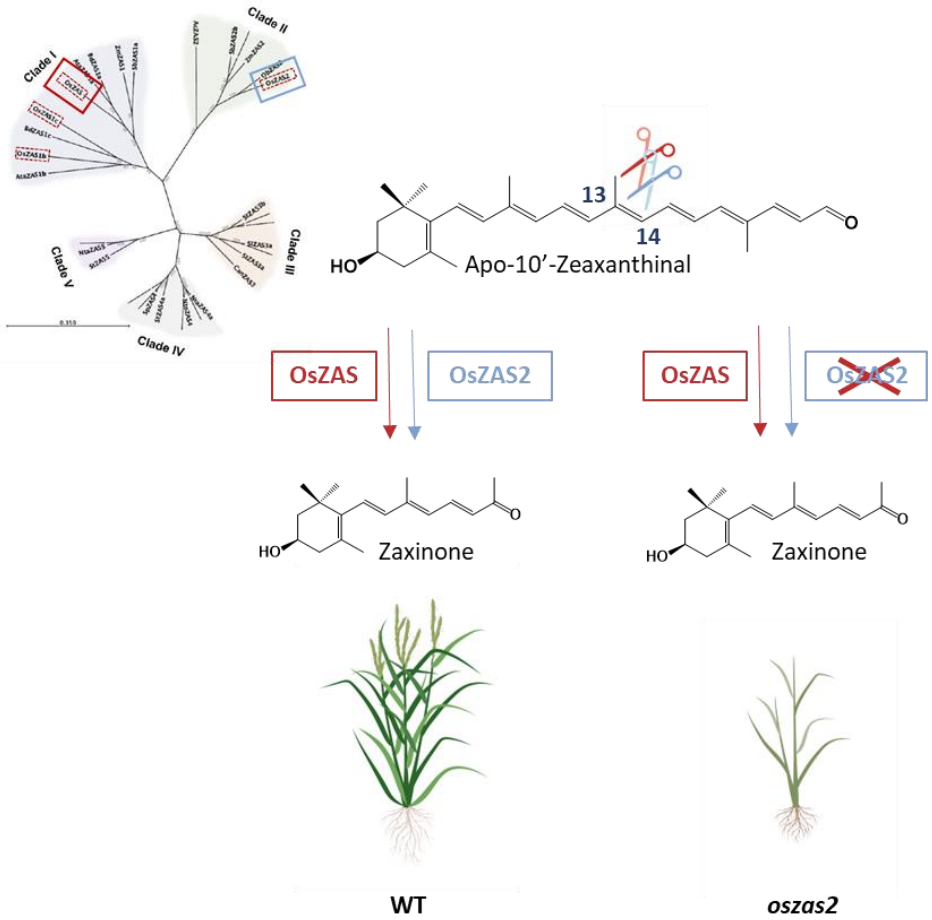

Schematic representation of OsZAS and OsZAS2 action in WT and oszas2 rice mutant. *OsZAS (Wang et al., 2019) and OsZAS2 are located in two different clades (phylogenetic tree from Ablazov et al., 2022), but they catalyze the same enzymatic reaction. In a WT rice plant, both OsZAS and OsZAS2 are involved in zaxinone production. In addition, both genes are inducted by phosphate starvation, are required for normal plant development, and regulate SLs content and the development of the AM symbiosis. OsZAS2 disruption led to about 40% less zaxinone root content compared to WT: the residual zaxinone content could be due to the activity of OsZAS suggesting that OsZAS and OsZAS2 show functional redundancy.*

4.2 Supplementary material

The supplementary data referred to the Chapter 4 are available at the following link:

https://oup.silverchair-cdn.com/oup/backfile/Content_public/Journal/plphys/191/1/10.1093_plphys_kiac472/1/kiac472_supplementary_data.pdf?Expires=1680886017&Signature=mPqF0S0lSjeK~ZW1xEovctOAKQ4RJfDKBVftk9FDclkias~FjyIpynka66e05Tzhz0ZGEbtMWwIFkpghIWTO2SpVJjXK0fTVYQ07XWCHStBeQjpEKdTQC7YfPPNlffo9GA9kFA~R7VmyRf-WTguFY10rOG49M9SKArxqywF7FMY0eEoAN866xAs9lLVbRAnIxtC8AEEBsedYx6POZMUNNUe0FbKKkgAW9SIe2DmXFU6wUQMUh44AkRPvrEe6buOqMYQg~of7lhXdpRf75fWtVbJxBfiXGbGW5MJPKDgRs9a3-49LIdj9fLuViiK0V-CzYAhJNDgN1LEDjrL9NIOLDw__&Key-Pair-Id=APKAIE5G5CRDK6RD3PGA

Chapter 5: The effect of zaxinone, a natural metabolite derived from carotenoids, on tomato plants

5.1 Introduction

Due to their 'static' nature, plants developed a series of strategies to adapt to the environmental and biotic stresses which affected them. Among these, plants produce hormones and chemical signals to coordinate their responses to external stimuli and communicate with the surrounding organisms (pathogens, symbionts, etc.) (Chaiwanon *et al.* 2016). Many of these compounds originate from the carotenoid pathways, for example, abscisic acid (ABA) and strigolactones (SLs), intensively studied since their discovery (Moise *et al.* 2014; Sun *et al.* 2018). In recent years, other apocarotenoids like β-cyclocitral, zaxinone, and anchorene are emerging as signaling molecules involved in plant development and stress response (Felemban *et al.* 2019; Fiorilli *et al.* 2019; Dickinson *et al.* 2019; Jia *et al.* 2019; Wang *et al.* 2019). In general, these carotenoid derivatives are produced by the oxidative cleavage of double conjugated bonds in the carotenoid backbone (Nisar *et al.* 2015; Ahrazem *et al.* 2016; Jia *et al.* 2018). This cleavage can be originated from a non-enzymatic process induced by reactive oxygen species (ROS) (Ramel *et al.* 2012; Havaux 2014). However, most plant apocarotenoids are formed by the action of a ubiquitous family of non-heme iron (II) dependent enzymes called Carotenoid Cleavage Dioxygenase (CCDs). In the model plant *Arabidopsis thaliana*, the CCD family comprises nine members, including five 9-*cis*-epoxy-carotenoid-dioxygenases (NCED2, NCED3, NCED5, NCED6, and NCED9) and four CCDs (CCD1, CCD4, CCD7, and CCD8) (Tan *et al.* 2003; Sui *et al.* 2013).

NCED, cleaving 9-*cis*-violaxanthin and 9-*cis*- neoxanthin, is responsible for the formation of xanthoxin, which is the ABA precursor (Nambara & Marion-Poll 2005; Ahrazem *et al.* 2016). ABA is a plant hormone with multiple functions, involved in

stomata closure regulation and water loss under drought conditions (Merilo *et al.* 2015) and the control of seed maturation and dormancy (Tuan *et al.* 2018).

CCD1 enzymes are generally less specific and can convert a wide variety of substrates, producing dialdehydes with different chain lengths and volatiles, involved in the aroma and flavour of diverse species (Vogel *et al.* 2008; Ilg *et al.* 2009, 2014). CCD4 is present in two forms: one, exclusive of *Citrus*, produces citraurin (Pan *et al.* 2012); the other one cleaves carotenoids either at the C7–C8 double bond in cryptoxanthin and zeaxanthin or at the C9–C10 double bond in bicyclic carotenoids (Rubio-Moraga *et al.* 2014; Bruno *et al.* 2015, 2016).

CCD7 and CCD8 are strigolactones (SL) biosynthesis enzymes that act sequentially in converting 9-*cis*-β-carotene, generated by the carotene isomerase DWARF27 (D27), into carlactone, the SL precursor. SLs are plant hormones that regulate different aspects of plant development, such as shoot branching, root architecture, and leaf senescence (Xie *et al.* 2010; Al-Babili & Bouwmeester 2015; Decker *et al.* 2017; Felemban *et al.* 2019). Moreover, they are exudated in the rhizosphere, where they act as an inducer of seed germination of root parasitic plants of the genera *Striga*, *Orobanche*, *Alectra*, and *Phelipanche* (Xie et al., 2010; Yoneyama *et al.* 2013). The photosynthetic capacity of these plants is not sufficient to provide the energy required for survival, therefore they infest host plants to achieve water and nutrients (Bouwmeester *et al.* 2003), negatively affecting yields and representing a severe agricultural problem (Parker, 2009).

In contrast, SLs take part in the establishment of the arbuscular mycorrhizal (AM) symbiosis (Akiyama *et al.* 2005; López-Ráez *et al.* 2015) and in the *Rhizobium*-legume interaction (Soto *et al.* 2010; Peláez-Vico *et al.* 2016). Briefly, the first mutualistic association involves around 80% of the land plants and allows an exchange of nutrients between the two partners (Genre *et al.* 2020). The plant provides photosynthetic products and lipids to the fungus that, in turn, improves the

plant mineral nutrition (Gutjahr 2014; Lanfranco *et al.* 2018). The second interaction involves rhizobia, soil bacteria able to convert atmospheric nitrogen into ammonia. They invade the legume root to form new organs, called nodules, in which the fixed atmospheric nitrogen is transferred to the plant in exchange for carbohydrates (Markmann and Parniske 2009).

Recent phylogenetic analysis of plant CCD orthologs led to the discovery of Zaxinone Synthase (ZAS), which is conserved in most land plants, but not in *Arabidopsis* or other members of *Brassicaceae* (Wang *et al.* 2019). *In vitro*, ZAS converts 3-OH-all-*trans*-β-apo-10'-carotenal into zaxinone, a growth-promoting apocarotenoid and a SL biosynthesis regulator (Wang *et al.* 2019). In rice, the loss-of-function *zas* mutant shows decreased zaxinone content in roots, retarded root and shoot growth, and increased SL levels. The rice genome encodes three OsZAS homologs, called OsZAS1b, OsZAS1c, and OsZAS2. OsZAS2 was recently shown to form zaxinone *in vitro*, to be expressed under phosphate starvation, and specifically in arbuscule-containing cells. The characterization of a CRISPR/Cas mutant line demonstrated that OsZAS2, in analogy to ZAS, determines rice growth, architecture, and SL content, and is required for optimal mycorrhization (Ablazov *et al.* 2022). The exogenous application of zaxinone not only restored the mutant phenotype, as expected, but also stimulated root growth in wild-type plants and, under low phosphate deficiency, decreases SL biosynthesis and release (Fiorilli *et al.* 2019; Wang *et al.* 2019).

In contrast to rice, in *Arabidopsis*, zaxinone acts as a positive regulator of SL, and ABA biosynthesis, and its application reduces hypocotyl growth by increasing ABA content (Ablazov *et al.* 2020). The presence of zaxinone in *Arabidopsis* suggests the existence of a ZAS-independent zaxinone biosynthetic route and indicates a general regulatory impact on the growth in both AM-host and non-host plants (Ablazov *et al.* 2020; Moreno *et al.* 2021).

Moreover, a recent study highlighted the positive impact of zaxinone and its analogs, called MiZax 3 and MiZax5 (Wang *et al.* 2020), on several monocots and dicots grown in different environments, pointing out their potential use as biostimulants. In particular, the effect of foliar application of these compounds on tomato *(Solanum lycopersicum)* not only improved the plants' fitness, increasing the plant height and the number of branches but also impacted the reproductive phase, enhancing the total number of flowers and fruits compared to the untreated condition (Wang *et al.* 2022).

In the current study, we investigated the effect of exogenous zaxinone given as root treatment on tomato plant development, mycorrhization, and responses to biotic and abiotic stress, probing the potential of this molecule on this important crop and model plant.

5.2 Material and methods

Plant material and growth conditions. Wild type and *slccd8* (kindly provided by Prof. Aly Radi, Newe Yaar Research Center, Volcani Institute - ARO) (Bari *et al.* 2019) tomato seeds (cv. Money Maker) were surface-sterilized in 50% sodium hypochlorite solution with 0.01 % Tween-20 for 15 min and pre-germinated on moistened filter paper with half-strength liquid Murashige and Skoog (MS) medium incubated at 30°C for 6 days. The pre-germinated seeds were transferred to light in controlled conditions (a 12 h photoperiod, 200-µmol photons m^{-2} $s^{-1,}$ 70% RH, and day/night temperature of 25/23 ºC) for 4 days. Well-developed seedlings (10 days old) were transferred in 50 ml falcon tubes or 2L magenta box with half-strength modified Hoagland nutrient solution (5.6 mM NH_4NO_3, 0.8 mM $MgSO_4.7H_2O$, 0.8 mM K_2SO_4, 0.18 mM $FeSO_4.7H_2O$, 0.18 mM $Na_2EDTA.2H_2O$, 1.6 mM $CaCl_2.2H_2O$, 0.8 mM KNO_3, 0.023 mM H_3BO_3, 0.0045 mM $MnCl_2.4H_2O$, 0.0003 mM $CuSO_4.5H_2O$, 0.0015 mM $ZnCl_2$, 0.0001 mM $Na_2MoO_4.2H_2O$ and with or without 0.4 mM $K_2HPO_4.2H_2O$, based on experiments) and grown in hydroponic conditions.

For phenotypic analyses, tomato seedlings were grown under the conditions described above, with the nutrient solution containing 0.4 mM $K_2HPO_4.2H_2O$ (+Pi) and 1 µM, 2.5 µM or 5 µM zaxinone (dissolved in Dimethyl sulfoxide; DMSO) or the corresponding volume of the solvent (control) for two to three weeks. The solution was changed twice a week, adding the chemical at each renewal.

For testing the zaxinone effect on tomato plants in the rhizotron system (48cm x 24 cm x 5cm box), the seedlings were grown in soil with half-strength modified Hoagland nutrient solution containing 0.4 mM $K_2HPO_4.2H_2O$ (+Pi) and 5 µM zaxinone for 21 days. The solution was changed twice a week, adding the chemical at each renewal. To increase the stability of the compounds, 1 µl/ml emulsifier (cyclohexanone + Atlas G1086 kindly provided by Mr. Han Rieffe of CRODA,

Gouda; Netherlands) was added into the nutrient solution. The root surface area was analyzed with the ImageJ software.

For SL analysis, tomato seedlings were transferred into 50 ml falcon tubes, containing the nutrient solution with 0.4 mM $K_2HPO4.2H_2O$ (+Pi) for one week. They were then subjected to phosphate deficiency (-Pi) for one week. On the day of root exudates collection, tomato plants were first treated with 5 µM zaxinone for 6 h, and then root exudates were collected for LC-MS/MS analysis and *Striga* bioassays.

For starch quantification 10-days old seedlings were transferred in 50 ml falcon tubes containing a modified Hoagland nutrient solution (500 µM Pi) and 5 µM zaxinone (dissolved in DMSO) or the corresponding volume of the solvent (mock) for three weeks. The solution was changed twice a week and plants were treated with the molecule once a week.

For gene expression analyses, seedlings were grown hydroponically as described above with the nutrient solution including 0.4 mM $K_2HPO4.2H_2O$ (+Pi) or without $K_2HPO_4.2H_2O$ (-Pi) for 7 days. Seedlings were further treated with zaxinone for 6 h, and tissues were collected.
For all experiments, synthetic zaxinone was purchased (customized synthesis) from Buchem B.V. (Apeldoorn, The Netherlands).

Plant and fungal materials for mycorrhization experiment. Tomato seeds (cv. M82 and Money Maker) were surface-sterilized in 70% ethanol with 0.01 % Tween-20 for 3 minutes and then in a 5% commercial hypochlorite in sterile H_2O for 13 minutes. Seeds were then transferred in Petri dishes with 0.6% plant agar (Duchefa, Haarlem, The Netherlands) medium, and germinated in the dark at 23 °C for five days. Seedlings were then moved to day/night conditions for another four days (16 h light (23 °C)/8 h dark (21 °C)) and then transferred to pots. Mycorrhizal plants (myc) were inoculated with *Funneliformis mosseae* (BEG12) commercial inoculum

(MycAgroLAb, France) mixed (30%) with sterile quartz sand. Plants were watered with a modified Hoagland nutrient solution containing low Pi concentration (50 µM Pi). We treated two sets of mycorrhizal tomato plants with different zaxinone concentrations (0.5 µM and 5 µM) once a week during the irrigation. All the plants were collected at 35 dpi (days post inoculation). For the molecular analyses, roots were immediately frozen in liquid nitrogen and stored at −80 °C. Some roots were dedicated for the morphometric evaluation according to Trouvelot *et al.* 1986: samples were stained with 0.1% cotton blue in lactic acid and the estimation of mycorrhizal parameters was performed using "Ramf" an open-source R package (https://github.com/mchiapello/Ramf) (Chiapello *et al.* 2019).

For the time-course experiment, a set of mycorrhizal and no-mycorrhizal tomato plants (cv. Money Maker) were grown with the same conditions described above in this paragraph. Plants were collected at 7, 21, and 35 dpi and used for molecular and morphological analysis.

***Striga hermonthica* seed germination bioassays.** *Striga hermonthica* seed germination bioassays were conducted by following the procedure described previously (Jamil *et al.* 2012). About 50-100 sterilized *Striga* seeds were spread on a glass fiber filter paper disc. Then 12 discs with *Striga* seeds were put on a sterilized filter paper and moistened with 3 ml sterilized water in a 90 mm Petri plate. The plates were sealed with parafilm and covered with aluminum foil. All the plates were kept at 30ºC for 10 days for pre-conditioning. On the 11th day, six dry discs with pre-conditioned seeds were selected and put in a 90 mm Petri dish. A filter paper ring moistened with 0.9 ml sterile MilliQ water was placed on the plate. The root exudates collected from zaxinone-treated tomato seedlings were applied at 50 µl on each six discs. Sterile MilliQ water and standard SL analog GR24 (2.5 µM) were included as a negative and positive control, respectively. After application, *Striga* seeds were incubated in dark at 30ºC for 24 hours. Germination (seeds with radicle emerging

through seed coat) was scored under a binocular microscope, and germination rate (%) was calculated.

Quantitative analysis of SLs in tomato root exudates. For the quantification of SLs in tomato root exudates, 50 ml of root exudates spiked with 0.672 ng of D6-5-deoxystrigol, was brought on a 500 mg/3 ml fast SPE C18 column preconditioned with 6 ml of methanol and 3 ml of water. After washing with 3 ml of water, SLs were eluted with 4 ml of acetone. The 4-deoxyorobanchol fraction (acetone-water solution) was concentrated in SL aqueous solution (~500 µl), followed by the extraction with 1 ml of ethyl acetate. 750 µl of SLs enriched organic phase was then transferred to 1.5 ml tube and evaporated to dryness under vacuum. The dried extract was dissolved in 100µl of acetonitrile: water (25:75, v:v) and filtered through a 0.22 µm filter for LC-MS/MS analysis. 4-deoxyorobanchol was analyzed by using HPLC-Q-Trap-MS/MS with MRM mode. Chromatographic separation was achieved on an Agilent 1200 HPLC system with a ZORBAX Eclipse plus C18 column (150 × 2.1 mm; 3.5µm; Agilent). Mobile phases consisted of water: acetonitrile (95:5, v:v, A) and acetonitrile (B), both containing 0.1% formic acid. A linear gradient was optimized as follows (flow rate, 0.2 ml/min): 0−10 min, 25 % to 100 % B, followed by washing with 100 % B and equilibration with 25 % B. The injection volume was 5 µl and the column temperature was maintained at 30°C for each run. The MS parameters were listed as follows: positive ion mode, ion source of turbo spray, ion spray voltage of 5500 V, curtain gas of 20 psi, collision gas of medium, gas 1 of 80 psi, gas 2 of 70 psi, turbo gas temperature of 400 °C, declustering potential of 60 V, entrance potential of 10 V, collision energy of 20 eV, collision cell exit potential of 15 V. The characteristic MRM transitions (precursor ion → product ion) were 347.1→233, 347.1→97 for orobanchol; 345.0→231.0, 345.0→327.0 for didehydroorobanchol; 365.0→268.0 for solanacol; 337→222, 337→97 for D6-5-deoxystrigol.

Quantification of starch. For starch extraction, excised root apparatus was rapidly blot-dried on filter paper and weighed. Samples, frozen in liquid nitrogen, were homogenized using a pestle. The samples were further homogenized in 0.5 mL of absolute ethanol. After the addition of 0.5 mL of 80% ethanol, the tubes were incubated at 70°C for 90 min and then centrifuged for 10 min at 11,337 × g and the pellet was resuspended in 1 mL of 80% ethanol. This step was repeated two times more. The pellets were finally resuspended in 400 μL of 0.2mM KOH and incubated at 95°C for 60 min. After neutralization with 70 μL of acetic acid, the samples were centrifuged for 10 min and the supernatant was used for starch quantification (Starch Test-Combination enzymatic analysis kit, cat. no. 207748; Boehringer, Mannheim, Germany), according to the manufacturer's instructions.

RNA library preparation and transcriptomic analysis. Tomato roots and shoots total RNA was extracted with TRIzol (Invitrogen, https://www.thermofisher.com) using a Direct-zol RNA Miniprep Plus Kit following the manufacturer's instructions (ZYMO RESEARCH; USA). RNA quality was checked with Agilent 2100 Bioanalyzer, and concentration was measured using a Qubit 3.0 Fluorometer. The cDNA libraries were constructed following standard Illumina protocols and paired-end sequenced on a HiSeq Illumina 4000 machine by the Bioscience core lab of KAUST. The reads quality was checked with FastQC (Babraham Bioinformatics; http://www.bioinformatics.babraham.ac.uk/projects/fastqc/), trimmed with Trimmomatic 0.36 ((Bolger *et al.* 2014) and quantified with Salmon 1.6.0 (parameters: -l A --validateMappings --gcBias --numGibbsSamples 20), using a transcriptome reference index build on Tomato genome (SL4.0) and transcriptome (ITAG4.0) files available on https://solgenomics.net/organism/Solanum_lycopersicum/genome. Expression matrices were created and imported into R environment with *tximport* 1.20.0 package (parameters: type="salmon", countsFromAbundance="lengthScaledTPM") (Soneson *et al.* 2015).

The whole dataset was split into “shoot” and “root” subsets and the function *DESeqDataSetFromTximport* from DESeq2 1.30.1 (Love *et al.* 2014) was used to create one R object with count information for each subset. The experimental design was set up to account for the two Zaxinone treatments (“mock” and “zax”) and the two Phosphate treatments (“P” and “Pstar”) with an interaction term (design = ~P_treatment + Zax_treatment + P_treatment: Zax_treatment). “Mock” and “control” were selected as reference levels for Zax_treatment and P_treatment variables, respectively. Further quality controls (PCA and heatmaps) were performed on *rlog* transformed count data; no outliers were identified. Differential expression analysis was performed with *DESeq2* and *results* functions. Five hypotheses were tested (Wald test): (i) the effect of Zax_treatment in “P” condition (comparison: “Zax_P vs mock_P”); (ii) the effect of Zax_treatment in “Pstar” condition (comparison: “Zax_Pstar vs mock_Pstar”); (iii) the effect of P_treatment in “mock” condition (comparison: “mock_Pstar vs mock_P”); (iv) the effect of P_treatment in “zax” condition (comparison: “zax_Pstar vs zax_P”) and (v) the differences in Zax_treatment” across P_treatment (interaction term). Genes with adjusted p-value ≤ 0.05 were considered differentially expressed. Functional enrichment analyses (GO and KEGG) and visualization were performed using gprofiler2 package (Kolberg *et al.* 2020).

Gene expression analysis. Roots of tomato seedlings were ground and homogenized in liquid nitrogen, and total RNA was isolated using a Direct-zol RNA Miniprep Plus Kit following the manufacturer’s instructions (ZYMO RESEARCH; USA). cDNA was synthesized from 1 µg of total RNA using iScript cDNA Synthesis Kit (BIO-RAD Laboratories, Inc, 2000 Alfred Nobel Drive, Hercules, CA; USA) according to the instructions in the user manual. The gene expression level was detected by real-time quantitative RT-PCR (qRT-PCR) performed using SYBR Green Master Mix (Applied Biosystems; www.lifetechnologies.com) in a CFX384 Touch™ Real-Time PCR Detection System (BIO-RAD Laboratories, Inc, 2000 Alfred Nobel Drive,

Hercules, CA; USA). Primers used for qRT-PCR analysis are listed in Supplementary, **Table 1**. The gene expression level was calculated by normalization of a ubiquitin (*SlUbq,* Solyc01g056940.2*)* housekeeping gene. The relative gene expression level was calculated according to the $2^{-\Delta\Delta}$CT method (Livak & Schmittgen 2001).

Osmotic stress induction and leaves transpiration rate. For the osmotic stress induction experiment, tomato (cv. M82) seeds were sterilized with the same method described for the mycorrhizal experiment. Ten-day-old seedlings were then transferred to pots containing quartz sterile sand. Plants were grown in a growth chamber for 21 days under 14 h light (24 °C)/10 h dark (20°C) regime and divided into two sets, one watered twice a week with a modified Hoagland nutrient solution containing 500 µM Pi concentration (+P) and one watered Hoagland nutrient solution with 50 µM Pi (-P). Then, the plants were transplanted in a hydroponic system, maintaining the +P or -P conditions. Osmotic stress was imposed with 10% (w/v) polyethylene glycol 6000 (PEG) completely dissolved in either +P (+P/+PEG) or –P (-P/+PEG) nutrient solution, corresponding to -1.61 MPa, following a modified protocol developed by Liu *et al.* (2015). All the plants (-P, +P, -P/+PEG e +P/+PEG) were samples at the 35 dpg (days post-germination) and samples were collected for molecular analysis.

For the leaves transpiration rate assay, tomato (cv. M82) 10-days old seedlings were transferred to pots containing quartz sterile sand and grown in a growth chamber under 14 h light (24 °C)/10 h dark (20 °C) regime. The treatment was performed directly on leaves and there were tested different compounds, GR24-rac (0.5 µM), zaxinone (0.5 µM), and the corresponding volume of the solvent as control. The measurement was carried out with a porometer (Decagon SC-1) at two time points: after 2 hours from the application of the molecules and after 24 hours.

Pathogenicity test on tomato upon *Botrytis cinerea* infection. For the pathogenicity test, tomato (cv. Money Maker) seeds were sterilized and germinated

using the same method described for the mycorrhizal experiment. After, 10 days old seedlings were transferred to pots containing quartz sterile sand. Plants were grown in a growth chamber for 21 days under 14 h light (24°C)/10 h dark (20°C) regime and watered with a modified Hoagland nutrient (500 µM Pi) and tap water, alternately. The treatments were carried out by dissolving the different molecules: GR24 (a SL synthetic analog), zaxinone, MiZax3, a zaxinone mimic (Wang *et al.* 2020), TIS108 (a SL inhibitor), or the corresponding volume of the solvent (acetone) as the control, in the nutrient solution or water to have a 10^{-6} M final concentration. Once leaves reached an adequate size, we placed a *Botrytis cinerea* (*Bc*) plug on 4 leaves per plant and monitored the infection after 48 and 96 hours. After 48 hours post-inoculation (hpi) the presence or the absence of the lesion was recorded while, after 96 hpi, for each lesion, the percentage of the necrotized leaf surface was evaluated. Seven plants for each condition were considered.

Statistics and reproducibility. All the experiments were performed with at least three biological replicates each. Statistical tests were carried out through One-way analysis of variance (One-way ANOVA) and Tukey's *post hoc* test, using a probability level of $P<0.05$. Statistical elaborations were performed using PAST ver.3 (Hammer *et al.*).

5.3 Results

Identification of the putative ZAS tomato homolog

Wang *et al*. (2019) described that the ZAS enzyme subgroup, responsible for zaxinone production, is distributed among moss, fern, monocots, and dicots but absent in *Brassicales*. Within Group 7 a ZAS tomato putative homologous gene, *SlZAS* (*Solyc08g066720*) was identified. Quantitative RT-PCR assays on tomato roots and shoots (**Figure 1**) showed that *SlZAS* was expressed only in roots and transcript levels increased under low Pi (-Pi) compared to normal (+P) conditions. This response to low Pi is similar to what has been observed for *OsZAS* (Wang *et al.* 2019).

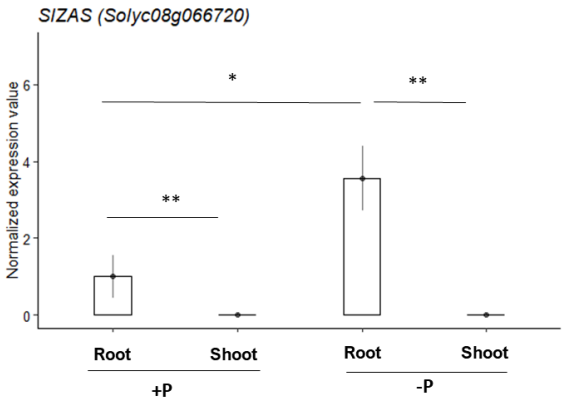

Figure 1. SlZAS expression pattern in tomato root and shoot. *The normalized expression value of SlZAS under +P (500 µM) and low Pi (50 µM) conditions in root and shoot tissue of 21-day-old tomato plants. Data are means ± SE (n=4). Significant values (by one-way Anova) are shown as follows: *P < 0.05; **P<0.01.*

Phenotypic characterization of tomato plants treated with zaxinone

To investigate the effect of zaxinone on tomato plant development, we treated hydroponically grown seedlings with 5 µM zaxinone. Plants exposed to zaxinone (Zax) showed an increase in root number and biomass, a higher number of leaves, and an increased shoot length compared to control plants (Mock) (**Supplementary figure 1**). We applied zaxinone also to plants grown in soil using the Rhizotron system that allows more detailed monitoring of root parameters (Wang *et al.* 2019);

we observed an increased root surface area and an increment in lateral root number. In addition, a higher shoot length and biomass were recorded (**Figure 2 a**). Taken together, our results showed a positive impact of zaxinone on the tomato vegetative phase with an enhancement of root and shoot growth, in analogy to what was observed in rice (Wang *et al.* 2019). In addition, a recent study highlighted that, in rice, zaxinone treatment triggered sugar-related metabolic processes leading to an increase in sugar and starch content (Wang, Alseekh, *et al.* 2021). We, therefore, quantified the starch level in the roots of hydroponically grown seedlings after three weeks of zaxinone application (5 µM), and an increase in starch content was observed (**Figure 2 b**).

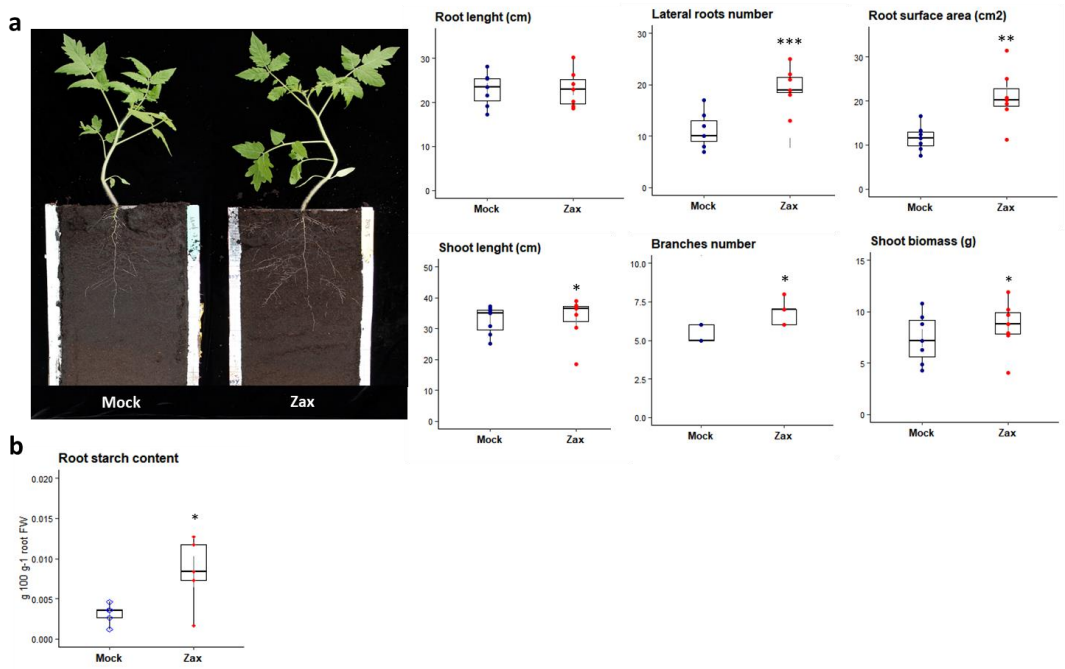

Figure 2. a. *Phenotypic evaluation of tomato plants treated (Zax) or not (Mock) with zaxinone (5 µM) grown in a Rhizotron system. Root number, root surface area, shoot length, biomass, and the number of branches were evaluated. n=7.* ***b.*** *Starch quantification in root tissues treated or not with zaxinone (5 µM) grown in +Pi condition (500 µM). n=5. Data represent ± SE. Significant values (by one-way Anova and t-test) are shown as follows: *P < 0.05; **P<0.01; ***P<0.001.*

Since in rice the growth-promoting effect of zaxinone was found to be dependent on SLs (Wang *et al.*, 2019), we tested whether this was the case also for tomato: we thus

applied 5 µM zaxinone to *slccd8*, a mutant line defective for a SL biosynthetic gene (Bari *et al.* 2019), grown hydroponically. Interestingly, the treatment did not promote root growth (root length, biomass, and root number) in the *slccd8* mutant (**Figure 3**), indicating that the effect of zaxinone is mediated by functional SL biosynthesis.

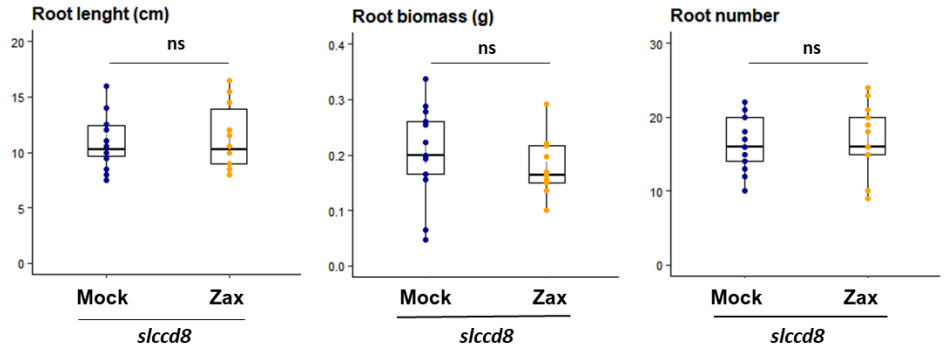

Figure 3. *Phenotypic evaluation of slccd8 mutant line tomato treated (Zax) or not (Mock) with zaxinone (5 µM) grown in a hydroponic system. Root length, biomass, and number were evaluated. n=15. Data represent ± SE. Significant values (by one-way Anova and t-test) are shown as follows: *P < 0.05; **P<0.01; ***P<0.001, ns: no significant difference.*

Effect of zaxinone on SL biosynthesis

Exogenous zaxinone treatment led to a reduction of SLs biosynthesis in rice (Wang *et al.* 2019) but an increase in Arabidopsis (Ablazov *et al.* 2020). To test the effect of exogenous zaxinone on SLs content in tomato, we quantified SLs in exudates of tomato plants treated with 5 µM zaxinone (Zax) or not treated (Mock) (**Figure 4a)**. Zaxinone application decreased significantly the orobancol-1 and solanacol content, while for dihydrorobanchol-1 and dihydrorobanchol-2 we also observed a decrease but not statistically significant. In addition, we performed a *Striga* parasitic plant seed germination assay on the Mock and Zax root exudates, using GR24, a SL synthetic analog, as a positive control. The results indicated a significantly decreased *Striga* seed germination of treated exudate compared to the control condition (**Figure 4b**).

Next, we determined the transcript level of SL biosynthetic genes *SlCCD7*, *SlCCD8*, and *SlMAX1* using q-RT-PCR. As shown in **Figure 4c**, the application of zaxinone induced a decrease, but not statistically significant, in the mRNA levels of SL biosynthetic genes in roots. These findings revealed that, as observed in rice, zaxinone exposure negatively regulated SLs biosynthesis and release.

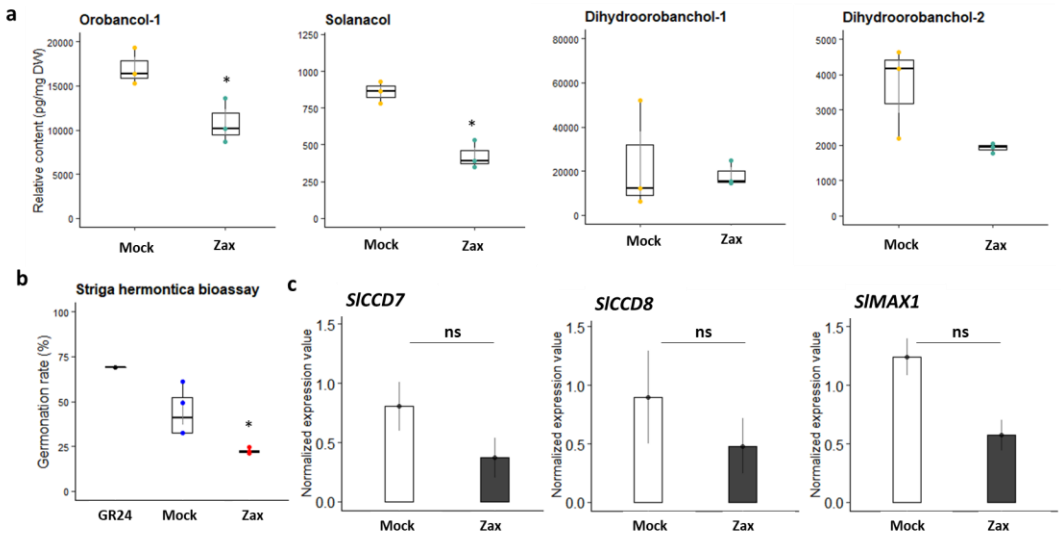

Figure 4. Effect of zaxinone on tomato SL biosynthesis and release. a. *Striga seeds germination rate upon treatment with exudates analyzed in response to zaxinone treatment (5 µM). GR24 was used as a positive control.* ***b.*** *Relative quantification of orobanchol-1, solanacol, dihydrorobanchol-1, and dihydrorobanchol-2 in root exudate of tomato treated or not with zaxinone. Data n = 3 biological replicates.* ***c.*** *qRT-PCR analysis of transcript levels of SL biosynthesis genes (SlCCD7, SlCCD8, and SlMAX1) transcript levels in tomato roots grown hydroponically under Pi starvation. Ubiquitin was used as a reference gene. Bars represent mean ± SE. Data n = 4 biological replicates. Statistical analysis was performed using one-way analysis of variance (ANOVA) and significant values are shown as follows: *P < 0.05, ns: no significant difference.*

Transcriptomic analysis (RNA-Seq) on tomato treated with zaxinone

We also analyzed the impact of a zaxinone short exposure (6 h) on tomato transcriptome using RNA sequencing (RNA-Seq) (**Figure 5**, **Supplementary figure 3**). We considered roots and shoots of plants treated (Zax) or not (Mock) with 5 µM zaxinone and grown under normal Pi condition (+Pi) or low Pi (-Pi). Reads were filtered for quality, cleaned from adapters, and transcripts were quantified with

Salmon (mapping-based mode on *Solanum lycopersicum* transcriptome index - EnsemblPlant SL.3 version). The zaxinone application in +Pi roots led to increased transcript levels in 210 genes and decreased transcript levels in 103 genes. Among the upregulated genes, we outlined two F-box/kelch-repeat proteins (*Solyc03g120320, Solyc12g088220*), a phosphate transporter PHO1-3 (*Solyc05g010060*), and a pleiotropic drug resistance protein (*Solyc09g091670*). The downregulated genes included, among others, two ABA receptors (*Solyc05g052420*, *Solyc03g095780*) and two high-affinity nitrate transporters (*Solyc11g069735*, *Solyc06g074990*).

For -Pi roots we found 12 up-regulated genes and 19 down-regulated genes. The upregulated genes comprised *Solyc03g120320* and *Solyc01g006050*, two genes in common with the RNA-Seq conducted on rice treated with zaxinone (after 2h, 6h, and 24h) (Wang, Alseekh, *et al.* 2021); among the downregulated genes we described *Solyc03g119660*, encoding for a protein annotated as PLANT CADMIUM RESISTANCE like, and *Solyc04g015210*, encoding for a disease resistance protein, present under both -Pi and +Pi conditions.

We detected a less significant impact on the shoot transcriptome (in the +Pi condition: 10 down-regulated genes and 1 up-regulated), which can be explained by the fact that zaxinone was applied to roots and for a short time.

If we consider, on the other hand, the two different Pi conditions, the root and shoot transcriptomes changed significantly. In the root grown under the -P condition we observed 3168 down-regulated genes and 4206 up-regulated genes. In the shoot, we reported 1363 down-regulated and 2382 up-regulated genes. Among the root genes strongly induced by Pi deficiency we found, as expected, *SlCCD7 (Solyc01g090660)* and *SlCCD8* (*Solyc08g066650*) (López-Ráez *et al.* 2008) and genes involved in Pi transport (*Solyc09g066410* and *Solyc05g010060*) or genes induced by Pi starvation like TPSII (*Solyc03g098010*). Likewise, in the shoot, *SlCCD8*, the phosphate starvation inducible gene TPSI1, and different phosphate transporters

(*Solyc09g066410*, *Solyc03g005530*, *Solyc09g090360*, *Solyc03g097840*, *Solyc05g010060*, and *Solyc09g090070*) were up-regulated upon Pi starvation.

To validate the RNA-Seq data, we monitored by qRT-PCR the transcript level of 7 selected genes that showed low to high response to zaxinone treatment (**Supplementary figure 2**): the results of this experiment fully confirmed the RNA-Seq expression patterns.

Gene Ontology (GO term) analysis of molecular function and biological process allowed us to identify upon zaxinone application the activation of genes involved in signaling receptor activity, molecular transducer activity, ABA, and hormone binding. Furthermore, enrichments with Kyoto Encyclopedia of Genes and Genomes (KEGG) showed that most of the genes regulated by zaxinone were related to the biosynthesis of secondary metabolites, like phenylpropanoids, stilbenoid, diarylheptanoid and gingerol. In addition, we analysed the expression of SL biosynthesis genes (*SlD27*, *SlCCD7*, *SlCCD8*, *SlMAX1*) and *SlZAS* using the same samples of the RNA-Seq experiment. After 6h, we observed a statistically significant decrease in *SlCCD7* and *SlZAS* in +Pi roots (**Supplementary figure 4**).

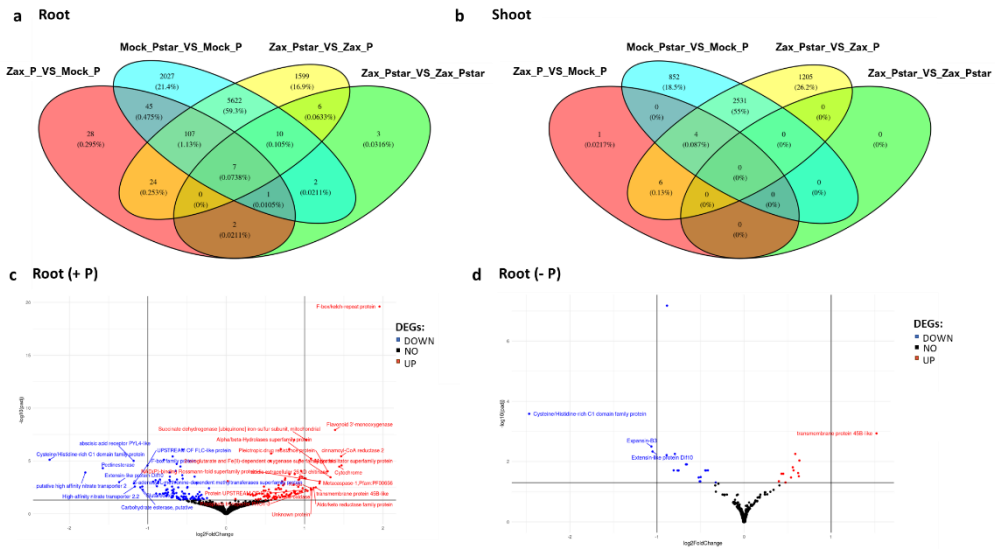

Figure 5. Analysis of differentially expressed genes (DEGs) in response to short exposure, 6 h, zaxinone treatment (5 µM). *a. Root Venn diagrams showing the numbers of genes that overlap*

between different conditions (Zas_P = plants grown in +P condition and treated with zaxinone; Mock_P = plant grown in +P condition and no treated; Zax_Pstarv = plants grown in P starvation and treated with zaxinone; Mock_Pstarv = plants grown in P starvation and no treated). b. Shoot Venn diagrams showing the numbers of genes that overlap between different conditions. c. Volcano plot representation of differential expression analysis of genes in the zaxinone-treatment versus Mock data sets, in roots grown in +P condition. The blue point represents the down-regulated genes, and the red ones are the up-regulated (padj ≤ 0.05, log2FC ≤ 0). The genes whose names are indicated are differentially expressed (padj < 0.05) and have a log2FC >1 or < -1. d. Volcano plot representation of differential expression analysis of genes in the zaxinone-treatment versus Mock data sets, in roots grown in P starvation. The blue point represents the down-regulated genes, and the red ones are the up-regulated (padj ≤ 0.05, log2FC ≤ 0). The genes whose names are indicated are differentially expressed (padj < 0.05) and have a log2FC >1 or < -1.

Zaxinone exogenous treatment affects AM symbiosis

As we demonstrated that in rice zaxinone and *OsZAS* influence AM colonization (Wang *et al.*, 2019; Votta *et al.*, 2022). At first, we investigated *SlZAS* expression levels during a time-course mycorrhization experiment (**Figure 6a**). In analogy to rice, SlZAS abundance in mycorrhizal roots increased at the early stage of colonization (7 dpi) and decreased significantly in the next stage (21 dpi) (Wang et al., 2019). By contrast, at the late stage (35 dpi), in tomato the SlZAS transcript remains downregulated compared to non-mycorrhizal roots while in rice we observed an upregulation of OsZAS. The expression profile of SlPT4, a tomato phosphate transporter encoding gene used as an AM marker (Figure 6b) and the morphological evaluation of mycorrhization by the method by Trouvelot et al. (1986, Figure 6c) confirmed the AM colonization progression.

To test the impact of exogenous zaxinone on the establishment of the AM symbiosis, we treated a set of mycorrhizal plants (cv. Money Maker and M82) with different zaxinone concentrations (0.5 µM and 5 µM) and assessed the colonization level by molecular and morphological analyses. We observed a significant decrease in the expression of *SlPT4*, a tomato phosphate transporter gene used as AM marker, in root samples (cv. Money Maker) treated with the highest zaxinone concentration (5 µM; **Figure 6c**). The same result was obtained in the M82 cultivar, where we also observed reduced *SlPT4* expression levels upon zaxinone supply; this result was in

line with the morphological data: treated plants showed lower values for all the evaluated mycorrhization parameters: frequency of mycorrhizal colonization (F%), the intensity of colonization (M%), and arbuscule abundance (a% and A%) compared to untreated plants (**Figure 6 d-e**).

Taken together these results confirmed that, as in rice (Wang *et al.* 2019; Votta *et al.* 2022), the exogenous application of zaxinone negatively impacts the AM symbiosis

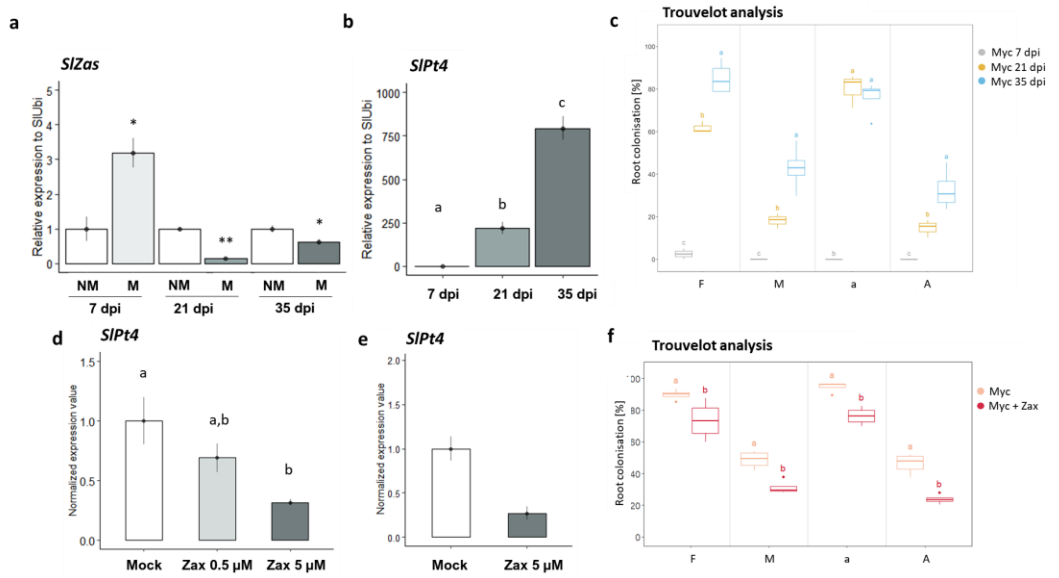

Figure 6. Zaxinone and mycorrhization. a. *SlZAS expression in mycorrhizal (M; inoculation with F. mosseae) or no-mycorrhizal (NM) roots of tomato cv. Money Maker-MM, during a time course experiment (7, 21, 35 dpi).* ***(b-c).*** *Analysis of arbuscular mycorrhizal level in tomato roots (cv. MM). The relative expression of SlPT4, an AM-marker gene, in the distinct stages of mycorrhization (7,21,35 dpi).* ***c.*** *Level of colonization expressed as F%: frequency of mycorrhizal, M%: intensity of mycorrhizal colonization, a%, and A%: arbuscule abundance in roots at 35 dpi.* ***d.*** *The expression level of SlPT4 in mycorrhizal roots (cv. MM) treated (Zax) or not (Mock) with zaxinone (0.5 µM and 5 µM) and colonized by F. mosseae at 35 days post inoculation (dpi). Ubiquitin was used as a reference gene.* ***(e-f).*** *Analysis of arbuscular mycorrhizal level in tomato roots (cv. M82) colonized by F. mosseae treated (myc+zax) or not (myc) with zaxinone (5 µM). The relative expression of SlPT4 in mycorrhizal roots treated or not with zaxinone. Level of colonization expressed as F%: frequency of mycorrhizal, M%: intensity of mycorrhizal colonization, a%, and A%: arbuscule abundance in roots at 35 dpi. For each experiment, we considered at least n=4 plants. Data are means ± SE. Significant values are shown with asterisks (*P < 0.05; **P<0.01; ***P<0.001) or different letters (P < 0.05).*

Zaxinone participates in the response to abiotic and biotic stresses

Recent studies have shown that among apocarotenoids, beyond the well-known ABA, there are many molecules involved in abiotic stress responses and biotic interactions (Felemban *et al.* 2019; Wang, Lin, *et al.* 2021). To investigate the possible involvement of zaxinone in responses to water stress, we measured the transpiration rate of untreated (control) or zaxinone-treated tomato leaves. In parallel, GR24 was used as a positive control, since it is known that SL exogenous application induced stomata closure (Visentin *et al.* 2016; Lv *et al.* 2018). The transpiration rate of leaves treated with GR24 significantly decreased compared to untreated leaves at the first time point (2h), remaining stable at the second time point (24 h). A similar pattern was observed in the case of the zaxinone treatment, suggesting a possible involvement of zaxinone in stomata regulation and, consequently, in acclimatization to water stress, as it was shown for SL (Visentin *et al.* 2016) (**Figure 7a**).

In addition, we evaluated whether *SlZAS* expression was responsive to drought. Gene expression profiles of *SlZAS, SlCCD8*, and *SlNCED1*, a marker gene for drought stress, were monitored in roots (**Figure 7b**) and shoot (data not shown) of plants exposed to osmotic stress (+PEG) at different Pi levels (+P: 500 μM, and -P: 50 μM). As expected, independently of the availability of Pi, the PEG treatment induced the expression of *SlNCED1,* the key gene for ABA biosynthesis, confirming the induction of the stress condition. In roots, *SlZAS* was upregulated by the osmotic stress under both Pi conditions. On the other hand, under low Pi conditions *SlCCD8*, was down-regulated by the osmotic stress as observed by Visentin *et al.* (2016). The

similar profile of *SlZAS* and *SlNCED1* further supports a potential involvement of *SlZAS* in the regulation of the osmotic stress response.

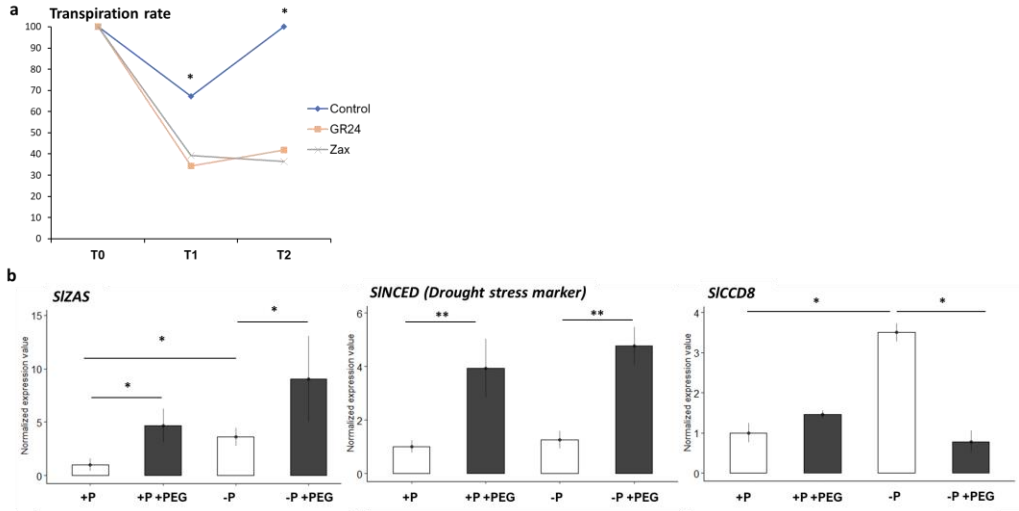

Figure 7. Zaxinone involvement in the response to abiotic stress. a. *Leaves transpiration rate before the treatment (T0), after 2 hours (T1), and 24 hours (T2). The molecules tested are shown in the legend (0.5 µM).* ***b.*** *The expression level of SlZAS, SlNCED1, and SlCCD8 in tomato roots exposed to osmotic stress (+PEG), grown in different Pi conditions (+P: 500 µM, and -P: 50 µM). Bars represent mean ± SE; a n = 5 biological replicates; b n = 4 biological replicates. Statistical analysis was performed using the t-student test and one-way analysis of variance (ANOVA). Significant values are shown with asterisks (*P < 0.05; **P<0.01; ***P<0.001).*

Finally, to investigate the possible role of zaxinone in pathogenic interactions we set up a pathogenicity assay on tomato using the fungal pathogen *Botrytis cinerea* (*Bc*). Plants were treated with GR24, zaxinone, Mizax3 (zaxinone mimic; (Wang *et al.* 2020), TIS108 (a SL inhibitor), and acetone, as control, which was given together with the nutrient solution 72 and 24 hours before *Bc* inoculation (**Figure 8a**). At 48 hours post inoculation (hpi), plants that received GR24 showed a lower percentage of leaves with symptoms compared to those treated with acetone. In contrast, in plants treated with zaxinone and MiZax3 the percentage of leaves showing the onset of symptoms was higher. This trend was confirmed at 96 hpi, when plants treated with MiZax3 and zaxinone presented a higher percentage of leaf necrotic area, while those treated with GR24 showed a slight, although not more statistically significant, decrease (**Figure 8b**). At both time points, TIS108-treated plants revealed

intermediate values. These results suggested that plants treated with zaxinone or its mimic were more susceptible to pathogen infection.

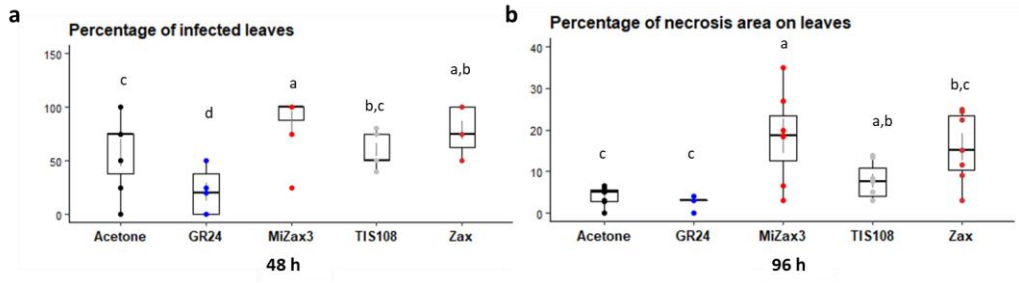

Figure 8. Zaxinone involvement in the response to biotic stress. a. *In vivo infection of B. cinerea on tomato leaves treated with acetone, GR24, MiZax3, TIS108, and zaxinone, used at concentration* 10^{-6}*M.* ***c****. The percentage of leaves that after inoculation showed the onset of symptoms at 48 hours post inoculation (hpi).* ***d.*** *The percentage of leaf necrotized area at 96 hpi. Bars represent mean ± SE; n = 4 biological replicates. Statistical analysis was performed using the t-student test and one-way analysis of variance (ANOVA). Significant values are shown with different letters (P < 0.05).*

5.4 Discussion

Zaxinone is a recently discovered apocarotenoid described as a growth regulator in rice (Wang *et al.* 2019). This molecule, in rice, regulates the development and plant architecture, possibly by suppressing SL biosynthesis. This metabolite is produced by the action of an enzyme belonging to the CCD family, ZAS, which is conserved in most land species, except for Brassicales. However, zaxinone is also present in plant species that lack *ZAS* genes, such as Arabidopsis, indicating that it can be synthesized *via* alternative routes independent of these enzymes (Mi *et al.* 2019; Wang *et al.* 2019; Ablazov *et al.* 2020). Notably, in contrast to what was observed in rice, zaxinone application on Arabidopsis inhibited the hypocotyl elongation and promoted both SL and ABA content, suggesting that it might act as a stress signal (Ablazov *et al.* 2020). In light of these observations, it would be important to characterize ZAS homologs and describe the impact of zaxinone on other plant species. Here, we characterized the *ZAS* homolog gene - *SlZAS* - in tomato plants, and we evaluated the effect of zaxinone exogenous supply on tomato vegetative growth, mycorrhization, and the response to abiotic and biotic stresses.

Our results presented many similarities with what was observed in rice (Wang et al., 2019), starting with the expression pattern of *SlZAS*, which was up-regulated upon Pi starvation and expressed in roots. To better characterize the functions of this gene within a collaboration with Dr. Gianfranco Diretto (ENEA, Rome) *slzas* mutants are currently being generated with the CRISPR/Cas9 technology. Moreover, to determine the enzymatic activity of SlZAS, *in vitro* assay as described by Wang *et al.* (2019) and Ablazov *et al.* (2022) will be performed.

Zaxinone exogenous treatment promotes tomato growth and reduces strigolactone synthesis

Zaxinone exogenous application on tomato plants grown hydroponically or in the soil showed a positive effect of the molecule, which enhanced root and shoot growth,

as observed in rice (Wang *et al.* 2019). In addition, a recent study highlighted that the long-term zaxinone foliar application also positively impacts tomato productivity, increasing the number of flowers and fruits (Wang *et al.* 2022). In rice, the molecular mechanisms at the basis of the growth effect exerted by exogenous zaxinone were associated with the stimulation of sugar metabolism and regulation of cytokinin homeostasis (Wang, Alseekh, *et al.* 2021). In analogy to the rice, we observed that the application of zaxinone led to starch accumulation in tomato roots, suggesting potential conserved mechanisms of action.

To evaluate the changes in tomato transcriptome after zaxinone treatment, we performed RNA-Seq analysis on plant exposure or not to the molecule and grown under high and low conditions of Pi. We found, as expected, a higher amount of DEGs when comparing the two Pi concentrations while the zaxinone treatment led to minor transcriptomic changes. In the +Pi root, genes involved in nitrate and phosphate metabolism and transport were expressed differently, highlighting plant responses' rapid activation.

As observed in the RNA-Seq conducted by (Wang, Alseekh, *et al.* 2021) on rice treated with zaxinone (after 2h, 6h, and 24h), we detected a less significant impact on the shoot transcriptome, probably caused by the nature of the treatment when using the hydroponic condition. Remarkably, we identified a tomato gene (*Solyc03g120320*) that is up-regulated in zaxinone tomato-treated roots (under both Pi conditions), whose rice homolog was also found up-regulated by the zaxinone treatment. This gene was found to be induced in tomato leaves during senescence (Ma *et al.* 2019) and its Arabidopsis (AT1G80440) homolog encoded an F-box protein targeting type-B ARR (Arabidopsis Response Regulator) proteins that negatively regulate the cytokinin response (Kim *et al.* 2013; Ma *et al.* 2019). Since in rice the treatment with zaxinone modulated the cytokinins content (Wang, Alseekh, *et al.* 2021), it would be interesting to quantify their content in zaxinone-

treated tomato roots and to further characterize the role of this F-box protein in both rice and tomato.

As previously mentioned, zaxinone was described, under low Pi conditions, as a negative regulator of SL biosynthesis in rice (Wang *et al.* 2019), but a positive regulator of SL levels in Arabidopsis (Ablazov *et al.* 2022). Here, the SLs exudates quantification and the *Striga* seed germination assay indicated a lower SLs content in exudates of zaxinone-treated plants compared to the control condition; this was also mirrored by a slight decrease, although not statistically significant, in the mRNA level of SL biosynthetic genes (*SlCCD7, SlCCD8,* and *SlMAX1)* in roots. These data are in line with what has been observed in rice, where zaxinone acts as a plant growth-promoting metabolite and, under certain conditions, a negative regulator of SLs biosynthesis.

Zaxinone exogenous treatment has a negative impact on mycorrhizal colonization

The impact of zaxinone on the biosynthesis of SLs, the demonstration that *OsZAS* guarantees the correct extent of AM root colonization (Votta *et al.* 2022), as well as the induction of *OsZAS* in rice mycorrhizal roots (Fiorilli *et al.* 2015), led, therefore, to investigate also in tomato the role of zaxinone on the AM symbiosis. By monitoring the SlZAS expression level in the different mycorrhization stages, we obtained a profile similar to that described in rice in the early stages of mycorrhization (7-21 dpi). Moreover, the phenotypic and molecular analysis conducted on two different tomato cultivars, Money Maker and M82, highlighted that exogenous zaxinone negatively impacts the AM symbiosis, confirming the results obtained in rice (Wang et al. 2019; Votta et al. 2022). We recently hypothesized that in rice the zaxinone exogenous application repressed the AM colonization level, probably due to the strong negative effect of this compound on SLs biosynthesis or to alterations to other plant hormones involved in the AM symbiosis (Votta *et al.* 2022). The same situation can be envisaged for tomato plants.

The analysis of *SlZAS* mutant plants, when available, can be instrumental to better clarifying this issue.

Zaxinone may play a role in the response to osmotic stress and fungal pathogen infection

In the last years, apocarotenoids were also found to play a prominent role in biotic and abiotic stress responses. In this context, to explore the potential role of zaxinone on water stress, we evaluated the transpiration rate of leaves treated with or not with zaxinone or GR24, here used as a positive control. Compared to controls, plants treated with both molecules showed a significantly lower transpiration rate, suggesting a potential zaxinone involvement in stomatal regulation and, consequently, in acclimatization to water stress, as already demonstrated for SLs (Visentin *et al.* 2016; Lv *et al.* 2018). Notably, under osmotic stress, the *SlZAS* expression pattern was similar to that of *SlNCED*, which is a marker for water stress. In contrast, *SlCCD8* was inhibited by the osmotic stress, confirming data reported by Cardinale *et al.* (2018), who proposed that this regulation promotes ABA biosynthesis and its translocation from root to stem. Taken together these preliminary results indicated a potential zaxinone implication in adaptation to water and osmotic stress, and suggest a possible zaxinone cross-talk with SLs and ABA (López-Ráez *et al., 2010*, Visentin *et al.*, 2016, Ruiz-Lozano *et al.*, 2016).

Finally, to analyze the zaxinone involvement in other biotic interactions besides the AM symbiosis, we set up a pathogenicity test on tomato leaves with the fungal pathogen *Botrytis cinerea* (*Bc*). Plants treated with zaxinone and MiZax3, a mimic of zaxinone (Wang *et al.* 2020), were more susceptible to fungal infection while plants treated with GR24 were more resistant, confirming the protective action of SLs (Torres-Vera et al., 2014, Marzec 2016). We can hypothesize that the zaxinone and MiZax3 growth promotion effect (Wang *et al.* 2019; Wang, Alseekh, *et al.* 2021) causes an increase in the sugar content of the leaves, thus promoting the growth of the pathogen. A further hypothesis points to an indirect action of the two compounds

that negatively affect the SLs biosynthesis and content in planta (Wang *et al.* 2019, 2020) thus reducing the resistance to pathogens (Torres-Vera *et al.* 2014, Marzec 2016). We can also speculate on the possible involvement of zaxinone and its mimic in modulating defense responses through crosstalk with other hormones (i.e., jasmonate, salicylic acid, ethylene) related to the plant's immune response. Further investigations are needed to clarify this issue.

Overall, these data represent the first contribution toward understanding the biological effect of zaxinone on tomato plants. In analogy to what has been observed in rice, this metabolite positively regulates tomato growth and development and affects the level of SLs, which participate in the control of many aspects of plant biology. Moreover, the potential role of zaxinone in plant responses to water stresses and plant-pathogenic interactions deserves further attention opening perspectives for future applications in agriculture, especially in light of climate change. As a future perspective, it would be helpful to obtain and characterize mutant lines to fully understand the role between *SlZAS* and zaxinone in tomato development processes and the responses to stresses.

5.5 Summary model

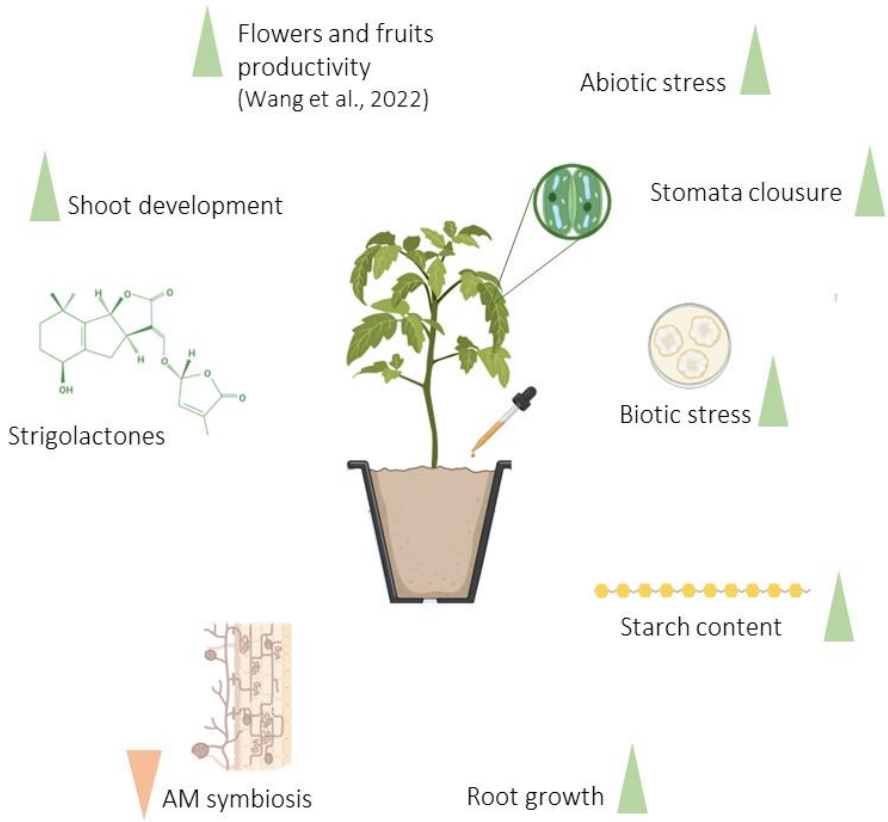

Summary diagram of the effect of exogenous zaxinone treatment on tomato plants. *Green arrows indicate a positive effect of zaxinone on root and shoot development (plants grown in hydroponics and soil), on starch content, on flowers and fruits production (upon a foliar treatment - Wang et al., 2022), and a putative involvement in biotic and abiotic stresses. Orange arrows indicate a negative impact of zaxinone application on SLs biosynthesis and release and on the AM symbiosis. Created with "Biorender".*

5.6 References

Ablazov A., Mi J., Jamil M., Jia K.-P., Wang J.Y., Feng Q., Al-Babili S. (2020) The Apocarotenoid Zaxinone Is a Positive Regulator of Strigolactone and Abscisic Acid Biosynthesis in Arabidopsis Roots. Frontiers in Plant Science, **578**.

Ablazov A., Votta C., Fiorilli V., Wang J.Y., Aljedaani F., Jamil M., Balakrishna A., Balestrini R., Liew K.X., Rajan C., Berqdar L., Blilou I., Lanfranco L., Al-Babili S. (2022) ZAXINONE SYNTHASE 2 *regulates growth and arbuscular mycorrhizal symbiosis in rice*. Plant Physiol.191(1):382-399

Ahrazem O., Gómez-Gómez L., Rodrigo M.J., Avalos J., Limón M.C. (2016) Carotenoid Cleavage Oxygenases from Microbes and Photosynthetic Organisms: Features and Functions. International Journal of Molecular Sciences **17**:1781.

Akiyama K., Matsuzaki K., Hayashi H. (2005) Plant sesquiterpenes induce hyphal branching in arbuscular mycorrhizal fungi. Nature **435**:824–827.

Al-Babili S., Bouwmeester H.J. (2015) Strigolactones, a Novel Carotenoid-Derived Plant Hormone. Annual Review of Plant Biology **66**:161–186.

Bari, V. K., Nassar, J. A., Kheredin, S. M., Gal-On, A., Ron, M., Britt, A., & Aly, R. (2019). CRISPR/Cas9-mediated mutagenesis of *CAROTENOID CLEAVAGE DIOXYGENASE* 8 in tomato provides resistance against the parasitic weed *Phelipanche aegyptiaca*. Scientific reports, **9**(1): 11438.

Bolger A.M., Lohse M., Usadel B. (2014) Trimmomatic: a flexible trimmer for Illumina sequence data. Bioinformatics **30**:2114–2120.

Bouwmeester, H. J., Matusova, R., Zhongkui, S., & Beale, M. H. (2003). Secondary metabolite signalling in host–parasitic plant interactions. Current opinion in plant biology, **6**(4): 358-364.

Bruno M., Beyer P., Al-Babili S. (2015) The potato carotenoid cleavage dioxygenase 4 catalyzes a single cleavage of β-ionone ring-containing carotenes and non-epoxidated xanthophylls. Archives of Biochemistry and Biophysics **572**:126–133.

Bruno M., Koschmieder J., Wuest F., Schaub P., Fehling-Kaschek M., Timmer J., Beyer P., Al-Babili S. (2016) Enzymatic study on AtCCD4 and AtCCD7 and their potential to form acyclic regulatory metabolites. Journal of Experimental Botany **67**:5993–6005.

Chaiwanon J., Wang W., Zhu J.-Y., Oh E., Wang Z.-Y. (2016) Information Integration and Communication in Plant Growth Regulation. Cell **164**:1257–1268.

Chiapello M., Das D., Gutjahr C. (2019) Ramf: An Open-Source R Package for Statistical Analysis and Display of Quantitative Root Colonization by Arbuscular Mycorrhiza Fungi. Frontiers in Plant Science **10**:1184.

Decker E.L., Alder A., Hunn S., Ferguson J., Lehtonen M.T., Scheler B., Kerres K.L., Wiedemann G., Safavi-Rizi V., Nordzieke S., Balakrishna A., Baz L., Avalos J., Valkonen J.P.T., Reski R., Al-Babili S. (2017) Strigolactone biosynthesis is evolutionarily conserved, regulated by phosphate starvation and contributes to resistance against phytopathogenic fungi in a moss, *Physcomitrella patens*. New Phytologist **216**:455–468.

Dickinson A.J., Lehner K., Mi J., Jia K.-P., Mijar M., Dinneny J., Al-Babili S., Benfey P.N. (2019) β-Cyclocitral is a conserved root growth regulator. Proceedings of the National Academy of Sciences **116**:10563–10567.

Felemban A., Braguy J., Zurbriggen M.D., Al-Babili S. (2019) Apocarotenoids Involved in Plant Development and Stress Response. Frontiers in Plant Science **10:**1168.

Fiorilli V., Vallino M., Biselli C., Faccio A., Bagnaresi P., Bonfante P. (2015) Host and non-host roots in rice: cellular and molecular approaches reveal differential responses to arbuscular mycorrhizal fungi. Frontiers in Plant Science **6:**636.

Fiorilli V., Wang J.Y., Bonfante P., Lanfranco L., Al-Babili S. (2019) Apocarotenoids: Old and New Mediators of the Arbuscular Mycorrhizal Symbiosis. Frontiers in Plant Science **10:**1186.

Genre A., Lanfranco L., Perotto S., Bonfante P. (2020) Unique and common traits in mycorrhizal symbioses. Nature Reviews Microbiology **18**:649–660.

Gutjahr C. (2014) Phytohormone signaling in arbuscular mycorhiza development. Current Opinion in Plant Biology **20**:26–34.

Hammer O., Harper D.A.T., Ryan P.D. PAST: Paleontological Statistics Software Package for Education and Data Analysis. :9.

Havaux M. (2014) Carotenoid oxidation products as stress signals in plants. The Plant Journal **79**:597–606.

Ilg A., Beyer P., Al-Babili S. (2009) Characterization of the rice carotenoid cleavage dioxygenase 1 reveals a novel route for geranial biosynthesis: A novel route for geranial formation. FEBS Journal **276**:736–747.

Ilg A., Bruno M., Beyer P., Al-Babili S. (2014) Tomato carotenoid cleavage dioxygenases 1A and 1B: Relaxed double bond specificity leads to a plenitude of dialdehydes, mono-apocarotenoids and isoprenoid volatiles. FEBS Open Bio **4**:584–593.

Jamil M., Kanampiu F.K., Karaya H., Charnikhova T., Bouwmeester H.J. (2012) Striga hermonthica parasitism in maize in response to N and P fertilisers. Field Crops Research **134**:1–10.

Jia K.-P., Baz L., Al-Babili S. (2018) From carotenoids to strigolactones. Journal of Experimental Botany **69**:2189–2204.

Jia K.-P., Dickinson A.J., Mi J., Cui G., Xiao T.T., Kharbatia N.M., Guo X., Sugiono E., Aranda M., Blilou I., Rueping M., Benfey P.N., Al-Babili S. (2019) Anchorene is a carotenoid-derived regulatory metabolite required for anchor root formation in Arabidopsis. Science Advances **5**:eaaw6787.

Kim H.J., Chiang Y.-H., Kieber J.J., Schaller G.E. (2013) SCF ^{KMD} controls cytokinin signaling by regulating the degradation of type-B response regulators. Proceedings of the National Academy of Sciences **110**:10028–10033.

Kohlen W., Charnikhova T., Lammers M., Pollina T., Tóth P., Haider I., Pozo M.J., de Maagd R.A., Ruyter-Spira C., Bouwmeester H.J., López-Ráez J.A. (2012) The tomato CAROTENOID CLEAVAGE DIOXYGENASE8 (SlCCD8) regulates rhizosphere signaling, plant architecture and affects reproductive development through strigolactone biosynthesis. The New Phytologist **196**:535–547.

Kolberg L., Raudvere U., Kuzmin I., Vilo J., Peterson H. (2020) gprofiler2 -- an R package for gene list functional enrichment analysis and namespace conversion toolset g:Profiler. F1000Research **9**:ELIXIR-709.

Lanfranco L., Fiorilli V., Venice F., Bonfante P. (2018) Strigolactones cross the kingdoms: plants, fungi, and bacteria in the arbuscular mycorrhizal symbiosis. Journal of Experimental Botany **69**:2175–2188.

Livak K.J., Schmittgen T.D. (2001) Analysis of Relative Gene Expression Data Using Real-Time Quantitative PCR and the $2^{-\Delta\Delta CT}$ Method. Methods 25:402–408.

López-Ráez, J. A., Charnikhova, T., Gómez-Roldán, V., Matusova, R., Kohlen, W., De Vos, R., ... & Bouwmeester, H. (2008). Tomato strigolactones are derived from carotenoids and their biosynthesis is promoted by phosphate starvation. New Phytologist, **178:** 863-874.

López-Ráez, J. A., Kohlen, W., Charnikhova, T., Mulder, P., Undas, A. K., Sergeant, M. J., ... & Bouwmeester, H. (2010). Does abscisic acid affect strigolactone biosynthesis? New phytologist, **187**(2): 343-354.

López-Ráez J.A., Fernández I., García J.M., Berrio E., Bonfante P., Walter M.H., Pozo M.J. (2015) Differential spatio-temporal expression of carotenoid cleavage dioxygenases regulates apocarotenoid fluxes during AM symbiosis. Plant Science **230**:59–69.

Love M.I., Huber W., Anders S. (2014) Moderated estimation of fold change and dispersion for RNA-seq data with DESeq2. Genome Biology **15**:550.

Lv S., Zhang Y., Li C., Liu Z., Yang N., Pan L., Wu J., Wang J., Yang J., Lv Y., Zhang Y., Jiang W., She X., Wang G. (2018) Strigolactone-triggered stomatal closure requires hydrogen peroxide synthesis and nitric oxide production in an abscisic acid-independent manner. New Phytologist **217**:290–304.

Ma X., Balazadeh S., Mueller-Roeber B. (2019) Tomato fruit ripening factor NOR controls leaf senescence. Journal of Experimental Botany **70**:2727–2740.

Markmann, K., & Parniske, M. (2009). Evolution of root endosymbiosis with bacteria: how novel are nodules?. Trends in plant science, **14**(2): 77-86.

Marzec M. (2016) Strigolactones as Part of the Plant Defence System. Trends in Plant Science **21**:900–903.

Merilo E., Jalakas P., Laanemets K., Mohammadi O., Hõrak H., Kollist H., Brosché M. (2015) Abscisic Acid Transport and Homeostasis in the Context of Stomatal Regulation. Molecular Plant **8**:1321–1333.

Mi J., Jia K.-P., Balakrishna A., Wang J.Y., Al-Babili S. (2019) An LC-MS profiling method reveals a route for apocarotene glycosylation and shows its induction by high light stress in Arabidopsis. The Analyst **144**:1197–1204.

Moise A.R., Al-Babili S., Wurtzel E.T. (2014) Mechanistic Aspects of Carotenoid Biosynthesis. Chemical Reviews **114**:164–193.

Moreno J.C., Mi J., Alagoz Y., Al-Babili S. (2021) Plant apocarotenoids: from retrograde signaling to interspecific communication. The Plant Journal **105**:351–375.

Nambara E., Marion-Poll A. (2005) Abscisic Acid Biosynthesis and Catabolism. Annual Review of Plant Biology **56**:165–185.

Nisar N., Li L., Lu S., Khin N.C., Pogson B.J. (2015) Carotenoid Metabolism in Plants. Molecular Plant **8**:68–82.

Pan Z., Zeng Y., An J., Ye J., Xu Q., Deng X. (2012) An integrative analysis of transcriptome and proteome provides new insights into carotenoid biosynthesis and regulation in sweet orange fruits. Journal of Proteomics **75**:2670–2684.

Felemban, A., Braguy, J., Zurbriggen, M. D., & Al-Babili, S. (2019). Apocarotenoids involved in plant development and stress response. Frontiers in Plant Science, **10**: 1168.

Peláez-Vico MA, Bernabéu-Roda L, Kohlen W, Soto MJ, López-Ráez JA (2016) Strigolactones in the Rhizobium-legume symbiosis: Stimulatory effect on bacterial surface motility and down-regulation of their levels in nodulated plants. Plant Science **245**: 119–127.

Ramel F., Birtic S., Ginies C., Soubigou-Taconnat L., Triantaphylidès C., Havaux M. (2012) Carotenoid oxidation products are stress signals that mediate gene responses to singlet oxygen in plants. Proceedings of the National Academy of Sciences **109**:5535–5540.

Rubio-Moraga A., Rambla J.L., Fernández-de-Carmen A., Trapero-Mozos A., Ahrazem O., Orzáez D., Granell A., Gómez-Gómez L. (2014) New target carotenoids for CCD4 enzymes are revealed with the characterization of a novel stress-induced carotenoid cleavage dioxygenase gene from Crocus sativus. Plant Molecular Biology **86**:555–569.

Ruiz-Lozano, J. M., Aroca, R., Zamarreño, Á. M., Molina, S., Andreo-Jiménez, B., Porcel, R., ... & López-Ráez, J. A. (2016). Arbuscular mycorrhizal symbiosis induces strigolactone biosynthesis under drought and improves drought tolerance in lettuce and tomato. *Plant, cell & environment*, ***39***(2): 441-452.

Soneson C., Love M.I., Robinson M.D. (2015) Differential analyses for RNA-seq: transcript-level estimates improve gene-level inferences. F1000Research 4:1521.

Soto MJ, Fernández-Aparicio M, Castellanos-Morales V, García-Garrido JM, Ocampo JA, Delgado MJ, Vierheilig H. 2010. First indications for the involvement of strigolactones on nodule formation in alfalfa (Medicago sativa). Soil Biology and Biochemistry 42: 383–385.

Sui X., Kiser P.D., Lintig J. von, Palczewski K. (2013) Structural basis of carotenoid cleavage: From bacteria to mammals. Archives of Biochemistry and Biophysics 539:203–213.

Sun T., Yuan H., Cao H., Yazdani M., Tadmor Y., Li L. (2018) Carotenoid Metabolism in Plants: The Role of Plastids. Molecular Plant 11:58–74.

Tan B.-C., Joseph L.M., Deng W.-T., Liu L., Li Q.-B., Cline K., McCarty D.R. (2003) Molecular characterization of the Arabidopsis 9-cis epoxycarotenoid dioxygenase gene family. The Plant Journal: For Cell and Molecular Biology 35:44–56.

Torres-Vera, R., García, J. M., Pozo, M. J., & López-Ráez, J. A. (2014). Do strigolactones contribute to plant defence?. Molecular Plant Pathology, 15(2): 211-216.

Trouvelot A., Kough J.L., Gianinazzi-Pearson V. (1986) Estimation of vesicular arbuscular mycorrhizal infection levels. Research for methods having a functional significance. Physiological and genetical aspects of mycorrhizae = Aspects physiologiques et genetiques des mycorhizes : proceedings of the 1st European Symposium on Mycorrhizae, Dijon, 1-5 July 1985.

Tuan P.A., Kumar R., Rehal P.K., Toora P.K., Ayele B.T. (2018) Molecular Mechanisms Underlying Abscisic Acid/Gibberellin Balance in the Control of Seed Dormancy and Germination in Cereals. Frontiers in Plant Science 9:668.

Visentin I., Vitali M., Ferrero M., Zhang Y., Ruyter-Spira C., Novák O., Strnad M., Lovisolo C., Schubert A., Cardinale F. (2016) Low levels of strigolactones in roots as a component of the systemic signal of drought stress in tomato. New Phytologist 212:954–963.

Vogel J.T., Tan B.-C., McCarty D.R., Klee H.J. (2008) The Carotenoid Cleavage Dioxygenase 1 Enzyme Has Broad Substrate Specificity, Cleaving Multiple Carotenoids at Two Different Bond Positions. Journal of Biological Chemistry 283:11364–11373.

Votta C., Fiorilli V., Haider I., Wang J.Y., Balestrini R., Petřík I., Tarkowská D., Novák O., Serikbayeva A., Bonfante P., Al-Babili S., Lanfranco L. (2022) Zaxinone Synthase controls arbuscular mycorrhizal colonization level in rice. The Plant Journal:tpj.15917.

Wang J.Y., Alseekh S., Xiao T., Ablazov A., Perez de Souza L., Fiorilli V., Anggarani M., Lin P.-Y., Votta C., Novero M., Jamil M., Lanfranco L., Hsing Y.-I.C., Blilou I., Fernie A.R., Al-Babili S. (2021) Multi-omics approaches explain the growth-promoting effect of the apocarotenoid growth regulator zaxinone in rice. Communications Biology 4:1–11.

Wang J.Y., Haider I., Jamil M., Fiorilli V., Saito Y., Mi J., Baz L., Kountche B.A., Jia K.-P., Guo X., Balakrishna A., Ntui V.O., Reinke B., Volpe V., Gojobori T., Blilou I., Lanfranco L., Bonfante P., Al-Babili S. (2019) The apocarotenoid metabolite zaxinone regulates growth and strigolactone biosynthesis in rice. Nature Communications 10:810.

Wang J.Y., Jamil M., Hossain Md.G., Chen G.-T.E., Berqdar L., Ota T., Blilou I., Asami T., Al-Solimani S.J., Mousa M.A.A., Al-Babili S. (2022) Evaluation of the Biostimulant Activity of Zaxinone Mimics (MiZax) in Crop Plants. Frontiers in Plant Science 13.

Wang J.Y., Jamil M., Lin P.-Y., Ota T., Fiorilli V., Novero M., Zarban R.A., Kountche B.A., Takahashi I., Martínez C., Lanfranco L., Bonfante P., de Lera A.R., Asami T., Al-Babili S. (2020) Efficient Mimics for Elucidating Zaxinone Biology and Promoting Agricultural Applications. Molecular Plant 13:1654–1661.

Wang J.Y., Lin P.-Y., Al-Babili S. (2021) On the biosynthesis and evolution of apocarotenoid plant growth regulators. Seminars in Cell & Developmental Biology 109:3–11.

Xie X., Yoneyama K., Yoneyama K. (2010) The Strigolactone Story. Annual Review of Phytopathology 48:93–117.

Yoneyama K., Kisugi T., Xie X., Yoneyama K. (2013) Chemistry of Strigolactones: Why and How do Plants Produce so Many Strigolactones? In: Molecular Microbial Ecology of the Rhizosphere. John Wiley & Sons, Ltd, pp 373–379.

5.7 Supplementary material

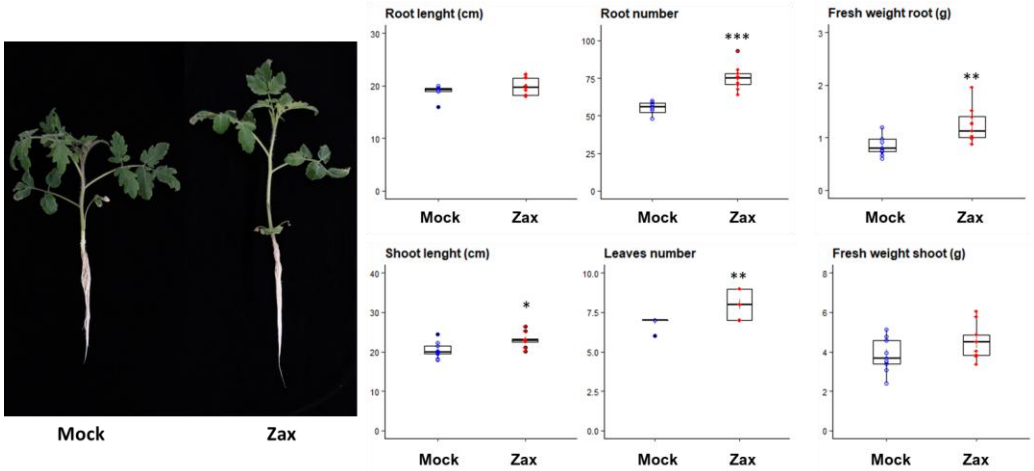

Supplementary figure 1. Phenotypic evaluation of tomato plants treated (Zax) or not (Mock) with zaxinone (5 µM) grown hydroponically. *Root number, root and shoot length, root and shoot biomass, and number of leaves were evaluated. n = 15. Data represent ± SE. Significant values (by one-way Anova) are shown as follows: *P < 0.05; **P<0.01; ***P<0.001.*

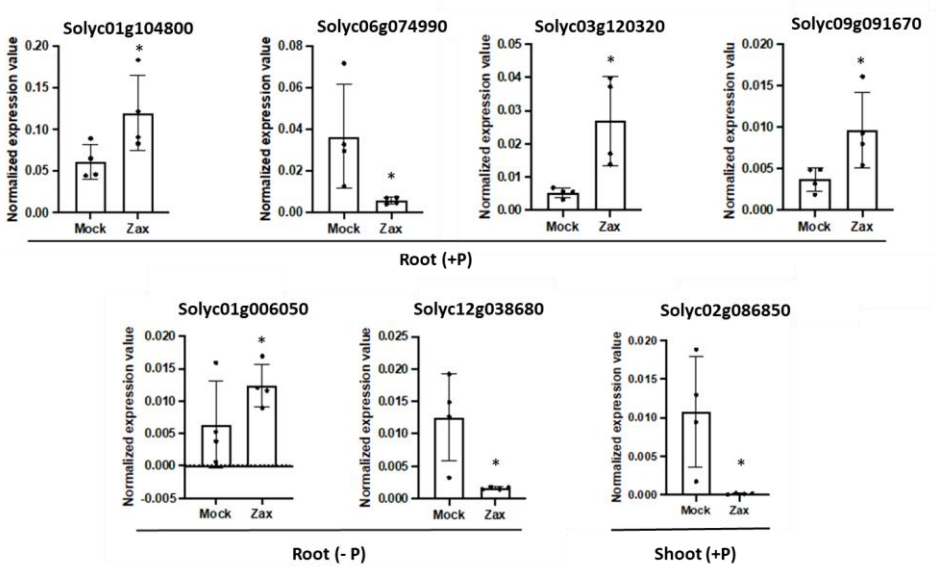

Supplementary figure 2. *Validation of RNAseq by q-RTPCR. 7 selected genes showing high to low fold change in expression upon zaxinone treatment. n=4 biological replicates. Data represent ± SE. Significant values (by one-way Anova) are shown as follows: *P < 0.05.*

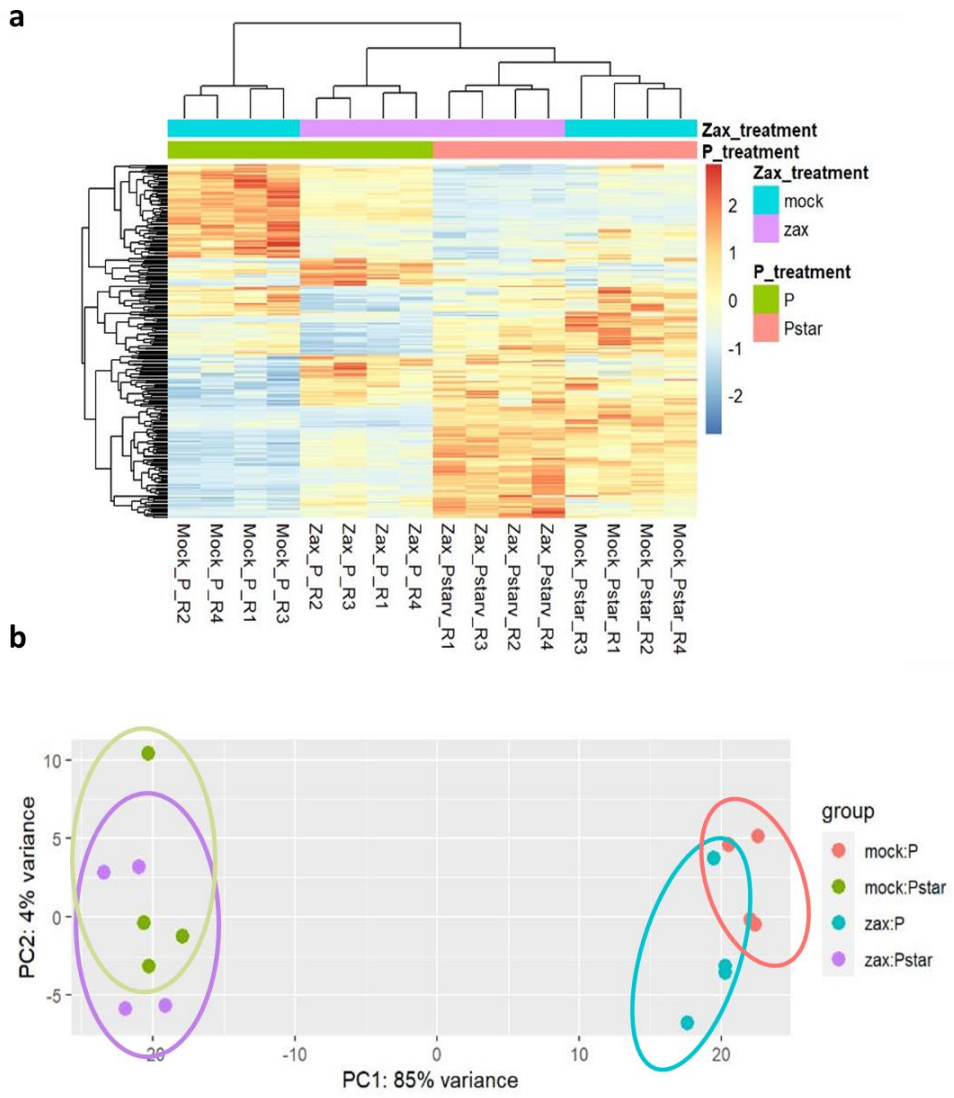

Supplementary figure 3. a. *Heatmap of zaxinone related DE genes in root.* ***b.*** *Principal component analysis (PCA) plots in root after zaxinone treatment (6h). n=4 biological replicates.*

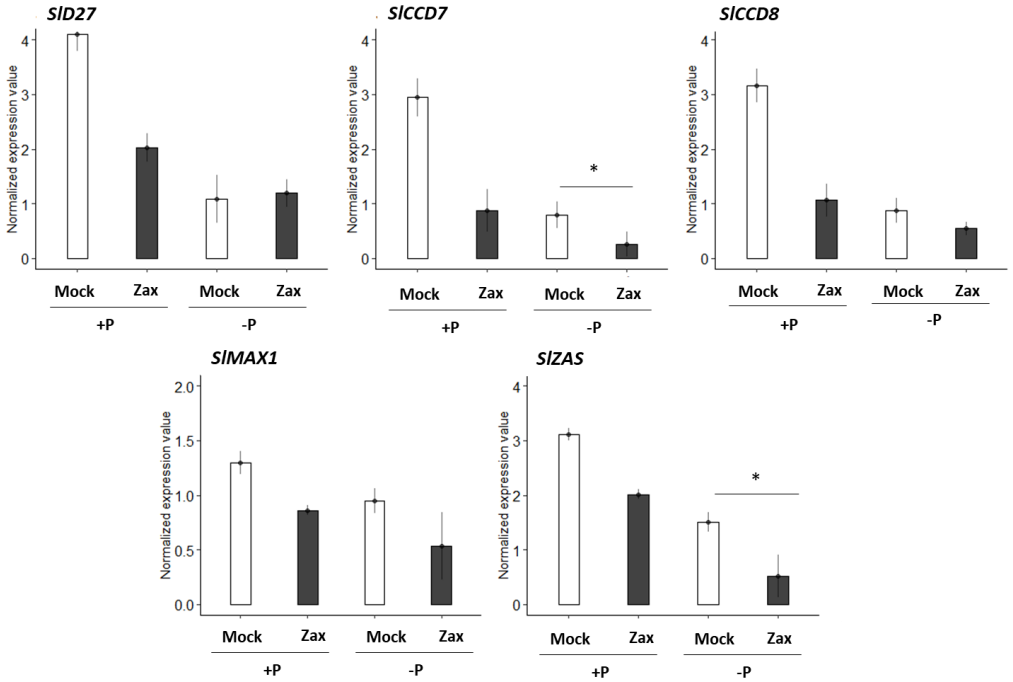

Supplementary figure 4. *Validation of SL biosynthesis genes (D27, CCD7, CCD8, MAX1) and ZAS by q-RT-PCR using RNASeq samples**.** Bar presented mean ± SE, n=4 biological replicates. Asterisks indicate statistically significant differences as compared to control by t-test (*p < 0.05).*

Experiment	Primer name	Sequence (5′–3′)
	***SlD27* F**	TCCCTAAGCCTATTCTTTCTCTG
	***SlD27* R**	TCACCTCACAAGGTCCAACTA
	***SlCCD7* F**	ACGGGTCAGGTTAAGTTTATG
	***SlCCD7* R**	CAACCATCTTCCCTCCTTTC
	***SlCCD8* F**	TGTACATGTTATGTGTAAAGCCAGTG
	***SlCCD8* R**	CACAGCAATCTGCAATCACA
	***SlMAX1* F**	GGTTCTGCAACAACATCCTTTAC
	***SlMAX1* R**	CAAACCCATGTTCCCTTG
	***SlZas1* F**	CCACGTTATGGTGATGCTAA
	***SlZas1* R**	TCACCACCACCTCATCATA
	***SlUbi* F**	TCCAGACCAGCAGAGATT
	***SlUbi* R**	CTCTAAGGCGAAGAACAAGG
Mycorrhizal plant	***SlPT4* F**	CCGAGACAAAAGGGAGATCAC
	***SlPT4* R**	CCAGAGACAGGTTTGCTAGTC
	***SlUbi* F**	ACCAAGCCAAAGAAGATCAAGC
	***SlUbi* R**	GTGAGCCCACACTTACCACAGT
Osmotic stress	***SlUbi* F**	ACCAAGCCAAAGAAGATCAAGC
	***SlUbi* R**	GTGAGCCCACACTTACCACAGT
	***SlNCED1* F**	ACCCACGAGTCCAGATTTC
	SlNCED1 R	GGTTCAAAAAGAGGGTTAG

Table 1. Primer sequences used in this study.

Chapter 6: Integration of Apocarotenoid Profile and Expression Pattern of Carotenoid Cleavage Dioxygenases during Mycorrhization in Rice

6.1 Introduction

Carotenoids represent an extended class of tetraterpene (C_{40}) lipophilic pigments, synthesized by all photosynthetic organisms (bacteria, algae, and plants) and by numerous non-photosynthetic microorganisms (Nisar *et al.* 2015). In plants, carotenoids are essential constituents of the photosynthetic apparatus, where they act as photoprotective pigments and take part in the light-harvesting process. Further, these pigments have ecological functions, providing flowers and fruits with specific colors and flavors that attract insects and other animals or, in contrast, as a repellent for pathogens and pests (Cazzonelli 2011).

The carotenoid structure, rich in electrons and conjugated double bonds, makes them susceptible to oxidation, which causes the breakage of their backbone and leads to a wide range of metabolites called apocarotenoids (Moreno *et al.* 2021). These compounds can be generated by non-enzymatic processes that are triggered by reactive oxygen species (ROS) (Harrison & Bugg 2014; Ahrazem *et al.* 2016) or by the action of a ubiquitous family of non-heme iron enzymes, called carotenoid cleavage dioxygenases (CCDs).

The genome of the model plant *Arabidopsis thaliana* comprises nine members of the CCD family, including five 9-*cis*-epoxy carotenoid dioxygenases (NCED2, NCED3, NCED5, NCED6, and NCED9) and four CCDs (CCD1, CCD4, CCD7, and CCD8) (Tan *et al.* 2003; Sui *et al.* 2013). In short, NCEDs catalyze the first step in abscisic acid (ABA, C_{15}) biosynthesis cleaving 9-*cis*-violaxanthin or 9'-*cis*-neoxanthin forming xanthoxin, the ABA precursor (Nambara & Marion-Poll 2005; Ahrazem *et al.* 2016). CCD1 cleaves several carotenoids and apocarotenoids at different positions along their carbon structure (Schwartz *et al.* 2001; Vogel *et al.* 2008; Ilg *et*

al. 2009, 2014) generating volatile compounds (i.e., β-ionone, β-cyclocitral, geranylacetone, and pseudoionone) in fruit and flowers of various plant species, and dialdehydes with several chain lengths (Moreno *et al.* 2021). CCD4 and CCD1 enzymes are known to produce apocarotenoid-derived pigments, flavors, and aromas *in planta*, but their biochemical functions differ considerably (Schwartz *et al.* 2001; Auldridge *et al.* 2006; Ilg *et al.* 2009). In plants, two different forms of CCD4 are present (Huang *et al.* 2009): one, exclusive of *Citrus*, is involved in citraurin formation and carotenoid turnover in different tissues (Pan *et al.* 2012), while the other type mediates the cleavage of bicyclic all-*trans*-carotenoids at the C9, C10 or C9', C10' double bond leading to apo-10'-carotenoids (C_{27}) and the corresponding C_{13} cyclohexenone outcome (i.e., β-ionone) (Bruno *et al.* 2015, 2016).

CCD7 and CCD8 are involved in strigolactone (SL) biosynthesis: CCD7 cleaves 9-*cis*-β-carotene (C_{40}) to give β-ionone and 9-*cis*-β-apo-10'-carotenal (C_{27}) while CCD8 leads to the conversion of 9-*cis*-apo-10'-carotenal (C_{27}) into carlactone, the SL precursor (Alder *et al.* 2012). In addition, CCD7 may also catalyse the initial 9,10 cleavage required for mycorradicin synthesis (Floss *et al.* 2008).

A recent survey on plant genomes identified another CCD subfamily, *Zaxinone Synthase* (*ZAS*), which is conserved in most land plants but missing in non-mycorrhizal species, i.e., *A. thaliana* (Fiorilli *et al.* 2019; Wang *et al.* 2019). *In vitro*, this enzyme cleaves a molecule of 3-OH-β-apo-10'-carotenal (C_{27}) at the C13-C14 double bond, generating zaxinone, a C_{18}-ketone (3-OH-β-apo-13-carotenone), and an unstable C_9-dialdehyde (Wang *et al.* 2019). Loss-of-function *zas* mutant showed a decreased zaxinone content in roots, reduced shoot, and root growth, and a higher SL level compared to wild-type rice plants (Wang *et al.* 2019). Phylogenetic analyses revealed that the rice genome encodes three *OsZAS* homologs, named *OsZAS1b*, *OsZAS1c*, and *OsZAS2* (Ablazov *et al.* 2022). Intriguingly, although *OsZAS2* is placed in a clade different from that of ZAS, it catalyses the same reaction, and both enzymes contribute to zaxinone production in rice (Ablazov *et al.* 2022).

Apocarotenoids play several roles in plants from the regulation of root and shoot developmental processes to plant responses to abiotic and biotic stresses (Moreno *et al.* 2021). They are also emerging signalling molecules implicated in plant-microbe interactions, including the arbuscular mycorrhizal (AM) symbiosis (Fiorilli *et al.* 2019).The AM symbiosis is one of the most ancient and widespread association, formed by approximately 70% of land plants (Wang & Qiu 2006; Brundrett 2009), including major crops, and soil fungi belonging to the *Glomeromycotina* group (Spatafora *et al.* 2016). The fungus facilitates the plant uptake of minerals, predominantly phosphorus (P) and nitrogen (N) (Smith *et al.* 2011), and the tolerance to biotic and abiotic stresses (Pozo *et al.* 2010; Chen *et al.* 2018). Meanwhile, the plant provides the fungus with photosynthetically fixed organic carbon. The establishment of the AM symbiosis includes several steps, starting with partners recognition *via* diffusible molecules, which activate the common symbiosis signaling pathway (MacLean *et al.* 2017) and trigger the development of fungus adhesion structures, called hyphopodia, on the root epidermis. These structures permit the fungus to enter the host root tissues and proliferate intercellularly and/or intracellularly (Bonfante & Requena 2011; Nadal & Paszkowski 2013). Finally, fungal hyphae invade the inner cortical layers, penetrate single cells and form highly branched tree-shaped hyphal structures, the arbuscules, where nutrient exchanges occur (Harrison 2012; Gutjahr & Parniske 2013). During these stages, the plant controls fungal expansion and symbiotic functions, by activating a series of cellular, metabolic, and physiological changes (Gutjahr 2014; Carbonnel & Gutjahr 2014). Among the environmental factors that regulate AM colonization, phosphate (Pi) availability is certainly one of the most crucial (Smith *et al.* 2011; Richardson *et al.* 2011). It has been recently shown that a complex gene network centered on the plant Pi starvation response actively supervises AM fungal development in roots acting at the local and systemic level (Shi *et al.* 2021; Das *et al.* 2022). Pi starvation also triggers the upregulation of genes involved in SLs biosynthesis (Yoneyama *et al.*

2007; Wang *et al.* 2017) while high Pi levels repress the expression of genes involved in the biosynthesis of carotenoids and SLs (Carbonnel & Gutjahr 2014).

SLs are the best-known plant molecules active in the pre-symbiotic AM interaction. In Pi-starved plants, SLs are produced by roots and exported to the rhizosphere, which directly stimulates AM fungal metabolism, gene expression, and hyphal branching, supporting the development of this symbiosis (Waters *et al.* 2017; Müller & Harrison 2019). Notably, Volpe *et al.* (2022) recently showed that SL biosynthesis is stimulated by chito-oligosaccharides released by AM fungi.

Studies of the last decade highlighted that other apocarotenoid compounds are involved in the AM symbiosis (Fiorilli *et al.* 2019 and reference therein). Among these, there is ABA, which is known for coordinating the plant's response to biotic and abiotic stress factors (Felemban *et al.* 2019; Moreno *et al.* 2021). The role of ABA in mycorrhizal colonization has been reported in different host plants: ABA is probably acting through synergistic and antagonistic interactions with other hormones (Herrera-Medina *et al.* 2007; Martín-Rodríguez *et al.* 2011; Charpentier *et al.* 2014). Specifically, ABA and SLs influence the outcome of the symbiosis, regulating each other reciprocally (López-Ráez *et al.* 2010). In contrast, an antagonistic interaction with ethylene (Martín-Rodríguez *et al.* 2011) and gibberellins (GA) (Floss *et al.* 2013; Martín-Rodríguez *et al.* 2016) was reported: ABA controls the normal development of arbuscules inhibiting ethylene production (Martín-Rodríguez *et al.* 2011). Moreover, this apocarotenoid modifies bioactive GA levels, acting on GA-biosynthesis and catabolism; and *vice versa* GA activates ABA catabolism, regulating AM formation (Martín-Rodríguez *et al.* 2016).
Other classes of apocarotenoids - blumenols (C_{13}) and mycorradicin (C_{14}) - were described as a signature for AM symbiosis since they are specifically accumulated in mycorrhizal plants (Walter *et al.* 2007; Hill *et al.* 2018; Moreno *et al.* 2021). They are associated with AM symbiosis establishment and maintenance (Walter *et al.*

2007; Floß *et al.* 2008; Floss *et al.* 2008; Fiorilli *et al.* 2019). Mycorradicins cause typical yellow/orange pigmentation of roots, which allowed the experts in the field to identify them for the first time (Scannerini & Bonfante-Fasolo 1977; Klingner *et al.* 1995; Floss *et al.* 2008). Blumenols are accumulated in the roots and shoots of host plants in direct correlation with the fungal colonization rate (Klingner *et al.* 1995; Maier *et al.* 1997; Walter *et al.* 2000; Fester *et al.* 2002; Strack & Fester 2006). Even if their biological role has not yet been clarified, blumenols have been proposed as foliar markers that allow rapid detection of AM symbiosis and screening of functional AM associations (Walter *et al.* 2010; Wang *et al.* 2018). In addition, zaxinone acts as a plant growth regulator controlling plant architecture and development (Wang *et al.* 2019). We recently demonstrated that *OsZAS* influences the extent of AM colonization, acting as a component of a regulatory network that involves SLs (Votta *et al.* 2022).

In the current study, to further explore the involvement of other apocarotenoids in the AM symbiosis we generated a qualitative and quantitative profile of apocarotenoids in roots and shoots of rice plants exposed to high/low Pi concentrations (+Pi and -Pi) and upon AM symbiosis. We quantified different non-hydroxylated and hydroxylated apocarotenoids in a time course experiment covering different stages of growth and AM development, by using an ultra-HPLC (UHPLC)-mass spectrometry (MS)-based approach (Mi *et al.* 2018) and, in parallel, we characterized the gene expression profiles of a set of CCDs genes. We also took advantage of chemometric tools such as Principal Component Analysis (Bro & K. Smilde 2014) and the low-level data fusion approach (Borràs *et al.* 2015), the latter used with the aim of combining and jointly exploring the information of the apocarotenoids and genes datasets.

6.2 Material and methods

Plant and fungal material Rice seeds of wild-type (cv. Nipponbare) were germinated in pots containing sand and incubated for 10 days in a growth chamber under 14 h light (23 °C)/10 h dark (21 °C). A set of plants (MYC) was inoculated with *Funneliformis mosseae* (BEG 12, MycAgroLab, France). The fungal inoculum (15%) was mixed with sterile quartz sand and used for colonization. A group of non-mycorrhizal plants (no-myc -Pi) was also set up. These two groups of plants (MYC and no-myc -Pi) were watered with a modified Long-Ashton (LA) solution containing 3.2 µM $Na_2HPO_4 \cdot 12H_2O$ (low Pi) and grown in a growth chamber under 14 h light (24 °C)/10 h dark (20 °C) regime. Another group of no-myc WT plants was watered with a LA containing 500 µM $Na_2HPO_4 \cdot 12\ H_2O$ (+Pi) and grown in the same condition described above; these plants were considered the no-myc + Pi samples. Plants for the three different conditions (MYC, no-myc -Pi, no-myc +Pi) were collected at three time points: 7 days post-inoculation (dpi), 21 dpi, and 35 dpi. For the molecular and metabolites analyses, roots and shoots samples were harvested and immediately frozen in liquid nitrogen and stored at -80°C. Some MYC roots were used for the morphological evaluation of mycorrhization according to Trouvelot *et al.* (1986): samples were clarified in KOH, stained with 0.1% cotton blue in lactic acid and the estimation of mycorrhizal parameters was performed using "Ramf" an open-source R package (https://github.com/mchiapello/Ramf) (Chiapello *et al.* 2019).

Qualitative and quantitative profiling of plant apocarotenoids (APOs). Following the method used by Mi *et al.* (2018), about 20 mg lyophilized root and shoot tissue powder was spiked with Internal Standards (IS) mixture (2 ng each standard) and extracted with 2 mL of methanol containing 0.1% BHT in an ultrasound bath (Branson 3510 ultrasonic bath) for 15 min, followed by the centrifugation. The supernatant was collected, and the pellet was re-extracted with 1 mL of the same solvent. The two supernatants were then combined and dried under

vacuum. The residue was re-dissolved in 150 mL of acetonitrile and filtered through a 0.22 mm filter for LC-MS analysis.

Analysis of apocarotenoids in plant tissue material was performed on a Dionex Ultimate 3000 UHPLC system coupled with a Q-Orbitrap- MS (Q-Exactive plus MS, Thermo Scientific) with a heated electrospray ionization source. Chromatographic separation was carried out on an ACQUITY UPLC BEH C18 column (100 x 2.1mm,1.7 mm) with a UPLC BEH C18 guard column (5 x 2.1mm, 1.7 mm) maintained at 35°C. UHPLC conditions including mobile phases and gradients were optimized based on the separation of APOs and the time needed for sample analysis. The quantification of APOs was calculated as follows: Amount [target APO] = Area [target APO]/Area [spiked IS] x Amount [spiked IS]/ mg materials.

Gene expression analysis. Total RNA was extracted from WT rice roots using the Qiagen Plant RNeasy Kit according to the manufacturer's instructions (Qiagen, Hilden; Germany). Following the producer's directives, samples were treated with TURBO™ DNase (Thermofischer). The RNA samples were routinely checked for DNA contamination through PCR analysis. Single-strand cDNA was synthesized from 1 μg of total RNA using Super-Script II (Invitrogen) according to the instructions in the user manual. Quantitative RT-PCR (qRT-PCR) was performed using a Rotor-Gene Q 5plex HRM Platform (Qiagen). All reactions were performed on at least three biological and three technical replicates. Baseline range and take-off values were automatically calculated using Rotor-Gene Q 5plex software. The transcript level of genes listed in **Supplemental Table 1** was normalized using *OsRubQ1* housekeeping gene (Güimil *et al.* 2005). Only take-off values leading to a Ct mean with a standard deviation below 0.5 were considered.

Statistics and reproducibility. Both experiments (plant apocarotenoid quantification and CCD gene expression analysis) were performed with at least three biological replicates each. Statistical tests were carried out through One-way analysis of variance (One-way ANOVA) and Tukey's *post hoc* test, using a probability level

of $P<0.05$. All statistical elaborations were performed using PAST statistical package version 4 (Hammer *et al.*).

Data quality assessment and preprocessing. Gene and apocarotenoid datasets were inspected to spot potential extreme samples or outliers. Different preprocessing approaches were tested, including autoscaling (i.e., column scaling to unit variance, followed by mean centering) and normalization to a unit area (i.e., the normalization factor of each sample was computed from its "area under the curve") followed by mean centering. Based on the ease of interpretation, we selected the following preprocessing: mean centering alone for the apocarotenoids dataset, and autoscale for the genes dataset. All modeling results were therefore obtained from the two datasets preprocessed as such. Regarding the analysis with the low-level data fusion approach (i.e., combining the two datasets into an individual one), a different sequence tailored to the issue of obtaining an equal representation of the two datasets was used, as described in the dedicated paragraph further in this Section (Data fusion approach).

Exploratory analysis. All chemometric models reported in this work are "exploratory", meaning that they describe the phenomena and natural groupings captured in the data, in an unsupervised manner (Li Vigni *et al.* 2013). To this aim, Principal Component Analysis (PCA) (Bro & K. Smilde 2014) was employed. This technique is exploited to capture, in sequence, the largest sources of variability by defining new variables (the so-called "Principal Components", PCs), which are summaries of the different pieces of information contained in the data. This "summarized" version of the information can be inspected with the scores and loadings plots, which are scatter plots obtained by plotting pairs (and sometimes triplets) of PCs. The scores plot allows inspecting the relationships among the samples and thus spotting possible groupings and tendencies of interest, and the loadings plot allows inspecting the relationships among the variables of the data, while at the same time providing an interpretation of the scores plot. In our study,

individual apocarotenoids and genes were identified by their systematic names and inspected in PCA as the samples. At the same time, the variables of the datasets were the combinations of three-time points (7, 21, and 35 dpi) and three conditions (MYC, no-myc -Pi, no-myc +P) for a total of nine combinations.

Data fusion approach. We used a low-level data fusion approach (Borràs *et al.* 2015) to combine and jointly explore the information of the apocarotenoids and genes datasets. In our study, the apocarotenoids dataset was joined with the genes dataset in the sample direction so that the nine variables (combinations of time points and conditions) were coherent between the two datasets, i.e., the information described by each column had to be the same in both datasets.

We performed the following data preprocessing and fusion sequence: (i) standard deviation scaling for each APO/gene quantification, (ii) fusion of the two data tables, (iii) group scale to give the two data tables the same importance (i.e., each dataset accounts for 50 % of the total variance of the resulting fused dataset), (iv) mean center. The new fused data table was then modelled with PCA, with the apocarotenoids and the genes as the samples (rows) and the combinations of time points and treatments as the variables (columns) (**Supplementary figure 1**).

6.3 Results

CCD gene expression pattern

We characterized the transcript level of a gene set of CCDs (*CCD1*, *CCD4a*, *CCD4b*, *CCD7*, *CCD8*, *ZAS1*, *ZAS1b*, *ZAS1c*, *ZAS2*) in mycorrhizal plants grown at low Pi (3.2 μM) and in non-mycorrhizal plants grown at low (3.2 μM) or high Pi (500 μM) during a time course experiment corresponding to early (7 dpi), middle (21 dpi) and late (35 dpi) stages of AM symbiosis development (**Supplementary Figure 2 A-B**). To assess the statistically significant differences, all samples were referred to the -Pi condition within each time point. As shown in the heatmap (**Figure 1 A**) referred to roots, *CCD1*, *CCD4a*, and *CCD4b* increase at 21 dpi in the +Pi condition compared to -Pi and MYC ones. Concerning the SLs biosynthesis genes, we observed an induction of *CCD7* in MYC roots at the middle and late stages (21, 35 dpi), while *CCD8* was induced at 7 dpi under the MYC condition, and, as expected (López-Ráez *et al.* 2008; Yoneyama *et al.* 2013), down-regulated under +Pi condition in the later time points (at 21 and 35 dpi). At the middle stage (21dpi) *ZAS1* showed an up-regulation in MYC samples and a down-regulation under +Pi. The *ZAS1* homolog, *ZAS1b* was upregulated at 21 dpi in MYC and +Pi roots, while a down-regulation was detected in MYC roots during the later stage. By contrast, *ZAS1c* was up-regulated at 35 dpi in MYC roots. Finally, the *ZAS2* expression level was induced at 21 dpi in +P (**Supplementary figure 3 A**).

The *CCDs* gene expression level in shoots (**Figure 1 B, Supplementary figure 3 B**) displayed several differences compared to roots. We detected induction of *CCD1* at 21 dpi in the +Pi condition, while its expression was down-regulated in the MYC condition at 21 and 35 dpi. *CCD4a* showed an expression profile similar to *CCD1*. By contrast, *CCD4b* displayed an opposite trend compared to *CCD4a* with an up-regulation at 35 dpi in the MYC condition. Moreover, *CCD4b* displayed an up-regulation at 7 dpi in the +Pi condition.

Considering SLs biosynthesis genes, while *CCD7* expression was not modulated across all conditions or time points, *CCD8* was up-regulated at 7 dpi (MYC and +Pi conditions) while it was down-regulated in the later stages (21 and 35 dpi) in the shoot of plants grown in +Pi and at 35 dpi in shoots of MYC plants. *ZAS1* displayed a down-regulation trend in all time points and conditions considered, with a statistically significant difference in mycorrhizal samples at 7 dpi. *ZAS1b*, and *ZAS1c*, showed an up-regulation in leaves of the MYC plant at the first time point (7 dpi) and 21 dpi upon +Pi. Lastly, *ZAS2* was barely detected in the shoot of plant growth at low Pi, while it showed an up-regulation at 21 dpi in MYC and +Pi conditions and a down-regulation in +Pi at 35 dpi.

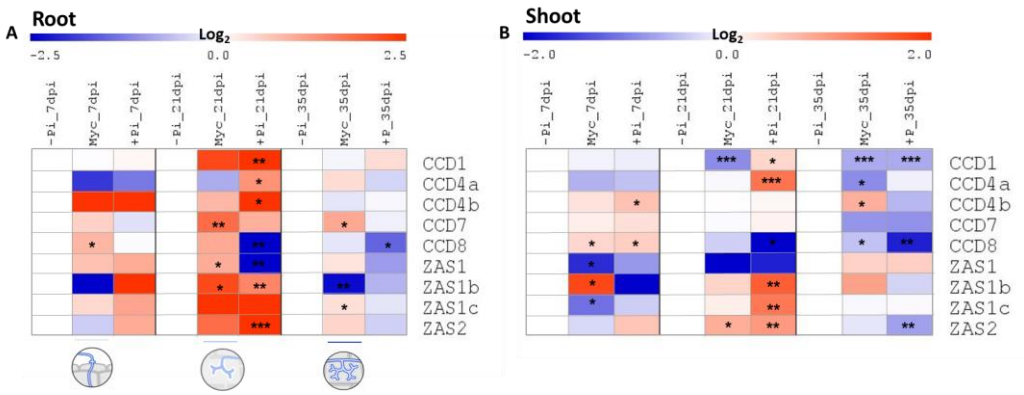

Figure 1. *Heatmap of root (A) and shoot (B) gene expression of the three-time points (7, 21, 35 dpi: days post inoculation) and the three analyzed conditions (-Pi, MYC, +Pi). Data are means ± SE (n<=4). For each gene and time point, the value of the corresponding -Pi sample was set to 1. Asterisks show statistically significant differences referred to the –Pi condition, separately for each time point, by one way-Anova (*P < 0.05; **P<0.01; ***P<0.001). The circles represented the different stages of mycorrhization: at the early stage (7 dpi), the fungus structures, hyphopodia, adhered to the root epidermis, during the middle stage (21 dpi), the arbuscules started their development that will be completed at the later stage (35 dpi). Heatmaps were generated with the MultiExperiment Viewer (MeV) software.-Pi: 3.2 µM Pi; MYC: mycorrhizal plants grown at 3.2 µM Pi; +Pi:500 µM Pi.*

We also compared the CCDs gene expression of shoot and root (Supplementary figure 4); at 7 dpi, we observed a statistically significant down-regulation of CCD1 and an up-regulation for CCD4b in shoots of -Pi, MYC, +Pi plants compared to the to -Pi root. At 21 dpi, root and shoot CCDs expression was similar, with a general

up-regulation of all analyzed genes (CCD1, CCD4a, CCD4b, CCD7, ZAS1b, ZAS1c, ZAS2), with the exception of CCD8 and ZAS1, compared to -Pi root. At the last time point (35 dpi), CCDs genes showed a rather similar expression pattern, but we noticed, compared to -P roots, an up-regulation of CCD4a in shoots of -Pi and +Pi plants, a down-regulation of CCD8 in root and shoot of +Pi plants and a down-regulation of ZAS1b in root MYC and shoot of -Pi and +Pi plants.

We used PCA (Bro & K. Smilde 2014) to assess the samples' natural grouping and clustering tendencies concerning different growth conditions (MYC, -Pi, +P) at the three-time points analysed. The loadings plot of **Figure 2 A** described the influence of the measured variables on the samples' distribution shown in the scores plot of **Figure 2 B**, which provided insights into this distribution.

In our study, the PCA model was obtained from the expression level of the set of genes analyzed in all samples, in which PC1 explained 43.88% (related to the gene expression level) and PC2 explained 22.23% (related to the plant developmental stage) of the total variance (**Supplementary figure 5**). PC1 and PC2 models highlighted that the middle developmental stage (21 dpi) in all growth conditions considered induced a different CCD expression pattern compared to the early and the later stages. We selected the model with 5 PCs, since PC3 (9.90%) and PC5 (5.53%) provided notable information related to the growth conditions, as shown in the loading plot (**Figure 2 A)**, while the scores plot (**Figure 2 B**) displayed a clear separation between the plant organs: root and shoot. More in detail, **Figure 2 B** showed that in root *CCD1* and *CCD7* expression was mainly influenced by Pi level, while *CCD8* by both Pi level and MYC condition. *CCD4a*, *ZAS1c*, and *ZAS1* expression was more affected by the time point than by the Pi level. By contrast, the *CCD4b* and *ZAS2* expression levels were mainly influenced by the Pi level. Concerning the shoot, *CCD1*, *CCD4a*, *CCD4b*, and *ZAS2* were located in the plot area influenced by the Pi level during the middle and late stages (21 and 35 dpi), while *CCD7* and *ZAS1c* fell in the plot area related to the MYC condition.

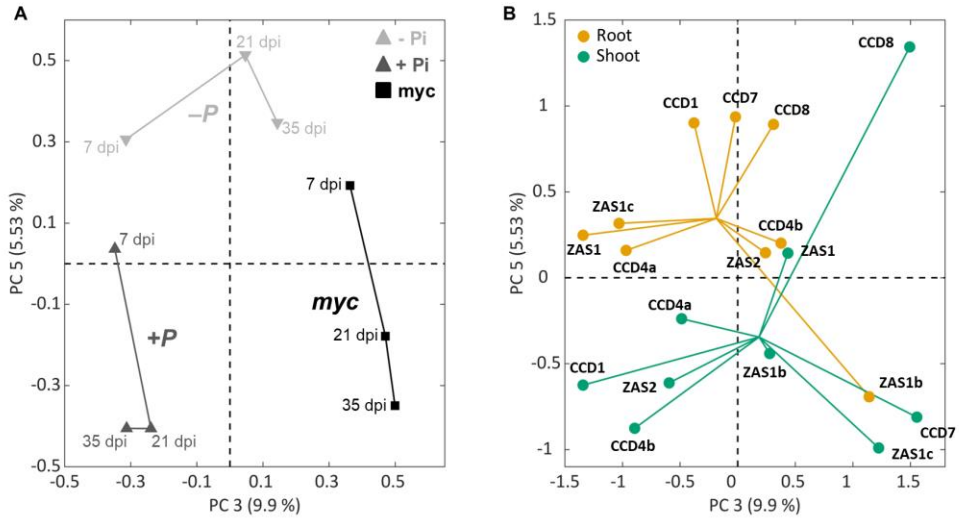

Figure 2. *PCA model of root and shoot CCDs genes expression across the three-time points and the three growth conditions (-Pi, MYC, +Pi). Loadings plot (A) and scores plot (B) show the third and fifth principal components. In the scores plot (B) for both groups the lines connecting each sample lead to the cluster center.*

Apocarotenoids profile

To profile non-hydroxylated and hydroxylated apocarotenoids (**Supplementary Table 2**) in roots and shoots of rice plants grown in high/low Pi concentration (+Pi and -Pi) and upon MYC condition, we used the ultra-HPLC (UHPLC)-mass spectrometry (MS)-based approach to get insight into the apocarotenoid compositions (Mi *et al.* 2018). To simplify this analysis, the statistically significant differences were referred to as the -Pi condition within each time point. The results showed a substantial difference between root and shoot in apocarotenoids quantification and distribution, in analogy to what has been observed in *CCDs* gene expression data.

Concerning the root (**Figure 3 A, Supplementary Figure 6 A**), we observed an increment of the content of Apo9 (β-ionone), Apo10, and their hydroxylated forms (OH-Apo9 and OH-Apo10) in MYC condition at 21 dpi and 35 dpi. In addition, Apo10 showed a higher accumulation in MYC roots and upon +Pi at 7 dpi. Likewise, at the same time point, the Apo11 level increased in the MYC condition, while it

decreased during the middle stage (21 dpi), contrary to its hydroxylated forms (OH-Apo 11 and OH-Apo 11-iso) which showed a strong accumulation. Moreover, at 35 dpi, all the β-apo-11-carotenoids (C_{15}) showed a statistically significant decrease upon +Pi. Apo12 and Apo14 displayed the same pattern at 35 dpi: both showed a higher accumulation in MYC and +Pi compared to -Pi. By contrast, we observed an increase of Apo13 in MYC and +Pi conditions during the early (7 dpi) and middle stages (21 dpi); its hydroxylated forms (OH-Apo13 and OH-Apo13-iso) also displayed a higher content at 7 dpi in the +Pi condition and 21 dpi in the MYC root. Moreover, at the later stage (35 dpi), OH-Apo13-iso showed a statistically significant higher and lower content in MYC and +Pi roots respectively. Finally, Apo15 and Apo15-iso displayed a higher level at 21 dpi in MYC and +Pi roots.

Concerning the shoot, the heatmap (**Figure 3 B**) showed that the non-hydroxylated apocarotenoids (from Apo 8 to Apo 15) displayed an overall similar profile: a general decrease at 7 and 35 dpi in +Pi condition compared to plants grown at -Pi, and an increase upon MYC and +P during the middle stage (21 dpi). Notably, Apo9, Apo10, Apo11, Apo12, Apo13, Apo14 and its isomer (Apo14-iso), and Apo15 levels decreased at 7 dpi in the +Pi condition. By contrast, at 21 dpi, Apo9, Apo10, Apo11, Apo12, Apo13, and Apo15 content increased in MYC and +Pi conditions, while Apo14 and its isomer showed an increment only for the MYC condition. At the later time point (35 dpi), we detected a decrease of Apo9, Apo12, and Apo14 e its isomer content in MYC plants.

The hydroxylated forms showed a profile similar to non-hydroxylated APO with an increased content at 21 dpi in the +Pi condition, and a decreasing trend in the MYC condition at 35 dpi. In detail, at 7 dpi, the OH-Apo11 isomer showed a statistically different increase in MYC condition. Further, at 21 dpi, OH-Apo8, OH-Apo10, OH-Apo11 and its isomer, OH-Apo12, OH-Apo13, OH-Apo15, and OH-Apo15 isomer strongly increase in +Pi. At the same time point, also OH-Apo11 isomer and OH-Apo13 levels increased in the MYC condition, while the OH-Apo10 content

decreased. At the later stage, OH-Apo10 and OH-Apo11 displayed an increased content at +Pi, while OH-Apo13-iso accumulation decreased in the shoot of plants grown in MYC and +Pi conditions. (**Supplementary Figure 6 B**)

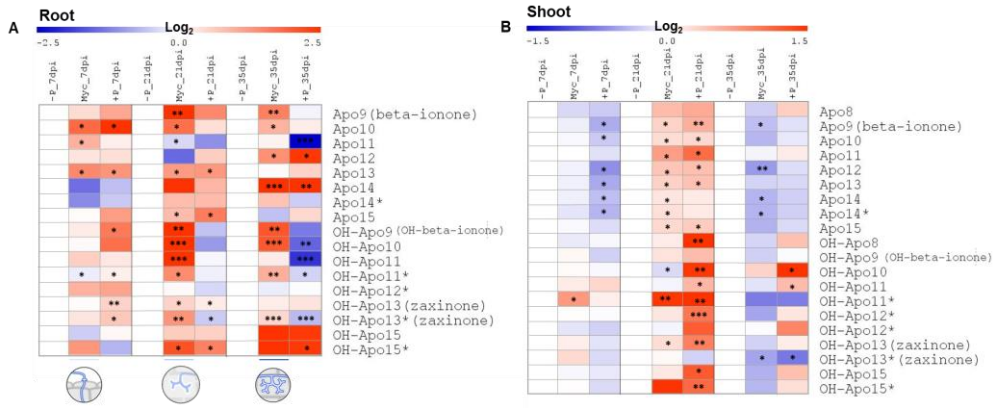

Figure 3. *Heatmap of root (A) and shoot (B) apocarotenoids quantification across the three time points and the three analyzed conditions (-Pi, MYC, +Pi). For each APOs and time point, the value of the corresponding -Pi was set to 1. Data are means ± SE (n<=4). Asterisks show statistically significant differences as compared to –P condition, separately for each time point, by one way-Anova (*P < 0.05; **P<0.01; ***P<0.001). The circles represented the different stages of mycorrhization: at the early stage (7 dpi), the fungus structures, called hyphopodia, adhered to the root epidermis, during the middle stage (21 dpi), the arbuscules started their development that will be completed at the later stage (35 dpi). The apocarotenoids indicated with asterisks represented the isoform of the corresponding apocarotenoid. Heatmaps were generated with the MultiExperiment Viewer (MeV) software.*

To inspect the apocarotenoid distribution to highlight possible interesting groupings through the different stages and identify if they were related to a specific Pi level or the MYC condition, a PCA was employed. In the apocarotenoids database, no outliers (i.e., samples with clearly inconsistent values and/or unexpected behaviors attributable to errors of measurement or to data acquisition problems) were identified, even if three apocarotenoids (OH-Apo10, Apo10, and Apo12) showed very high values across all time points and treatments (**Supplementary Figure 7**). To better model the information of the rest of the samples, these three extreme samples were removed from the apocarotenoids dataset and projected at a later stage to inspect their position in the final PCA model.

In the PCA model referred to apocarotenoids, PC1 explained 43.88% (related to apocarotenoid quantification) and PC2 explained 22.23% (related to growth conditions) of the total variance (**Supplementary figure 8**). PC1 and PC2 models highlighted the apocarotenoids strictly related to MYC condition (OH-Apo9; Apo11; OH-Apo11; OH-Apo13iso). Further, we adopted the PCA model PC2 combined with PC3, where PC3 explained 2.55% of the total variation, upon the propensity of samples to regroup following the temporal trend described in the loading plot (**Figure 4 A**). In the plot chart, at 7 dpi all the growth conditions were clustered in the same area. Here, the majority of the analysed shoot apocarotenoids (Apo9, Apo11, OH-Apo11 isomer, OH-Apo13, OH-Apo13 isomer, and Apo15) were located, suggesting that their content was mainly influenced by the growth time than by the growth condition.

The score plot (**Figure 4 B)** displayed a clear separation between the apocarotenoids quantified in roots or shoots. In-depth, in root OH-Apo9, OH-Apo11, Apo11, and OH-Apo13 isomer were mainly influenced by mycorrhization in different time points (21 dpi and 35 dpi). Instead, APO14 seems to be dependent on the Pi level and MYC condition. However, in shoot OH-Apo9, OH-Apo12 and OH-Apo15 were linked to the +Pi condition. OH-Apo8, the OH-Apo12 isomer, and the OH-Apo15 isomer depended on the Pi level at the middle stage (21 dpi).

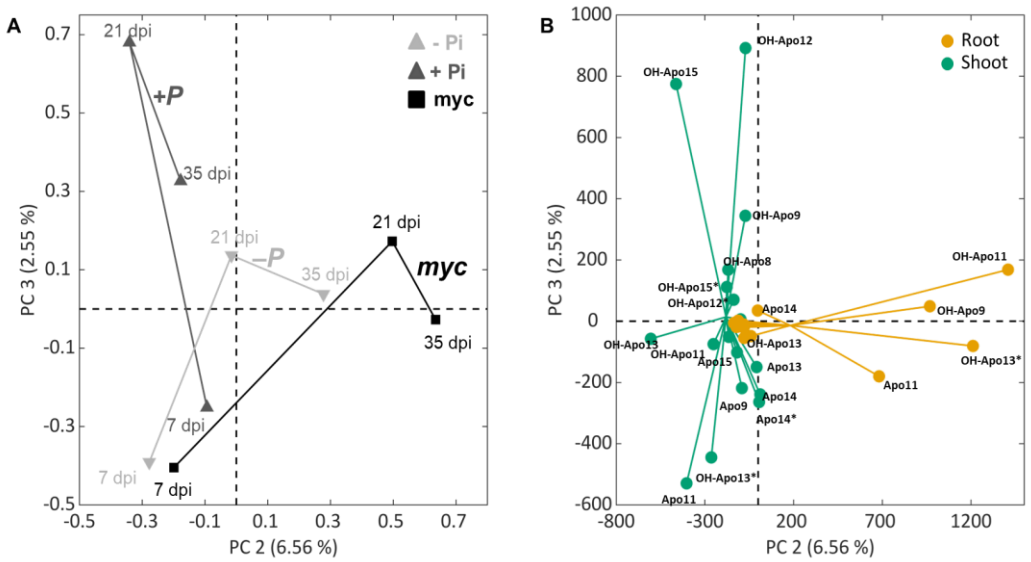

Figure 4. *PCA model of root and shoot APOs across the three-time points and the three growth conditions (-Pi, MYC, +Pi). Loadings plot (A) and scores plot (B) showing the second and third principal components. In the scores plot (B) for both groups the lines connecting each sample lead to the cluster center.*

Data fusion

Finally, to combine and investigate the potential correlation between apocarotenoids and CCD genes, we used a low-level data fusion approach (Borràs *et al.* 2015) to combine the two datasets into an individual fused one, also modelled with PCA.

In the PCA model specified to genes expression and apocarotenoids profiles joined, PC1 explained 29.65% and PC2 explained 26.81% of the total variance (**Figure 5 A-B**). From the loading plot (**Figure 5 A**) we observed the grouping of the samples interpretable by the temporal trend (7, 21, 35 dpi). As reported for the previous score plots referred to individual categories (genes and apocarotenoids), in Figure 5B we observed a clear separation between plant organs. In more detail, genes and apocarotenoids in the left upper part of the score plot (**Figure 5 B**) were more related to the early stage (7 dpi). Here, we found mainly shoot apocarotenoids, *CCD8* expressed in both root and shoot, and *ZAS1c* in the root. By contrast, the lower left part of the plot, clustered exclusively apocarotenoids and genes (*CCD7* and *ZAS1*)

modulated in the root, depended on the MYC condition during the middle and later stages. In particular, Apo9 (β-ionone), Apo10, and their hydroxylated forms (OH-Apo9 and OH-Apo10) were grouped in this plot area, suggesting their possible involvement during the AM colonization process. Further, in the same area, we highlighted the association between *CCD7* and one of its cleavage products, Apo9 (β-ionone).

In addition, this group highlighted the correlation between *ZAS1*, responsible for the OH-Apo13 (zaxinone) or zaxinone isomer synthesis, and its precursors (OH-Apo10 and OH-Apo12).

In the shoot, most of the *CCD* genes (*CCD1*, *CCD4a*, *CCD7*, *ZAS1b*, *ZAS1c*, and *ZAS2*) were mainly influenced by the Pi level and by the growing time (21 dpi and 35 dpi) similarly to some genes (*CCD1*, *CCD4a*, *CCD4b*, and *ZAS2*) in the root. Moreover, the right plot area clustered the majority of shoot apocarotenoids. On the whole, apocarotenoids profiles in the shoot seem to be more influenced by the time points (7, 21, 35 dpi) and Pi availability, while, in the root, most apocarotenoids and genes were mainly influenced by mycorrhization.

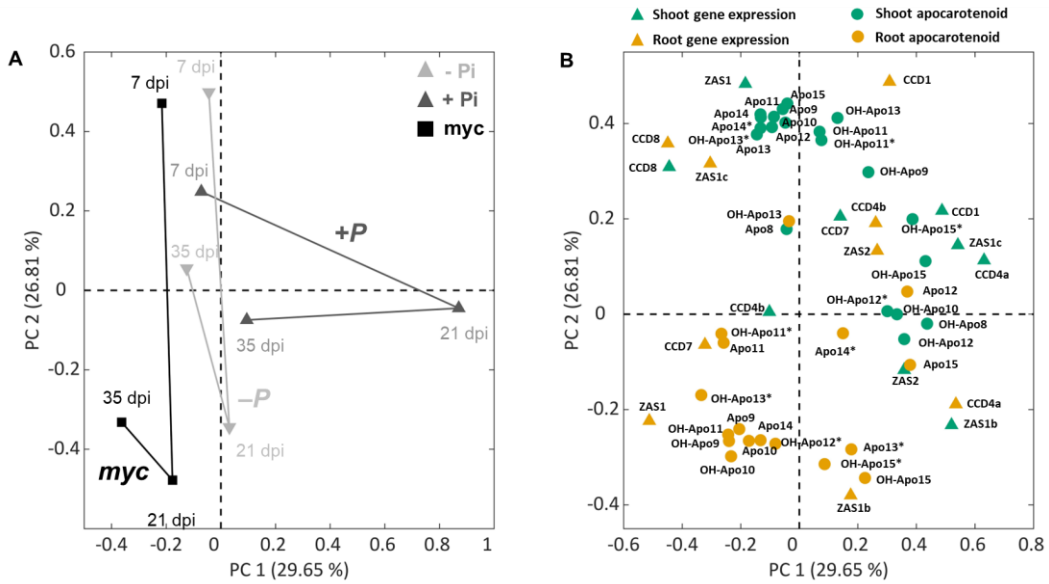

Figure 5. *PCA model of root and shoot genes and apocarotenoids datasets fused and analysed across the three-time points and the three growth conditions (-Pi, MYC, +Pi). Loadings plot (A) and scores*

plot (B) show the first and second principal components. The apocarotenoids indicated with asterisks represent the isoform of the corresponding apocarotenoid.

6.4 Discussion and conclusion

In recent years, plant apocarotenoids are emerging not only as carotenoid breakdown products but as metabolites with active roles in regulating physiological and developmental processes and plant-(a)biotic interactions (Zheng *et al.* 2021). In particular, some apocarotenoids were associated with the establishment and maintenance of AM symbiosis (Fiorilli *et al.* 2019). Investigations over the last decade indicate that beyond SLs, ABA, mycorradicins, and blumenols (Walter *et al.* 2007; Floss *et al.* 2008; Hill *et al.* 2018; Wang *et al.* 2018; Fiorilli *et al.* 2019), other apocarotenoids may play a role in this mutualistic association. For example, zaxinone, generated by the activity of the CCD subfamily Zaxinone Synthases, was shown to control the extent of AM root colonization with a complex interplay with SLs (Votta *et al.* 2022; Ablazov *et al.* 2022). To further explore the involvement of other apocarotenoids in the AM symbiosis in this work we developed a combined approach: we profiled apocarotenoids in rice roots and shoots across a time course (7, 21, 35 dpi) experiment of AM colonization by LC-MS (Mi *et al.* 2018) and, in parallel, we monitored the expression pattern of a set of CCD genes. To highlight genes and apocarotenoids more specifically related to the AM association, we analysed plants grown in low and high Pi conditions.

The results show that the AM colonization, although confined to the root system, can trigger a systemic response which is evident from the modulation of *CCDs* gene expression and apocarotenoid content in rice shoots. The effect on epigeous organs exerted by AM root colonization has been already described in other species (Fiorilli *et al.* 2009, 2018; Zouari *et al.* 2014). In addition, our analysis indicates that both mycorrhization and Pi availability triggered an organ-specific response with differential modulation of genes and apocarotenoids in roots *versus* shoots (**Figures 3 and 4**).

In particular, in roots Apo9 e OH-Apo9 e Apo10 e OH-Apo10 are much more abundant in the MYC samples across almost all the time points analysed and do not accumulate under +Pi; this profile suggests that they may be important for the AM colonization process. Apo9 is β-ionone, a cleavage product of several CCD enzymes (CCD1, CCD4, and CCD7) which was shown to have a role in plant-fungal interactions (Wilson *et al.* 1981; Sharma *et al.* 2012). However, its specific involvement in the AM symbiosis has not been characterized yet. As in our dataset, CCD7 displays an AM-responsive expression profile and it is involved in SLs biosynthesis, we envisage that β-ionone accumulation in AM roots is mainly due to CCD7 activity. It is worth noting that CCD7 could also be involved in the synthesis of blumenol-type metabolites and mycorradicin that accumulate in roots in the late stage of AM colonization (Wang *et al.* 2018; Fiorilli *et al.* 2019); however, due to lack of authentic standards, we could not monitor these metabolites.

Interestingly, we observed the accumulation at the middle and late stages of mycorrhization of zaxinone and OH-Apo10, which is the precursor of zaxinone, suggesting that mycorrhization stimulates multiple steps of this branch of the apocarotenoid biochemical pathway. Notably, the expression of *ZAS1* (and partially *ZAS2*) was also highly influenced by the MYC condition in roots, confirming its correlation with zaxinone (**Figure 1 and 5**). The association between *CCD8* and *ZAS1* at 7 dpi is in line with previous data showing their interplay at the early stage of the AM symbiosis (Votta *et al.* 2022).

Apo11 level increased at 7 dpi and decreased at 21 dpi, while OH-Apo11 and OH-Apo11 isomers could be associated with the 21 dpi MYC condition. Importantly, the apocarotenoids Apo11 and OH-Apo11 were recently described as being part of an alternative zeaxanthin epoxidase-independent pathway to produce ABA (Jia *et al.* 2022). Moreover, these compounds act like ABA in maintaining seed dormancy and inducing the expression of ABA-responsive genes (Zheng *et al.* 2021; Jia *et al.*

2022). In light of these findings, we could hypothesize that Apo11 and OH-Apo11, could be involved in the AM symbiosis, and deserve more investigations along the whole colonization process and in relation to what has been already described for ABA in mycorrhizal roots (López-Ráez *et al.* 2010; Pozo *et al.* 2015).

The composition of shoot apocarotenoids seems to be most influenced by the time point considered. At 7 dpi, we observe a trend to a decrease of most apocarotenoids, especially in the +Pi compared to -Pi condition. At 21 dpi, the MYC and +Pi conditions showed a similar pattern with a general increase in the level of several apocarotenoids. At 35 dpi, MYC and +Pi conditions again displayed a similar profile, but with a general decrease of several apocarotenoids content. From these observations, it can be speculated that the similarity between the MYC and the +Pi conditions could mirror the Pi nutritional status since the AM symbiosis guarantees an improved Pi mineral nutrition mimicking the high Pi condition (Zouari *et al.* 2014). Moreover, our data indicate that the OH-Apo11 isomer deserves more investigation as it could be considered a shoot marker of the early stage of AM colonization.

We also attempted to associate the expression of specific genes with the accumulation of specific apocarotenoids with a data fusion approach as the genes involved in the production of many apocarotenoids are largely unknown. The reliability of the approach was confirmed by the association between *ZAS1* and zaxinone and its precursor in roots and by the correlation between *CCD7* and β-ionone (**Figure 5**). In this context, we can speculate that *CCD1* and *CCD4a* are linked to the production of OH-Apo15 and its isomer, since they are correlated in the shoot and both organs, respectively (**Figure 5**). Interestingly, a fungal *CCD*, *NosACO*, mediates Apo15 (retinal) production, indicating *CCD1/4* or yet unidentified CCDs involved in Apo15 formation during AM symbiosis. In addition, the expression of *ZAS1* in shoots is also related to the accumulation of zaxinone,

suggesting a direct involvement of the enzyme in endogenous zaxinone production in shoots.

Over the years, the carotenoid metabolic pathway has been also investigated and manipulated to convert this knowledge into sustainable agriculture strategies. Recent studies highlighted how carotenoid biosynthesis and accumulation seem to positively impact the resistance of plants to abiotic stresses, such as high-light, increased temperature, and drought (Uarrota et al. 2018; Kim et al. 2018; Swapnil et al. 2021), represents a promising option for developing resilient crops (Stra et al. 2023). Among the apocarotenoids, many studies involved the well-characterized SLs biosynthesis or signaling based on the control of parasite plants, the efficiency of nutrient assimilation and crop development. With the increasing technologies available, future research should also investigate other carotenoid pathways to understand how they can influence the phenotype and other desirable traits in crops, focussing, in addition, on the impact on rhizospheric interactions and exploring the possibility of improving beneficial interactions to generate crops with better performance.

In conclusion, our data show the specific profiles of *CCD* genes and apocarotenoids across different stages of the AM symbiosis and Pi conditions, possibly highlighting novel markers at both local and systemic levels. Moreover, this combined approach seems a promising tool to further dissect this complex metabolic pathway suggesting putative links between enzymatic activities and apocarotenoids production.

6.5 Summary model

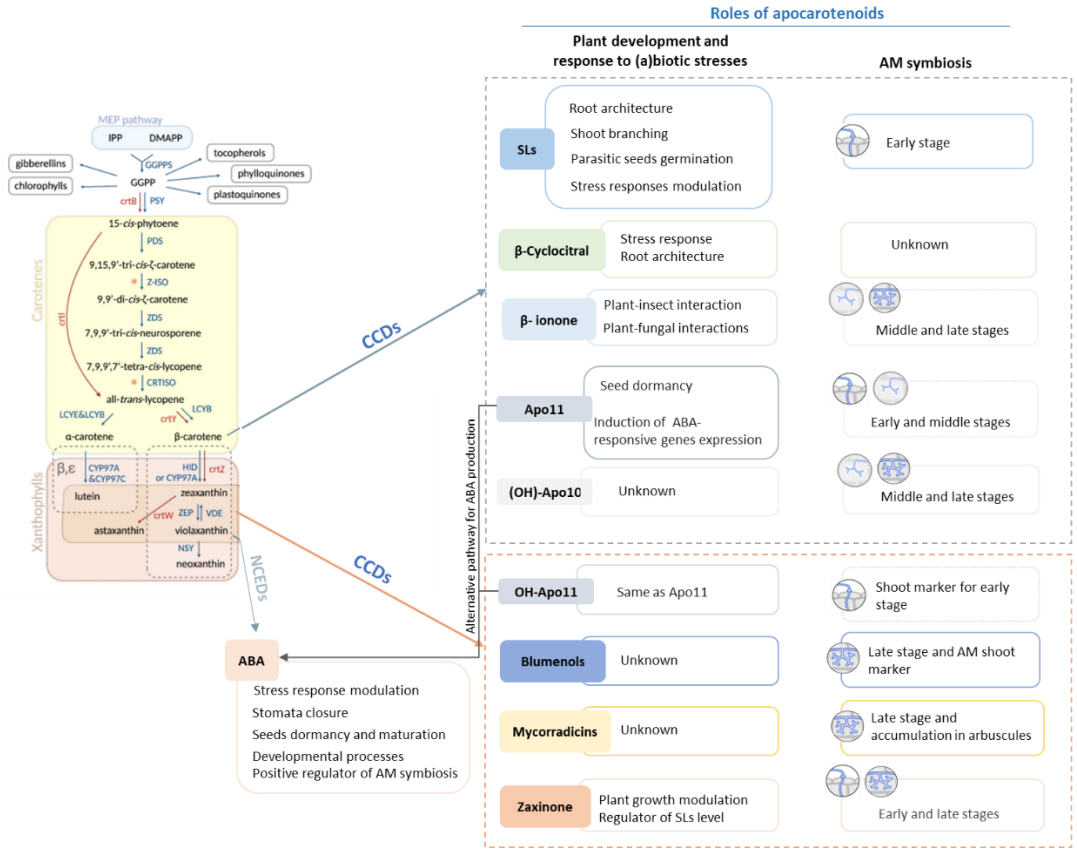

Overview diagram of biosynthesis and function of plant apocarotenoids. *For each apocarotenoid the principal functions discovered in plants are listed, differentiating their role in plant development and response to (a)biotic stresses and their involvement during the AM symbiosis. The boxes with dotted lines indicate a putative role. The circles represented the different stages of mycorrhization: at the early stage (7 dpi), the fungus structures, called hyphopodia, adhered to the root epidermis, during the middle stage (21 dpi), the arbuscules started their development that will be completed at the later stage (35 dpi). The biosynthetic pathway diagram is modified from Stra et al. (2023).*

6.6 References

Ablazov A., Votta C., Fiorilli V., Wang J.Y., Aljedaani F., Jamil M., Balakrishna A., Balestrini R., Liew K.X., Rajan C., Berqdar L., Blilou I., Lanfranco L., Al-Babili S. (2022) ZAXINONE SYNTHASE 2 regulates growth and arbuscular mycorrhizal symbiosis in rice. Plant Physiology **191**:382–399.

Ahrazem O., Gómez-Gómez L., Rodrigo M.J., Avalos J., Limón M.C. (2016) Carotenoid Cleavage Oxygenases from Microbes and Photosynthetic Organisms: Features and Functions. International Journal of Molecular Sciences **17**:1781.

Alder A., Jamil M., Marzorati M., Bruno M., Vermathen M., Bigler P., Ghisla S., Bouwmeester H., Beyer P., Al-Babili S. (2012) The path from β-carotene to carlactone, a strigolactone-like plant hormone. Science (New York, NY) **335**:1348–1351.

Auldridge M.E., McCarty D.R., Klee H.J. (2006) Plant carotenoid cleavage oxygenases and their apocarotenoid products. Current Opinion in Plant Biology **9**:315–321.

Bonfante P., Requena N. (2011) Dating in the dark: how roots respond to fungal signals to establish arbuscular mycorrhizal symbiosis. Current Opinion in Plant Biology **14**:451–457.

Borràs E., Ferré J., Boqué R., Mestres M., Aceña L., Busto O. (2015) Data fusion methodologies for food and beverage authentication and quality assessment – A review. Analytica Chimica Acta **891**:1–14.

Bro R., K. Smilde A. (2014) Principal component analysis. Analytical Methods **6**:2812–2831.

Brundrett M.C. (2009) Mycorrhizal associations and other means of nutrition of vascular plants: understanding the global diversity of host plants by resolving conflicting information and developing reliable means of diagnosis. Plant and Soil **320**:37–77.

Bruno M., Beyer P., Al-Babili S. (2015) The potato carotenoid cleavage dioxygenase 4 catalyzes a single cleavage of β-ionone ring-containing carotenes and non-epoxidated xanthophylls. Archives of Biochemistry and Biophysics **572**:126–133.

Bruno M., Koschmieder J., Wuest F., Schaub P., Fehling-Kaschek M., Timmer J., Beyer P., Al-Babili S. (2016) Enzymatic study on AtCCD4 and AtCCD7 and their potential to form acyclic regulatory metabolites. Journal of Experimental Botany **67**:5993–6005.

Carbonnel S., Gutjahr C. (2014) Control of arbuscular mycorrhiza development by nutrient signals. Frontiers in Plant Science **5**:462.

Cazzonelli C.I. (2011) Carotenoids in nature: insights from plants and beyond. Functional Plant Biology **38**:833.

Charpentier M., Sun J., Wen J., Mysore K.S., Oldroyd G.E.D. (2014) Abscisic Acid Promotion of Arbuscular Mycorrhizal Colonization Requires a Component of the PROTEIN PHOSPHATASE 2A Complex. Plant Physiology **166**:2077–2090.

Chen M., Arato M., Borghi L., Nouri E., Reinhardt D. (2018) Beneficial Services of Arbuscular Mycorrhizal Fungi – From Ecology to Application. Frontiers in Plant Science **9**:1270.

Das D., Paries M., Hobecker K., Gigl M., Dawid C., Lam H.-M., Zhang J., Chen M., Gutjahr C. (2022) PHOSPHATE STARVATION RESPONSE transcription factors enable arbuscular mycorrhiza symbiosis. Nature Communications **13**:477.

Felemban A., Braguy J., Zurbriggen M.D., Al-Babili S. (2019) Apocarotenoids Involved in Plant Development and Stress Response. Frontiers in Plant Science **10**:1168.

Fester T., Schmidt D., Lohse S., Walter M., Giuliano G., Bramley P., Fraser P., Hause B., Strack D. (2002) Stimulation of carotenoid metabolism in arbuscular mycorrhizal roots. Planta **216**:148–154.

Fiorilli V., Catoni M., Miozzi L., Novero M., Accotto G.P., Lanfranco L. (2009) Global and Cell-Type Gene Expression Profiles in Tomato Plants Colonized by an Arbuscular Mycorrhizal Fungus. The New Phytologist **184**:975–987.

Fiorilli V., Vannini C., Ortolani F., Garcia-Seco D., Chiapello M., Novero M., Domingo G., Terzi V., Morcia C., Bagnaresi P., Moulin L., Bracale M., Bonfante P. (2018) Omics approaches revealed how arbuscular mycorrhizal symbiosis enhances yield and resistance to leaf pathogen in wheat. Scientific Reports **8**:9625.

Fiorilli V., Wang J.Y., Bonfante P., Lanfranco L., Al-Babili S. (2019) Apocarotenoids: Old and New Mediators of the Arbuscular Mycorrhizal Symbiosis. Frontiers in Plant Science **10:**1186.

Floß D.S., Hause B., Lange P.R., Küster H., Strack D., Walter M.H. (2008) Knock-down of the MEP pathway isogene 1-deoxy-d-xylulose 5-phosphate synthase 2 inhibits formation of arbuscular mycorrhiza-induced apocarotenoids, and abolishes normal expression of mycorrhiza-specific plant marker genes. The Plant Journal **56**:86–100.

Floss D.S., Levy J.G., Levesque-Tremblay V., Pumplin N., Harrison M.J. (2013) DELLA proteins regulate arbuscule formation in arbuscular mycorrhizal symbiosis. Proceedings of the National Academy of Sciences **110**:E5025–E5034.

Floss D.S., Schliemann W., Schmidt J., Strack D., Walter M.H. (2008) RNA interference-mediated repression of MtCCD1 in mycorrhizal roots of Medicago truncatula causes accumulation of C27 apocarotenoids, shedding light on the functional role of CCD1. Plant Physiology **148**:1267–1282.

Güimil S., Chang H.-S., Zhu T., Sesma A., Osbourn A., Roux C., Ioannidis V., Oakeley E.J., Docquier M., Descombes P., Briggs S.P., Paszkowski U. (2005) Comparative transcriptomics of rice reveals an ancient pattern of response to microbial colonization. Proceedings of the National Academy of Sciences **102**:8066–8070.

Gutjahr C. (2014) Phytohormone signaling in arbuscular mycorhiza development. Current Opinion in Plant Biology **20**:26–34.

Gutjahr C., Parniske M. (2013) Cell and Developmental Biology of Arbuscular Mycorrhiza Symbiosis. Annual Review of Cell and Developmental Biology **29**:593–617.

Hammer O., Harper D.A.T., Ryan P.D. PAST: Paleontological Statistics Software Package for Education and Data Analysis. :9.

Harrison M.J. (2012) Cellular programs for arbuscular mycorrhizal symbiosis. Current Opinion in Plant Biology **15**:691–698.

Harrison P.J., Bugg T.D.H. (2014) Enzymology of the carotenoid cleavage dioxygenases: Reaction mechanisms, inhibition and biochemical roles. Archives of Biochemistry and Biophysics **544**:105–111.

Herrera-Medina M.J., Steinkellner S., Vierheilig H., Ocampo Bote J.A., García Garrido J.M. (2007) Abscisic acid determines arbuscule development and functionality in the tomato arbuscular mycorrhiza. New Phytologist **175**:554–564.

Hill E.M., Robinson L.A., Abdul-Sada A., Vanbergen A.J., Hodge A., Hartley S.E. (2018) Arbuscular Mycorrhizal Fungi and Plant Chemical Defence: Effects of Colonisation on Aboveground and Belowground Metabolomes. Journal of Chemical Ecology **44**:198–208.

Huang F.-C., Molnár P., Schwab W. (2009) Cloning and functional characterization of carotenoid cleavage dioxygenase 4 genes. Journal of Experimental Botany **60**:3011–3022.

Ilg A., Beyer P., Al-Babili S. (2009) Characterization of the rice carotenoid cleavage dioxygenase 1 reveals a novel route for geranial biosynthesis: A novel route for geranial formation. FEBS Journal **276**:736–747.

Ilg A., Bruno M., Beyer P., Al-Babili S. (2014) Tomato carotenoid cleavage dioxygenases 1A and 1B: Relaxed double bond specificity leads to a plenitude of dialdehydes, mono-apocarotenoids and isoprenoid volatiles. FEBS Open Bio **4**:584–593.

Jia K.-P., Mi J., Ali S., Ohyanagi H., Moreno J.C., Ablazov A., Balakrishna A., Berqdar L., Fiore A., Diretto G., Martínez C., de Lera A.R., Gojobori T., Al-Babili S. (2022) An alternative, zeaxanthin epoxidase-independent abscisic acid biosynthetic pathway in plants. Molecular Plant **15**:151–166.

Kim, H. S., Ji,C.Y., Lee,C.-J., Kim, S.-E., Park, S.-C., andKwak, S.-S. (2018).Orange: a target gene for regulating carotenoid homeostasis and increasing plant tolerance to environmental stress in marginal lands. J. Exp. Bot. 69. 4: 3393–3400.

Klingner A., Bothe H., Wray V., Marner F.-J. (1995) Identification of a yellow pigment formed in maize roots upon mycorrhizal colonization. Phytochemistry **38**:53–55.

Li Vigni M., Durante C., Cocchi M. (2013) Chapter 3 - Exploratory Data Analysis. In: Marini F (ed) Data Handling in Science and Technology. Elsevier, pp 55–126.

López-Ráez J.A., Charnikhova T., Gómez-Roldán V., Matusova R., Kohlen W., De Vos R., Verstappen F., Puech-Pages V., Bécard G., Mulder P., Bouwmeester H. (2008) Tomato strigolactones are derived from carotenoids and their biosynthesis is promoted by phosphate starvation. New Phytologist **178**:863–874.

López-Ráez J.A., Kohlen W., Charnikhova T., Mulder P., Undas A.K., Sergeant M.J., Verstappen F., Bugg T.D.H., Thompson A.J., Ruyter-Spira C., Bouwmeester H. (2010) Does abscisic acid affect strigolactone biosynthesis? New Phytologist **187**:343–354.

MacLean A.M., Bravo A., Harrison M.J. (2017) Plant Signaling and Metabolic Pathways Enabling Arbuscular Mycorrhizal Symbiosis. The Plant Cell **29**:2319–2335.

Maier W., Hammer K., Dammann U., Schulz B., Strack D. (1997) Accumulation of sesquiterpenoid cyclohexenone derivatives induced by an arbuscular mycorrhizal fungus in members of the Poaceae. Planta **202**:36–42.

Martín-Rodríguez J.A., Huertas R., Ho-Plágaro T., Ocampo J.A., Turečková V., Tarkowská D., Ludwig-Müller J., García-Garrido J.M. (2016) Gibberellin–Abscisic Acid Balances during Arbuscular Mycorrhiza Formation in Tomato. Frontiers in Plant Science **7**:1273.

Martín-Rodríguez J.Á., León-Morcillo R., Vierheilig H., Ocampo J.A., Ludwig-Müller J., García-Garrido J.M. (2011) Ethylene-dependent/ethylene-independent ABA regulation of tomato plants colonized by arbuscular mycorrhiza fungi. New Phytologist **190**:193–205.

Mi J., Jia K.-P., Wang J.Y., Al-Babili S. (2018) A rapid LC-MS method for qualitative and quantitative profiling of plant apocarotenoids. Analytica Chimica Acta **1035**:87–95.

Moreno J.C., Mi J., Alagoz Y., Al-Babili S. (2021) Plant apocarotenoids: from retrograde signaling to interspecific communication. The Plant Journal **105**:351–375.

Müller L.M., Harrison M.J. (2019) Phytohormones, miRNAs, and peptide signals integrate plant phosphorus status with arbuscular mycorrhizal symbiosis. Current Opinion in Plant Biology **50**:132–139.

Nadal M., Paszkowski U. (2013) Polyphony in the rhizosphere: presymbiotic communication in arbuscular mycorrhizal symbiosis. Current Opinion in Plant Biology **16**:473–479.

Nambara E., Marion-Poll A. (2005) Abscisic Acid Biosynthesis and Catabolism. Annual Review of Plant Biology **56**:165–185.

Pan Z., Zeng Y., An J., Ye J., Xu Q., Deng X. (2012) An integrative analysis of transcriptome and proteome provides new insights into carotenoid biosynthesis and regulation in sweet orange fruits. Journal of Proteomics **75**:2670–2684.

Pozo M.J., Jung S.C., López-Ráez J.A., Azcón-Aguilar C. (2010) Impact of Arbuscular Mycorrhizal Symbiosis on Plant Response to Biotic Stress: The Role of Plant Defence Mechanisms. In: Koltai H, Kapulnik Y (eds) Arbuscular Mycorrhizas: Physiology and Function. Springer Netherlands, Dordrecht, pp 193–207.

Pozo M.J., López-Ráez J.A., Azcón-Aguilar C., García-Garrido J.M. (2015) Phytohormones as integrators of environmental signals in the regulation of mycorrhizal symbioses. New Phytologist **205**:1431–1436.

Richardson A.E., Lynch J.P., Ryan P.R., Delhaize E., Smith F.A., Smith S.E., Harvey P.R., Ryan M.H., Veneklaas E.J., Lambers H., Oberson A., Culvenor R.A., Simpson R.J. (2011) Plant

and microbial strategies to improve the phosphorus efficiency of agriculture. Plant and Soil **349**:121–156.

Scannerini S., Bonfante-Fasolo P. (1977) Unusual plasties in an endomycorrhizal root. Canadian Journal of Botany **55**:2471–2474.

Schwartz S.H., Qin X., Zeevaart J.D. (2001) Characterization of a Novel Carotenoid Cleavage Dioxygenase from Plants *. Journal of Biological Chemistry **276**:25208–25211.

Sharma V., Singh G., Kaur H., Saxena A.K., Ishar M.P.S. (2012) Synthesis of β-ionone derived chalcones as potent antimicrobial agents. Bioorganic & Medicinal Chemistry Letters **22**:6343–6346.

Shi J., Zhao B., Zheng S., Zhang X., Wang X., Dong W., Xie Q., Wang G., Xiao Y., Chen F., Yu N., Wang E. (2021) A phosphate starvation response-centered network regulates mycorrhizal symbiosis. Cell **184**:5527-5540.e18.

Smith S.E., Jakobsen I., Grønlund M., Smith F.A. (2011) Roles of Arbuscular Mycorrhizas in Plant Phosphorus Nutrition: Interactions between Pathways of Phosphorus Uptake in Arbuscular Mycorrhizal Roots Have Important Implications for Understanding and Manipulating Plant Phosphorus Acquisition. Plant Physiology **156**:1050–1057.

Spatafora J.W., Chang Y., Benny G.L., Lazarus K., Smith M.E., Berbee M.L., Bonito G., Corradi N., Grigoriev I., Gryganskyi A., James T.Y., O'Donnell K., Roberson R.W., Taylor T.N., Uehling J., Vilgalys R., White M.M., Stajich J.E. (2016) A phylum-level phylogenetic classification of zygomycete fungi based on genome-scale data. Mycologia **108**:1028–1046.

Strack D., Fester T. (2006) Isoprenoid metabolism and plastid reorganization in arbuscular mycorrhizal roots. New Phytologist **172**:22–34.

Sui X., Kiser P.D., Lintig J. von, Palczewski K. (2013) Structural basis of carotenoid cleavage: From bacteria to mammals. Archives of Biochemistry and Biophysics **539**:203–213.

Swapnil, P., Meena, M., Singh, S. K., Dhuldhaj, U. P., Harish,, and Marwal, A. (2021). Vital roles of carotenoids in plants and humans to deteriorate stress with its structure, biosynthesis, metabolic engineering and functional aspects. Curr. Plant Biol. 26, 100203.

Tan B.-C., Joseph L.M., Deng W.-T., Liu L., Li Q.-B., Cline K., McCarty D.R. (2003) Molecular characterization of the Arabidopsis 9-cis epoxycarotenoid dioxygenase gene family. The Plant Journal: For Cell and Molecular Biology **35**:44–56.

Uarrota, V. G., Stefen, D. L. V., Leolato, L. S., Gindri, D. M., and Nerling, D. (2018). Revisiting carotenoids and their role in plant stress responses: From biosynthesis to plant signaling mechanisms during stress, in Antioxidants and antioxidant enzymes in higher plants. Eds. D. K. Gupta, J. M. Palma and F. J. Corpas (Cham: Springer International Publishing), 207–232.

Vogel J.T., Tan B.-C., McCarty D.R., Klee H.J. (2008) The Carotenoid Cleavage Dioxygenase 1 Enzyme Has Broad Substrate Specificity, Cleaving Multiple Carotenoids at Two Different Bond Positions. Journal of Biological Chemistry **283**:11364–11373.

Volpe V., Chialva M., Mazzarella T., Crosino A., Capitanio S., Costamagna L., Kohlen W., Genre A. Long-lasting impact of chitooligosaccharide application on strigolactone biosynthesis and fungal accommodation promotes arbuscular mycorrhiza in Medicago truncatula. New Phytologist 2023.

Votta C., Fiorilli V., Haider I., Wang J.Y., Balestrini R., Petřík I., Tarkowská D., Novák O., Serikbayeva A., Bonfante P., Al-Babili S., Lanfranco L. (2022) Zaxinone synthase controls arbuscular mycorrhizal colonization level in rice. The Plant Journal **111**:1688–1700.

Walter M.H., Fester T., Strack D. (2000) Arbuscular mycorrhizal fungi induce the non-mevalonate methylerythritol phosphate pathway of isoprenoid biosynthesis correlated with accumulation of the 'yellow pigment' and other apocarotenoids: Mycorrhizal induction of isoprenoid biosynthesis. The Plant Journal **21**:571–578.

Walter M.H., Floß D.S., Hans J., Fester T., Strack D. (2007) Apocarotenoid biosynthesis in arbuscular mycorrhizal roots: Contributions from methylerythritol phosphate pathway isogenes and tools for its manipulation. Phytochemistry **68**:130–138.

Walter M.H., Floss D.S., Strack D. (2010) Apocarotenoids: hormones, mycorrhizal metabolites and aroma volatiles. Planta **232**:1–17.

Wang J.Y., Haider I., Jamil M., Fiorilli V., Saito Y., Mi J., Baz L., Kountche B.A., Jia K.-P., Guo X., Balakrishna A., Ntui V.O., Reinke B., Volpe V., Gojobori T., Blilou I., Lanfranco L., Bonfante P., Al-Babili S. (2019) The apocarotenoid metabolite zaxinone regulates growth and strigolactone biosynthesis in rice. Nature Communications **10**:810.

Wang B., Qiu Y.-L. (2006) Phylogenetic distribution and evolution of mycorrhizas in land plants. Mycorrhiza **16**:299–363.

Wang W., Shi J., Xie Q., Jiang Y., Yu N., Wang E. (2017) Nutrient Exchange and Regulation in Arbuscular Mycorrhizal Symbiosis. Molecular Plant **10**:1147–1158.

Wang Y., Wang M., Li Y., Wu A., Huang J. (2018) Effects of arbuscular mycorrhizal fungi on growth and nitrogen uptake of Chrysanthemum morifolium under salt stress (L.-S.P. Tran, Ed.). PLOS ONE **13**:e0196408.

Waters M.T., Gutjahr C., Bennett T., Nelson D.C. (2017) Strigolactone Signaling and Evolution. Annual Review of Plant Biology **68**:291–322.

Wilson D.M., Gueldner R.C., Mckinney J.K., Lievsay R.H., Evans B.D., Hill R.A. (1981) Effect ofβ-lonone onaspergillus flavus andaspergillus parasiticus growth, sporulation, morphology and aflatoxin production. Journal of the American Oil Chemists' Society **58**:A959–A961.

Yoneyama K., Kisugi T., Xie X., Yoneyama K. (2013) Chemistry of Strigolactones: Why and How do Plants Produce so Many Strigolactones? In: Molecular Microbial Ecology of the Rhizosphere. John Wiley & Sons, Ltd, pp 373–379.

Yoneyama K., Xie X., Kusumoto D., Sekimoto H., Sugimoto Y., Takeuchi Y., Yoneyama K. (2007) Nitrogen deficiency as well as phosphorus deficiency in sorghum promotes the production and exudation of 5-deoxystrigol, the host recognition signal for arbuscular mycorrhizal fungi and root parasites. Planta **227**:125–132.

Zheng X., Yang Y., Al-Babili S. (2021) Exploring the Diversity and Regulation of Apocarotenoid Metabolic Pathways in Plants. Frontiers in Plant Science **12**:787049.

Zouari I., Salvioli A., Chialva M., Novero M., Miozzi L., Tenore G.C., Bagnaresi P., Bonfante P. (2014) From root to fruit: RNA-Seq analysis shows that arbuscular mycorrhizal symbiosis may affect tomato fruit metabolism. BMC Genomics **15**:221.

6.7 Supplementary material

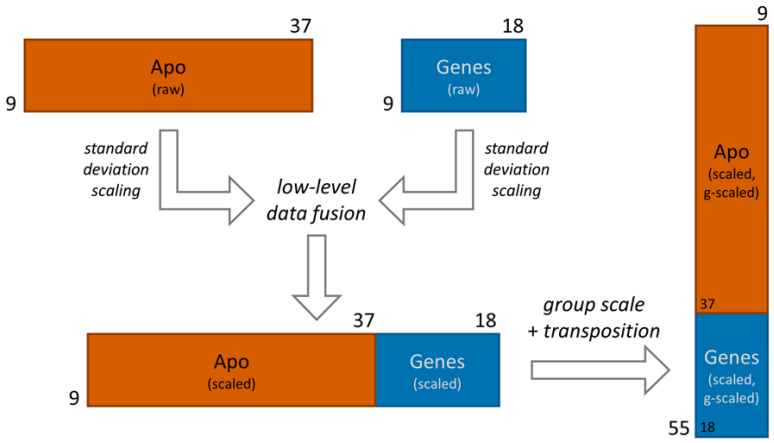

Supplementary Figure 1. *Data-fusion setup: the apocarotenoids and CCDs genes datasets were concatenated along the direction of time-growth conditions combinations (9), and after applying the preprocessing sequence described in Section Data fusion approach, the fused dataset was transposed and analysed with PCA with the apocarotenoids and CCDs genes as the samples and the time-growth conditions as the variables.*

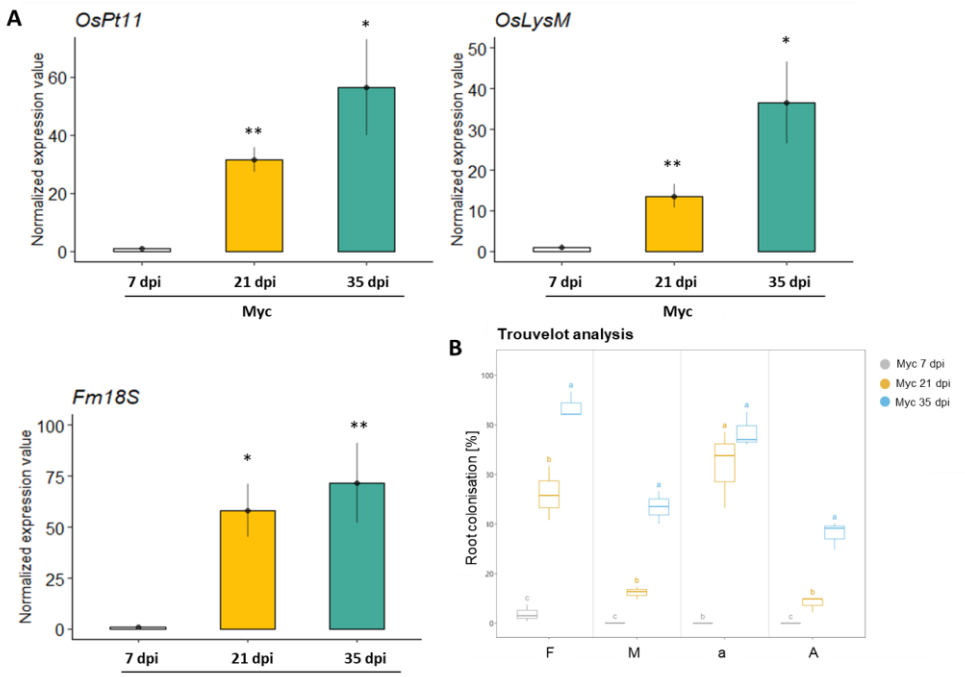

Supplementary figure 2. *Mycorrhization level in rice mycorrhizal plants grown in three-time points (7, 21, 35 dpi: days post inoculation). (A) Rice OsPT11 (Phosphate transporter 11) and OsLysM, and the fungal 18S rRNA expression pattern. Rubisco was used as a reference gene. Bars represent mean ± SE. Data n = 4 biological replicates. Asterisks indicate statistically significant differences referred to 7 dpi by one way-Anova (*P < 0.05; **P<0.01; ***P<0.001). (B) Morphological evaluation of root colonization with the method developed by Trouvelot et collegues (Trouvelot et al., 1986).T he estimation of mycorrhizal parameter, as F%: frequency of mycorrhizal, M%: intensity of mycorrhizal colonization, a%: arbuscule abundance in the mycorrhizal root part, and A%: arbuscule abundance in roots, was performed using "Ramf" an open-source R package (Chiapello et al. 2019). N=3. Significant values are shown with different letter (P < 0.05).*

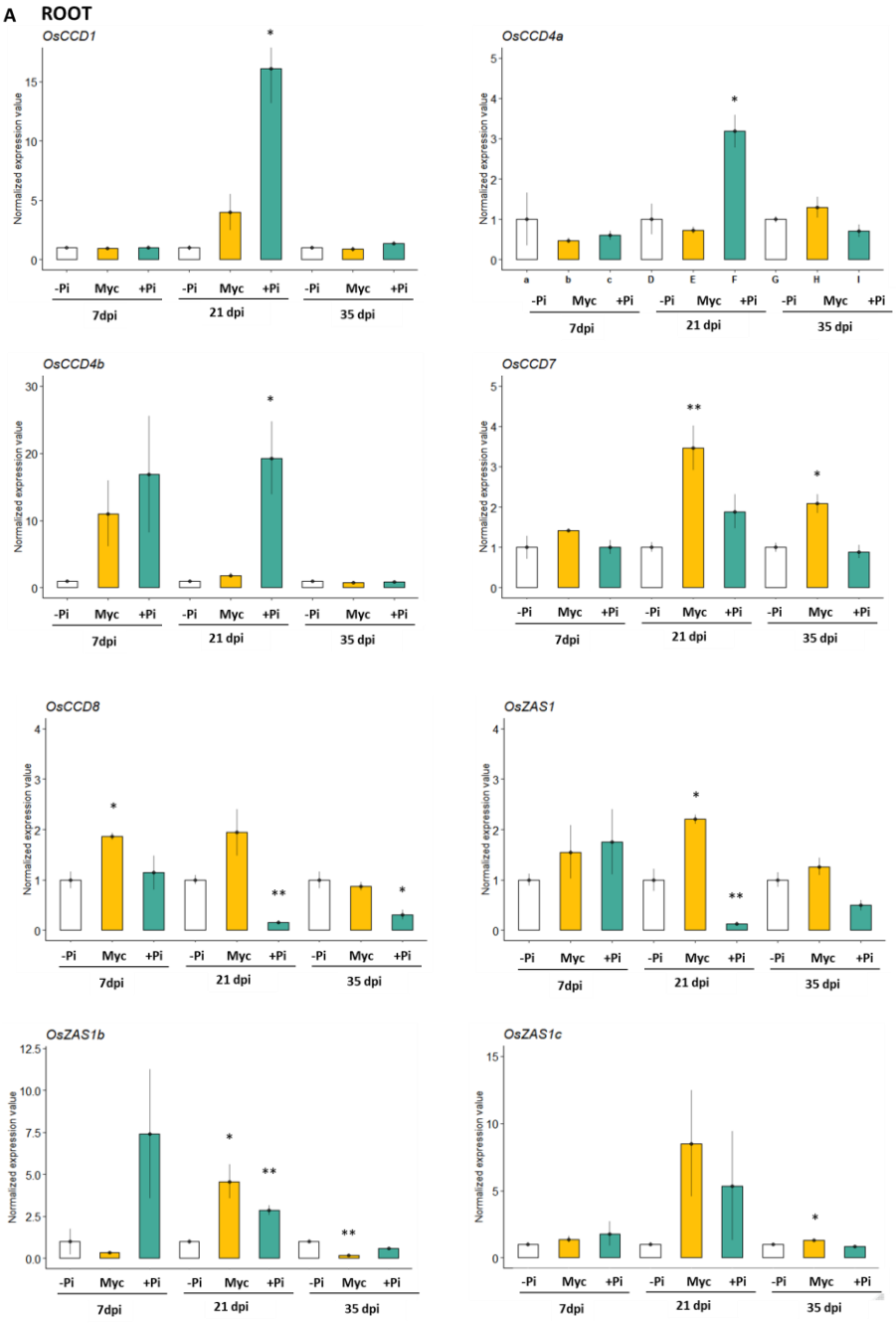
A ROOT
OsCCD1
OsCCD4a
OsCCD4b
OsCCD7
OsCCD8
OsZAS1
OsZAS1b
OsZAS1c
Normalized expression value
-Pi
Myc
+Pi
7dpi
21 dpi
35 dpi

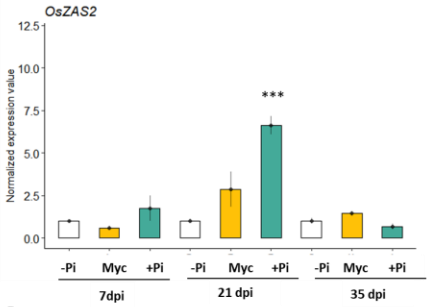
OsZAS2
Normalized expression value
12.5
10.0
7.5
5.0
2.5
0.0
***
-Pi Myc +Pi -Pi Myc +Pi -Pi Myc +Pi
7dpi
21 dpi
35 dpi

B **SHOOT**

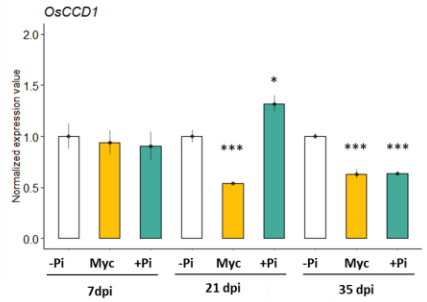
OsCCD1
Normalized expression value
2.0
1.5
1.0
0.5
0.0
*
***
***
***
-Pi Myc +Pi -Pi Myc +Pi -Pi Myc +Pi
7dpi
21 dpi
35 dpi

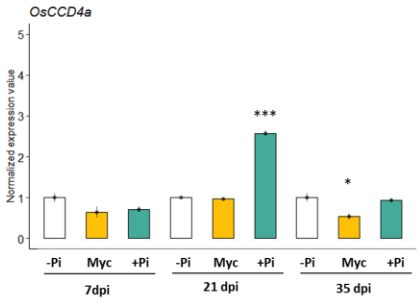
OsCCD4a
Normalized expression value
5
4
3
2
1
0
***
*
-Pi Myc +Pi -Pi Myc +Pi -Pi Myc +Pi
7dpi
21 dpi
35 dpi

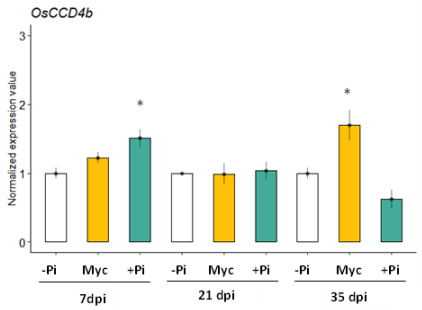
OsCCD4b
Normalized expression value
3
2
1
0
*
*
-Pi Myc +Pi -Pi Myc +Pi -Pi Myc +Pi
7dpi
21 dpi
35 dpi

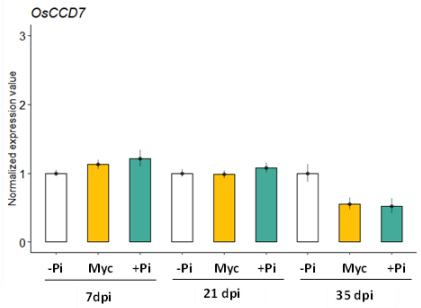
OsCCD7
Normalized expression value
3
2
1
0
-Pi Myc +Pi -Pi Myc +Pi -Pi Myc +Pi
7dpi
21 dpi
35 dpi

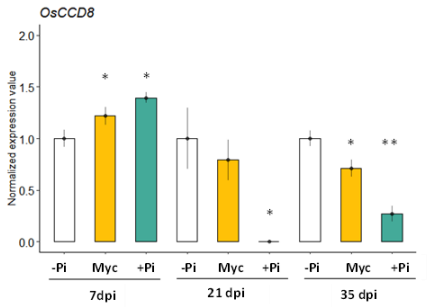
OsCCD8
Normalized expression value
2.0
1.5
1.0
0.5
0.0
*
*
*
*
**
-Pi Myc +Pi -Pi Myc +Pi -Pi Myc +Pi
7dpi
21 dpi
35 dpi

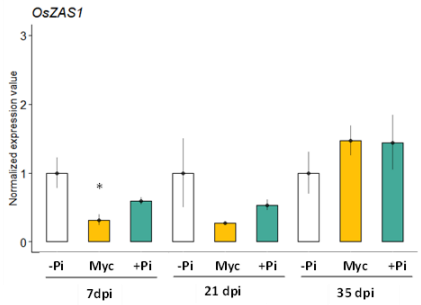
OsZAS1
Normalized expression value
3
2
1
0
*
-Pi Myc +Pi -Pi Myc +Pi -Pi Myc +Pi
7dpi
21 dpi
35 dpi

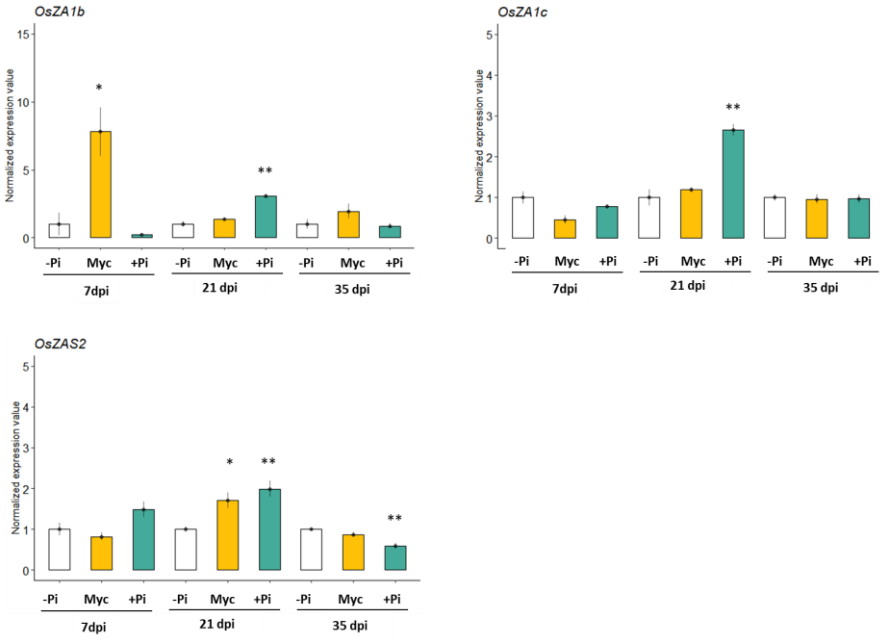

Supplementary figure 3. *qRT-PCR analysis of transcript levels of CCDs genes (CCD1, CCD4a, CCD4b, CCD7, CCD8, ZAS1, ZAS1b, ZAS1c, ZAS2) transcript levels in rice root (A) and shoot (B) grown in three time points (7, 21, 35 dpi: days post inoculation) and three conditions (-Pi, MYC, +Pi). Ubiquitin was used as a reference gene. Bars represent mean ± SE. Data n = 4 biological replicates. Asterisks indicate statistically significant differences referred to the –Pi condition, separately for each time point, by one way-Anova (*P < 0.05; **P<0.01; ***P<0.001).*

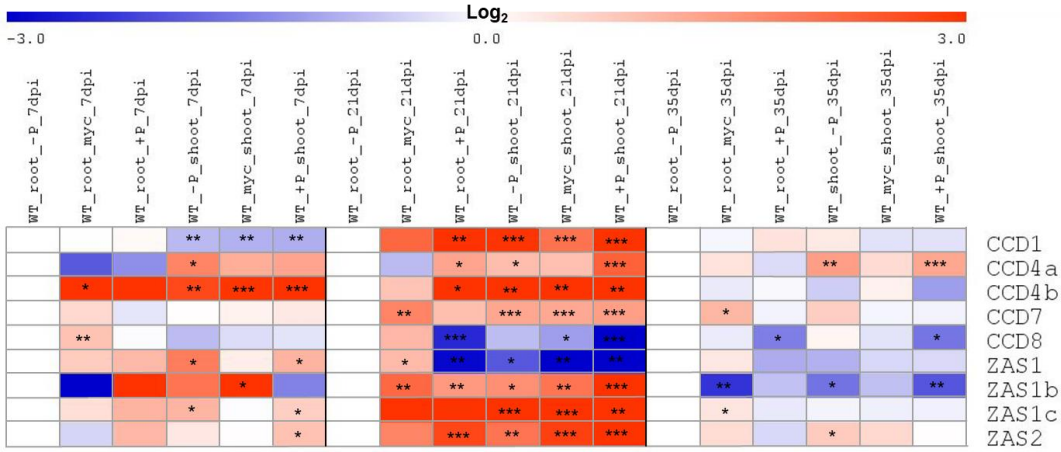

Supplementary figure 4. *Heatmap of root and shoot gene expression of the three-time points (7, 21, 35 dpi: days post inoculation) and the three analyzed conditions (-Pi, myc, +Pi). Data are means ± SE (n<=4). For each gene and time point, the value of the corresponding -Pi root sample was set to 1. Asterisks indicate statistically significant differences referred to the –Pi condition, separately for each time point, by one way-Anova (*P < 0.05; **P<0.01; ***P<0.001). Heatmaps were generated with the MultiExperiment Viewer (MeV) software.*
-Pi: 3.2 µM Pi; myc: mycorrhizal plants grown at 3.2 µM Pi; +Pi:500 µM Pi.

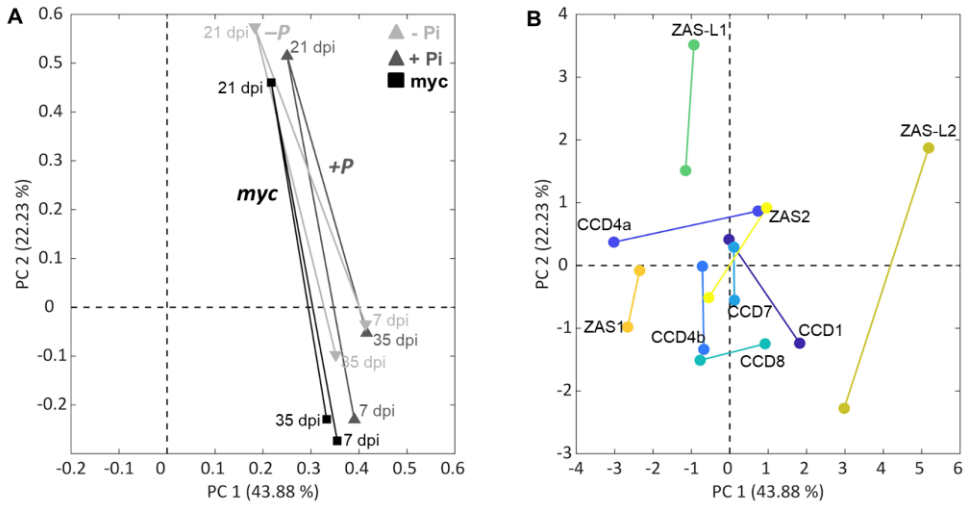

Supplementary figure 5. *PCA model of root and shoot CCDs genes through the three-time point and the three growth conditions (no-myc -P, MYC, no-myc +P). Loading plot (A) and score plot (B) with the first and second principal components.*

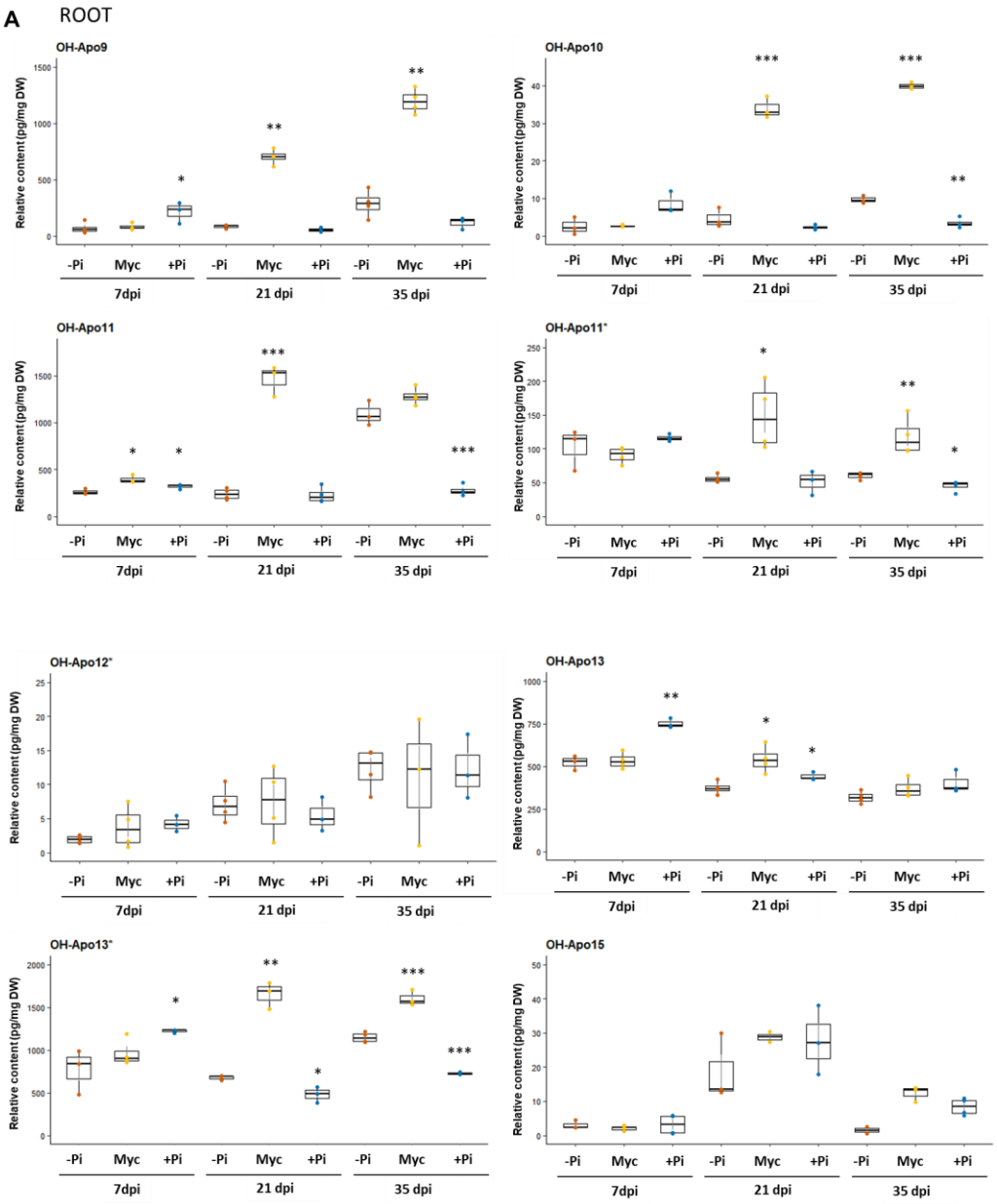
A
ROOT
OH-Apo9
OH-Apo10
OH-Apo11
OH-Apo11*
OH-Apo12*
OH-Apo13
OH-Apo13*
OH-Apo15
Relative content (pg/mg DW)
-Pi
Myc
+Pi
7dpi
21 dpi
35 dpi

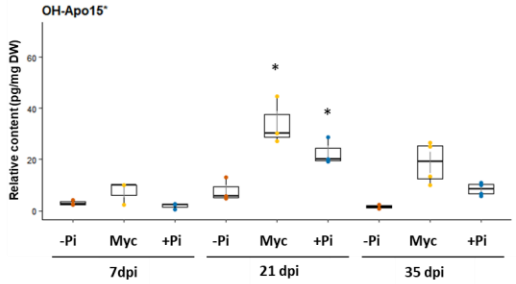
OH-Apo15*
Relative content (pg/mg DW)
-Pi
Myc
+Pi
7dpi
21 dpi
35 dpi

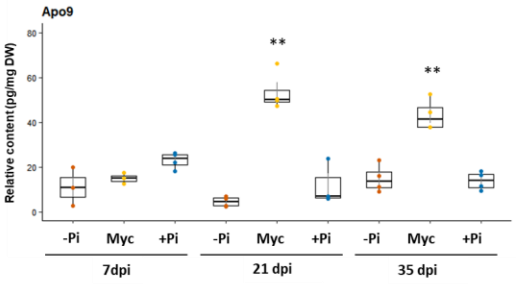
Apo9
Relative content (pg/mg DW)
-Pi
Myc
+Pi
7dpi
21 dpi
35 dpi

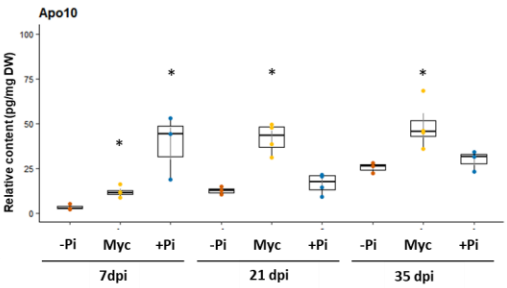
Apo10
Relative content (pg/mg DW)
-Pi
Myc
+Pi
7dpi
21 dpi
35 dpi

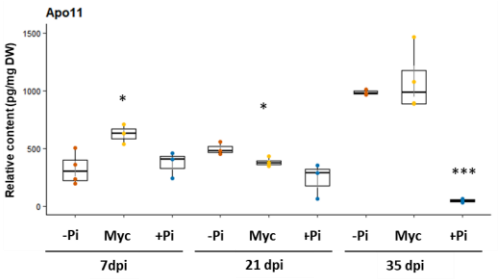
Apo11
Relative content (pg/mg DW)
-Pi
Myc
+Pi
7dpi
21 dpi
35 dpi

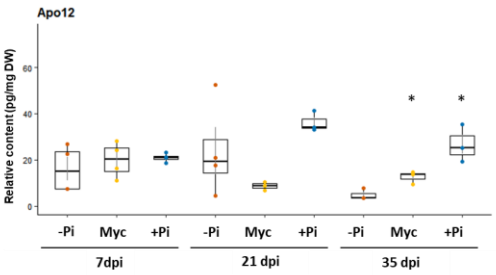
Apo12
Relative content (pg/mg DW)
-Pi
Myc
+Pi
7dpi
21 dpi
35 dpi

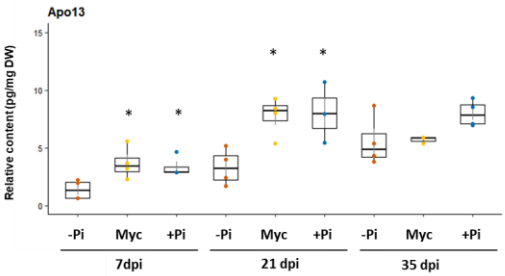
Apo13
Relative content (pg/mg DW)
-Pi
Myc
+Pi
7dpi
21 dpi
35 dpi

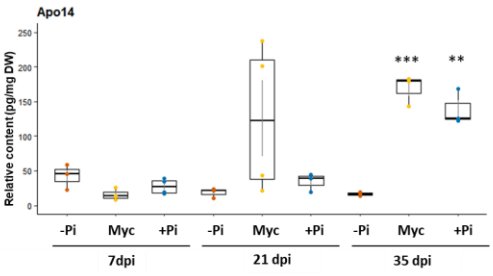
Apo14
Relative content (pg/mg DW)
-Pi
Myc
+Pi
7dpi
21 dpi
35 dpi

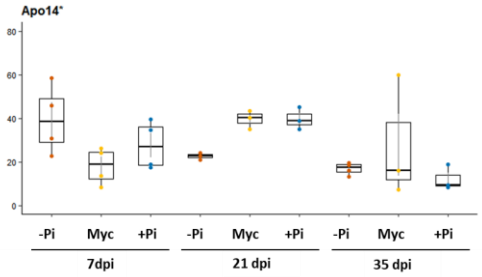
Apo14*
80
60
40
20
0
-Pi
Myc
+Pi
-Pi
Myc
+Pi
-Pi
Myc
+Pi
7dpi
21 dpi
35 dpi

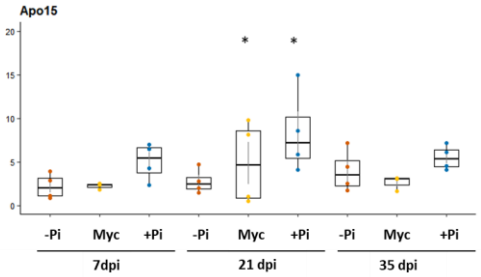
Apo15
20
15
10
5
0
*
*
-Pi
Myc
+Pi
-Pi
Myc
+Pi
-Pi
Myc
+Pi
7dpi
21 dpi
35 dpi

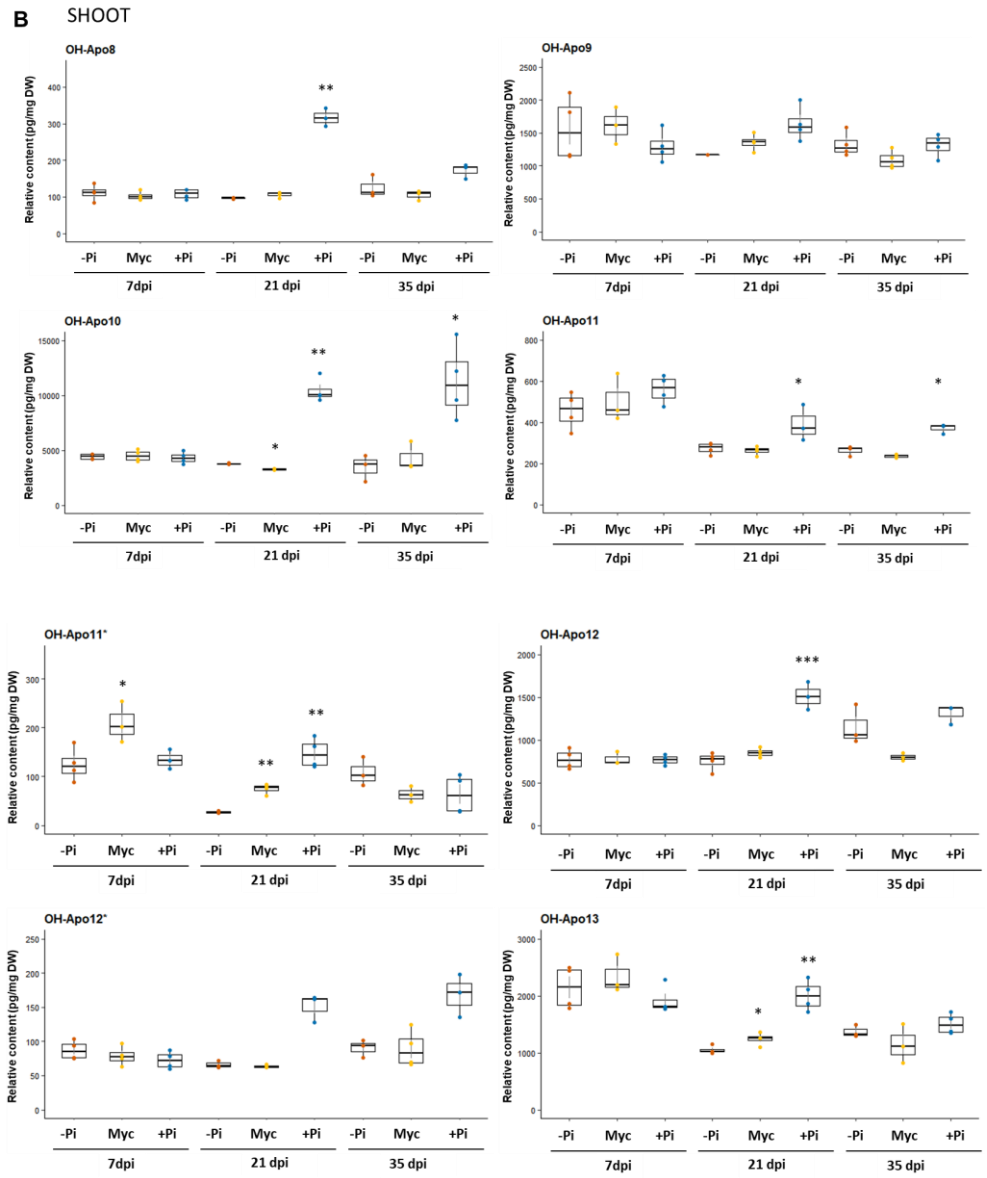
B
SHOOT
OH-Apo8
OH-Apo9
OH-Apo10
OH-Apo11
OH-Apo11*
OH-Apo12
OH-Apo12*
OH-Apo13
Relative content (pg/mg DW)
-Pi
Myc
+Pi
7dpi
21 dpi
35 dpi

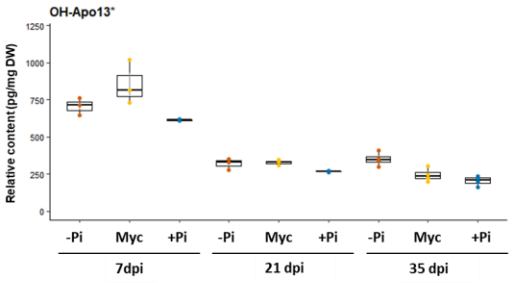
OH-Apo13*
Relative content (pg/mg DW)
1250
1000
750
500
250
0
-Pi Myc +Pi -Pi Myc +Pi -Pi Myc +Pi
7dpi
21 dpi
35 dpi

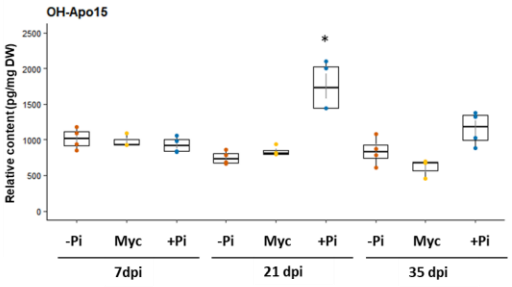
OH-Apo15
Relative content (pg/mg DW)
2500
2000
1500
1000
500
0
*
-Pi Myc +Pi -Pi Myc +Pi -Pi Myc +Pi
7dpi
21 dpi
35 dpi

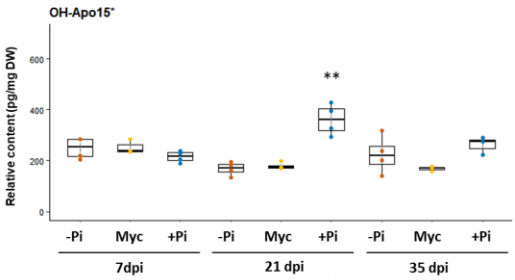
OH-Apo15*
Relative content (pg/mg DW)
600
400
200
0
**
-Pi Myc +Pi -Pi Myc +Pi -Pi Myc +Pi
7dpi
21 dpi
35 dpi

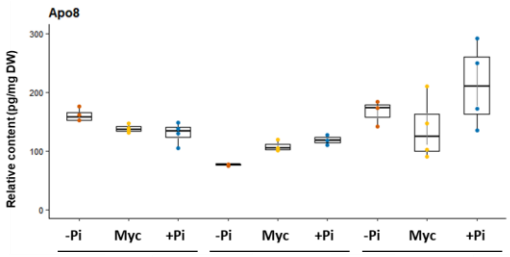
Apo8
Relative content (pg/mg DW)
300
200
100
0
-Pi Myc +Pi -Pi Myc +Pi -Pi Myc +Pi
7dpi
21 dpi
35 dpi

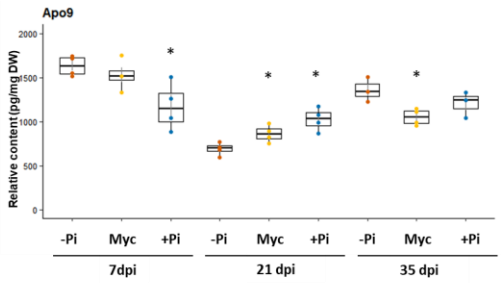
Apo9
Relative content (pg/mg DW)
2000
1500
1000
500
0
*
-Pi Myc +Pi -Pi Myc +Pi -Pi Myc +Pi
7dpi
21 dpi
35 dpi

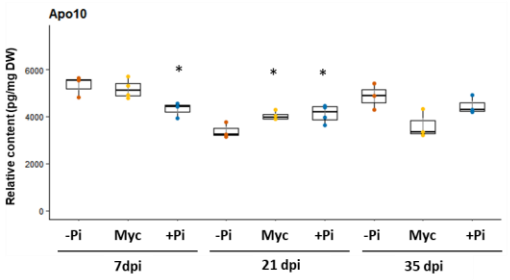
Apo10
Relative content (pg/mg DW)
6000
4000
2000
0
*
-Pi Myc +Pi -Pi Myc +Pi -Pi Myc +Pi
7dpi
21 dpi
35 dpi

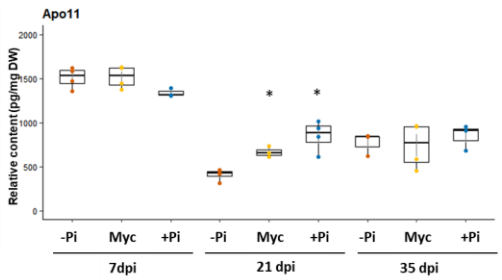
Apo11
Relative content (pg/mg DW)
2000
1500
1000
500
0
*
-Pi Myc +Pi -Pi Myc +Pi -Pi Myc +Pi
7dpi
21 dpi
35 dpi

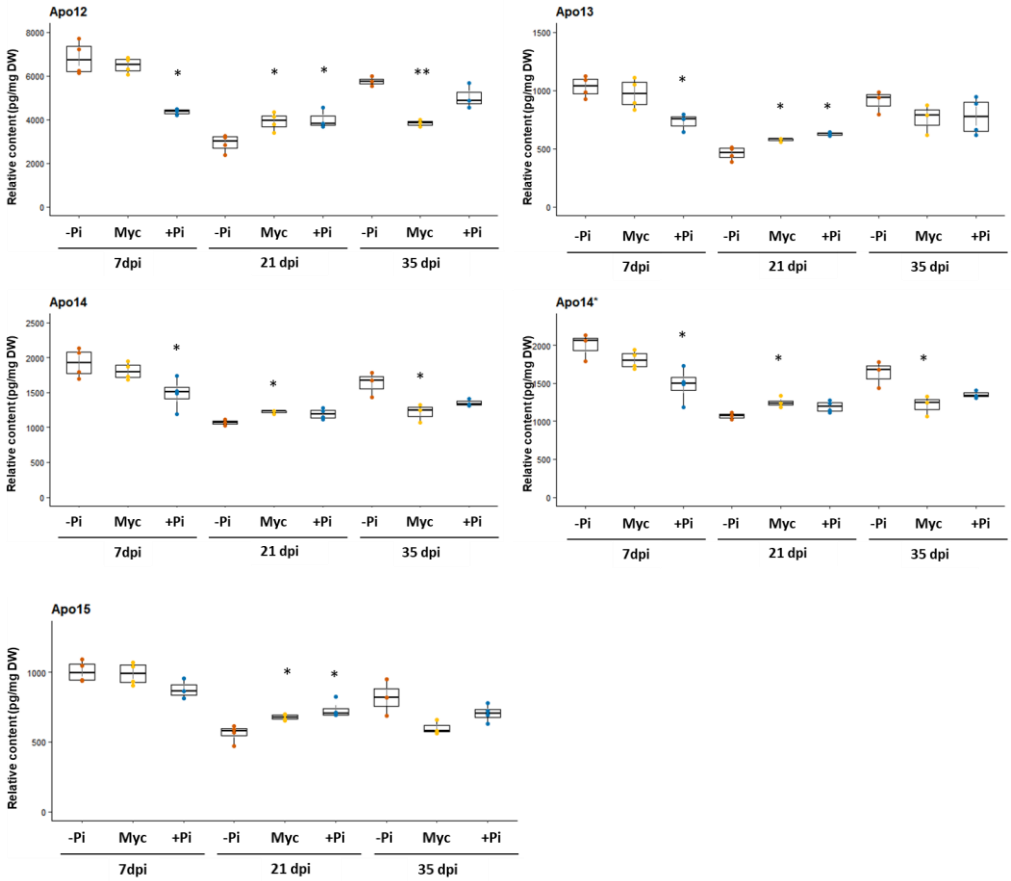

Supplementary Figure 6. *Apocarotenoids quantification across the three time points and the three analyzed conditions (-Pi, MYC, +Pi). Data are means ± SE (n<=4). Asterisks indicate statistically significant differences as compared to –P condition, separately for each time point, by one way-Anova (*P < 0.05; **P<0.01; ***P<0.001). The apocarotenoids indicated with asterisks represented the isoform of the corresponding apocarotenoid.*

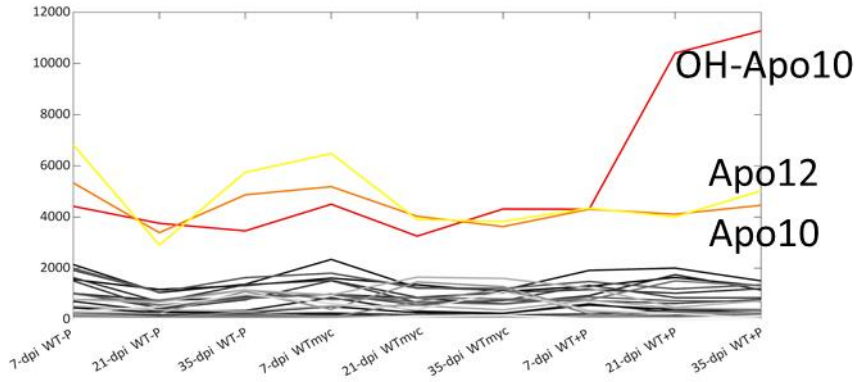

Supplementary Figure 7. *Plot of the raw apocarotenoids dataset. The three shoot apocarotenoids with extreme values (OH-Apo10, Apo12 and Apo10) are clearly visible and highlighted with warm colors.*

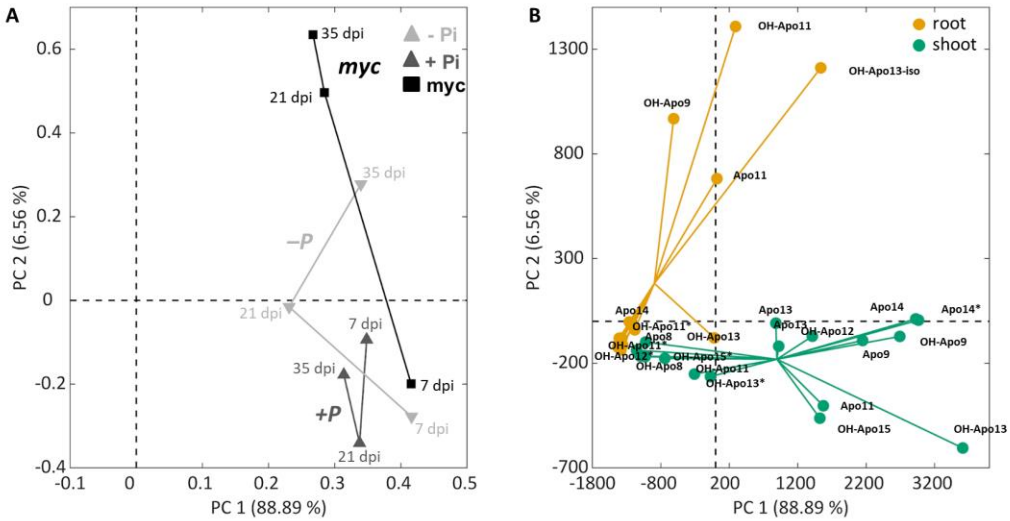

Supplementary figure 8. *PCA model of root and shoot apocarotenoids across the three growth stages and conditions (no-myc -P, MYC, no-myc +P). Loading plot (A) and score plot (B) with the first and second principal components. The apocarotenoids indicated with asterisks represent the isoform of the corresponding apocarotenoid.*

Experiment	Primer name	Sequence (5′–3′)
qRT-PCR	***OsRubQ1 F***	GGGTTCACAAGTCTGCCTATTTG
	OsRubQ1 R	ACGGGACACGACCAAGGA
	OsPt11 F	GAGAAGTTCCCTGCTTCAAGCA
	OsPt11 R	CATATCCCAGATGAGCGTATCATG
	OsCCD1 F	CAATGTCTGCTGATCCGGTG
	OsCCD1 R	TCACGCTGATTGTTTTGCCA
	OsCCD4a F	CGGGCTTCAACATCATGC
	OsCCD4a R	TAGCTCTCATGTGCTCCAG
	OsCCD4b F	CCAAACTTCTTCGCTGGCTT
	OsCCD4b R	GTGCATGGAGTAGGGAAGGT
	OsCCD7 F	CATTGGAAAAGTGAGGTTCCTTTGG
	OsCCD7 R	AATGCACTTGGAAAACGAG
	OsCCD8 F	GTTCCAGTACACGGACAAG
	OsCCD8 R	ACTGCCTCTCGTTGCTA
	OsZAS1 F	CTCCATTCGACCGTCTCAATCT
	OsZAS1 R	TGGCTTCTGTCTGGTTTTCTCA
	OsZAS1b F	GACCAAAACGGTGCCATCC
	OsZAS1b R	CTCCCTTTCCAGTGGATGCT
	OsZAS1c F	GCAGCAGCTTACCACCAAAC
	OsZAS1c R	GTGCGAAATTGCTCTCGGTG
	OsZAS2 F	CATCTAGGGAAGAGCCCAGC
	OsZAS2 R	TGGCTGCTTATTCCACCCAG

Supplementary Table 1. *Primer sequences used in this study.*

Abbreviation	Name	Formula	Structural formula
Apo9	β-apo-9'-carotenal (β-ionone)	$C_{13}H_{20}O$	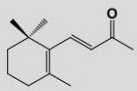
Apo10	β-apo-10'-carotenal	$C_{27}H_{36}O$	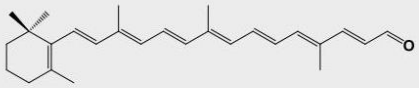
Apo11	β-apo-11-carotenal	$C_{15}H_{22}O$	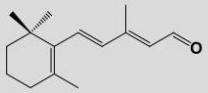
Apo12	β-apo-12'-carotenal	$C_{25}H_{34}O$	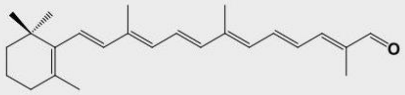
Apo13	β-apo-13-carotenone	$C_{18}H_{26}O$	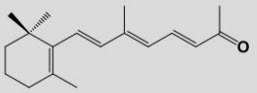
Apo14	β-apo-14'-carotenal	$C_{22}H_{30}O$	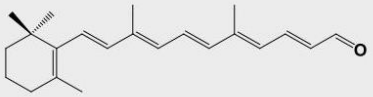
Apo15	β-apo-15-carotenal	$C_{20}H_{28}O$	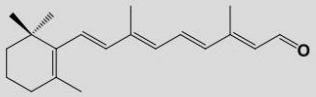
OH-Apo8	3-OH-β-apo-8'-carotenal	$C_{30}H_{40}O_2$	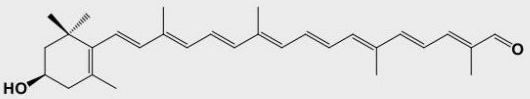
OH-Apo9	3-OH-β-apo-8'-carotenal (OH- β-ionone)	$C_{13}H_{20}O_2$	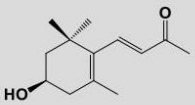
OH-Apo10	3-OH-β-apo-10'-carotenal	$C_{27}H_{36}O_2$	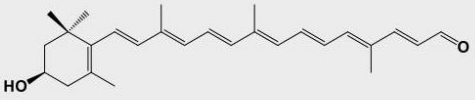

OH-Apo11	3-OH-β-apo-11-carotenal	$C_{15}H_{22}O_2$	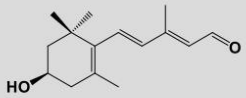
OH-Apo12	3-OH-β-apo-12'-carotenal	$C_{25}H_{34}O_2$	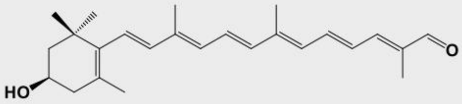
OH-Apo13	3-OH-β-apo-13-carotenone (zaxinone)	$C_{18}H_{26}O_2$	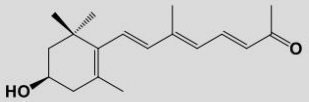
OH-Apo14	3-OH-β-apo-14'-carotenal	$C_{22}H_{30}O_2$	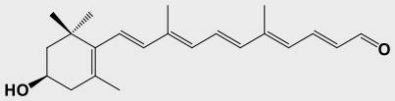
OH-Apo15	3-OH-β-apo-15-carotenal	$C_{20}H_{28}O_2$	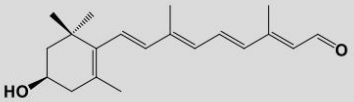

Supplementary Table 2. *A summary with non-hydroxylated and hydroxylated apocarotenoids analyzed in this study, the formula, corresponding name, and structural formula are indicated for each abbreviation.*

Chapter 7: General conclusions

My thesis, and the research work behind, focused mainly on zaxinone, a natural apocarotenoid with plant growth-promoting activity. The work has been carried out in collaboration with the group of Prof. Salim Al-Babili (KAUST, King Abdullah University of Science and Technology) which in 2019 led to the first publication on zaxinone and the gene responsible for its biosynthesis, *Zaxinone Synthase* (*OsZAS*) in rice plants (Wang *et al.* 2019).

Tracing back the history of plant apocarotenoids, the first to be discovered and characterized in the mid-1960s were abscisic acid (ABA) (Liu & Carns 1961) and strigolactones (SLs) (Cook *et al.* 1966). For years research has been looking at these plant hormones, to unravel the mechanisms under their biosynthesis, signalling, metabolism, and cross-talk with other hormones (for example, auxins, cytokinins, ethylene, and gibberellins) (Ross & O'Neill 2001; Hayward *et al.* 2009; Ross *et al.* 2011; Wang & Irving 2011). These studies highlighted the biological functions of these hormones and their role in the regulation of several aspects of plant biology and interactions with biotic and abiotic factors.

In recent years, thanks to the rapid development and improvement of analytical and sequencing techniques, our knowledge of apocarotenoids and the underlying metabolic pathways have been extensively increased. Other apocarotenoids were identified and characterized such as β-cyclocitral, which was found to be involved in stress responses (Dickinson *et al.* 2019), and anchorene and zaxinone with plant growth-promoting properties (Dickinson *et al.* 2019; Wang *et al.* 2019; Ablazov *et al.* 2020). Besides their role in plant development and in abiotic stress response, apocarotenoids are emerging as a key regulator of plant-(micro)organism interactions, such as the volatile compounds α- and β-ionone and loliolide, which influence plant–herbivore interactions (Moreno et al., 2021), and the C13 and C14

compounds, blumenols and mycorradicin, which are strongly associated with the establishment of AM symbiosis (Fiorilli et al., 2019).

In my PhD, I contributed to characterizing the involvement of zaxinone and zaxinone synthase in plant development and in the arbuscular mycorrhizal (AM) interaction.

First, we highlighted some of the mechanisms behind the plant growth promotion given by an exogenous zaxinone supply. In rice, zaxinone triggered sugar-related metabolic processes and influenced the root at the cellular level and induced an increase in root starch content and glycosylation of cytokinins (Wang *et al.* 2021) (**Chapter 2**).

In **Chapter 3**, our study described the function of *OsZAS* and zaxinone in the AM symbiosis regulation; we showed that *OsZAS* takes part in the mechanisms underpinning the early symbiotic programs that are instrumental in achieving normal mycorrhization levels, influencing both SLs and D14-L signaling pathways (Votta *et al.* 2022).

Moreover, we explored the role of *OsZAS2*, one of the other three *OsZAS* homologs encoded by the rice genome (Ablazov *et al.* 2022). This gene, besides *OSZAS*, is also involved in zaxinone production, is crucial for rice growth and development and is a further determinant of SL content and a regulator of mycorrhization level (**Chapter 4**).

Considering that zaxinone and the *OsZAS* homologous genes are present in other plant species, in **Chapter 5**, we investigated the impact of this apocarotenoid on tomato (*Solanum lycopersicum*), another important crop. As observed in rice, a zaxinone exogenous treatment positively regulates tomato growth, increases the starch content in roots, and affects SL biosynthesis. Furthermore, we highlighted the potential role of zaxinone in response to water stresses and in plant-pathogenic interactions, opening prospects for future investigations and applications in agriculture.

Finally, in the last chapter (**Chapter 6**), we explored the possible involvement of other apocarotenoids in the AM colonization process, by monitoring how their content change during different stages of mycorrhization, possibly highlighting novel markers at both local and systemic levels. The integration of metabolites and expression data of *CCD* genes has emerged as a promising tool to dissect this complex metabolic pathway suggesting putative links between enzymatic activities and apocarotenoid production.

In conclusion, my PhD work is a contribution to apocarotenoids research, and in particular to zaxinone. On the whole, the data presented in this thesis have highlighted the relevance of this metabolite on plant growth and have opened applicative perspectives of its use in agriculture as a biostimulant (Wang *et al. 2022*). There are still many issues that deserve investigation: for example, how zaxinone is perceived by plants and if and how zaxinone moves across different plant organs or even outside in the rhizosphere. Its involvement in plant-microbe interactions other than the AM symbiosis should also be analysed as well as its contribution to plant responses to abiotic stresses such as drought, which is a big challenge of modern agriculture. It would also be interesting to know to what extent plant growth-promoting effects of zaxinone, which we described in rice and tomato, occur in other plant species and what are the relationships with other phytohormones or bioactive metabolites of this versatile and fascinating plant metabolic pathway.

7.1 Reference

Ablazov A., Mi J., Jamil M., Jia K.-P., Wang J.Y., Feng Q., Al-Babili S. (2020) The Apocarotenoid Zaxinone Is a Positive Regulator of Strigolactone and Abscisic Acid Biosynthesis in Arabidopsis Roots. Frontiers in Plant Science **578.**

Ablazov A., Votta C., Fiorilli V., Wang J.Y., Aljedaani F., Jamil M., Balakrishna A., Balestrini R., Liew K.X., Rajan C., Berqdar L., Blilou I., Lanfranco L., Al-Babili S. (2022) ZAXINONE SYNTHASE 2 *regulates growth and arbuscular mycorrhizal symbiosis in rice*. Plant Physiol.191(1):382-399.

Cook C.E., Whichard L.P., Turner B., Wall M.E., Egley G.H. (1966) Germination of Witchweed (Striga lutea Lour.): Isolation and Properties of a Potent Stimulant. Science **154**:1189–1190.

Dickinson A.J., Lehner K., Mi J., Jia K.-P., Mijar M., Dinneny J., Al-Babili S., Benfey P.N. (2019) β-Cyclocitral is a conserved root growth regulator. Proceedings of the National Academy of Sciences **116**:10563–10567.

Hayward A., Stirnberg P., Beveridge C., Leyser O. (2009) Interactions between Auxin and Strigolactone in Shoot Branching Control. Plant Physiology **151**:400–412.

Liu W.-C., Carns H.R. (1961) Isolation of Abscisin, an Abscission Accelerating Substance. Science **134**:384–385.

Ross J., O'Neill D. (2001) New interactions between classical plant hormones. Trends in Plant Science **6**:2–4.

Ross J.J., Weston D.E., Davidson S.E., Reid J.B. (2011) Plant hormone interactions: how complex are they? Physiologia Plantarum **141**:299–309.

Votta C., Fiorilli V., Haider I., Wang J.Y., Balestrini R., Petřík I., Tarkowská D., Novák O., Serikbayeva A., Bonfante P., Al-Babili S., Lanfranco L. (2022) Zaxinone synthase controls arbuscular mycorrhizal colonization level in rice. The Plant Journal **111**:1688–1700.

Wang J.Y., Alseekh S., Xiao T., Ablazov A., Perez de Souza L., Fiorilli V., Anggarani M., Lin P.-Y., Votta C., Novero M., Jamil M., Lanfranco L., Hsing Y.-I.C., Blilou I., Fernie A.R., Al-Babili S. (2021) Multi-omics approaches explain the growth-promoting effect of the apocarotenoid growth regulator zaxinone in rice. Communications Biology **4**:1–11.

Wang J.Y., Haider I., Jamil M., Fiorilli V., Saito Y., Mi J., Baz L., Kountche B.A., Jia K.-P., Guo X., Balakrishna A., Ntui V.O., Reinke B., Volpe V., Gojobori T., Blilou I., Lanfranco L., Bonfante P., Al-Babili S. (2019) The apocarotenoid metabolite zaxinone regulates growth and strigolactone biosynthesis in rice. Nature Communications **10**:810.

Wang J. Y., Jamil M., Hossain M. G., Chen G. T. E., Berqdar, L., Ota, T., Blilou I., Asami T., Al-Solimani S. J., Mousa M. A. A., Al-Babili S. Evaluation of the Biostimulant Activity of Zaxinone Mimics (MiZax) in Crop Plants. Frontiers in Plant Science, 13.

Wang Y.H., Irving H.R. (2011) Developing a model of plant hormone interactions. Plant Signaling & Behavior **6**:494–500.

List of publications

- Wang J.Y., Alseekh S., Xiao T., Ablazov A., Perez de Souza L., Fiorilli V., Anggarani M., Lin P.-Y., **Votta C.,** Novero M., Jamil M., Lanfranco L., Hsing Y.-I.C., Blilou I., Fernie A.R., Al-Babili S. (2021) Multi-omics approaches explain the growth-promoting effect of the apocarotenoid growth regulator zaxinone in rice. Communications Biology 4:1–11.

- Fiorilli V., Maghrebi M., Novero M., **Votta C.,** Mazzarella, T., Buffoni B., Astolfi S., Vigani, G. (2022). Arbuscular Mycorrhizal Symbiosis Differentially Affects the Nutritional Status of Two Durum Wheat Genotypes under Drought Conditions. Plants, 11(6), 804.

- **Votta C**.*, Fiorilli V*., Haider I., Wang J. Y., Balestrini R., Petřík I., Tarkowská D., Novák O., Serikbayeva A., Bonfante P., Al-Babili S., Lanfranco L. (2022). Zaxinone synthase controls arbuscular mycorrhizal colonization level in rice. The Plant Journal, 111(6), 1688-1700.

- Ablazov A.*, **Votta C.***, Fiorilli V., Wang J. Y., Aljedaani F., Jamil M., Balakrishna A., Balestrini R., Liew K. X., Rajan C., Berqdar L., Blilou I., Lanfranco L., Al-Babili S. ZAXINONE SYNTHASE 2 regulates growth and arbuscular mycorrhizal symbiosis in rice. Plant Physiol.191(1):382-399.

Poster and oral presentation conferences

- **Votta C**., Fiorilli V., Gómez-Ariza J., Fornara F., Lanfranco L. The expression of Rhizophagus irregularis *RiPEIP1* gene in rice promotes plant growth and mycorrhizal colonization. **4th international Molecular Mycorrhiza Meeting** (**iMMM**), Turin, Italy 6 - 8 February 2019. (Poster presentation)

- Fiorilli V., **Votta C**., Wang J.,Haider I., Jamil M. , Mi J. , Baz L. , Saito Y. , Boubacar A. Kountche1 , Kun- Peng Jia1 ,Guo X. , Balakrishna A.,Ntui V. , Reinke B., Volpe V., Gojobori T. , Blilou I. , Lanfranco L. , Bonfante P., Al-Babili S. Zaxinone, a natural apocarotenoid, is involved in the establishment of the arbuscular mycorrhizal symbiosis. **4th international Molecular Mycorrhiza Meeting** (**iMMM**), Turin, Italy 6 - 8 February 2019. (Poster presentation)

- **Votta C**., Fiorilli V., Gómez-Ariza J., Fornara F., Lanfranco L. Rice plants expressing the Rhizophagus irregularis *RiPEIP1* gene show enhanced growth and incresed level of mycorrhizal colonization. **International Society for Molecular Plant-Microbe Interactions (IS-MPMI) XVIII Congress,** Glasgow, Scotland 14-18 July 2019. (Poster presentation)

- Fiorilli V., Haider I., **Votta C**., Wang J., Jamil M., Mi J., Kountche B.,Jia K., Balakrishna A., Lanfranco L., Bonfante P., Al Babili S. Zaxinone, a natural apocarotenoid, is involved in the establishment of the arbuscular mycorrhizal symbiosis. **International Society for Molecular Plant-Microbe Interactions (IS-MPMI) XVIII Congress,** Glasgow, Scotland 14-18 July 2019**.** (Poster presentation)

- **Votta C**., Fiorilli V., Gómez-Ariza J., Fornara F., Lanfranco L. "The heterologous expression of the Rhizophagus irregularis RiPEIP1 gene in rice plants leads to enhanced growth and mycorrhizal colonization", VI International Plant Science Conference (IPSC)-114° Congresso della Società Botanica Italiana, Padova, 4 - 7 September 2019. (Oral presentation)
- **Cristina Votta**, Valentina Fiorilli, Jian You Wang, Silvia De Rose, Alessandro Silvestri, Teresa Mazzarella, Aparna Balakrishna, Muhammad Jamil, Salim Al-Babili, Luisa Lanfranco. The effect of zaxinone, a natural metabolite derived from carotenoids, on tomato plants. 116° Congresso della Società Botanica Italiana, 8 - 10 September 2021, online. (Oral presentation)

Acknowledgments

Having come to the end of my PhD, I must thank the people who have accompanied me over the years.

In primis, I want to express the sincerest gratitude to Prof. Luisa Lanfranco for her complete availability and trust in me from the beginning, and to Prof. Valentina Fiorilli for guiding me since my first year in the lab and outside, and for having the patience to wait for me to "walk with my legs."

I thank Prof. Salim Al-Babili and his group for the seven months spent in his lab at KAUST. This period was very formative for me, allowing me to grow from a scientific and social point of view and get to know different people and cultures. I especially thank Eric for his invaluable and constant help in and out of KAUST.

I thank Dr.ssa Raffaella Balestrini for welcoming me into her lab and following me during the *in situ* hybridization; and all the people who dedicated their time in the lab and beyond, sharing their knowledge with me, especially Mara, Alessandro, Matteo, and Veronica.

Thanks to all my colleagues, with whom over the years we have shared ideas and support in the lab and in fields, lunches, beers, and even some running together. In particular, I thank Teresa and Andrea for their endless support, our laughter and hard times spent together without discouraging us, and for being, more simply, my friends.

Finally, I thank the people who love me and believe in me. My friends Sara and Marta have been by my side since we were children (has it been 20 years?). My mom Gianna and dad Felice, examples of all the lessons that are not learned from books and whom I hope to never forget. My sisters Simona (Mozza) and Franci for growing up together and sharing memories and emotions that have led us to be the people we

are. Andrea for his daily support and for making me feel sheltered from all the fears that are part of the "future".